The role of the AHNAK protein in breast cancer: Implications for tumour metastasis and chemoresistance

by

Tanja Andréa Davis

Dissertation presented for the degree of
Doctor of Philosophy in the
Faculty of Science at
Stellenbosch University

Promotor: Prof. Anna-Mart Engelbrecht

Co-promotor: Dr. Benjamin Loos

December 2016

The financial assistance of the National Research Foundation (NRF) towards this research is hereby acknowledged. Opinions expressed and conclusions arrived at, are those of the author and are not necessarily to be attributed to the NRF.

Declaration

By submitting this dissertation electronically, I declare that the entirety of the work contained therein is my own, original work, that I am the sole author thereof (save to the extent explicitly otherwise stated), that reproduction and publication thereof by Stellenbosch University will not infringe any third party rights and that I have not previously in its entirety or in part submitted it for obtaining any qualification.

This dissertation includes one original paper published in a peer-reviewed journal. The development and writing of the paper were the principal responsibility of myself.

December 2016

Abstract

Introduction – Cancer continues to have a significant impact on society. While there has been much success in characterising tumours and identifying targetable markers, two major problems are still faced today, namely therapeutic failure and advanced progression of the disease. The human AHNAK protein is a giant scaffold protein involved in multiple cellular processes and has now also been suggested to be associated with cancer, particularly with regards to tumour metastasis and chemoresponse. However, limited information and several contradicting findings have contributed to a poor understanding of the role of AHNAK in cancer. Thus, we aimed to characterise the AHNAK protein in cancer by determining the role of the protein in the chemotherapeutic response of breast cancer to doxorubicin (DXR) and also in cellular migration.

Methods – For the *in vitro* model the non-metastatic DXR-sensitive epithelial-like MCF-7 and metastatic DXR-resistant mesenchymal-like MDA-MB-231 cell lines were used. We performed DXR treatments and assessed AHNAK's protein expression and intracellular localisation. We also assessed these properties in a tumour-bearing mouse model. AHNAK knockdown and overexpression was achieved by means of transient plasmid transfections in both cell lines and following DXR treatments we assessed apoptotic marker expression, cell cycle modulation, epithelial-mesenchymal transition (EMT) marker expression and cellular migration.

Results – DXR induced dose-independent and dose-dependent changes in AHNAK protein expression in MCF-7 and MDA-MB-231 cells, respectively, but it did not affect its intracellular localisation in these cells. In the tumour-bearing mouse model DXR also induced dose-dependent changes in AHNAK expression without affecting its localisation, similar to the MDA-MB-231 cells. In the MDA-MB-231 cells, DXR promoted apoptosis inhibition by decreasing cPARP and cCasp7 expression. Knockdown of AHNAK prevented this inhibition while overexpression induced a similar inhibitory effect. With cell cycle analyses we observed that DXR also resulted in S phase arrest in these cells. AHNAK knockdown completely prevented the DXR-induced cell cycle arrest while overexpression was sufficient to cause such an arrest on its own. No significant effects were observed with these experiments in the MCF-7 cells. DXR induced EMT in the MCF-7 cells but AHNAK knockdown or overexpression did not affect this. In MDA-MB-231 cells DXR treatment showed a trend of decreased EMT and while AHNAK knockdown had no effect on this, its overexpression showed clearer evidence of EMT reduction. AHNAK knockdown also had no major effects on cell migration in both cell lines, although its overexpression generally decreased cellular migration.

Conclusions – We show that AHNAK plays a novel role in the DXR-response of breast cancer cells and this involved AHNAK's expression, apoptosis inhibition and cell cycle modulation. Possible

molecular mechanisms are proposed but require further investigation. Our results regarding the role of AHNAK in tumour cell migration is less clear and contradicting when compared to other studies. These results may have potential therapeutic implications with regards to the modulation of DXR response to improve treatment efficacy.

Opsomming

Inleiding - Kanker het steeds 'n beduidende impak op die samelewing. Terwyl daar groot sukses in die karakterisering van gewasse en die identifisering van teikenbare merkers gemaak is, word twee groot probleme steeds vandag ervaar, naamlik terapeutiese mislukking en gevorderde progressie van die siekte. Die menslike AHNAK proteïen is 'n reuse steier proteïen betrokke by verskeie sellulêre prosesse en dit word ook voorgestel dat die proteïen verband hou met kanker, veral ten opsigte van kanker metastase en chemo-reaksie. Beperkte inligting en verskeie weersprekende bevindinge het egter bygedra tot 'n swak begrip van die rol van AHNAK in kanker. ‘n Oogmerk van hierdie studie is dus om AHNAK in kanker beter te karakteriseer deur die rol van die proteïen in chemoterapeutiese reaksie van borskanker teenoor doxorubicin (DXR) en ook in sellulêre migrasie te bepaal.

Metodes - Vir die *in vitro* model is die nie-metastatiese DXR-sensitiewe epiteel-agtige MCF-7 en metastatiese DXR-weerstandige mesenkiemale MDA-MB-231 sellyne gebruik. Ons het DXR behandelings uitgevoer en AHNAK proteïen uitdrukking en intrasellulêre lokalisering bepaal. Ons het hierdie eienskappe ook in 'n kanker muis model bepaal. AHNAK uitklopping en ooruitdrukking is bereik deur middel van tydelike plasmied transfeksies in beide sellyne. DXR behandelinge is uitgevoer en daarna is apoptotiese merker uitdrukking, selsiklus modulasie, epiteel-mesenkiemale oorgang (EMO) merker uitdrukking en sellulêre migrasie bepaal.

Resultate - DXR het dosis-onafhanklike en dosis-afhanklike veranderinge in AHNAK proteïen uitdrukking in MCF-7 en MDA-MB-231 selle, onderskeidelik, veroorsaak maar het geen invloed op intrasellulêre lokalisering gehad nie. Met die kanker muis model het DXR ook dosis-afhanklike veranderinge in AHNAK uitdrukking veroorsaak sonder ‘n verandering in lokalisering, soortgelyk aan dié in MDA-MB-231 selle. In die MDA-MB-231 selle het DXR apoptose inhibering bevorder deur cPARP en cCasp7 uitdrukking te verminder. AHNAK uitklopping het hierdie inhibisie verhinder terwyl ooruitdrukking tot ‘n soortgelyke inhiberende effek gelei het. Selsiklus analise het getoon dat DXR ook tot S-fase blokkering gelei het in hierdie selle. AHNAK uitklopping het die selsiklus blokkering heeltemal verhoed terwyl ooruitdrukking voldoende was om ‘n soortgelyke blokkering op sy eie teweeg te bring. Geen beduidende effekte was waargeneem met hierdie eksperimente in die MCF-7 selle nie. DXR het EMO bevorder in die MCF-7 selle maar AHNAK uitklopping of ooruitdrukking het geen invloed op dit gehad nie. In MDA-MB-231 selle het DXR behandeling 'n tendens van verminderde EMO getoon en terwyl AHNAK uitklopping geen effek op hierdie gehad het nie, het ooruitdrukking duideliker bewyse van EMO vermindering getoon. AHNAK uitklopping het ook nie 'n groot uitwerking op sel migrasie in beide sellyne gehad nie, alhoewel ooruitdruking sellulêre migrasie oor die algemeen verminder het.

Gevolgtrekkings - Ons bewys dat AHNAK 'n nuwe rol speel in die DXR-reaksie van borskanker en dit betrek AHNAK uitdrukking, apoptose inhibering en selsiklus modulasie. Moontlike molekulêre

meganismes word voorgestel, maar verdere ondersoek word vereis. Die resultate met betrekking tot die rol van AHNAK in kankersel migrasie is minder duidelik en weerspreek sekere studies. Hierdie resultate het moontlike potensiële terapeutiese implikasies met betrekking tot die modulasie van DXR-reaksie om behandeling doeltreffendheid te verbeter.

Acknowledgements

I am sincerely indebted to the following:

My husband John, words can not express how much your support means to me. Thank you for your endless patience throughout my years of studying. Thank you for always being there and for taking care of everything else so that I can focus on my studies. I am truly blessed with the best husband a PhD student could hope for.

My supervisor, Prof Anna-Mart Engelbrecht, thank you so much for always believing in me. Thank you for the coutless opportunities to grow as a researcher, for always being willing to listen and give advice in tough times and for taking me in as one of your “children”. It has been an immense privilege to be your student.

My co-supervisor, Dr Ben Loos, thank you for your support and technical guidance. Thank you for always being willing to answer a quick question even in those very busy times.

To Bali, thank you for your leadership, your valuable input and for always being willing to help. Thank for always having an open door, even if it was just to chat.

To my friends and family, thank you for patiently waiting for me to finish my studies. Your continued support has meant a great deal to me.

To Gustav, thank for your help with the animal study, for all your inspiring ideas, and for the good conversations during those long hours in animal house.

To Ashwin, Lize, Rozanne and Megan, thank you for help throughout the project and always being willing to answer countless questions.

To the CRG and DSG research groups, thank you for all the fun times and making those long days and busy times more bearable.

To the staff of the Physiological Sciences department, thank you for guidance, support and for providing a friendly environment.

To my collaborators, Dr Jade Peres and Prof Sharon Prince, thank you for your contributions to this study and for teaching me molecular cloning.

Lastly, to the National Research Foundation (NRF) and the Maree Stander Bursary for financial support.

Table of contents

List of figures

List of tables

List of conference contributions and publications

International

- **Davis, T.**, Loos, B., Peres, J., Prince, S. and Engelbrecht, A-M. Investigating the function of the AHNAK protein in doxorubicin resistance. International Journal of Molecular Medicine *36*, S63. [Published abstract]

  Oral presentation at the 20th World Congress on Advances in Oncology & the 18th International Symposium on Molecular Medicine in Athens, Greece, October 2015

National

- **Davis, T.**, Loos, B., Peres, J., Prince, S. and Engelbrecht, A-M. Investigating the role of the AHNAK protein in breast cancer response to doxorubicin.

  Oral presentation at the 43rd annual Physiology Society of Southern Africa (PSSA) congress in Bloemfontein, South Africa, September 2015

- **Davis, T.**, Peres, J., Prince, S., Loos, B., and Engelbrecht, A-M. The human AHNAK protein has a novel role in the cellular response to doxorubicin. [Abstract to be published]

  Oral presentation at the 44th annual Physiology Society of Southern Africa (PSSA) congress in Cape Town, South Africa, August 2016. Awarded Wyndham prize for best student oral presentation.

Publications

The majority of the content in section 1.6 has been published as a review article entitled “AHNAK: The giant jack of all trades”. For the purpose of the literature review, the article text was modified only to include recently published literature that followed publication of the article.

- **Davis, T.**, Loos, B. and Engelbrecht, A-M. (2014). AHNAK: The giant jack of all trades. Cellular Signalling *26*, 2683-2693.

- Van Niekerk, G., **Davis, T.** and Engelbrecht, A-M. (2015). Was the evolutionary road towards adaptive immunity paved with endothelium? Biology Direct 10:47.

- Van Niekerk, G., **Davis, T.** and Engelbrecht, A-M. (2015). Bone marrow fat: What is it good for? Seminars in Arthritis and Rheumatism 45:5, p14

- Rautenbach, A., Goldswain, T., **Davis, T.**, Engelbrecht, A-M and Makunga, N. Pharmacological analysis and elucidation of the cytotoxicity of Dodonaea viscosa L. Jacq. in breast cancer cell lines and in a tumour-bearing mouse model. Phytomedicine. Currently being revised before resubmission, Ref. No.: PHYMED-D-15-00253

- Kruger, M., le Roux, H., **Davis, T.** and Engelbrecht, A-M. The effect of MKP-1 inhibition on the cytotoxicity of chemotherapeutic drugs in breast cancer. Article submitted.

Abbreviations

ABC	-	ATP-binding cassette
ANCOVA	-	Analysis of covariance
ANOVA	-	Analysis of variance
ATM	-	Ataxia-telangiectasia mutated
ATR	-	ATM and Rad-3-related
β-DG	-	Beta-dystroglycan
BBB	-	Blood-brain barrier
BM	-	Basement membrane
BSA	-	Bovine serum albumin
$CaCl_2$	-	Calcium chloride
Casp7	-	Caspase 7
Ca_v	-	L-type voltage-gated calcium
Cav3	-	Caveolin 3
CAZ	-	Components of active zone
cCasp7	-	Cleaved caspase 7
ccRCC	-	Clear cell renal cell carcinoma
cPARP	-	Cleaved PARP
CNS	-	Central nervous system
CO_2	-	Carbon dioxide
CRU	-	Central repeated unit
Cterm	-	C-terminal
CTLs	-	Cytotoxic CD8+ effector T cells
DMEM	-	Dulbecco's modified eagle medium
DNA	-	Deoxyribonucleic acid
DXR	-	Doxorubicin

DYSF	-	Dysferlin
EC	-	Endothelial cells
ECM	-	Extracellular matrix
EDTA	-	Ethylenediaminetetraacetic acid
EGF	-	Epidermal growth factor
EGFR	-	Epidermal growth factor receptor
EGTA	-	Triethylene glycol diamine tetraacetic acid
EMT	-	Epithelial-mesenchymal transition
ERK	-	Extracellular signal regulated kinase
FBS	-	Fetal bovine serum
FGF	-	Fibroblast growth factor
Fig.	-	Figure
FITC	-	Fluorescein isothiocyanate
HBSS	-	Hanks' balanced salt solution
HCl	-	Hydrogen chloride
HER2	-	Human epidermal growth factor receptor 2
HRP	-	Horseradish peroxidase
IAP	-	Inhibitor of apoptosis protein
ICC	-	Immunocytochemistry
IHC	-	Immunohistochemistry
IL-2	-	Interleukin 2
JNK	-	c-Jun N-terminal kinase
LB	-	Lysogeny broth
LGMD2A	-	Limb girdle muscular dystrophy 2A
LGMD2B	-	Limb girdle muscular dystrophy 2B
MAPK	-	Mitogen-activated protein kinase
MAPKK	-	Mitogen-activated protein kinase kinase

MD	-	Muscular dystrophy
MET	-	Mesenchymal-epithelial transition
MIF	-	Macrophage migration inhibitory factor
MK2	-	MAP kinase-activated protein kinase 2
MMC	-	Mitomycin C
Na_3VO_4	-	Sodium orthovanadate
NaCl	-	Sodium chloride
NaF	-	Sodium fluoride
NF-κB	-	Nuclear transcription factor-κB
NFAT	-	Nuclear factor of activated T cells
NK	-	Not known
OD	-	Optical density
P-gp	-	P-glycoprotein
p	-	p-value
pAkt	-	Phosphorylated Akt
PARP	-	Poly-ADP-ribose polymerase
PBS	-	Phosphate-buffered saline
pDNA	-	Plasmid DNA
PDZ	-	PSD-95/Discs-large/ZO-1
PI	-	Propidium iodide
PI3K	-	Phosphatidylinositol 3-kinase
pIRβ	-	Phospho-insulin receptor-β
PKA	-	Protein kinase A
PKB	-	Protein kinase B
PKCα	-	Protein kinase C alpha
PLCγ	-	Phospholipase C gamma
PMSF	-	Phenylmethylsulfonyl fluoride

PNS	-	Peripheral nervous system
PPARγ	-	Peroxisome proliferator-activated receptor-γ
PTEN	-	Phosphatase and tensin homologue deleted on chromosome 10
PVDF	-	Polyvinylidene fluoride
R-Smads	-	Regulatory Smad proteins
RACKs	-	Receptors for activated C kinase
RIPA	-	Radioimmunoprecipitation assay
RNA	-	Ribonucleic acid
ROS	-	Reactive oxygen species
RT	-	Room temperature
RTK	-	Receptor tyrosine kinase
SDS	-	Sodium dodecyl sulphate
SEM	-	Standard error of the mean
shRNA	-	short hairpin-RNA
SLE	-	Systemic lupus erythematosus
STAT3	-	Signal transducer and activator of transcription 3
TBS-T	-	Tris-buffered saline-tween
TCR	-	T cell antigen receptor
tGFP	-	turbo green fluorescent protein
TGF-β	-	Transforming growth factor-β
TNF	-	Tumour necrosis factor
TOP2	-	Topoisomerase II
TRAIL	-	TNF-related apoptosis-inducing ligand
UV	-	Ultraviolet light
VEGF	-	Vascular endothelial growth factor
vs.	-	versus
WB	-	Western blot

ZEB	-	Zinc-finger E-box-binding
ZO-1	-	Zonula occludens 1

Units and symbols

A	-	amps
aa	-	amino acids
bp	-	basepairs
hrs	-	hours
kb	-	kilobases
kDa	-	kilodalton
l	-	litre
min	-	minute
mg	-	milligram
ml	-	millilitre
mm^3	-	cubic millimetre
mM	-	millimolar
ng	-	nanogram
nm	-	nanometre
rpm	-	rotations per minute
U	-	unit
V	-	volt
°C	-	degrees Celsius
®	-	registered
™	-	trademark
µg	-	microgram
µM	-	micromolar
µl	-	microliter

Chapter 1 : Literature Review

1.1 Cancer

Cancer is arguably the most well-known, and perhaps feared, disease known to mankind. The first descriptions originate in ancient Egypt where mummies displayed fossilised bone tumours (American Cancer Soceity, 2014). The Edwin Smith Papyrus, part of an ancient Egyptian textbook dating back to 3000 BC, describes cases of breast cancer and notes that “there is no treatment”. Only 2000 years later, in 370-460 BC, the disease is named: first as *carcinos* and *carcinoma* by Hippocrates and then in 28-50 BC as *cancer* by the Roman physician Celsus. The first surgeries aimed at treating cancer were performed in the 16th-18th centuries while the field of cancer epidemiology started in the 18th century (American Cancer Society, 2014).

Today, cancer represents a significant burden on society. In 2012, 14.1 million new cases were diagnosed while 8.2 million people succumbed to the disease (Ferlay et al., 2013). These numbers represent an 11% and 7.9% increase, respectively, when compared to 2008. Furthermore, cancer also accounts for the second highest number of noncommunicable disease-related deaths world-wide in 2012 (World Health Organization, 2014). Statistics for under-developed countries are even less favourable, representing 57% of all new cases and 65% of all deaths in 2012 (Ferlay et al., 2013). Statistics for South Africa are however limited since recorded cancer data is only available up to 2009. The Globocan initiative reports projected rates of 77 400 new cases and 47 400 deaths for South Africa in 2012. Perhaps more alarming is that when age-standardised rates of incidence and mortality are compared between countries, South Africa falls below first-world countries such as the United States of America and the United Kingdom in terms of incidence, but ranks above these countries in terms of mortality. Globally, the most frequently diagnosed cancer among men are lung cancer, with prostate in a close second. However, cancer mortality among men is most commonly as a result of lung cancer, followed by liver, stomach, colorectum and prostate cancers. In women, breast cancer is most frequently diagnosed, followed by colorectum, lung and cervix uteri cancers, while mortality is due to breast followed by lung, colorectum, cervix uteri and stomach cancers (Ferlay et al., 2013). A different picture can be seen in South Africa. South African men are most frequently diagnosed with prostate cancer followed by lung, colorectum and oesophageal cancers while mortality is mostly due to lung, followed by prostate, oesophageal, and colorectum cancers. South African women are most frequently diagnosed with breast followed by cervix uteri, lung and colorectum cancers and mortality is mostly due to cervix uteri followed by breast, lung and colorectum cancers (Ferlay et al., 2013).

1.2 Treatment

Cancer treatment started, historically, with radical surgeries, even before the age of anaesthesia or specialised surgical techniques (American Cancer Society, 2014). Significant progress was made throughout the 18th-20th centuries that refined surgical techniques and lead to improved outcomes while pioneering research aimed at understanding the disease paved the way to the possibility of novel treatment options. Soon after the discovery of X-rays in 1895, the advantages of radiation therapy in the treatment of cancer was realised and the first report of a positive outcome came only one year later (Connell and Hellman, 2009). The idea of treating cancer with drugs started in the late 1930's and early 1940's when the positive effect of hormonal therapy and nitrogen mustard, respectively, on cancer was observed (Huggins and Hodges, 1941; Gilman, 1963; Chabner and Roberts, 2005; DeVita and Chu, 2008). The revolution of chemotherapy and the success that came with it lead the way in cancer treatment for many decades, and in some ways, still are. With increased understanding of cellular biology in the late 20th century, and the changes present in cancer, came the era of targeted therapy which focusses on specific molecules altered in cancer, or even in a specific type of cancer (Chabner & Roberts, 2005).

Treatment today draws benefit from all the different kinds of therapy. It has long been known that a combination of drugs and therapies yield improved response rates and increased survival while limiting the possibility of toxic side-effects or acquired resistance (Al-Lazikani et al., 2012; Devita et al., 1975). Radiation is often administered before or after surgery while drugs, chemotherapeutic or targeted, can be administered in a neoadjuvant (beforehand) or adjuvant (together with) setting with the radiation-surgery regime. The choice of treatment regime made by the physician is influenced by three main aspects: (1) the type of cancer, (2) the extent or stage of cancer and (3) the age and presence of comorbidities of the patient.

(1) Location and subtype of cancer

Different types of anti-cancer drugs have shown superior efficacy against certain cancer types. This is especially true for targeted therapies where specific targets have shown prevalence in certain cancers. For instance, platinum-based chemotherapeutic drugs, such as cisplatin and carboplatin, are routinely used to treat lung cancers, while those that harbour mutations in the epidermal growth factor receptor gene (EGFR) are also treated with tyrosine kinase inhibitors such as erlotinib (Lemjabbar-Alaoui et al., 2015). In breast cancer, patients with tumours positive for the overexpression/amplification of the human EGFR 2 (HER2) gene are treated with HER2-targeting agents such as trastuzumab while patients with hormone responsive tumours are treated with endocrine therapy. Those lacking any specific target receive chemotherapy, often in the form of anthracyclines or taxanes (Goldhirsch et al., 2013).

(2) Extent or stage of cancer

With diagnosis of early stage cancer surgical excision is often preferred as a first-line treatment, provided the tumour is considered resectable. This is normally coupled with either radiation or drug therapy to improve the outcome, as is the case in both lung and breast cancer (Lemjabbar-Alaoui et al., 2015; Senkus et al., 2013). Treatment of advanced cancer is more complicated and consists normally of some form of systemic therapy. Often, treatment is aimed only at controlling the disease; such as in lung cancer where prophylactic brain radiation is given due to the high frequency of metastatic spread to this area, or as in metastatic breast cancer, which is largely considered as incurable (Cardoso et al., 2012; Lemjabbar-Alaoui et al., 2015).

(3) Age and comorbidities

The range of available treatment options can be limited by the presence of comorbidities and the general health of a patient, of which both are major complicating factors in elderly patients. The key factor is a good performance status: a scale ranging from zero (good health and active) to five (dead) that was designed by the Eastern Cooperative Oncology Group to describe the progression of the disease and its impact on the patient's general health (Oken et al., 1982). Another complicating factor is that elderly patients are normally excluded from clinical trials resulting in very limited information regarding safe and optimal treatment of the disease. Chemotherapy in elderly patients may be avoided or limited to single-agent therapy due to increased presence of toxic side-effects, although it has been suggested that elderly breast cancer patients can receive the same treatments as their younger counterparts provided they have a good performance status (Gridelli et al., 2003; Rosenkranz et al., 2006).

1.3 Doxorubicin

Doxorubicin (DXR, tradename Adriamycin) is one of the most valuable chemotherapeutic drugs developed to date. Together with daunorubicin and epirubicin, it belongs to the family of anthracycline antibiotics isolated from the actinobacterium *Streptomyces peucetius* 46 years ago (Arcamone et al., 2000; Cortés-Funes and Coronado, 2007). DXR has a complex structure which consists of an aromatic ring system containing a quinone bound to an aminoglycoside (fig. 1.1) (Cortés-Funes and Coronado, 2007; Cutts et al., 2005). Only minor differences are observed in the structure of DXR versus daunorubicin (presence of a C-14 hydroxyl group) and epirubicin (orientation of the sugar C-4 hydroxyl group) and yet DXR is more effective and has a broader spectrum of activity that the latter versions (Cortés-Funes and Coronado, 2007). DXR is used to treat many solid tumours, including lung, breast, ovarian, gastric, liver, Hodgkin's and non-Hodgkin's lymphoma, sarcoma's, multiple myeloma's and pediatric cancers, while daunorubicin is primarily used to treat

acute myeloid leukemia and epirubicin to treat gastric and breast cancer (Cortés-Funes and Coronado, 2007; Gewirtz, 1999; Thorn et al., 2011).

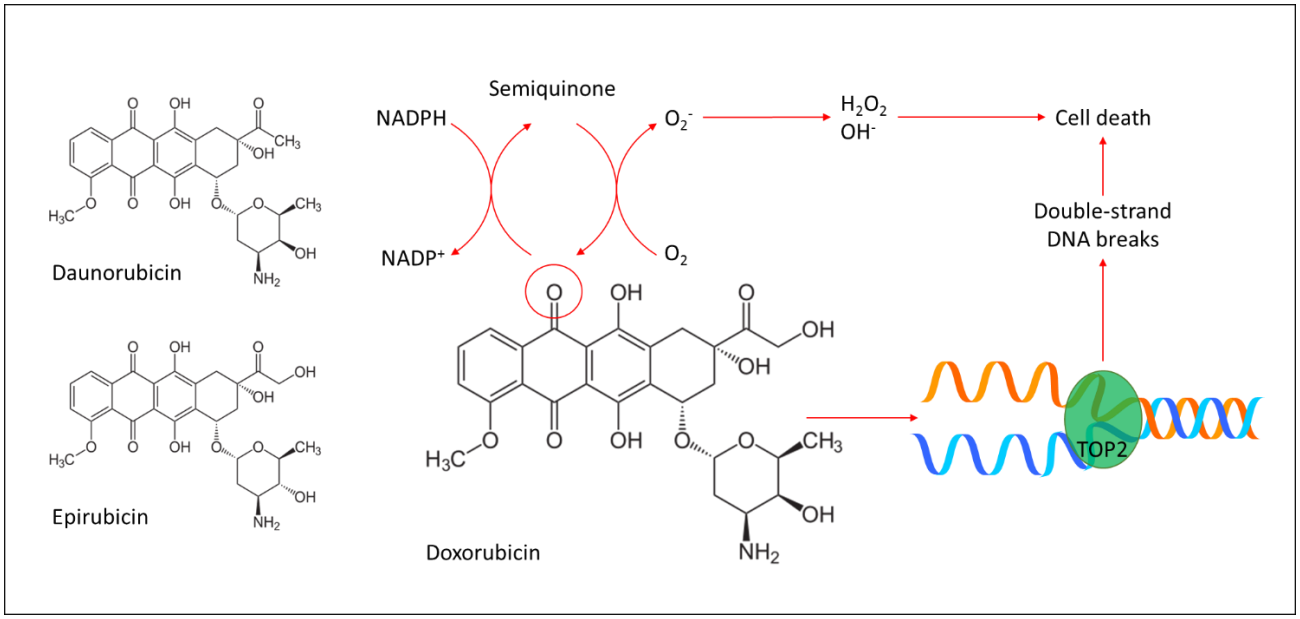

Figure 1.1: Chemical structure of the anthracyclines daunorubicin, epirubicin and DXR, and DXR main mechanisms of action. TOP2 – topoisomerase II.

Unfortunately, the full potential of DXR can not be exploited in a clinical setting due to the presence of serious side-effects. This can include gastrointestinal problems, acute vomiting, alopecia, hematopoietic suppression, liver damage, nephropathy and even, indirectly, cognitive impairment (Octavia et al., 2012; Tacar et al., 2013). Of most concern however is the development of cardiotoxicity, which develops in a cumulative dose-dependent manner and presents as dilated cardiomyopathy, cardiac dysfunction and even subsequent heart failure and death (Zhang et al., 2009).

1.3.1 Molecular mechanisms of action

Several mechanisms of action have been proposed for the cytotoxicity imposed by DXR and are mostly closely associated with its structure. Once DXR enters a cell through passive diffusion, it accumulates significantly within the cytoplasm, but even more so in the nucleus where it has high affinity for DNA (Tacar et al., 2013). Here DXR has the ability to bind and inhibit the DNA-repair enzyme topoisomerase II (TOP2) (Cortés-Funes and Coronado, 2007; Gewirtz, 1999; Tacar et al., 2013). This represents one of the primary mechanisms for DXR-induced cell death. TOP2 is responsible for the unwinding and separation of the DNA strands and is thus essential for processes such as DNA replication and transcription (Palchaudhuri and Hergenrother, 2007; Tacar et al., 2013). By binding the enzyme DXR stabilises the TOP2-DNA complex after the enzyme has made a double-strand cleavage, effectively preventing the enzyme from completing its function and increasing the

presence of DNA strand breaks leading to cell death via apoptosis (fig 1.1) (Gewirtz, 1999; Nitiss, 2009). DXR can also intercalate DNA on its own by forming non-covalent bonds with base pairs which results in the inhibition of DNA and RNA polymerases and subsequently DNA replication and transcription (Cummings et al., 1991; Gewirtz, 1999; Tacar et al., 2013). In addition, a cytotoxic response can also be elicited by the formation of DXR-DNA adducts (Cutts et al., 2005; Swift et al., 2006).

Another major mechanism of cytotoxicity for DXR is the generation of reactive oxygen species (ROS). The quinone ring structure of DXR can undergo redox cycling with the formation of a semiquinone free radical through NADPH dependent reduction (fig. 1.1) (Cummings et al., 1991). The free radical can either be rapidly transferred to oxygen molecules, forming superoxide radicals and restoring DXR to its original state, or the semiquinone radical can continue to damage DNA by itself (Cummings et al., 1991; Gewirtz, 1999). Alternatively, through a series of events the superoxide radical can generate hydrogen peroxide and hydroxyl radicals which also have the potential to cause DNA damage and lipid peroxidation (Cummings et al., 1991). In addition, the formation of oxygen radicals are also possible through the association of DXR with iron (Gewirtz, 1999).

Generation of ROS is suggested to be the major cause of cardiotoxicity associated with DXR treatment (Berthiaume and Wallace, 2007; Kalyanaraman et al., 2002). It is expected that ROS would have the most significant effect at or near the site of its generation, which is most likely the mitochondria in cardiomyocytes (Berthiaume and Wallace, 2007). It has been reported that DXR accumulates in both the nucleus and mitochondria in the heart, and, compared to other tissues, the heart also has a significantly higher load of mitochondria due to its high-energy demand. Furthermore, the inner mitochondrial membrane also contains a significant amount of cardiolipins for which DXR has a high affinity (Berthiaume and Wallace, 2007). Cardiomyocytes may also be more susceptible to damage induced by DXR due to inherently lower levels of superoxide dismutase, catalase, and glutathione peroxidase, leaving the cells vulnerable to the effects of superoxide and hydrogen peroxide (Kalyanaraman et al., 2002; Liu and Tan, 2003; Marklund et al., 1982). These findings support the notion that mitochondria represent the major site of damage in the heart. In addition to the reactions leading to the generation of ROS described above, ROS can also potentially be generated through reduction of DXR by complex one of the electron transport chain, which is also located in the inner mitochondrial membrane (Berthiaume and Wallace, 2007).

The mechanisms underlying DXR's cytotoxicity have been studied extensively, both *in vitro* and *in vivo*, and the apoptosis-inducing mechanisms described above are well supported and accepted. Whether the trigger for a tumour cell to die is protein-associated DNA damage or ROS-associated DNA damage remains unclear though.

Findings from early studies suggested that lower concentrations of DXR mainly trigger apoptosis through protein-associated DNA damage, while higher concentrations lead to oxidative stress (Di et

al., 2009; Gewirtz, 1999). It was found in one study that apoptosis was maximally induced in lymphoblastic leukaemia cells at a concentration of 1 μM while only a high concentration treatment of 100 μM DXR for 12 hrs showed oxidative damage (Müller et al., 1997). Another study reported significant hydroxyl radical formation in both intact and fractionated MCF-7 breast cancer cells after exposure to 200 μM DXR where resistance was conferred by increased expression of glutathione peroxidase (Sinha et al., 1989).

Even though insight into the mechanism of DXR within a cell is provided by studies where high concentrations were used, it remains uncertain whether it has any relevance with regards to a clinical setting. There are however also several studies that report on the generation of ROS with low concentrations of DXR. One study reported increased ROS production in colon adenocarcinoma cells after treatment with 0.18 μM for 14-48 hrs while another detected significant ROS levels in osteosarcoma cells after a 24 hr treatment with 0.4 μM DXR (Tsang et al., 2003; Ubezio and Civoli, 1994). Friesen *et al.* found that antioxidants such as reduced glutathione, N-acetylcysteine and superoxide dismutase protected leukaemia cells from apoptosis induced by 0.18-1.84 μM DXR after 30 hrs (Friesen et al., 1999).

The concentration of DXR used for treatment may very well be an important factor that determines the specific molecular trigger for apoptosis induction and/or cell death, however it is also likely that other aspects, such as exposure time and cell type/genetic background, are also involved. Rogalska *et al.* detected a significant rise in ROS levels in ovarian cancer cells after DXR treatment with 0.27 μM for 2-24 hrs but not after 48 hrs (Rogalska et al., 2011). In another study, significant and rapid ROS production after 20-30 min exposure to 18.4 μM DXR was reported while DXR-induced cell death, observed after 48 hrs, was associated rather with reduced mitochondrial respiratory activity and cytosolic ATP levels; however, it is unclear whether the initial short term events had any effect or perhaps lead to the long term effects (Kuznetsov et al., 2011). In a study by Di *et al.* the antioxidants glutathione and N-acetylcysteine protected wild-type MCF-7 breast cancer cells from death induced by 1 μM DXR treatment for 2 hrs, however it failed to have any statistically significant effect on p53-null MCF-7 cells (Di et al., 2009).

With regards to non-cancerous cells, specifically cell types implicated in DXR-induced cardiotoxicity, there is overwhelming evidence that death is oxidant induced and it was also suggested that the mechanisms involved in cell death between these cells and cancer cells are indeed different (Mukhopadhyay et al., 2009; Octavia et al., 2012). Using a fairly low concentration of DXR (0.5 μM), Wang *et al*. showed that the apoptotic death of bovine aortic endothelial cells and adult rat cardiomyocytes, where associated with an early production of ROS, could be prevented by antioxidants and were independent of p53. In contrast, human ovarian teratocarcinoma (PA-1) and human breast cancer (MCF-7) cells failed to show any ROS (after 4 hrs) although a dependency on p53 was detected (Wang et al., 2004). In another study, the production of ROS in normal cells (rat cardiomyocytes, H9C2) were also reported, although it was only detected after a 16 hr treatment

with 0.9 μM DXR but in conjunction with other apoptotic markers (Kluza et al., 2004). In this study however, an early increase in ROS was detected in rat mammary adenocarcinoma cells (MTLn3) even before apoptotic markers were observed. The authors also made a surprising discovery of increased mitochondrial mass upon DXR treatment that was restricted to the cancer cells, although the reason behind this remains unclear (Kluza et al., 2004).

Evidence strongly supports ROS as the major mechanism of cell death in cardiotoxicity while the mechanism(s) in tumour cells remains controversial. The possibility of distinct mechanisms between these cell types harbour a crucial advantage – therapeutic strategies can be developed that could alleviate the associated cardiotoxicity without affecting the effectiveness of DXR. In addition, this could possibly relieve dose limitations, allowing the use of higher concentrations that would ensure killing of all tumour cells which would prevent recurring tumours, especially DXR-resistant tumours. However, this would require a more complete understanding of the mechanisms involved in DXR-induced death of tumour cells.

1.3.2 DXR delivery innovations

DXR is administered through arterial injection or infusion and like many other chemotherapeutic drugs its primary target is rapidly-dividing tumour cells. However, unwanted targeting of normal cells also occurs, as evident by the associated toxic side-effects. Since its introduction into clinical use, various modifications pertaining to the drug delivery system have been investigated that could help improve its effectiveness and decrease its impact on normal cells. By coupling DXR to nanoparticles or cell-penetrating peptides, increased cytotoxic effects have been shown in various tumour cells and *in vivo*, often at lower concentrations compared to unconjugated DXR (Aroui et al., 2009a, 2010; Barraud et al., 2005). An advantage of conjugating DXR to some form of a carrier system is that it can aid in avoiding recognition by drug-export proteins commonly found in resistant cells, resulting in increased drug retention. Furthermore, in an *in vivo* setting, increased accumulation in the tumour tissue is also readily achieved since the carrier system can easily enter the tissue through the defective and leaky vasculature of the tumour (Aroui et al., 2010; Tacar et al., 2013).

By taking tumour-specific properties into account, such as environmental pH, additional modifications can be made to carrier systems that can also contribute to improved outcomes. Lee *et al.* reported that increased cellular toxicity in DXR-resistant MCF-7 cells and tumour growth suppression in mouse xenografts were aided by pH-triggered release of DXR from polymeric micelles, while Du *et al.* produced a dual pH-sensitive DXR-coupled nanoparticle that facilitated both enhanced cellular uptake and triggered intracellular drug release, thus increasing the effectiveness of the drug in a breast cancer stem cell line (Du et al., 2011; Lee et al., 2005).

Other modifications involve coupling additional molecules that are commonly overexpressed in tumours to facilitate targeting of DXR specifically to the tumour, avoiding accumulation in unwanted organs and thus the associated dangerous side-effects. Studies reporting on the coupling of DXR to

anti-CD19-labelled liposomes, transferrin-labelled liposomes or HER2-targeting nanoparticles all reported improved effectiveness *in vivo* when comparing tumour growth suppression and survival times with those of non-targeting controls (Agadjanian et al., 2012; Cheng and Allen, 2008; Li et al., 2009b). Most importantly though, the studies also reported significantly higher accumulation of DXR in tumour tissue compared to other tissues, with particularly low levels in the heart. These results emphasise the usefulness of targeting DXR carrier systems in limiting or even preventing DXR-induced cardiotoxicity.

Since individual tumours can display significant heterogeneity, Lowery *et al.* chose a different strategy to achieve tumour-specific targeting of DXR (Lowery et al., 2011). A peptide capable of recognising only irradiated tumour cells was produced and used to label a DXR-coupled liposome. Not only did the carrier system display enhanced effectiveness at killing irradiated tumour cells *in vitro* and suppressing tumour growth *in vivo*, it facilitated significant accumulation only in irradiated tumours and not in other organs or even irradiated normal tissues. This technique shows great promise as it can be applied across multiple cancer types and can facilitate DXR targeting to the entire tumour volume, circumventing any potential problems associated with molecular heterogeneity of tumours where residual cells can remain post-treatment and ultimately result in tumour recurrence.

Many studies describing the use of various carrier systems to enhance drug effectiveness while limiting off-target toxicity took advantage of one of DXR's inherent properties in order to determine these responses, namely autofluorescence. In particular, Hwang *et al.* (following up with HER2-DXR nanoparticle study mentioned above) made use of this ability and in conjunction with some of the latest imaging techniques was able to quantitatively determine nanoparticle efficacy and monitor targeting capacity at macro and micro scales as well as the therapeutic efficacy trajectory (Hwang et al., 2012). As new frontiers are reached in imaging techniques the ability to monitor drug action, distribution and pharmacokinetics will greatly improve, and this will hold significant benefits for the continued development of therapeutics, particularly for DXR.

1.3.3 Pro-tumour effects

DXR has become widely known for its superiority in anti-tumour actions. However, no drug is perfect and often certain conditions are required to ensure proper functioning. Apart from its toxic side-effects, several studies have found that DXR can even have pro-tumour activities under sub-optimal conditions (Han et al., 2013). Treatment of various types of cancer cells with low concentrations of DXR and/or transient exposure have shown that DXR is capable of promoting tumour progression and malignancy and in some occasions, resistance too. This is mainly achieved through the induction of epithelial-mesenchymal transition (EMT), albeit through different mechanisms. EMT is an important regulatory process transforming epithelial cells to a more mesenchymal-like phenotype that is commonly associated with acquiring of metastatic abilities and will be discussed in the following section. A transient exposure of SiHa cervical cancer cells to a low dose of 0.1 μM DXR

was shown to induce temporary resistance to both DXR and cisplatin, another DNA damaging drug (Yeh et al., 2003). The resistance was found to be associated with increased nuclear transcription factor-κB (NF-κB) activity. Further evidence for a role in DXR-induced activation of NF-κB was reported in another study where DXR was shown to provoke a series of events that led to EMT induction (Li et al. 2011). NF-κB was found to play a central role in a positive feedback loop for this pathway, further amplifying the effects of the DXR. However, in this study the concentration of DXR used was quite high (46 μM), and whether this can be reached in an *in vivo* or clinical setting seems highly unlikely. DXR was also shown to induce EMT in BGC-823 gastric cancer cells following a dose of 0.74 μM for 24 hrs (Han et al., 2013). Here, it was shown that the EMT was mediated by β-catenin, a protein that regulates the expression of EMT transcription factors. In several liver cancer cell lines, with an epithelial phenotype, DXR was shown to induce EMT by activating signal transducer and activator of transcription 3 (STAT3) (Hu et al., 2012). Knockdown of STAT3 reversed the DXR-induced changes, but was unable to reverse the EMT in a mesenchymal-like liver cancer cell line, suggesting that the STAT3-mediated EMT might be restricted to DXR-induction. Another signalling molecule implicated in DXR-induced EMT is transforming growth factor-β (TGF-β). It was reported in two separate studies that a low dose of DXR, 0.05 μM and 0.025 μM in HCT116 colon cancer cells and 4T1 murine breast cancer cells respectively, induced EMT by activating the TGF-β/Smad pathway (Bandyopadhyay et al., 2010; Li et al., 2015). An increase in DXR resistance was also reported in both studies. A third study reported similar findings in BT-20 breast cancer cells following treatment with 0.31 μM DXR (Chen et al., 2013). DXR increased TGF-β expression and activity resulting in the activation of EMT. Here, an increase in β-catenin was also reported. DXR can thus have multiple influences driving tumour progression and malignancy, yet the molecular crosstalk remains unclear. These studies highlight not only the importance of ensuring optimal conditions for DXR treatment but also of a complete understanding of its effects as both has significant implications for cancer treatment.

1.3.4 DXR resistance

Resistance to chemotherapeutic drugs are often a limiting factor in the treatment of cancer and can have severe consequences in terms of patient prognosis and survival. Resistance to DXR has been observed frequently and can be acquired or intrinsic of nature. The molecular mechanisms implicated in acquired resistance are typically investigated *in vitro* by exposing sensitive cancer cells to increasing concentrations of DXR over an extended period of culture where after comparisons are drawn between the newly resistant cell line and the parental cell line. Intrinsic mechanisms of resistance are often investigated by comparing cell lines that are naturally sensitive and resistant to the drug.

A variety of mechanisms can transform a sensitive cancer cell into a resistant cell (Gottesman, 2002). Increased drug efflux via the energy-dependent ATP-binding cassette (ABC) transporters are not only the best characterised mechanism but often represents the main cause of resistance in several

cancers, such as leukaemias, breast and lung cancers and sarcomas (Gottesman et al., 2002; Szakács et al., 2006). P-glycoprotein (P-gp), a member of the ABC family, recognises hydrophobic drugs and can provide significant resistance to several drugs such as vinblastine, etoposide, imatinib, methotrexate and DXR (Szakács et al., 2006).

Strong correlations between increased P-gp expression and DXR resistance have been shown *in vitro* and in clinical tumour samples where even moderate increases in P-gp expression can effectively induce resistance (Mechetner et al., 1998; Pajic et al., 2009). Acquired DXR resistance mediated by increased P-gp expression has been suggested to be the result of hypomethylation of the promoter area of the P-gp gene (Chekhun et al., 2006). While a methylated promoter area is more constricted in chromatin and deacetylated histones, a low level of, or absent, methylation of the promoter allows for a more open conformation, facilitating increased expression of the gene.

Another mechanism commonly observed in DXR resistance involves a defective phosphatase and tensin homologue deleted on chromosome 10 (PTEN) protein and the subsequent activation of the phosphatidylinositol 3-kinase (PI3K)/Akt (also known as protein kinase B, PKB) pathway. PTEN functions as a negative regulator of PI3K, preventing the phosphorylation and activation of Akt and its anti-apoptotic and cell growth and survival functions (Tanaka and Grossman, 2003). Introduction of a functional PTEN into prostate cancer cells with defective PTEN resulted in decreased levels of pAkt and increased sensitivity to DXR, while *in vivo* it resulted in significant growth suppression of established tumours from DXR-resistant bladder cancer cells (Grünwald et al., 2002; Tanaka and Grossman, 2003). Defective PTEN regulation is often a result of inactivating mutations; mutations preventing its lipid and protein phosphatase abilities are capable of inducing DXR resistance, and can thus represent an important mechanism of intrinsic resistance (Steelman et al., 2008).

1.4 Metastasis

With approximately 90% of all cancer-related deaths resulting from the metastatic spread of primary tumours, metastasis is arguably the most clinically relevant field of cancer research (Christofori, 2006; Monteiro and Fodde, 2010; Spano et al., 2012). With this in mind, research has experienced a horizontal expansion; without neglecting the importance of understanding tumourigenesis and its prevention, massive effort has been placed on understanding tumour progression and dissemination.

Metastasis is defined as the spread of a primary tumour to distant sites in the body and involves a series of sequential steps (fig. 1.2). This involves the loss of adhesion and dissociation from the primary tumour, invasion of the local environment, intravasation into either, or both, the lymphatic and vasculature system, survival in these systems, extravasation at a distant secondary site and the

colonisation and growth of a secondary tumour at this site (Coghlin and Murray, 2010; Duffy et al., 2008; Steeg, 2006; Valastyan and Weinberg, 2011).

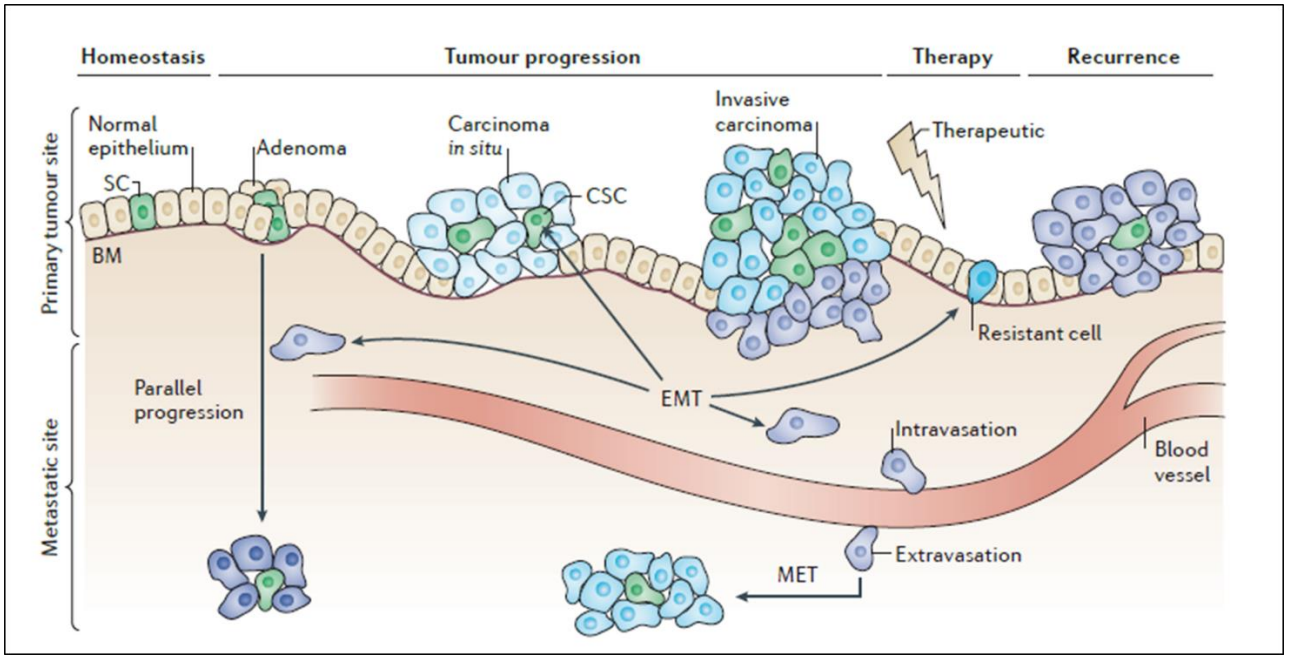

Figure 1.2: The metastatic process showing both early and late dissemination models and the role of EMT in these processes. CSC – cancer stem cell; EMT – epithelial-mesenchymal transition; MET – mesenchymal-epithelial transition; SC – stem cell. (De Craene and Berx, 2013).

Traditionally, the metastatic phenotype was seen as the end-product of a series of culminating genetic aberrations and mutations during tumour progression (Coghlin and Murray, 2010; Duffy et al., 2008; Klein, 2008). This follows a model of somatic evolution where a small population of cells described as the “fittest of the fit” would only disseminate late, after the formation of a large primary tumour. However, increasing evidence are supporting a second model, originally hypothesised more than 10 years ago (Bernards and Weinberg, 2002). In this model, the mutant alleles predisposing a cell to metastasise are acquired early in tumourigenesis, along with the other mutations driving tumourigenesis in the first place. The tumour cells can disseminate early from the primary tumour and would diverge genetically and obtain full malignancy at a distant site (fig 1.2) (Coghlin and Murray, 2010; Duffy et al., 2008; Klein, 2008, 2009). The actual contributions of these models to metastatic cancer in a clinical setting is however still uncertain as there are both supporting evidence and unanswered questions for each of the models.

Through whichever model, it is clear that the acquisition of the metastatic phenotype involves a complex and intricate collection of molecular signalling pathways that facilitate the changes necessary for cell migration and invasion (Spano et al., 2012). One process that has been associated with these changes is EMT (fig. 1.2).

1.5 EMT

EMT represents a biological reprogramming process where apical-basal polarised, stationary epithelial cells undergo significant transcriptomic changes to facilitate transition into a front-rear polarised, motile mesenchymal-like cell (Kalluri and Weinberg, 2009; Zeisberg and Neilson, 2009). The process provides a certain extent of phenotypic plasticity since the reverse, mesenchymal-epithelial transition (MET), is also possible. EMT is employed in both physiological and pathophysiological settings in order to achieve distinct functional outcomes and has been classified into three types (Kalluri and Weinberg, 2009; Micalizzi et al., 2010; Zeisberg and Neilson, 2009). Type I EMT takes place during developmental processes such as implantation, embryogenesis and organ development. This type of EMT is transient and physiological and facilitates the spatial and temporal remodelling and diversification of tissue to ensure proper morphogenesis. Type II EMT takes place during repair-associated activities such as tissue regeneration, wound healing and organ fibrosis. It is driven and dependent on injury and inflammation and can be both physiological and pathophysiological. Lastly, type III EMT takes place in tumour cells and is associated with the invasive and metastatic properties of a malignant tumour. Partial EMT is also often observed in tumours, where epithelial and mesenchymal markers can be shed and gained, respectively, to different extents (Christofori, 2006; Kalluri and Weinberg, 2009; Lamouille et al., 2014; Micalizzi et al., 2010; Zeisberg and Neilson, 2009).

Multiple changes and adaptations take place during EMT that ultimately enable the transition and are often grouped into three major events, namely genetic reprogramming, dissolution of cellular adhesions and junctions and reorganisation of the cytoskeleton. The EMT process starts with the genetic reprogramming which entails significant changes on the transcriptomic level that mediate the phenotypic changes. Basically, the expression of genes regulating epithelial characteristics are downregulated while those that regulate mesenchymal characteristics are upregulated (table 1.1) (Lamouille et al., 2014). Several transcription factors have been shown to facilitate these changes, including Snail, TWIST and zinc-finger E-box-binding (ZEB) transcription factors (De Craene and Berx, 2013; Lamouille et al., 2014). These transcription factors can mediate both the suppression and activation of genes and may even converge on the same genes or drive each other's expression (Peinado et al., 2007).

Snail1 (also known to as Snail or SNAI1) and Snail2 (also known to as Slug or SNAI2) belong to the Snail family of zinc-finger transcription factors (Lamouille et al., 2014; Peinado et al., 2007). These transcription factors suppress gene activity through binding of E-box sequences within the promoter regions. Multiple signalling pathways can activate Snail and Slug, including TGF-β/Smad-3, PI3K/Akt, NF-κB, WNT/β-catenin and growth factors that function through receptor tyrosine kinases

(RTKs) such as epidermal growth factor (EGF) and fibroblast growth factor (FGF). Increased expression of these transcription factors have been found in various cancers, such as breast, lung, colon, ovarian and melanoma, and have been correlated with metastasis, invasion and poor survival. TWIST1 (or TWIST) forms part of the large basic helix-loop-helix family. Several other members of the family, such as TWIST2, E12 and E47, have also been implicated in EMT although TWIST is the best characterised with the most support for a role in cancer. TWIST also recognises E-box sequences in promoter regions and subsequently recruits additional proteins to facilitate gene suppression or activation. TWIST can be activated by the mitogen-activated protein kinase (MAPK), TGF-β, WNT and vascular endothelial growth factor (VEGF) pathways. Increased expression has been found in breast, gastric, liver and prostate cancers and has also shown to correlate with metastasis, invasion and poor survival. The ZEB transcription factor family are also zinc-finger transcription factors and comprises of ZEB1 (also known as δEF1) and ZEB2 (also known as SIP1). Like Snail and TWIST, ZEB transcription factors also binds E-box promoter sequences, resulting in either gene suppression or activation, although Snail and TWIST can also facilitate the activation of ZEB transcription factors. In addition, the TGF-β, NF-κB, WNT/β-catenin and MAPK pathways can also activate the ZEB transcription factors. Increased expression of these transcription factors has been found in ovarian, gastric, pancreatic and colon cancers and has been shown to correlate with histological type and poor survival (Lamouille et al., 2014; Peinado et al., 2007).

The dissolution of cellular adhesions and junctions are primarily achieved through the downregulation of epithelial characteristics. The most important epithelial marker that is suppressed is arguably E-cadherin. E-cadherin, a member of the cadherin family, is a single-span transmembrane glycoprotein that binds and interacts with other E-cadherin proteins in neighbouring cells (Beavon, 2000; Yilmaz and Christofori, 2009). Through this homophyllic interaction E-cadherin physically connects neighbouring cells and mediates intercellular adhesion, forming what is referred to as adherens junctions. On the inside of the cell, the cadherin-catenin complex is formed which further stabilises the external bonds. E-cadherin binds β-catenin or γ-catenin, followed by the recruitment of α-catenin and the p120 protein. This complex also links E-cadherin, and the junction, to the cytoskeleton through interaction with actin (Beavon, 2000; Yilmaz and Christofori, 2009). During EMT activation, E-cadherin expression can be suppressed by Snail, Slug, ZEB1, ZEB2 and TWIST, highlighting its central role in the loss of epithelial characteristics (Bolós et al., 2003; Cano et al., 2000; Comijn et al., 2001; Eger et al., 2005; Yang et al., 2004). Loss of E-cadherin results in the physical disruption of adherens junctions and detachment from the epithelial layer. In addition, the cadherin-catenin complex is also disrupted and β-catenin, under the influence of the WNT signalling pathway, is then free to accumulate in the nucleus where it functions as a transcription factor controlling the expression of other pro-migratory and pro-invasive genes (Beavon, 2000; Christofori, 2006; Yilmaz and Christofori, 2009). Similar to the increased expression of the various transcription factors that can suppress E-cadherin, a loss of E-cadherin has been shown to correlate with metastasis, invasion and poor prognosis (Chen et al., 2003; Hunt et al., 1997; Tamura et al.,

1996). Also associated with the loss of E-cadherin expression is the gain of N-cadherin expression (Gravdal et al., 2007; Micalizzi et al., 2010; Yilmaz and Christofori, 2009). N-cadherin, also a classical member of the cadherin protein family, provides weaker and more transient adhesive properties and serves as a marker for mesenchymal-like cells. Its increased expression has been shown to be facilitated by TGF-β, ZEB2 and TWIST (Alexander et al., 2006; Araki et al., 2011; Vandewalle et al., 2005). This swop in cadherin expression is often referred to as the "cadherin-switch" and has been shown to be associated with tumour progression, metastasis and clinical recurrence (Bussemakers and Schalken, 2000; Gravdal et al., 2007; Yilmaz and Christofori, 2009). Several other proteins are also downregulated during the loss of epithelial characteristics, including claudin and occludin, which facilitates the disruption of tight junctions, and connexin, which facilitates the disruption of gap junctions (Ikenouchi et al., 2003; Lamouille et al., 2014; Vandewalle et al., 2005). Integrins are transmembrane proteins that link the extracellular matrix with the intracellular cytoskeleton and thus also functions in cell adhesion (Christofori, 2006; Yilmaz and Christofori, 2009). Significant changes in the repertoire of integrins present at the cell membrane have been observed during EMT that ultimately favours pro-migratory and pro-invasive activities.

In order for a cell to be motile, as with the end-product of EMT, it has to undergo significant changes in its shape in order to form a front or leading edge and a rear edge (Guarino, 2007). These changes are mediated by the reorganisation of its cytoskeleton. Cellular protrusions, such as filopodia and lamellipodia, that drive motility are formed by the polarisation of cortical actin and assembly into filaments (Guarino, 2007; Savagner, 2001). Several proteins regulate these events including the RhoGTPase family members Rac1, RhoA and Cdc42. The large and complex RhoGTPase family is made up of signalling proteins that transmit signals from the extracellular surface, such as growth factor receptors and adhesion receptors, to intracellular effector proteins that modulate the actin cytoskeleton (Yilmaz and Christofori, 2009). RhoA, and its effector protein $p160^{ROCK}$, was shown to be required for the actin cytoskeletal remodelling observed during TGF-β-induced EMT (Bhowmick et al., 2001). It was showed in another study that in colorectal cancer cells inhibition of EMT resulted in decreased activities of RhoA and Rac1, as well as epithelial cellular morphology and decreased migration (Gulhati et al., 2011).

The composition of intermediary filaments within a cell also undergo dramatic changes during EMT. Cytokeratin intermediary filaments are predominantly found in epithelial states and are subsequently suppressed during EMT. This is accompanied by the increased expression of Vimentin intermediary filaments and is also associated with tumour aggressiveness (Boyer et al., 1989; Kokkinos et al., 2007; Willipinski-Stapelfeldt et al., 2005). It has been suggested that Vimentin is central in the acquisition of the mesenchymal state and is often used as a marker for this state (Mendez et al., 2010). Expression of Vimentin can induce a mesenchymal state in epithelial cells which is reversed upon its silencing. Furthermore, it also leads to decreased adhesion and increases cell motility (Mendez et al., 2010). Vimentin expression has been shown to be induced by both Snail and ZEB2

and it has also been shown to be upregulated during TGF-β and WNT/β-catenin induced EMT (Bindels et al., 2006; Gilles et al., 2003; Olmeda et al., 2007; Yook et al., 2006; Zhao et al., 2008). In the clinical setting, increased Vimentin has been shown to positively correlate with both metastasis and invasion (Gilles et al., 1996; Lang et al., 2002).

The EMT process is known to be complex, with the involvement of numerous signalling pathways and a vast number of effectors. Several of these proteins are well characterised and are frequently used as markers for the identification of active EMT or MET (Zeisberg and Neilson, 2009). Even though increased research efforts into metastasis and specifically the identification of the important role of EMT in metastasis, have significantly improved our understanding on metastasis, new signalling pathways and effectors are still being discovered, emphasising the need for continued research and a more complete understanding.

Table 1.1: Biomarkers for EMT

Epithelial state (lost during EMT)		***Mesenchymal-state (gained during EMT)***	
Marker	*Functional area*	*Marker*	*Functional area*
E-cadherin	Cell adhesion	N-cadherin	Cell adhesion
β-catenin (plasma membrane-associated)	Cell adhesion	β-catenin (nuclear)	Transcription factor
ZO-1	Tight junctions	Syndecan-1	Transmembrane heparin sulphate proteoglycan
Cytokeratins	Intermediary filament	Vimentin	Intermediary filament
Claudins	Tight junctions	α-Smooth muscle actin	Microfilaments
Desmoplakin	Desmosomes	Fibronectin	ECM
Laminin-1	ECM	Laminin-5	ECM
		Snail	Transcription factor
		ZEB	Transcription factor
		TWIST	Transcription factor

ECM – extracellular matrix; EMT – epithelial-mesenchymal transition; ZO-1 – zonula occludens 1. (Thiery and Sleeman, 2006; Zeisberg and Neilson, 2009).

1.6 AHNAK: The giant jack of all trades

A major event in the history of science was the decoding of the human genome. However, deciphering the proteome remains an elusive task. A molecular and functional characterisation is yet to be determined for a vast number of proteins, including nucleoprotein AHNAK.

Twelve years ago it was pointed out that the mystery of AHNAK still continues (Amagai, 2004). Up till then, studies only revealed subtle hints regarding the biological role of AHNAK. However, research in the last 12 years has provided more foundation for these hints as well as new directions for investigation. The implicated cellular processes or pathways seem distinct, ranging from a role in the formation of the blood brain barrier, in cell architecture and migration, to the regulation of cardiac calcium channels and muscle membrane repair (Benaud et al., 2004; Gentil et al., 2005; Haase et al., 2005; Huang et al., 2007; Shankar et al., 2010).

1.6.1 The giant protein

AHNAK, or nucleoprotein AHNAK, is adequately referred to as a giant protein based on its estimated size of approximately 700 kDa (629.1 kDa according to sequence data in UniProtKB, Q09666) (Shtivelman et al., 1992). It is also known as desmoyokin; the desmoyokin protein was identified a few years ahead of AHNAK but it was soon discovered that the two proteins share significant homology and are in fact the same protein (Hashimoto et al., 1993). Originally, it was said to be transcribed from an intron-less gene located on chromosome 11q12, however recent data suggests that alternative splicing takes place from a multi-exon gene, which is consistent with sequence data in the genomic database Ensembl (ENSG00000124942) (Kudoh et al., 1995; de Morrée et al., 2012; Shtivelman et al., 1992). The protein structure of AHNAK is of a tripartite nature, where the bulk of the protein, approximately 4 300 amino acids, is comprised of 128-residue repetitive elements (Hohaus et al., 2002; Shtivelman et al., 1992). These in turn contain an internal repetitive feature consisting of seven amino acid residues. Flanking the central domain are the N- and C-terminal domains with sizes of 251 and 1 002 amino acids, respectively (Hohaus et al., 2002; Shtivelman et al., 1992). Structural predictions of the central domain modelled a structure resembling a β-strand with alternating hydrophilic and hydrophobic residues generating a thin polyionic rod flanked by the terminal domains (Shtivelman et al., 1992). Sites for various protein interactions are scattered across the protein, although the majority is in the C-terminal. A PDZ domain is located within the N-terminal (fig. 1.3) (Komuro et al., 2004). Also known as GLGF or DHR domains, PDZ (PSD-95/Discs-large/ZO-1) domains consist of an 80-90 residue motif that is fairly common not only in human proteins but also in other metazoans, and have undeniably been associated with protein-protein interactions (Nourry et al., 2003).

A second AHNAK protein, AHNAK2, has also been identified (Komuro et al., 2004). Significant homology is shared with the gene, located on chromosome 14q32, and since the two proteins also share several features, the AHNAK family of proteins was established. AHNAK2 is also a giant

protein, with an estimated size of approximately 600 kDa, and has the same tripartite protein structure as that of AHNAK. It is also suggested that they share some intracellular localisations, and hence possibly some functions; however, there has been only one report describing a function for AHNAK2 and thus far, AHNAK has not been implicated in this field. AHNAK2 was recently found to interact with FGF1 under stress conditions (Kirov et al., 2015). This interaction takes place in the C-terminal of AHNAK2 and was shown to be required for stress-induced secretion of FGF1. Co-translocation and co-localisation of both proteins at the plasma membrane and with F-actin was also observed. It was thus suggested that AHNAK2 functions as a scaffold by localising FGF1 at the plasma membrane and possibly providing a link to the actin cytoskeleton (Kirov et al., 2015). The AHNAK proteins have also been reported to have some similarity to periaxin (Han and Kursula, 2014). Although the sequence homology is quite low, the proteins do share some characteristics with regards to their genomic splicing events and protein structure. Periaxin also contains a PDZ domain and is said to be important in the myelination of the peripheral nervous system (Han and Kursula, 2014).

Several intracellular locations have been reported for AHNAK including the nucleus, cytoplasm and plasma membrane (Benaud et al., 2004; Masunaga et al., 1995; Shtivelman et al., 1992; Sussman et al., 2001). Although the presence of both a nuclear localisation signal and a nuclear export signal have been suggested for AHNAK, its intracellular trafficking also seems to be dependent on cell type, the formation of cell-cell contacts, extracellular calcium concentrations and phosphorylation status (Benaud et al., 2004; Hashimoto et al., 1995; Sussman et al., 2001).

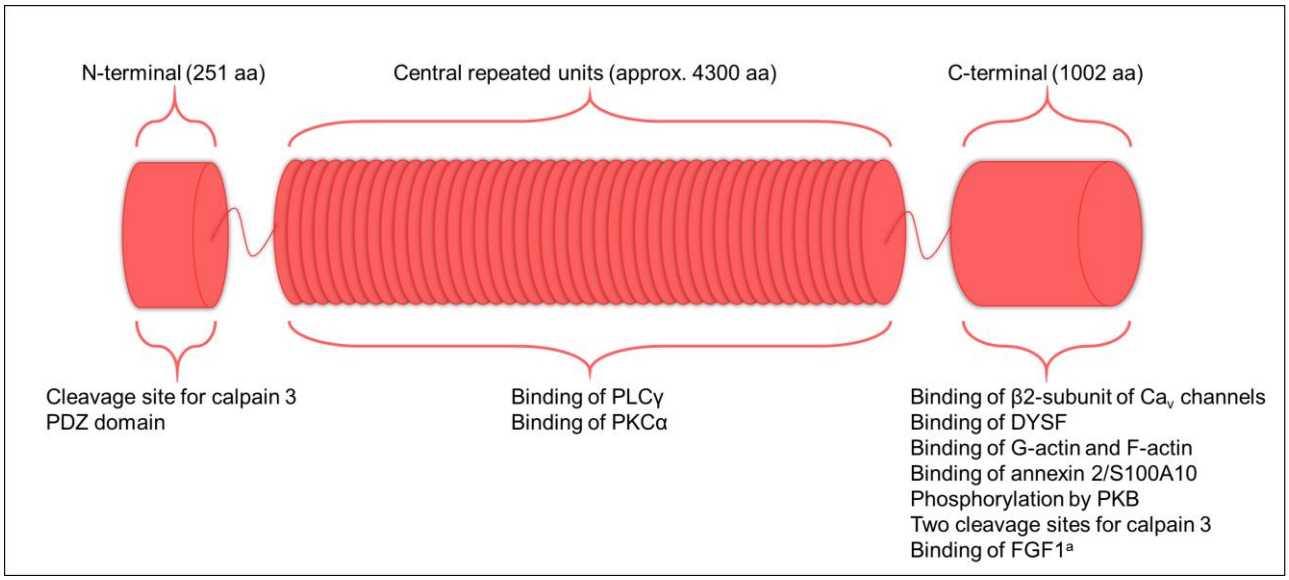

Figure 1.3: AHNAK protein structure depicting its tripartite nature and various binding sites. a – Refers to AHNAK2. (Davis et al., 2014)

1.6.2 Deciphering the function of AHNAK

Numerous studies have contributed to deciphering the function of AHNAK and the diversity between the various fields of research are quite remarkable. A common feature in the majority of these studies is the fact that AHNAK forms part of multi-protein complexes, most likely acting as a structural scaffold. In addition to the more prominent roles that have been described to date, a few other studies have also been reported that include potential roles for AHNAK that are less known.

Initial mouse models showed that AHNAK-null mice are viable, fertile and show no obvious phenotypic defect, leading to the speculation that AHNAK2 might fulfil a compensatory role in some areas of functioning (Komuro et al., 2004; Kouno et al., 2004). However, recent studies suggest otherwise. It was reported that AHNAK-null mice displayed stunted growth and reduced adipose tissue, although the authors did not elaborate on this finding (Lee et al., 2014). A second study reported that AHNAK-null mice exhibited lower body and fat weight than their wild type counterparts; this effect was even more drastic when mice were fed a high fat diet, indicating that the ability to discern this phenotype might be linked to the diet of the mice (Kim et al., 2010). The group suggested that the observed resistance to diet-induced obesity was associated with changes in the levels of certain amino acids, which were appropriately related to fat metabolism. Two follow-up studies by the same groups have since characterised the effect of AHNAK knockout more fully (Shin et al., 2015a, 2016). Again, AHNAK-null mice displayed decreased body weight on both normal and high-fat diets; these changes were minor at six weeks but significant at 18 weeks, indicating that an adequate growth period is also required for this phenotype. Control mice gained considerable weight on the high-fat diet over the 18 weeks while AHNAK-null mice showed complete resistance. The decrease in body weight was shown to be a result of smaller fat pads and decreased total fat. AHNAK-null mice on the high-fat diet also had decreased triglycerides and total and low-density lipoprotein cholesterol, and increased glucose tolerance and insulin sensitivity. The groups investigated these effects further with an *in vitro* model of adipogenesis and found that AHNAK functions as an important regulator of adipocyte differentiation induced by the bone morphogenetic protein (BMP)/Smad-1/Smad-5 signalling pathway (fig. 1.4). AHNAK was shown to interact with and is required for the nuclear translocation of Smad-1 and Smad-5. During BMP-induced differentiation, knockdown of AHNAK prevented Smad-mediated transcription of peroxisome proliferator-activated receptor-γ (PPARγ), a central regulator of adipocyte differentiation. Overexpression of the AHNAK CRU units increased PPARγ expression. Additionally, increased levels of phospho-insulin receptor-β (pIRβ), pAkt, and Glut4 were also detected in AHNAK-null mice fed high-fat diets, which also explains the observed phenotypic effects. It was thus suggested that AHNAK is required for differentiation of pre-adipocytes by functioning in the BMP/Smad-1/Smad-5 pathway, and that loss of AHNAK would limit the generation of adipocytes and ultimately fat (Shin et al., 2015a, 2016).

In another study, a possible role for AHNAK in DNA repair via non-homologous end-joining was suggested after the group showed that AHNAK interacts with the DNA ligase IV-XRCC4 complex

and assisted in the binding of the complex to DNA (Stiff et al., 2004). These results could explain a nuclear localisation for AHNAK, which has previously been reported, as well as the presence of a nuclear localisation signal in its sequence (Shtivelman et al., 1992; Sussman et al., 2001). Unfortunately though, no studies have been performed to follow-up on these results.

Lastly, AHNAK was identified as a novel antigen in systemic lupus erythematosus (SLE) (Sköldberg et al., 2002). The cleavage of autoantigens by granzyme B and caspase 3 is commonly observed in systemic autoimmune diseases, and it was shown that the AHNAK protein can be cleaved by both proteases. Although the authors did not elaborate on the significance of AHNAK as an autoantigen in SLE, it was suggested that AHNAK's internal repetitive domain might prime the protein as a target for autoimmune reactions. In addition, the presence of antinuclear antigens is characteristic of SLE, with a prevalence of 95% in patients, which could contribute to the susceptibility of AHNAK as a target in SLE (Mok and Lau, 2003; Sköldberg et al., 2002).

Throughout the years several groups have published on multiple studies aimed at characterising AHNAK and together they provide strong support for a role for AHNAK in particular research areas, including cell signalling and contacts, calcium channel regulation and membrane repair. These areas have become the focus points for AHNAK-based research and will be discussed in more detail in the following sections.

1.6.3 Cell signalling and cell contacts

One of the first reports investigating AHNAK's function implicated the protein in the signalling pathways downstream of protein kinase C-alpha (PKCα) and phospholipase C-gamma (PLCγ) owing to its ability to interact with and activate both of these proteins (Lee et al., 2008; Sekiya et al., 1999). AHNAK was suggested to serve as a scaffold protein linking the above-mentioned proteins; by activating PKCα, arachidonic acid is released near PLCγ which is then activated by the concerted action of the available arachidonic acid and AHNAK (Lee et al., 2004). It was shown that the activation of PKCα also resulted in the activation of a downstream c-Raf/mitogen activated protein kinase kinase (MAPKK)/extracellular signal regulated kinase (ERK) cascade and that the interactions between AHNAK, PKCα and PLCγ involved the central repeated units of AHNAK (Lee et al., 2008; Sekiya et al., 1999). The sequence of these events does however seem to be reversed; PLC is typically positioned upstream from PKC since its enzymatic action produces diacylglycerol, an essential co-factor for conventional PKC isozymes such as PKCα (Newton, 2010). Scaffold proteins are however also known to be critical regulators of PKC activity by localising the enzymes at specific subcellular sites and in close proximity to co-factors, other regulatory proteins or substrates. In particular, a group of proteins known as receptors for activated C kinase (RACKs) have been identified to bind specific PKC isozymes (Mochly-Rosen et al., 1991; Newton, 2010). In addition to performing the customary scaffold protein function of localising its interacting protein

partners, these RACKs have also been reported to have the ability to relieve the binding PKC isozyme from an autoinhibitory state and producing an active PKC isozyme in the absence of PKC co-factors (Newton, 2010; Ron and Mochly-Rosen, 1995). Furthermore, RACKs can also provide support for PLCγ; binding of PLCγ to RACKs inhibits subsequent PKC binding, however a PKC-RACK complex does not prevent the binding of PLCγ to RACKs (Disatnik et al., 1994). The protein-scaffold interactions and outcomes illustrated by RACKs seem similar to what was observed for AHNAK, PKCα and PLCγ, however whether AHNAK and the RACK proteins themselves share any similarities is currently unknown.

Specific expression patterns of AHNAK in tissues from the nervous system have provided potential roles for the protein, although they seem to differ between the central- (CNS) and peripheral nervous systems (PNS). In the PNS AHNAK was suggested to play a role in myelination, a process performed by Schwann cells (fig. 1.4). The process is strictly dependent on adhesion to laminin-containing basement membranes which is facilitated by the transmembrane dystroglycan-dystrophin complex (von Boxberg et al., 2014; Salim et al., 2009). In Schwann cells, AHNAK knockdown was shown to result in altered morphology, increased detachment from laminin substrate and decreased levels of β-dystroglycan (β-DG) which also showed altered intracellular localisation (Salim et al., 2009). During development, AHNAK was shown to be highly expressed during the period of laminin deposition and myelination, concomitantly with increased β-DG expression. These results were further explored in a recently published follow-up study (von Boxberg et al., 2014). Co-immunoprecipitation experiments revealed that AHNAK and β-DG indeed co-localises and interacts, and that AHNAK knockout mice displayed altered distribution and decreased levels of β-DG. The expression levels of dystrophin-116 were also decreased and mice showed instances of abnormal myelinated fibres. In addition, Schwann cells isolated from the mice displayed decreased migrational velocity and increased rigidity, and it was determined that the organisation of the actin cytoskeleton was negatively affected (von Boxberg et al., 2014). These results led the authors to hypothesise that AHNAK interacts with the dystroglycan-dystrophin complex and that a lack of AHNAK impairs the integrity of the complex and subsequent binding to the basement membrane via laminin, ultimately resulting in abnormal myelination events. The dystroglycan-dystrophin complex also binds F-actin, linking it to the plasma membrane; again, weakening of the complex might have resulted in the altered morphology, migration and stiffness shown by these cells. AHNAK could thus potentially also serve as a molecular and/or structural link between the actin cytoskeleton and the basement membrane receptor complex (von Boxberg et al., 2014). Interestingly, periaxin, the only protein outside the AHNAK family that shows some homology, is also important in the myelination of the PNS. Whether these proteins are somehow connected in this process is unclear; both proteins can bind β-DG complexes but they do not seem to co-localise in myelinating Schwann cells (von Boxberg et al., 2014; Salim et al., 2009).

In the CNS AHNAK was suggested to play a role in the formation of the blood-brain barrier (BBB) (fig. 1.4) (von Boxberg et al., 2006; Gentil et al., 2005). Specific expression was detected in endothelial cells (EC) forming the BBB, while EC lacking BBB properties, including tumour angiogenic EC, showed decreased AHNAK levels (Gentil et al., 2005). AHNAK was localised to the plasma membrane, specifically at the tight junctions, where a co-localisation with zonula occludens 1 (ZO-1), a known tight junction protein, was also observed. An *in vitro* model representing a functional BBB showed the translocation of AHNAK from the cytoplasm to the plasma membrane following the establishment of the BBB (Gentil et al., 2005). A similar model was also employed to investigate the effects of a bacterial toxin on the BBB (Boveri et al., 2006). In addition to causing a significant increase in the permeability of the BBB, AHNAK was shown to redistribute from the EC tight junctions to the cytoplasm, supporting the findings for the intracellular distribution of AHNAK (Boveri et al., 2006; Gentil et al., 2005). Furthermore, AHNAK was found to be significantly up-regulated upon spinal cord injury (von Boxberg et al., 2006). The increased expression was detected in cells possessing barrier properties and the distribution specifically delineated the cavity formed at the lesion site, suggestive of forming a barrier around the site of damage (von Boxberg et al., 2006).

The results obtained in the above-mentioned studies describe different roles for AHNAK in the CNS and PNS, although β-DG might represent a common link between these roles. AHNAK has the ability to bind β-DG in Schwann cells and this associates AHNAK with an indirect role in myelination of PNS axons (von Boxberg et al., 2014). In the CNS, β-DG is expressed in a number of cells, including oligodendrocytes (Colognato et al., 2007; Zaccaria et al., 2001). Here, β-DG is also reported to function as a laminin receptor, and is said to be important for oligodendrocyte differentiation and myelination (Colognato et al., 2007). However, an interaction and role for AHNAK in myelination of the CNS seems unlikely, since it has been reported that AHNAK is not expressed in these cells (von Boxberg et al., 2014). β-DG is however also expressed in EC of the BBB and might also assist in maintaining the integrity of BBB (Zaccaria et al., 2001; del Zoppo et al., 2006). Here, an interaction between β-DG and AHNAK is possible but is yet to be determined.

Recently another function for AHNK in the CNS was reported (Shin et al., 2015b). This study also made use of AHNAK-null mice and showed that a loss of AHNAK lead to increased neurogenesis. Increased cell proliferation was observed in the hippocampal dentate gyrus of AHNAK-null mice as well as increased neuronal differentiation and migration of mature neurons from the subgranular zone to the granular cell layer of the dentate gyrus (Shin et al., 2015b). The molecular mechanism behind this function is however unknown. Neurogenesis and differentiation are complex processes modulated by numerous signalling pathways. A possible avenue to explore could involve potential interactions with Smad proteins, as with adipocyte differentiation described above, since the induction of hippocampal neuronal differentiation by brain-derived neurotrophic factor or TGF-β2 has previously been shown to be mediated by Smad-2/Smad-4 transcriptional control (Lu et al., 2005).

AHNAK has also been associated with the formation of cell-cell contacts, as reported by the group of Sussman *et al.* (fig. 1.4) (Sussman et al., 2001). In epithelial cells, the intracellular location of AHNAK was shown to be dependent on the level of confluency of the *in vitro* culture; AHNAK displayed a nuclear localisation in subconfluent cells compared to either a cytoplasmic or plasma membrane-associated localisation in confluent cells. The presence of a nuclear localisation signal and a nuclear export signal identified within AHNAK's protein sequence was involved in its translocation, as well as its phosphorylation by Akt. Low levels of active Akt were observed in subconfluent cultures, which significantly increased upon the formation of cell-cell contacts when confluency was reached, while treatment with a PI3K (upstream of Akt) inhibitor resulted in decreased levels of phosphorylated AHNAK located in the nucleus (Sussman et al., 2001).

A subsequent study investigating the role of AHNAK at the plasma membrane revealed similar results. The group of Benaud *et al.* showed that, upon reaching confluency, AHNAK redistributed from the cytoplasm to the plasma membrane in epithelial cells (Benaud et al., 2004). Furthermore, AHNAK was shown to form part of a multimeric protein complex at the plasma membrane which included actin and the heterotetrameric complex of annexin 2/S100A10. Exposure of confluent cells to low calcium conditions, a condition which destabilises cell-cell contacts, resulted in a cytoplasmic localisation for both AHNAK and annexin 2/S100A10. In addition, the AHNAK/annexin 2/S100A10 complex was also shown to co-localise and interact with membrane lipid rafts. Knockdown of annexin 2 resulted in a secondary reduction in AHNAK that was now cytoplasmic while knockdown of AHNAK resulted in a flattened cellular morphology, similar to that seen when cells were exposed to low calcium conditions, as well as disorganisation of the actin cytoskeleton. Treating confluent cells with cytochalasin D, which disrupts the actin cytoskeleton, also resulted in altered AHNAK localisation (Benaud et al., 2004).

Based on the results obtained in these studies, it can be suggested that calcium-dependent formation of cell-cell contacts initiates a signalling pathway which, most likely via Akt-mediated phosphorylation, results in the translocation of AHNAK to the plasma membrane where a protein complex is formed with annexin 2/S100A10 and the actin cytoskeleton (Benaud et al., 2004; Sussman et al., 2001). A role for the calcium-sensitive, phospholipid-binding protein annexin 2 in membrane dynamics has been well described; by binding actin filaments its function includes regulating actin filament turnover and membrane ruffles as well as endocytic events such as intracellular trafficking of macropinosomes and endosomal transport (Grieve et al., 2012; Hayes et al., 2006; Merrifield et al., 2001; Morel et al., 2009). Furthermore, annexin 2 is involved in establishing cell-cell contacts by recruiting proteins important for cell-cell adhesion and the formation of adherens junctions (Grieve et al., 2012; Hansen, 2002; Yamada et al., 2005). The calcium-insensitive S100A10 protein is mostly tightly bound to annexin 2 and while this interaction provides protection from degradation, S100A10 is also reported to be required for several membrane-related functions along with annexin 2 (Rescher and Gerke, 2008; Sayeed et al., 2013). Indeed, a recent three-dimensional

structure determination revealed that both the annexin 2 and S100A10 moieties were required for recruitment and complex formation with AHNAK (Dempsey et al., 2012). The studies described above correspond with annexin 2's role in establishing cell-cell contacts, implicating AHNAK in these events, while a recent study linked AHNAK to membrane ruffling and endocytic events. AHNAK, annexin 2 and S100A10 were required for invasion of epithelial cells by *Salmonella* bacteria (Jolly et al., 2013). This type of infection requires extensive actin remodelling and membrane ruffling to engulf the bacteria, and the three implicated proteins were shown to be significantly enriched at the sites of infection, while a decrease in either of the proteins resulted in decreased number of infections (Jolly et al., 2013). Taken together, AHNAK's interaction with annexin 2/S100A10 implicates the protein in some of the heterotetrameric complex's roles in membrane dynamics. The precise function of AHNAK within this multi-protein complex remains unclear though; it might function purely as a scaffold providing structural support to the complex and perhaps additional components or it might have a more active role by taking part in signal transduction.

1.6.4 Regulation of calcium channels

The majority of research investigating the molecular function of AHNAK has, however, focused on the protein's interaction with the L-type voltage-gated calcium (Ca_v) channels in cardiomyocytes (fig. 1.4). Ca_v channels are heteromultimers consisting of pore-forming α1- and regulatory β-subunits, as well as other auxiliary subunits. In cardiac cells they represent a major calcium-influx controlling channel that is activated following an action potential and transduces the signal to the inside of the cell, effectively performing excitation-contraction coupling (Bers, 2000; Catterall et al., 2005).

After determining that AHNAK can bind to and interact with the β2-subunit of the $Ca_v1.2$ channel, which contains the α1C isoform as the pore-forming subunit, subsequent studies reported that AHNAK localises to the sarcolemma, specifically the T-tubules where Ca_v channels are predominantly found, and that AHNAK was most likely phosphorylated by protein kinase A (PKA), suggesting a possible role in β-adrenergic regulation of Ca_v channels (Haase et al., 1999; Hohaus et al., 2002).

Regulation of the Ca_v channels through this pathway has been well described; following stimulation by the sympathetic nervous system, β-adrenergic receptors are activated resulting in the production of cyclic adenosine monophosphate by adenylyl cyclase. These second messengers activate PKA which translocates to the plasma membrane where it can phosphorylate both the α1- and β2-subunits of the channel (Kamp and Hell, 2000). In addition, AHNAK was also shown to interact with both G- and F-actin, indicating that AHNAK might form part of a regulatory network transducing signals from the cytoskeleton to the channels (Hohaus et al., 2002). The integrity of the actin cytoskeleton has indeed been previously shown to be important in regulating the calcium current through Ca_v channels, not only in cardiac cells but also in vascular smooth muscle cells and osteoblasts (Galli and DeFelice, 1994; Lader et al., 1999; Li et al., 2011; Nakamura et al., 2000). However, further studies elucidated a more direct role for AHNAK. By investigating the effect of a

mutated AHNAK fragment, the group of Haase *et al.* found that wild type endogenous AHNAK functions as an inhibitor of the $Ca_v1.2$ channel, regulating the current of the channel (Haase et al., 2005). Binding of the Ile5236Thr-fragment resulted in increased calcium current compared to the wild type AHNAK, an effect that was unaltered by the addition of isoprenaline, a known stimulator of the β-adrenergic receptor. The authors concluded that, under basal conditions, AHNAK binds the β2-subunit of the channel, thereby limiting calcium influx; while upon β-adrenergic stimulation and subsequent phosphorylation by PKA, AHNAK releases the subunit, allowing proper functioning and increased calcium influx (Haase et al., 2005). The results obtained also supported those of a previous study where fragments of the AHNAK C-terminal competing with endogenous whole protein relieved the β2-subunit from the enforced negative regulation (Alvarez et al., 2004). Interestingly, the Ile5236Thr mutant AHNAK was identified by screening a cohort of patients diagnosed with hypertrophic cardiomyopathy and although it represents a rare genetic variant with no apparent association with the disease, it remains a functional gain-of-function mutation which could affect individual contractile functioning of the heart (Haase et al., 2005).

A role for AHNAK in regulating calcium flux through Ca_v channels was also identified in other cell types, albeit with contradicting findings. AHNAK was shown to be important for calcium influx in CD4+ T cells as well as cytotoxic CD8+ effector T cells (CTLs) (fig. 1.4) (Matza and Flavell, 2009; Matza et al., 2008, 2009). In these cells, AHNAK was suggested to be required for the membrane expression of the calcium channel possibly through its interaction with the β2-subunit; however, the specific Ca_v channel isoform involved was $Ca_v1.1$, which contains the α1S pore-forming subunit. AHNAK deficiency, whether in AHNAK-null mice or by means of siRNA knockdown, resulted in decreased calcium influx leading to defective CD4+ T cell activation and proliferation and reduced CTL cytolytic activity (Matza et al., 2008, 2009). Furthermore, AHNAK was also shown to be required for calcium influx in osteoblasts (Shao et al., 2009). One of the main functions of regulatory β-subunits is to assist in the membrane targeting of the α1-subunit, therefore, in conjunction with the results obtained in these studies, one could suggest that AHNAK assists the β2-subunit in steering the pore-forming subunit to the plasma membrane as well as stabilising the completed channel, thus allowing a fully functioning channel to form (Chien et al., 1995). Possible explanations for the contrasting roles in Ca_v channel regulation between these studies and those described above could be attributed to the specific cell type involved (excitable vs. non-excitable), the purpose of calcium inside the cell (excitation coupling vs. signalling molecule) or perhaps the Ca_v channel isoform itself ($Ca_v1.2$ vs. $Ca_v1.1$).

Recently, another association has been made between AHNAK and Ca_v channels (fig. 1.4). In pre-synaptic neurons, Ca_v channels ($Ca_v2.1$ and $Ca_v2.2$ with pore-forming subunits α1A and α1B, respectively) interact with synaptic laminin and assist in the formation and stabilisation of so-called active zones, areas of neurotransmitter release (Nishimune et al., 2004). In an attempt to identify how these Ca_v channels are connected to the active zone, Carlson *et al.* identified the cytoskeletal

components of the Ca_v channel protein complex, which was shown to include AHNAK (Carlson et al., 2010). Localisation of AHNAK at the pre-synaptic nerve terminals was also observed and it was suggested that AHNAK might function to link the Ca_v channel to the actin cytoskeleton through the regulatory β2 subunit, as with the $Ca_v1.2$ channels in cardiac cells. These results were supported in another recent study that identified AHNAK as part of the "components of active zone" (CAZ) complex (Yao et al., 2014). Interestingly, this study aimed at identifying proteins interacting with the huntingtin protein, the causative mutational protein in the neurodegenerative Huntington's disease. AHNAK was identified along with other proteins known to be important in the CAZ complex, which was also identified as the active zone component connected with the Ca_v channel in the abovementioned study. Indeed, the $Ca_v2.1$ channel was used in this study as a marker for the synaptosome fraction. It is clear that AHNAK forms part of the active zone through protein interactions, although whether AHNAK is actively part of the functions of the active zone (and can be classified as a CAZ protein as suggested in the latter study), or merely functions as a cytoskeleton link (as suggested in the former study) is currently unknown.

1.6.5 Membrane repair

A significant amount of research has also focused on AHNAK's potential involvement in the repair of the plasma membrane in skeletal muscle after injury. This commenced with a report identifying the protein as a marker for enlargeosomes; distinct non-secretory vesicles that undergo rapid exocytosis following calcium influx (fig. 1.4) (Borgonovo et al., 2002; Chieregatti and Meldolesi, 2005). In general, the regulated exocytosis of non-secretory vesicles is considered to have two purposes, firstly to facilitate the translocation of membrane proteins such as receptors to the cell surface, and secondly, to translocate membrane patches to the plasma membrane (Chieregatti and Meldolesi, 2005). Enlargeosomes are thought to fall under the latter category, with the specific function of decreasing cell surface tension allowing membrane repair to take place. In addition, exocytosis of enlargeosomes might also be required for cell surface enlargement during differentiation (Borgonovo et al., 2002; Chieregatti and Meldolesi, 2005). In resting PC12-27 cells, a neurosecretion-defective clone rich in enlargeosomes, AHNAK staining labelled the inner cytoplasmic rim just below the plasma membrane (Borgonovo et al., 2002). However, upon stimulation with the calcium ionophore ionomycin, significant AHNAK labelling was observed at the plasma membrane. This labelling showed increased levels, was long-lasting and punctate, as would be expected from membrane fusion events (Borgonovo et al., 2002).

The specific function of AHNAK within enlargeosomes is however unknown, even though several studies commonly use the protein as a marker for these vesicles, including studies focussed on understanding and characterising the vesicles (Cocucci et al., 2008; Prada et al., 2007; Racchetti et al., 2010, 2012). The process of membrane resealing through intracellular vesicles has been extensively studied and several have reported on the participation of the cell cytoskeleton. This can

occur on multiple levels and differs amongst the phases of repair. Following the calcium-influx stimulus that accompanies membrane disruption, vesicles are rapidly recruited to the site of damage; since these vesicles are not docked at the plasma membrane they require a trafficking machinery and the kinesin and myosin motor proteins, as well as microtubules, have been shown to be important here (Abreu-Blanco et al., 2012; Bi et al., 1997; McDade and Michele, 2014). Depolarisation of the cortical actin cytoskeleton is also required since this allows the vesicles to rapidly move to the site of damage and fuse with the membrane without obstruction (Abreu-Blanco et al., 2012; Miyake et al., 2001). Following successful patching of the membrane, both the membrane and the cortical cytoskeleton needs to be restored in order to allow complete healing (Abreu-Blanco et al., 2012). Since AHNAK has previously been shown to be able to bind actin and to be involved in remodelling the actin cytoskeleton, it could be that the function of AHNAK present within enlargeosomes might be within one of the phases of membrane resealing. A role in the second phase might be more likely though, since AHNAK is localised within enlargeosomes during recruitment to the damaged membrane, while after fusion it is localised at the membrane. Interestingly, annexin 2 has also been localised to enlargeosomes, although instead of co-localising with AHNAK as shown in previous studies, it is present on the cytosolic-face of the vesicle membrane, suggesting it might take part in vesicle response to the calcium stimulus (Lorusso et al., 2006).

Perhaps the best evidence supporting a role for AHNAK in membrane repair stems from an interaction with dysferlin (fig. 1.4). Dysferlin is highly expressed in skeletal muscle and mutations in the associated gene leading to decreased and/or abnormal dysferlin protein are known to cause limb girdle muscular dystrophy 2B (LGMD2B), distal anterior compartment myopathy and miyoshi myopathy, collectively referred to as dysferlinopathies (Huang et al., 2007). At present, it is clear that dysferlin functions in membrane repair processes; dysferlin-deficient mice display impaired membrane repair, which is also the pathological mechanism implicated in human patients suffering from the diseases (Bansal et al., 2003; Huang et al., 2007; Wallace and McNally, 2009). The molecular mechanism of this role is however not completely understood, although dysferlin is presumed to mediate vesicle fusion events (Cenacchi et al., 2005). Recent studies have proposed three different possibilities; firstly, that dysferlin-containing vesicles transported by microtubules and kinesin fuses with lysosomes at the site of damage in order to form a large membrane ‘plug’ while the second, in contrast, suggested that dysferlin tethers individual exocytic lysosomes to the damaged site resulting in the secretion of acid sphingomyelinase which then facilitates membrane repair (Defour et al., 2014; McDade and Michele, 2014). In a third study it was found that, in addition to proposed roles in membrane repair, dysferlin is required for maintaining and stabilising calcium homeostasis and T-tubule function during membrane stress (Kerr et al., 2013).

The group of Huang *et al.* reported a calcium-independent interaction between the far-carboxyl end of AHNAK and the C2A domain of dysferlin, as well as with its homolog, myoferlin (Huang et al.,

2007). Since calcium-induced signalling is associated with membrane repair, this type of interaction indicates that AHNAK can also bind to dysferlin under normal conditions. AHNAK was also shown to co-localise with dysferlin at the sarcolemma of muscle fibres, while redistribution to the cytoplasm along with dysferlin during muscle regeneration was observed. Importantly, a secondary reduction in AHNAK was observed in muscle tissue sections from dysferlinopathy patients, which suggests that dysferlin might function to localise and stabilise AHNAK at the plasma membrane through its transmembrane domain. This is also reminiscent of the situation described by Benaud *et al.* where knockdown of annexin 2 resulted in a secondary reduction of AHNAK protein levels (Benaud et al., 2004). Furthermore, dysferlin interacts with the annexin 2/S100A10 heterotetramer in a calcium and membrane injury-dependent manner, suggesting that AHNAK might form part of a similar multiprotein complex (Lennon et al., 2003). Indeed, these proteins have all been identified to be contained in dysferlin-complexes in skeletal muscle cells and tissues (de Morrée et al., 2010). It is known that the influx of calcium following membrane rupture serves as the signal for membrane repair processes and, as previously shown, a calcium signal was also involved in the translocation of AHNAK from the cytoplasm to the plasma membrane (Benaud et al., 2004). The protein sequence of AHNAK is not reported to contain any calcium-binding sites, however annexin 2 most likely serves as the intermediate; binding of calcium to annexin 2 activates the protein resulting in subsequent recruitment of S100A10 and AHNAK, followed by translocation to the plasma membrane (Rezvanpour et al., 2011). This sequence of events is similar to previously reported findings (Benaud et al., 2004). Structure analyses have determined that the region of the AHNAK protein reserved for the heterotetramer complex of annexin 2/S100A10 is small enough to allow adequate space for the docking of additional complex proteins at the membrane, such as dysferlin (Dempsey et al., 2012; Rezvanpour et al., 2011). Support for the requirement of a fully functional dysferlin-protein complex was recently reported. In bovine coronary arterial endothelial cells, silencing of AHNAK expression produced the same effect as silencing of dysferlin, i.e. decreased lysosomal fusion and acid sphingomyelinase activation upon induction of Fas ligand (Han et al., 2012). Possibly regulating this multiprotein complex is calpain 3; a muscle-specific member of the non-lysosomal cysteine protease calpain family and which is also the characteristic mutational target in LGMD2A (Huang et al., 2008). Huang *et al.* were able to show that calpain 3 interacted with and cleaved AHNAK, causing it to lose its ability to bind dysferlin (Huang et al., 2008). Tissue sections from LGMD2A patients revealed increased levels of AHNAK at the sarcolemma. These results suggest that in the dysferlin protein complex, calpain 3 regulates AHNAK turnover and thus the AHNAK-dysferlin interaction as well (Huang et al., 2008).

A recent study investigating the localisation of AHNAK in muscular dystrophies, specifically LGMD2B and LGMD2A, reported some intriguing findings which might shed light on the dysregulation of AHNAK and possibly enlargeosomes inthese diseases (Zacharias et al., 2011). Skeletal muscle tissue sections of patients with LGMD2B and LGMD2A were compared to normal tissue sections. Tissue sections from the diseased patients showed changes typical of muscular dystrophy (MD),

including increased endomysial fibrosis. While normal tissue sections displayed a sarcolemma-associated labelling for AHNAK, tissue sections from LGMD2B showed significantly reduced labelling at the membrane and very strong labelling outside the muscle fibre in the endomysium. In LGMD2A tissue sections, AHNAK labelling at the sarcolemma either remained constant or was slightly reduced; however, a significant amount of AHNAK staining was also observed in the endomysium. Through co-staining with the respective markers it was determined that neither infiltrating immune cells, the basal lamina nor MD-associated fibrosis were the likely sources for the AHNAK present in the endomysium, thus suggesting the muscle fibre itself as a possible source. By utilising an *in vitro* model, the authors determined that myotubes are capable of secreting small vesicles which tested positive for AHNAK. Although these vesicles seem to resemble enlargeosomes, which in the case of MD might be dysregulated in such a manner that they are actually secreted out of the muscle fibre instead of repairing the sarcolemma (perhaps because components necessary for a functional complex tethered to the damaged membrane are missing), the specific origin of the proteins and identification of the vesicles requires further investigation (Zacharias et al., 2011). In this study, the loss of AHNAK at the sarcolemma was restricted to LGMD2B tissue sections, which is in agreement with the finding of Huang *et al.* in LGMD2B patients, as described above, therefore reinforcing the suggestion that dysferlin might function to stabilise AHNAK at the sarcolemma. However, this contradicts with the findings of Huang *et al.* in LGMD2A patients also described above, emphasising the need for further investigation.

1.6.6 Tumour progression

Research into the molecular function of AHNAK over the last couple of years has experienced yet another change in direction, with the focus predominantly on tumour metastasis. Numerous studies have implicated the protein in several events related to tumour metastasis, such as PI3K/Akt signalling pathway, actin cytoskeleton reorganisation, formation of pseudopodial protrusions and EMT.

It all started with several large-scale, mostly proteomic-based studies. A proteome analysis of purified pseudopodial protrusions from an invasive variant of transformed MDCK cells revealed the presence of AHNAK and active Akt, while differential protein expression analysis of the A549 lung cancer cell line undergoing TGF-β-induced EMT showed increased expression of AHNAK and annexin 2 (Jia, 2005; Keshamouni et al., 2006). Furthermore, treatment of the invasive breast cancer cell line SUM-52PE with PD173074, an inhibitor of receptor tyrosine kinases including the PI3K pathway, resulted in decreased levels of phosphorylated AHNAK (Pal et al., 2006). Taken together, these findings correspond to the studies of Sussman *et al.* (2001) and Benaud *et al.* (2004) which suggested a signalling pathway that includes Akt, AHNAK and the annexin 2/S100A10 complex. These findings would suggest that increased expression of AHNAK, phosphorylated by Akt and in complex with annexin 2, are associated with tumour progression, metastasis and invasion. Two other

studies showed AHNAK to be highly abundant in lipid rafts isolated from melanoma and breast cancer cell lines; while the first found no association with the degree of malignancy, the second found AHNAK to be inversely correlated with the degree of malignancy (Baruthio et al., 2008; Caruso and Stemmer, 2011). Additional studies reported differential expression in metastatic and non-metastatic cell lines, enrichment in purified pseudopods and decreased gene expression in tumours following knockdown of SCUBE3 (an activator of signalling pathways leading to angiogenesis, degradation of the extracellular matrix and EMT) (see table 1.2) (Chen et al., 2006; Chou et al., 2013; Parisis et al., 2013).

Table 1.2: Large-scale studies implicating AHNAK in cancer and metastasis

Type of study	***Experimental environment***	***Findings / remarks***	***Reference***
Proteome analysis	Purified pseudopodia	AHNAK detected	(Jia, 2005)
Differential protein expression	Lung cancer cell line (A549) undergoing EMT (induced)	Increased expression	(Keshamouni et al., 2006)
Differential phosphoprotein	Breast cancer cell line (SUM-52PE) treated with RTK-inhibitor	Decreased pAHNAK	(Pal et al., 2006)
Proteome analysis	Lipid rafts of four melanoma cell lines	Highly abundant	(Baruthio et al., 2008)
Proteome analysis	Lipid rafts of four breast cancer cell lines	Highly abundant	(Caruso and Stemmer, 2011)
Differential gene & protein expression	Metastatic (TMC-1) vs non-metastatic (SC-M1) gastric cancer cell lines	Decreased gene & protein expression	(Chen et al., 2006)
Differential gene expression	*HER-2* overexpressing primary cell line	Decreased gene expression	(Chen et al., 2010)
Differential gene expression	Angiotropic vs non-angiotropic melanoma tumours	Decreased gene expression	(Lugassy et al., 2011)
Quantitative phosphoproteome analysis	Metastatic (MDA-MB-231) vs non-metastatic (MCF-7) breast cancer cell line	Increased pAHNAK	(Kabir et al., 2012)
Differential protein expression	Laryngeal carcinoma tissues from 83 patients compared to surrounding normal tissues	Increased expression, correlated with patient survival	(Dumitru et al., 2013)
Mutational screening	ccRCC tissues from 99 patients	Presence of recurrent mutations	(Guo et al., 2011; Xu et al., 2012)
Proteome analysis	Purified pseudopodia from migrating MCF-7 cells (induced)	Enriched	(Parisis et al., 2013)
Differential gene expression	*SCUBE3*$^{-/-}$ lung adenocarcinoma tumours	Decreased gene expression	(Chou et al., 2013)

Quantitative whole-proteome analysis	ccRCC tumour samples compared to normal kidney samples	Increased protein expression, capable of distinguishing between sample types	(White et al., 2014)
Transcriptome and proteome analysis	Various cell lines representing different states of EMT	Attenuated expression	(Thomson et al., 2011)
Phosphoproteome analysis	Tumourigenic (SCC-9) vs non-tumourigenic (HaCaT)	Decreased serine phosphosites	(Winck et al., 2014)
Differential gene expression	Non-tumourigenic (208F) vs Ras-transformed (FE-8)	Decreased expression	(Zuber et al., 2000)
Differential gene expression	Acute lymphocytic leukaemia patients	Increased expression, correlated with relapse	(Chiaretti et al., 2004)
Differential gene expression[a]	Pancreatic cancer vs normal tissues (meta-analysis)	Increased expression	(Goonesekere et al., 2014)
Whole-exome sequencing	Matched metastatic melanoma tumour vs normal (eight patient samples)	Mutated epitope presentation detected	(Cohen et al., 2015)
Differential gene expression	Complete vs incomplete response, patient tumour biopsies (pre-treatment)	Increased expression	(Lopes-Ramos et al., 2015)
Differential gene expression	Isogenic cisplatin-resistant vs cisplatin-sensitive ovarian cancer cell lines	Increased expression	(Cheng et al., 2006)
Differential protein expression	Cisplatin-resistant vs parental neuroblastoma cell lines	Increased expression	(Piskareva et al., 2015)
Quantitative whole proteome analysis	Irradiated breast cancer cells	Increased expression	(Kim et al., 2015)
Quantitative proteome analysis	Melanoma vs melanocyte cell lines, membrane enriched samples	Decreased expression	(Sheppard et al., 2015)

[a] – Refers to AHNAK2.

Even though these large-scale studies identifying AHNAK among a multitude of other proteins are limited in describing the details of AHNAK's involvement within these processes on a molecular level, they do have the potential to point to other processes within tumourigenesis that might be worthwhile investigating. As an example, investigating possible associations or correlations between the individual proteins themselves might yield some attractive results. In the study by Dumitru *et al.* AHNAK in combination with macrophage migration inhibitory factor (MIF) were strong predictors of

poor survival in laryngeal carcinoma (Dumitru et al., 2013). In addition, in the study by White *et al.*, MIF was identified along with AHNAK as being significantly dysregulated in clear cell renal cell carcinoma (ccRCC) samples compared to normal kidney samples (White et al., 2014). Here, it is noteworthy to mention that MIF has recently been shown to be a novel regulator of autophagy, a highly regulated process of self-degradation with known ties to tumourigenesis (El Bounkari and Bernhagen, 2012; Yang and Klionsky, 2010). Results obtained from these large-scale studies can also strengthen or add value to follow-up studies. A group led by Dumitru recently reported on the use of FoxP3, a forkhead transcription factor implicated in cancer, as a prognostic marker for different types of head and neck cancer. When combining the marker, and the inflammation marker cyclooxygenase-2, with expression data for AHNAK, significantly stronger prognostic values were obtained for survival of patients with laryngeal carcinoma (Weller et al., 2014).

Studies specifically investigating the role of AHNAK in cancer are especially limited. Recently, Shankar *et al.* turned their focus to AHNAK after discovering that it was significantly enriched in purified pseudopodia of six different metastatic cancer cell lines (Shankar et al., 2010). Further investigation revealed that the knockdown of AHNAK resulted in pseudopodial retraction, impaired tumour cell migration and invasion as well as EMT reversal. The actin cytoskeleton network was also affected and administration of an actin-stabilising drug, jasplakinolide, reversed the effects brought about by the knockdown, such as cell shrinkage and rounding (Shankar et al., 2010). In addition, AHNAK has been included in an EMT profiler array (EMT-RT^2 Profiler PCR Array, SAAB Bioscience, Qiagen) and its expression (both gene and protein) decreased along with other mesenchymal markers during MET (Finetti et al., 2015).

Another recent study reported similar findings with regards to tumour cell migration and invasion. AHNAK gene expression was shown to be significantly higher in seven different mesothelioma cell lines compared to the control mesothelial cell line (Sudo et al., 2014). Furthermore, knockdown of AHNAK resulted in decreased migration and invasion of the cancer cells. Mice xenograft models were also established with four of the mesothelioma cell lines and AHNAK expression was detected, where the immunohistochemistry staining revealed an interesting localisation pattern. AHNAK was found to be localised in both the cytoplasm and at the plasma membrane in the single sarcomatoid xenograft tumour, while in the remaining three epithelioid tumours AHNAK was restricted to the plasma membrane. These results were confirmed in tumour specimens from patients; however the reason for this localisation pattern is unknown (Sudo et al., 2014). AHNAK also seems to play a role in the migration of non-cancerous cells. Aortic smooth muscle cells isolated from AHNAK knockout mice displayed decreased migration compared to wild type cells upon stimulation with platelet derived growth factor (Lim et al., 2013). In this model, the loss of AHNAK was associated with decreased phosphorylation of ERK and inhibition of Rac proteins, important components regulating cytoskeleton dynamics in migrating cells (Lim et al., 2013). The role for AHNAK in cell migration in both metastatic tumour cells and normal cells suggests that AHNAK is dysregulated in the cancer

setting; this most likely occurs either on an expression level, as suggested by the various large-scale studies, or via post-translational modification such as phosphorylation by Akt.

Lastly, an interesting link between AHNAK-containing vesicles and cancer was suggested in a recent study and even though AHNAK could be indirectly linked with cellular migration, the findings rather support an association between AHNAK and tumour progression (fig. 1.4) (Silva et al. 2016). Silva *et al.* reported on the directional transfer of microvesicles from aggressive breast cancer cells to non-transformed fibroblasts when in co-culture. The group found that AHNAK was the most abundant component of these vesicles and that the protein was also required for the formation of the vesicles. The outcome of vesicle transfer between the two cell lines was increased fibroblast migration and the authors cautiously suggested that this could assist tumour cells in establishing a beneficial tumour microenvironment that would favour growth, invasion and metastasis. The microvesicles identified in this study could be similar to enlargeosomes in neuronal cells described earlier. Indeed, the group did report similarities following ultrastructural analysis and also identified annexin 2 as part of the vesicle components. Since the general function of these vesicles and that of enlargeosomes differ greatly, it suggests that AHNAK is not directly involved in the individual functions of these vesicles but rather that AHNAK is only involved in the formation of these vesicles, which is also supported by the findings of the recent study (Silva et al. 2016).

In contrast to the above-mentioned studies where AHNAK was described as a protein that promotes the progression of cancer, it has also been suggested to function as a tumour suppressor. Through a series of experiments the group of Lee *et al.* elegantly described AHNAK as an important component of the TGF-β/Smad signalling pathway (fig. 1.4) (Lee et al., 2014). AHNAK was shown to be capable of binding the regulatory Smad 1-3 proteins while knockdown of AHNAK under stimulation by TGF-β resulted in decreased phosphorylation and activation of Smad-3. AHNAK assisted in the translocation of Smad-3 to the nucleus where it was shown to be important in the binding of phospho-Smad-3 to the c-Myc promoter, also under TGF-β stimulation, resulting in decreased c-Myc expression. In addition, AHNAK was also shown to block the inhibitory activities of Smad-7, thus further promoting the action of Smad-3. The outcome of the AHNAK-mediated activities was revealed by cell cycle analysis; overexpression of AHNAK resulted in significant accumulation of cells in the G_0/G_1 phase, and thus in cell cycle arrest. These results were confirmed by showing that the expression of cyclin D1/D2 was decreased, while the expression of $p21^{Waf/Cip}$ and $p27^{Kip1}$ were increased in AHNAK-overexpressing cells. When the authors expanded their findings to a tumour model, they showed that cervical cancer cells overexpressing AHNAK had decreased tumourigenic capabilities and that transformed AHNAK knockout mice displayed increased hyperplasia and reduced regulatory Smad activities. Taken together the authors suggested that, upon stimulation by TGF-β, AHNAK supports the transcription-related functions of regulatory Smads which results in the attenuation of cell cycle progression, ultimately preventing cell proliferation, by regulating c-Myc activity as well as other related factors (Lee et al., 2014). TGF-β

has also been shown to initiate the EMT process and, indeed, a large-scale study has shown before that AHNAK expression is increased in cells undergoing EMT induced by TGF-β (Bhowmick et al., 2001; Keshamouni et al., 2006; Miettinen et al., 1994). The authors of this study did state that AHNAK deficient cells displayed a reduced EMT phenotype and markers in response to TGF-β; however, these experiments were performed in non-tumourigenic HaCaT cells and the authors failed to elaborate on this in light of their other findings. In a recent follow-up study, the group confirmed the suppressive effect of AHNAK on c-Myc expression when they showed that knockdown of AHNAK sufficiently upregulated c-Myc to allow for the generation of induced pluripotent stem cells when co-transfected with other required markers (Lim et al., 2015).

Further supporting the role of AHNAK as a tumour suppressor is a recent study by Sheppard *et al.* (Sheppard et al., 2015). Decreased protein expression was observed in three melanoma cell lines compared with normal melanocytes. This decrease was suggested to be the result of both transcriptional and post-translational control, as only two of the cell lines showed decreased mRNA expression. These findings were further supported by an analysis of data sets from the Gene Expression Omnibus database, which revealed decreased expression in metastatic melanoma. Interestingly, annexin 2 also showed decreased gene and protein expression in the melanoma cell lines and decreased E-cadherin expression followed after AHNAK knockdown. This led the authors to suggest that these proteins form a complex at the cell membrane that is collectively downregulated during the acquisition of a metastatic phenotype, resulting in decreased cellular adhesion (Sheppard et al., 2015).

The findings implicating AHNAK in cancer are intriguing; several studies, both large-scale and specific, support a role in tumour progression and several in tumour suppression. It can however be suggested that AHNAK may indeed function as both and that its functioning is under tight control, most likely by the specific signalling pathways activated in the cell. This seems especially likely if one considers the significant diversity of AHNAK's functions across cell types. As an example, AHNAK has been shown to interact with the Smad proteins on two different occasions, although the upstream signalling molecule differs; BMP in adipocyte differentiation and TGF-β in tumour suppression. In addition, TGF-β itself is known to mediate both pro- (particularly in EMT) and anti-tumour effects and so the signalling molecules controlling TGF-β can indirectly control AHNAK (Heldin et al., 2009).

Recent studies have also suggested that there may be a correlation between AHNAK expression and a tumour cell's response to chemotherapy. One study employed a strategic genome-wide analysis to identify genes whose expression correlates with tumour cell invasion as well as with chemotherapeutic response (Hsu et al., 2013). AHNAK was identified as part of an eight-gene signature capable of predicting a cell line's invasiveness and its response to tubulin-binding and targeted therapies. Specifically, AHNAK showed a positive correlation with invasiveness as well as with targeted therapy response but a negative correlation with tubulin-binding therapy response (Hsu

et al., 2013). AHNAK was also included in a gene signature capable of predicting complete response to neoadjuvant chemoradiotherapy in rectal cancer, although this signature could not be validated against independent data sets (Lopes-Ramos et al., 2015).

A positive correlation between AHNAK and cisplatin resistance has also been reported on two separate occasions. Chen *et al.* reported increased gene expression in four pairs of isogenic cisplatin-resistant and cisplatin-sensitive ovarian cancer cell lines, while Piskareva *et al.* reported increased protein expression in cisplatin-resistant versus parental neuroblastoma cell lines (Cheng et al., 2006; Piskareva et al., 2015). By comparing the mitochondrial and endoplasmic reticulum fractions of two metastatic breast cancer cell lines, Leong *et al.* showed that AHNAK protein expression significantly decreased following induction of apoptosis by a DXR-TRAIL treatment regime (Leong et al., 2012). These results are surprising, since AHNAK is not reported to be present at these intracellular locations. Furthermore, it is evident that further studies are necessary to delineate the expression levels of AHNAK in response to DXR and TRAIL separately, especially since the lethal effect of these two agents are transduced by two different apoptotic pathways (Leong et al., 2012). In contrast, AHNAK protein expression was increased following radiation of breast cancer cells, indicating the AHNAK responds differently based on the therapeutic method (Kim et al., 2015).

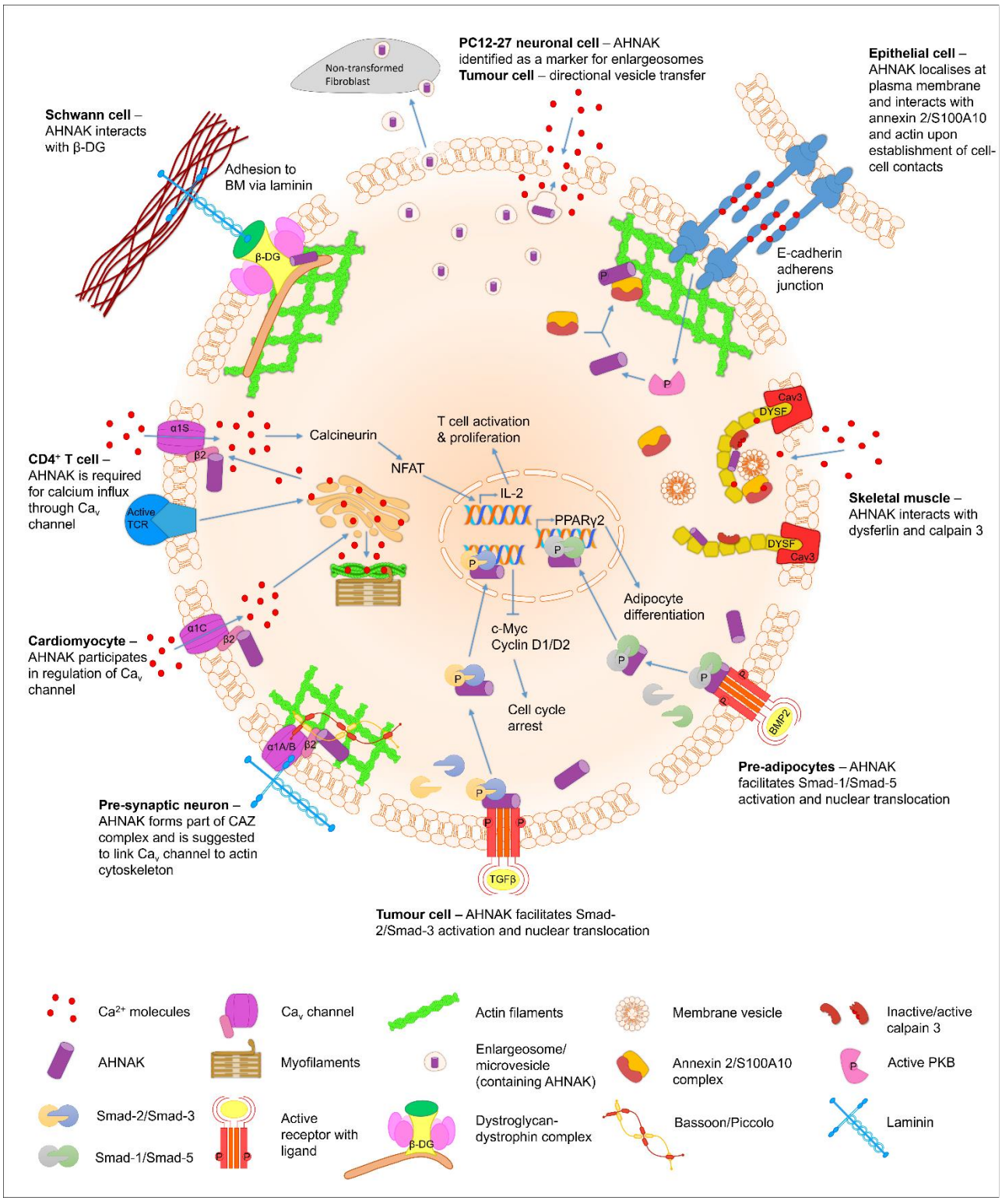

Figure 1.4: Biological processes where AHNAK have been suggested to function. (Davis et al., 2014)

1.6.7 Fitting all the AHNAK-pieces together

Based on the literature reviewed here it is clear that the giant protein AHNAK is involved in a variety of cellular processes and pathways (see fig. 1.4). These processes or pathways are quite distinct

and seem to be related to or dependent on the nature of the cell/tissue type. This would suggest some kind of cell- or tissue-specific regulation. Whether regulation on the transcriptional level takes place is still largely uncertain, however it does seem likely given that specific expression patterns in the CNS and PNS most likely define AHNAK's function in the formation of the BBB and myelination. In terms of post-translational regulation, phosphorylation by two kinases, PKA and Akt, has been reported and further possibilities governed by TGF-β most likely exist. AHNAK's functionality is probably also affected by the reported cleavage by calpain 3. It can, however, be suggested that either cellular calcium levels or calcium-mediated signalling represent a likely regulatory mechanism, especially since the majority of AHNAK's proposed functions involve calcium in some way or another (table 1.3). Translocation of AHNAK has been shown in several studies and it seems likely that its function might also be regulated by its intracellular trafficking. Based on the majority of the studies discussed, it can be suggested that AHNAK probably exerts its function(s) at the plasma membrane since, in most cases, this represents its final destination with redistribution to the cytoplasm observed in abnormal or inactive circumstances. However functional activity at other intracellular locations cannot be ruled out, especially since AHNAK was reported to function in the nucleus on three occasions (Lee et al., 2014; Shin et al., 2015a; Stiff et al., 2004). Understanding the rationale behind AHNAK's intracellular trafficking could assist in explaining its role in disease pathology as changes in localisation have already been observed in dysferlinopathies and mesothelioma.

Table 1.3: Possible correlations between AHNAK and calcium signalling processes

Biological role of AHNAK	***Cell/ tissue type***	***State of cell/process when AHNAK's location is:***		***Role of Ca^{2+} in implicated cellular process associated with AHNAK***	***Reference***
		Cytoplasmic	***Plasma membrane-associated***		
Blood-brain barrier	Endothelial	Absent/damaged	Active/formation	Required for assembly and integrity of adherens and tight junctions, which determines BBB permeability	(Ballabh et al., 2004; Boveri et al., 2006; Gentil et al., 2005)
Cell-cell contacts	Epithelial	Subconfluent	Confluent	Required for formation of E-cadherin-mediated cell-cell contacts	(Benaud et al., 2004; Sussman et al., 2001)
Ca_v channel regulation	Cardiomyocytes	NK	Normal	Influx initiates signalling cascade resulting in contraction	(Bers, 2000; Haase et al., 2005)
Ca_v channel regulation	$CD4^+$ T cells & $CD8^+$ CTL	NK	Active[a]	Influx initiates signalling cascade necessary for proper functioning of cells during immune response	(Matza et al., 2008, 2009)
Enlargeosomes	PC12-27 (Neuronal)	Rest	Active	Signals exocytosis of vesicles	(Chieregatti and Meldolesi, 2005)
Membrane repair	Skeletal muscle tissue	(Regeneration – no proposed function for AHNAK yet)	Normal / physiological sarcolemma injury[b]	Influx initiates repair system	(Huang et al., 2007; Wallace and McNally, 2009)

[a] - AHNAK plasma membrane-associated localisation implied but not shown (see text). [b] - Under normal conditions contraction-induced sarcolemmal injury represents a common physiological event, however in the absence of functioning repair systems it can lead to progressive myonecrosis, representing a pathological event (Wallace and McNally, 2009). NK – not known

Even though the last 12 years have provided valuable clues, AHNAK's exact function remains uncertain. The role suggested for AHNAK in regulating calcium current in cardiomyocytes specifically seems quite promising; however, future research needs to focus on establishing how this translates to other Ca_v channels such as those in T cells where the net effect on the calcium current seems to be the opposite of that in cardiomyocytes. Furthermore, $Ca_v1.2$ channels present in cardiomyocytes can also be found in smooth muscle cells, endocrine cells and neuronal cell bodies, therefore it needs to be investigated whether AHNAK fulfils the same role in these cell types (Catterall et al., 2005). In addition, since AHNAK has now been shown to interact with four different Ca_v channels it also needs to be investigated whether it can bind to other members of the family, which could implicate a role for AHNAK in several other functions.

Also, it is becoming clear that AHNAK often binds and interacts with several different proteins, forming multiprotein complexes. It has been suggested before – and now it seems even more likely – that AHNAK functions as a scaffold protein facilitating the assembly of a different set of proteins required for each of the different cellular processes or pathways described above. For instance, in terms of membrane repair in skeletal muscle, this could include dysferlin, calpain 3 and possibly caveolin 3 and annexin 2/S100A10, while in cell cytoarchitecture, and perhaps also in tumour metastasis, this can include annexin 2/S100A10 and the actin cytoskeleton network. This characteristic is at the heart of AHNAK's proposed roles, serving as a molecular bridge between the diversity of the associated biological processes. Indeed, the only proposed roles where protein interactions for AHNAK are not known are in the formation of the BBB and in enlargeosomes, although it is most likely that their identification is just a matter of time. Both the size and protein structure of AHNAK lends it the unique abilities of facilitating the binding of multiple proteins and providing the necessary support and stability for the assembled complexes (Dempsey et al., 2012; Han and Kursula, 2014). Furthermore, the functional classification of AHNAK as a scaffold protein is supported by the presence of a PDZ domain within its protein structure. PDZ domains are known to facilitate proteins' interactions with carboxyl-terminals of other proteins, other PDZ domains and even lipids; therefore proteins containing these domains are often localised at specific cellular sites where they assist in the assembly of functional units that mediate signalling events or receptor localisation (Nourry et al., 2003).

So far, relatively large clouds of uncertainty still cover the biological role of AHNAK in membrane repair and tumour metastasis, which suggests that a shift in focus towards these areas is needed. Especially in the case of the latter, where the majority of studies so far are gene/protein-expression based, more work is urgently needed in order to determine how and where AHNAK fits into the complex process of tumour metastasis. Regulatory mechanisms are evidently of great importance and identifying the upstream signalling pathways controlling AHNAK will help to clarify its role in tumour progression and metastasis.

Future research should continue to strive to identify novel interacting partners for AHNAK in different models as well as any possible associated regulatory mechanisms. To date, methods such as co-immunoprecipitation and immunocytochemistry and –histochemistry have greatly assisted in describing the molecular environment of AHNAK. Protein, domain and 3D structural analyses coupled with computational bioinformatics can further aid in identifying additional interacting proteins and imaging techniques such as fluorescence resonance energy transfer, correlative light and electron microscopy and the design of fluorochrome-tagged fusion proteins can aid in describing protein interactions under different experimental conditions. Making use of animal models in contextually different but related disease states can also aid in expanding the molecular environment. Targeted mutations and making use of inhibitors acting on specific signalling molecules can help in understanding the role of any associated signalling pathways. In addition, characterising AHNAK2, and perhaps periaxin, can also be of great value.

To assume that the functional roles of AHNAK described here are the only functions would be naïve, although its inherent diversity in terms of biological roles makes identifying new areas worth investigating challenging. However, it is always of utmost importance never to allow a narrow-minded view in research; indeed, taking the diversity of AHNAK into account might prove to be of value when identifying novel areas of investigation. As an example, the fact that AHNAK is phosphorylated by Akt opens up a whole plethora of possibilities since Akt itself is known to be an important mediator of numerous cellular processes. One such process is autophagy and together with the association between AHNAK, MIF, autophagy and cancer mentioned earlier, it might support an endeavour into this area of investigation. Furthermore, with the aim of describing AHNAK's function on a molecular level, one field of research might benefit from the other. For instance, it is has been shown that AHNAK is capable of regulating calcium influx through an interaction with the channel itself and, recently, a new field of research into tumour metastasis has emerged which focuses on impaired calcium signalling and its effect on tumour cell migration and invasion (Prevarskaya et al., 2011). Also, in the study of Benaud *et al.* AHNAK was reported to be involved in the organisation of the actin cytoskeleton while the latter is also important for other cellular processes such as cell migration and mitochondrial transport in neuronal axons (Hollenbeck, 2005; Yamazaki et al., 2005). Lastly, AHNAK is known to interact with the annexin 2/S100A10 complex and, through its ability to bind negatively charged membrane components, annexin 2 has previously been shown to be involved in the organisation of membrane domains as well as in certain endo- and exocytosis events (Gerke et al., 2005). Thus, by keeping an open mind, protein-interaction or co-localisation studies in other fields of research might broaden the scope of AHNAK's involvement even further.

Taken together, even though its exact function remains unclear, the studies published in the last 12 years have contributed significantly to making AHNAK less of a mystery, and hopefully with the aid of further research into the various biological areas, the mystery of AHNAK will be solved in the next decade.

1.7 Problem statement

Cancer is a devastating disease that knowns no prejudice and most importantly, no limits. It is projected that 8.8 million people worldwide died from this disease in 2015, including approximately 54 600 South Africans (Ferlay et al., 2013). Two major problems that are contributing to these alarming statistics is the failure of anti-cancer therapies and the advanced progression of the disease. These two problems stem from two separate cellular processes, namely therapeutic response and cellular invasion and migration respectively, but they are connected in a positive feedback loop.

Even though significant progress has been made in characterising tumours and identifying targetable markers, oncologists are still faced with the burden of trying to overcome the high occurrence of therapeutic failure and resistance. It has become clear that tumour resistance is a multifactorial process and that the scope of each individual resistance mechanism needs to be characterised. This is clear from clinical studies; even though drug efflux via membrane transporters were thought to be a major mechanism of tumour resistance, inhibitors of these transporters, such as verapamil, have not lead to the expected reduction in tumour resistance (Gottesman, 2002). Furthermore, limited treatment options are available for metastatic cancers and oncologists are often forced to prescribe intense treatment regimens consisting of multiple chemotherapeutic drugs. However, resistance is common in these advanced cancers which contributes significantly to the high mortality rates observed with metastatic disease (Chen, 2012; Christofori, 2006).

To be able to effectively modulate the therapeutic response of cancer cells to improve the outcome, the molecular components of the response needs to be identified and understood. This is particularly important in the age of personalised medicine. AHNAK represents a potential novel component in the cellular therapeutic response. Even though several studies have successfully characterised the protein in some of its other functions, information regarding the role of AHNAK in cancer is very limited. Basal AHNAK expression has been compared to the chemotherapeutic sensitivity of certain drugs to identify correlations while a change in AHNAK expression has been reported in only a few studies under different conditions (Hsu et al., 2013; Leong et al., 2012; Silva et al., 2016). Thus, in order to determine whether AHNAK is indeed involved in therapeutic response, a more complete investigation is needed, which serves as the rationale for this study.

This comprehensive research study has a strong basic molecular component, incorporating several clinically relevant aspects. DXR was used as chemotherapeutic treatment since it is a common chemotherapeutic drug used to treat many different cancers, including the chosen model of breast cancer. We also selected treatment doses that would represent both an inefficient treatment outcome, which may potentially promote tumour progression, as well as an effective treatment dose

in order to determine whether AHNAK is associated with a specific type of response. We also chose breast cancer cell lines that show different responses to DXR as well as different capacities for cellular migration.

1.7.1 Hypothesis

We hypothesised that AHNAK is involved in the DXR-response of breast cancer cells, and that AHNAK may thus play a role in the development of DXR resistance.

1.7.2 Aims

We aimed to identify a possible association between AHNAK and DXR-response by:

1. Determining the effect of DXR on AHNAK in breast cancer cells
2. Determining the effect of AHNAK on the DXR-specific response in breast cancer cells

We also aimed to characterise the role of AHNAK in tumour metastasis by:

3. Determining the role of AHNAK in EMT and cellular migration
4. Determining whether a possible link exists between AHNAK, DXR and cellular migration

1.7.3 Objectives

To achieve our aims, we established the following objectives:

1. Investigate the effect of DXR on AHNAK's protein expression and localisation, through Western blot and immunofluorescence experiments respectively, in an *in vitro* model consisting of the MCF-7 and MDA-MB-231 cell lines and in an *in vivo* tumour-bearing mouse model
2. Obtain and generate mammalian expression plasmids containing regions of the human AHNAK protein to facilitate AHNAK overexpression as well as plasmids containing shRNA specifically targeting AHNAK to facilitate AHNAK knockdown
3. Investigate the effect of AHNAK on DXR cytotoxicity and apoptosis induction in MCF-7 and MDA-MB-231 cells following AHNAK knockdown and overexpression
4. Investigate the effect of AHNAK on DXR-induced modulation of the cell cycle in MCF-7 and MDA-MB-231 cells following AHNAK knockdown and overexpression
5. Investigate the effect of AHNAK on cellular migration by assessing EMT marker expression and cellular migration with Western blot and scratch assays respectively, in MCF-7 and MDA-MB-231 cells following AHNAK knockdown and overexpression and DXR treatment

Chapter 2 : Materials and Methods

2.1 Molecular cloning

2.1.1 DNA plasmids and bacterial strain

A GIPZ™ Lentiviral shRNA set (Dharmacon, GE Healthcare) was purchased to facilitate knockdown of AHNAK. The set contains four plasmids that express short hairpin RNA's (shRNA) targeting four different regions of the AHNAK transcript and one plasmid containing a scrambled sequence shRNA (non-targeting, serves as negative control). These plasmids were designated pGIPZ-AHNAK1-4 and pGIPZ-sc. The plasmid set was purchased as glycerol stocks (four frozen stocks of *Escherichia coli* (*E. coli*) cells, each expressing one of the plasmids). Inoculums were prepared by stabbing each glycerol stock with a sterile 200 µl pipette tip and then ejecting the tip into a glass vial containing 5 ml growth media. Incubation of inoculums took place overnight at 37°C with shaking at approximately 200 rpm. Growth media for these cells consisted of low salt lysogeny broth (LB) medium (10 g/l tryptone, 5 g/l yeast extract, 5 g/l NaCl, pH 7) and 100 µg/ml carbenicillin antibiotic (Sigma-Aldrich).

The pM-DY and pC-DY plasmids containing inserts of four repeated units from the CRU domain and the C-terminal domain of AHNAK, respectively, in a pcDNAI/Amp backbone (Invitrogen, Life Technologies) was a kind gift from Prof Silvère van der Maarel (Leiden University Medical Center, Leiden, The Netherlands). The pcDNA3.1 (+) plasmid was a kind gift from Prof Sharon Prince (University of Cape Town, Cape Town, South Africa). Both plasmids contain the ampicillin resistance marker and transformed bacterial cultures were grown in normal LB medium (10 g/l tryptone, 5 g/l yeast extract, 10 g/l NaCl, pH 7) and 100 µg/ml ampicillin.

The *E. coli* strain DH5α, kindly provided by Prof Sharon Prince (University of Cape Town, Cape Town, South Africa), was used in all molecular cloning experiments.

2.1.2 Preparation of competent cells

Competent cells of the DH5α strain were prepared with the $CaCl_2$ method (Seidman et al., 1997). A 5 ml inoculate was grown overnight with shaking at 37°C in LB medium without antibiotics. On the following day, 1 ml of the culture was used to inoculate 100 ml of LB medium, without antibiotics, and the culture was grown for 2-3 hrs until an optical density (OD) of 0.5-0.8 was reached at 595 nm. The culture was then centrifuged at 3000 rpm for 10 min at 4°C. The pellet was gently resuspended in 1 ml of ice-cold 100 mM $CaCl_2$. Another 30 ml of ice-cold 100 mM $CaCl_2$ was added, gently inverted to mix and incubated on ice for 1 hr. After incubation the culture was centrifuged at 3000 rpm for 10 min at 4°C and the pellet was resuspended again in 1 ml ice-cold 100 mM $CaCl_2$.

Aliquots were prepared as glycerol stocks (final concentration 15% glycerol) and were prepared for storage at -80°C through flash freezing in liquid nitrogen.

2.1.3 Bacterial transformation

For transformation of *E. coli* cells with plasmid DNA (pDNA), an aliquot of competent cells were allowed to thaw on ice. Approximately 70-100 ng of pDNA was added to the cells and incubated on ice for 10 min. The cells were heat-shocked at 42°C for 2 min and then transferred immediately onto ice to incubate for another 5 min. A volume of 300 µl LB medium, without antibiotic, was added to the cells and incubated while shaking for 60-90 min at 37°C. After incubation, 50 µl of cells were spread onto LB-agar plates (with the appropriate antibiotics) and allowed to absorb for 10 min at room temperature (RT) before being incubated upside-down overnight at 37°C. The following day, colonies was picked by gently stabbing the colony with a sterile 200 µl pipette tip. The tip was ejected into 5 ml LB medium (with the appropriate antibiotics) and the inoculum was incubated overnight at 37°C with shaking.

2.1.4 Plasmid extraction – miniprep

To identify positive clones, pDNA extractions were performed with the QIAprep® Spin Miniprep Kit (Qiagen®). The kit was used according to the manufacturer's instructions and all steps, including centrifugation steps, were performed at RT. Briefly, 2 ml of an overnight culture was pelleted by centrifugation at 8000 rpm for 3 min and then resuspended in 250 µl of buffer P1 (resuspension buffer). An equal volume of buffer P2 (cell lysis buffer) was added and the culture was gently mixed by inversion 4-6 times. Next, 350 µl of buffer N3 (neutralisation buffer) was added and immediately mixed by inversion 4-6 times. The lysate was centrifuged at 13000 rpm for 10 min. The supernatant was added to the QIAprep® spin column and centrifuged at 13000 rpm for 1 min. The flow-through was discarded and the spin column was washed with 750 µl buffer PE (wash buffer) through centrifugation at 13000 rpm for 1 min. The flow-through was again discarded and the spin column was placed in a centrifuge eppie. Another centrifugation step at 13000 rpm for 1 min was performed to remove any residual wash buffer. Finally, to elute the pDNA, the spin column was placed in a clean centrifuge eppie and 50 µl of nuclease-free water was added to the spin column, allowed to incubate for 1 min and then centrifuged at 13000 rpm for 1 min. The amount of extracted pDNA was quantified with a NanoDrop 2000c (Thermo Scientific) instrument.

2.1.5 Plasmid extraction – maxiprep

For large scale pDNA extractions the PureYield™ Plasmid Maxiprep System (Promega) was used. The kit was used according to the manufacturer's instructions and all steps, including centrifugation

steps, were performed at RT. An overnight culture of 250 ml was pelleted by centrifugation at 5320 rpm for 10 min. The pellet was resuspended in 12 ml Cell Resuspension Solution. An equal volume of the Cell Lysis Solution was added and the culture was mixed by inversion 3-5 times. The culture was allowed to incubate for 3 min before 12 ml Neutralisation Solution was added and mixed by inversion 10-15 times. The lysate was then centrifuged at 6300 rpm for 30 min. For purification and elution, the PureYield™ Clearing Column was placed securely on top of the PureYield™ Maxi Binding Column and then connected to a vacuum pump. One half of the lysate was poured into the PureYield™ Clearing Column and allowed to pass through both columns before the remaining lysate was poured in and allowed to pass through the columns. The vacuum pump was stopped and the PureYield™ Clearing Column discarded, leaving only the PureYield™ Maxi Binding Column connected to the vacuum pump. The column was washed with 5 ml Endotoxin Removal Wash and then with 20 ml Column Wash. The column was then dried for 5 min with the vacuum pump switched on. The column was removed and placed in a clean 50 ml centrifuge tube. Three elution steps was performed. First, a volume of 1 ml nuclease-free water was added to the column, allowed to incubate for 5 min and then centrifuged at 3370 rpm for 5 min. The elute was transferred to a clean centrifuge eppie and the elution step was repeated with 500 µl nuclease-free water and then with 250 µl nuclease-free water. The amount of extracted pDNA was quantified with a NanoDrop 2000c (Thermo Scientific) instrument.

2.1.6 Restriction enzyme digests and ligation reactions

For restriction enzyme digest reactions approximately 1 µg of pDNA was cut with the restriction enzymes *Eco*RI (10 U) and *Bam*HI (20 U) in a double digest reaction (cut with both enzymes at the same time) in 2X Tango buffer, as recommended by the manufacturer (Thermo Scientific). Digests were incubated for 1-3 hrs at 37°C. Digest products were separated on a 0.8% agarose gel at 80 V for between 1.5 and 2.5 hrs.

Ligation reactions with linearised pDNA and inserts was based on the following equation:

$$\frac{100\ ng\ plasmid\ \times kb\ size\ of\ insert}{kb\ size\ of\ plasmid} \times \frac{3}{1} = ng\ of\ insert\ required$$

If necessary, the calculated amount of insert required was adjusted to avoid exceeding the maximum volume of the ligation reaction (20 µl) while still maintaining an insert-vector ratio of 3:1. Ligations were performed in 1X ligation buffer with 1 U of T4 DNA ligase (Promega) and incubated overnight at 4°C.

2.1.7 DNA purification from agarose gels

Purification of pDNA following restriction enzyme digestion and agarose gel electrophoresis was performed with the Wizard® SV Gel and PCR Clean-up System (Promega). The pDNA was obtained from the gel by cutting out the correctly sized band with a clean scalpel and placing it in a centrifuge eppie. The weight of the gel piece was determined by weighing the eppie before and after adding the gel piece. A volume of 10 µl Membrane Binding Solution was added per 10 mg gel piece. The gel mixture was briefly vortexed and incubated at 50-65°C for 10 min or until the gel was completely dissolved. The SV Minicolumn was assembled by placing the column into the Collection Tube. The dissolved gel mixture was then added to the column and incubated for 1 min at RT. The column was centrifuged at 14000 rpm for 1 min and the flow-through was discarded. A volume of 700 µl Membrane Wash Solution was added to the column and centrifuged again at 14000 rpm for 1 min. This step was repeated with 500 µl Membrane Wash Solution and centrifugation for 5 min. The assembly was centrifuged again with the lid open to allow any remaining ethanol from the wash solution to evaporate. The column was transferred to a clean centrifuge eppie and 50 µl nuclease-free water was added to the centre of the column. The column was allowed to incubate for 1 min before centrifuging at 14000 rpm for 1 min. The pDNA elute was saved and the amount of purified pDNA was quantified with a NanoDrop 2000c (Thermo Scientific) instrument.

2.2 Cell lines

Human breast adenocarcinoma cells lines, MCF-7 (non-metastatic, DXR-sensitive) and MDA-MB-231 (metastatic, DXR-resistant), as well as the Cos-7 (monkey kidney fibroblast) cell line, were kindly provided by Prof Sharon Prince (University of Cape Town). The cell lines were cultured in growth medium consisting of Dulbecco's Modified Eagle Medium (DMEM) (Gibco®, ThermoFisher Scientific) supplemented with 10% fetal bovine serum (FBS) (Capricon Scientific) and maintained in humidified incubators set to 37°C and 5% CO_2. Cells were regularly passaged through trypsinisation with 0.25% Trypsin-EDTA (Gibco®, ThermoFisher Scientific). For all experiments, cells were seeded in the appropriate dishes and allowed to settle for either one day (MDA-MB-231) or two days (MCF-7) before beginning the experiment.

2.3 DXR treatments

DXR stock solutions were prepared by resuspending 10 mg doxorubicin hydrochloride (Sigma-Aldrich) in 5.071 ml pure DMEM. Stock solutions were filtered before further use and stored at -20°C. Working solutions were prepared immediately before treatment under sterile conditions with further dilutions made in growth medium. For DXR treatments, the cell monolayer (approximately 80%

confluent) was refreshed with growth media containing the appropriate concentration of DXR for either 24 or 48 hrs.

2.4 MTT assay

MTT assays quantify mitochondrial reductive capacity and were performed as a measure of cell viability. Briefly, the yellow tetrazolium MTT dye is reduced by mitochondrial reductase enzymes to form insoluble purple formazan crystals. These crystals are then dissolved in an acidified alcohol to form a coloured solution. The amount of formazan formed is directly proportional to the amount of metabolically healthy cells. MTT (thiazolyl blue tetrazolium bromide, Sigma-Aldrich) solution was prepared to a concentration of 0.01 g/ml in phosphate-buffered saline (PBS). All MTT assays were performed in 24-well cell culture plates. For each well, media was aspirated and cells were treated with 125 µl MTT solution and 375 µl PBS. After 90 min incubation at 37°C, the MTT was removed and 500 µl of Isopropanol/Triton-X solution (50:1, 1% HCl-Isopropanol to 0.1% Triton-X) was added. The plates were gently shaken for approximately 5 min to allow the crystals to dissolve. Colorimetric readings were measured at a wavelength of 595 nm with an EL800 universal microplate reader (Bio-Tek Instruments Inc.) and the KC Junior software (Bio-Tek Instruments Inc.).

2.5 Transfections

The XtremeGene HP transfection reagent (Roche) was used to transfect pDNA into both the MCF-7 and MDA-MB-231 cell lines. Recommended protocols for each cell line from the manufacturer was used as starting point for optimising a transfection protocol. The pGIPZ-sc plasmid was used during the optimisation process as the pGIPZ plasmids also express turbo-Green Fluorescent Protein (tGFP). Various conditions such as cell confluency, amount of pDNA and the ratio of pDNA:transfection reagent were tested in a 24-well cell culture plate format. Transfection efficiency was determined by visualising tGFP expression with live cell imaging with the 10X objective on the Olympus® Cell^R system and Olympus® IX81 inverted fluorescence microscope (Olympus® Biosystems, GMBH Japan) with a Xenon-Arc burner (Olympus® Biosystems, GMBH Japan) as light source and a UBG triple-bandpass emission filter cube (Chroma).

Once optimised, the following protocols were used in all transfections. For MCF-7 cells, cells were transfected at a confluency of 80-85%. A total of 2 µg pDNA was transfected per well (6-well plate) or 0.5 µg pDNA per well (24-well plate) in a ratio of 1:3 with the transfection reagent, prepared in 200 µl pure DMEM per well (6-well plate) or 50 µl pure DMEM (24-well plate). pDNA-transfection reagent complexes were allowed to incubate for 40 min at RT before adding to wells in a drop-wise

manner. Transfection took place over 48 hours. For MDA-MB-231 cells, cells were transfected at a confluency of 75-80%. A total of 2 µg (6-well plate) or 0.5 µg (24-well plate) pDNA was transfected per well in a ratio of 1:2 with the transfection reagent, prepared in 200 µl or 50 µl pure DMEM, respectively. Complexes were allowed to incubate for 20 min at RT before adding to wells in a drop-wise manner. Transfection took place over 48 hours.

For transfections in 96-well cell culture plates, master-mix complexes of 1 µg per 100 µl pure DMEM were prepared. Each cell line's respective ratio for pDNA-transfection reagent was maintained and were allowed to incubate for their respective incubation times, as described above. The complexes were then aliquoted (10 µl) into the appropriate wells.

Transfection in Cos-7 cells were performed according to the manufacturer's recommended protocol (2 µg pDNA in a ratio of 1:2 with transfection reagent, 30 min incubation for complex formation and 48 hr transfection).

For experiments where DXR treatments followed pDNA transfection, cells were transfected as described above. Following the 48 hr transfection period, media was removed from the wells and replaced with fresh media supplemented with the appropriate concentration of DXR.

2.6 Caspase-Glo® assay

The Caspase-Glo® Assay (Promega) is a luminescent assay that measures the activities of caspase 3 and caspase 7 (markers of apoptosis). The assay employs a luminogenic substrate that is cleaved only by active caspase 3/7 to produce a luminescent signal that is directly proportional to the amount of caspase activity present within the sample. The assay was performed according to manufacturer's instructions and all experiments were performed in 96-well cell culture plates. All steps were performed in reduced light environments as the reagent is light sensitive. The Caspase-Glo® reagent was prepared immediately before use by allowing the components to equilibrate to RT and then mixing the Caspase-Glo® buffer solution with the Caspase-Glo® substrate. Following transfection and treatment of cells, as described in above sections, an equal volume of Caspase-Glo® reagent was added to the media in each well (100 µl). The plates were allowed to incubate for 2 hrs at RT where after the entire contents of the wells were transferred to white-walled 96-well plates. These plates were used for taking the luminescence readings as it prevents cross-over signal from neighbouring wells. Luminescence was measured with a GloMax® 96 Microplate Luminometer (Promega) and the GloMax® software (Promega) using pre-installed settings for the Caspase-Glo® Assay.

2.7 Flow cytometry

Flow cytometry was used to assess cell cycle distribution of a whole cell population. Propidium iodide (PI) was chosen to label cellular DNA. PI intercalates into the major groove of double-stranded DNA and is capable of producing a strong fluorescent signal (excitation at 488 nm, emission at 600 nm). The intensity of the fluorescent signal is directly proportional to the amount of DNA present; thus, cells in G_2/M phase will have double the intensity of cells in G_1 phase while cells in S phase will have intensities between G_1 and G_2/M. Since PI is also capable of binding double-stranded RNA, RNase A was used to degrade cellular RNA and to ensure that only cellular DNA is measured. PI and RNase A was purchased from Sigma. PI stock solutions were prepared to a concentration of 1 mg/ml in PBS and stored at 4°C covered in foil. Working solutions were prepared by further dilution with PBS to a final concentration of 50 µg/ml. Purchased RNase A had a concentration of 29 mg/ml and was stored at -20°C. Working solutions were prepared in PBS to a concentration of 100 µg/ml.

For flow cytometry, experiments were conducted in 6-well cell culture plates. Media was removed from the wells and washed once with warmed PBS. Cells were trypsinised in 500 µl trypsin and triplicate wells of each experimental group were pooled to form one sample. To obtain any remaining cells left in the wells, the wells were rinsed with PBS that was then added to the corresponding sample. The samples were centrifuged at 1750 rpm for 4 min and washed once with PBS. Cells were fixed by resuspending the pellet in ice-cold 70% ethanol while vortexing (to avoid the formation of clumps) and incubated on ice for 1 hr. The cells were then centrifuged at 3000 rpm for 5 min and washed twice with PBS. The pellet was resuspended in 50 µl RNase A and 400 µl PI and the cells were allowed to stain for 30 min at RT. The cells were acquired and processed with the BD FACSDiVa v6.1.3 software on the BD FACSAria™ cell sorter (Benton Dickinson, USA) with a minimum of 10000 events. Results were analysed on ModFit LT software (Verity software house, Inc., ME, USA) to determine the percentage of cells in each phase of the cell cycle (apoptosis peaks were excluded during the analysis).

2.8 Wound healing assay

Wound healing assays, also known as scratch assays, were performed to assess cellular migration. The assay is based on the ability of cells, from a confluent monolayer, to move into and refill a gap over time. In order to exclude the effects of cellular proliferation, cells are treated with a cytostatic agent such as Mitomycin C (MMC). MMC is a powerful DNA crosslinker and inhibits the synthesis of DNA. MMC was purchased from Sigma and prepared to a concentration of 0.4 mg/ml in sterile PBS. Aliquots were covered in foil as MMC is light sensitive and stored at 4°C. The optimal concentration required for inhibition of cellular proliferation was determined in dose response experiments. MCF-7

and MDA-MB-231 cells were seeded onto sterile glass microscope coverslips in 6-well cell culture plates. Cells were treated with a concentration range derived from literature, namely 1 µg/ml, 2 µg/ml, 5 µg/ml and 10 µg/ml (Connolly et al., 2010; Goel and Gude, 2011; Li et al., 2012). After 24 hrs cells were prepared for staining with the nuclear dye Hoechst. The coverslips were removed from the wells and gently washed with PBS. Cells were fixed with 100% ice-cold methanol for 5 min and washed three times with PBS. A volume of 200 µl 10 µg/ml Hoechst 33342 (prepared in PBS, Sigma-Aldrich) were added onto each coverslip and incubated for 10 min to allow for staining of DNA. After staining, the coverslips were washed three times with PBS before being mounted onto a glass microscope slide with Dako Fluorescent Mounting Medium (Dako). Slides were allowed to dry at RT for 1 hr, sealed with clear nail polish and left to dry another hour. Slides were stored at -20°C. For fluorescent imaging, a total of nine images, at random fields of view, per slide were acquired on a Nikon Eclipse E400 microscope equipped with a DS-Fi2 colour digital camera (Nikon, Japan) with a DAPI barrier filter (excitation 340-380 nm, emission 435-483 nm). Nuclear counts were performed as an indication of cellular proliferation and compared to control groups at 0 and 24 hrs.

For wound healing assays experiments were conducted in 6-well cell culture plates. Following 48 hr transfection, three wounds, or scratches, were made in each well with a sterile 200 µl pipette tip. The wells were washed once with warmed PBS to remove debri and refreshed with growth media. Control images at the 0 hr time-point were then taken. Brightfield images were acquired with the 4x objective on an Olympus® Cell^R system and Olympus® IX81 inverted fluorescence microscope (Olympus®, GMBH Japan). The microscope is equipped with a temperature-controlled incubator system that was set to 37°C and a motorized stage control that allows exact positions to be saved and accessed at a later point in time. For each well, the X, Y and Z coordinates of three positions across the three wounds were saved and applied in subsequent time-points. After the first images were acquired, the wells were refreshed with growth media supplemented with the appropriate concentration of DXR and MMC and incubated covered in foil. Since both DXR and MMC are light sensitive, it was decided to start with the treatment immediately after the first images were taken at 0 hr in order to avoid any prolonged exposure to light during the saving of the positions and image acquisition. Subsequent images were taken at 6 hr, 12 hr, 18 hr, and 24 hr time-points.

Analyses of the images acquired during the wound healing assay were performed with ImageJ software. The area of wounds were calculated, in µm, by the software by demarcating the wounded area along the migration front on scaled images.

The following formula was used to calculate the percentage of wound closure:

$$\frac{wound\ area\ at\ (0\ hr) - wound\ area\ (x\ hr)}{wound\ area\ (0\ hr)} \times 100\ = \%\ wound\ closure\ at\ x\ hr$$

The rate of wound closure was determined with the following equation:

$$\frac{\%\ wound\ closure\ (x\ hr)}{x} = rate\ of\ wound\ closure\ at\ x\ hr\ (\%.hr^{-1})$$

2.9 Western blots

2.9.1 Protein harvest from cells

For protein harvest cells were seeded in 6-well cell culture plates. The radioimmunoprecipitation assay (RIPA) buffer (65 mM Tris, 154 mM NaCl, 1% NP-40, 1% Na-deoxycholate, 5 mM EDTA, 5 mM EGTA, 0.1% SDS, pH 7.4) was used for cell lysis. Protease and phosphatase inhibitors (1 µg/ml Aprotinin, 1 µg/ml Leupeptin, 1 mM PMSF, 1 mM Na_3VO_4, 1 mM NaF and 1 µg/ml Benzamidine) were added to the RIPA buffer immediately before use.

Following treatments, media was removed from the wells and the cells were trypsinised with 500 µl trypsin. The trypsinised cells from triplicate wells were pooled into one sample per experimental group. Samples were centrifuged at 2500 rpm for 5 min (MCF-7) or 1500 rpm for 3 min (MDA-MB-231). Pellets were washed twice with PBS before resuspension in 200 µl RIPA buffer and were incubated on ice for 1 hr. Samples were then sonicated at 5 Amps for 10 sec while on ice and stored at -80°C before further processing. This freeze-thaw step was included to further promote the disruption of cellular membranes. When thawed, the foam (produced during sonication) was allowed to settle before centrifuging the samples at 13300 rpm for 2 min to pellet debri. The supernatant was removed and transferred to a clean centrifuge eppie. Extracted protein samples were stored at -80°C.

2.9.2 Protein harvest from tissues

Tumour tissues were allowed to thaw on ice. A volume of 300-700 µl RIPA buffer (with protease and phosphatase inhibitors) was added to the tissue depending on its size. Surgical scissors, cleaned with 100% ethanol, was used to cut tissues into smaller pieces while on ice. The tissue was then homogenised with a KineMatica Polytron™ PT2100 homogeniser (Fisher Scientific) while on ice. The homogeniser was thoroughly cleaned with both distilled water and RIPA buffer between each tissue sample. The homogenised tissues was allowed to incubate on ice for 2 hrs before centrifuging at 12000 rpm for 20 min at 4°C. The supernatant, containing the extracted protein, was carefully removed while avoiding debri and fat and transferred to a clean centrifuged eppie and stored at -80°C.

2.9.3. Bradford assay and sample preparation

The Bradford assay was performed to quantify the amount of extracted protein in a sample. A 5X Bradford stock solution was prepared with 500 mg Coomassie Brilliant Blue G-250 dissolved in 250 ml 95% ethanol and 500 ml phosphoric acid (filled to 1 l with distilled water) and filtered until brown. Working solutions were prepared at 1X concentration and filtered until brown. For each assay, a standard curve was prepared with bovine serum albumin (BSA, Roche) consisting of the following points: 0 µg (blank), 2 µg, 4 µg, 8 µg, 12 µg, 16 µg and 20 µg, in a final volume 100 µl and added to 900 µl Bradford reagent. For each sample, 5 µl was diluted in 95 µl distilled water and 900 µl Bradford reagent. Absorbancies were measured on a Cecil CE 2021 spectrophotometer (Cecil Instruments) set to a wavelength of 595 nm and zeroed with a blank containing 100 µl distilled water and 900 µl Bradford reagent. Dilutions of samples were made in RIPA buffer if readings fell outside the standard curve.

Results from the Bradford assay were used to calculate the volume of sample required to load either 20 µg or 50 µg of total protein. A 3X Laemli's sample buffer was used to prepare protein lysates for Western blots in a ratio of 2:1 (protein:buffer) with final concentrations (1X) of 62.5 mM Tris (pH 6.8), 4% SDS, 10% glycerol, 0.03% bromophenol blue and 5% beta-mercaptoethanol.

2.9.4 Western blots

For Western blot experiments, one general protocol was followed for the majority of proteins while a separate protocol was followed for AHNAK.

2.9.4.1 General Western blot protocol

Western blot samples were prepared with the sample buffer either beforehand (stored at -80°C) or fresh. Before use, samples were mixed by vortex, heated at 95°C for 5 min and pulsed in a benchtop centrifuge. Samples were separated on 12% acrylamide gels prepared with the TGX™ Stain-Free™ FastCast™ Acrylamide Kit (Bio-Rad). These gels contain trihalo compounds that bind tryptophan residues within proteins without causing any changes in protein mobility. Upon exposure to UV light, a reaction takes place that produces a fluorescent signal that can be easily detected on both the acrylamide gel and transferred membrane. This technology allows one to obtain the total protein data for a Western blot which can be used for normalisation. The BLUeye Prestained Protein ladder (Genedirex®) was used as a molecular weight marker and the Tris/Glycine/SDS running buffer (Bio-Rad) was used for gel electrophoresis. Gels were run at 100 V for 10 min and then at 150 V until the dye front reached the bottom of the gel (approximately 90 min). Gels were exposed to UV light for 2.5 min on the ChemiDoc™ MP System (Bio-Rad) to activate the Stain-Free™ properties of the gel. For protein transfer, the Trans-Blot® Turbo™ RTA Mini PVDF Transfer kit (Bio-Rad) was used according the manufacturer's instructions. Briefly, a polyvinylidene fluoride (PVDF) membrane was

activated in 100% methanol for 10 sec before soaking in the supplied transfer buffer for approximately 2 min, along with the blotting papers. Transfer stacks were assembled and the transfer was performed in the Trans-Blot® Turbo Transfer System under the following conditions: 2.5 A, 25 V 10 min. Following protein transfer, membranes were rinsed in 100% methanol and allowed to air-dry to promote fixation of proteins onto membranes. When dry, membranes were re-wetted in 100% methanol and then washed in tris-buffered saline-tween (TBS-T, 20 mM Tris, 137 mM NaCl, pH 7.6, 0.1% Tween-20). Total protein images of membranes were obtained under UV light on the ChemiDoc™ MP System. Membranes were blocked in 5% milk (prepared in TBS-T) for 1 hour. After blocking membranes were washed three times for 5 min each in TBS-T. For primary antibody incubation, membranes were placed inside 50 ml centrifuge tubes containing the primary antibody (prepared in TBS-T, according to table 2.1) and placed on a rotator overnight at 4°C. On the following day, membranes were removed from the primary antibody and washed three times for 5 min each with TBST-T. Membranes were then incubated on secondary antibody (also in 50 ml centrifuge tubes, prepared in TBST-t , table 2.1) for 1 hr on a roller at RT. Membranes were washed three times for 5 min each before being developed on the ChemiDoc™ MP system with the Clarity™ ECL Substrate (Bio-Rad).

Table 2.1: Details of antibodies used in Western blot experiments

Primary Antibody	***Molecular Weight***	***Concentration***	***Secondary Antibody***	***Concentration***
KIS (AHNAK)	~700 kDa	WB: 1:10 000	Anti-rabbit-HRP	1:10 000
		ICC: 1:100	Anti-rabbit-FITC	1:200
		IHC: 1:500	Anti-rabbit-FITC	1:200
V16 (AHNAK)	~700 kDa	WB: 1:200	Anti-goat-HRP	1:10 000
cPARP	89 kDa	WB: 1:1000	Anti-rabbit-HRP	1:10 000
cCasp 7	18 kDa	WB: 1:1000	Anti-rabbit-HRP	1:10 000
E-cadherin	135 kDa	WB: 1:1000	Anti-rabbit-HRP	1:5000 (MDA-MB-231) 1:10 000 (MCF-7)
Vimentin	57 kDa	WB: 1:1000	Anti-rabbit-HRP	1:10 000
Snail	29 kDa	WB: 1:1000	Anti-rabbit-HRP	1:10 000

All primary antibodies, with the exception of KIS, were obtained from Cell Signalling. Secondary anti-rabbit-HRP is also from Cell Signalling, and anti-rabbit-FITC is from Jackson ImmunoResearch. Abbreviations: WB – Western blot; ICC – immunocytochemistry; IHC – immunohistochemistry; HRP – horseradish peroxidase; FITC – fluorescein isothiocyanate.

2.9.4.2. AHNAK Western blot protocol

Western blot samples were prepared fresh for each experiment. Samples were mixed by vortex, heated at 95°C for 5 min and pulsed in a benchtop centrifuge. Samples were separated on 7.5% acrylamide gels prepared with the TGX™ Stain-Free™ FastCast™ Acrylamide Kit (Bio-Rad). The HiMark™ Pre-stained Protein ladder (Thermo Scientific) was used as a molecular weight marker and the Tris/Glycine/SDS running buffer (Bio-Rad) was used for gel electrophoresis. Gels were run at 100 V for 10 min and then at 200 V for 1.5-2 hrs. Gels were exposed to UV light for 2.5 min on the ChemiDoc™ MP System (Bio-Rad) to activate the Stain-Free™ properties of the gel. Proteins were transferred onto Immobilon-FL 0.45 µm PVDF membranes (Merck Millipore) in a wet-transfer system with cold Towbin transfer buffer (25 mM Tris, 192 mM Glycine, 10% methanol, 0.05% SDS). Membranes were activated in 100% methanol for 15 sec before being soaked in transfer buffer for 5 min, along with extra thick blotting paper (Bio-Rad). Transfer stacks were assembled and placed into a tank along with an ice-pack. Proteins were transferred under constant ampere of 200 mAmps for 2 hr. Following protein transfer, membranes were rinsed in 100% methanol and allowed to air-dry to promote fixation of proteins onto membranes. When dry, membranes were re-wetted in 100% methanol and then washed in TBS-T. Total protein images of membranes were obtained under UV light on the ChemiDoc™ MP System. Membranes were blocked in 5% milk (prepared in TBS-T) for 1 hour. After blocking membranes were washed three times for 5 min each in TBS-T. For primary antibody incubation, membranes were placed inside 50 ml centrifuge tubes containing the primary antibody (prepared in TBS-T, according to table 2.1) and placed on a rotator overnight at 4°C. On the following day, membranes were removed from the primary antibody and washed three times for 5 min each with TBST-T. Membranes were then incubated on secondary antibody (also in 50 ml centrifuge tubes, prepared in TBST-t , table 2.1) for 1 hr on a roller at RT. Membranes were washed three times for 5 min each before being developed on the ChemiDoc™ MP system with the Clarity™ ECL Substrate (Bio-Rad). The KIS antibody, designed to recognise the internal CRU region of the AHNAK protein, was a kind gift from Dr Jacques Baudier (French Institute of Health and Medical Research, Paris, France). The V16 antibody, designed to recognise the C-terminal domain of AHNAK, was purchased from Santa Cruz Biotechnology Inc.

2.9.4.3. Analysis of Western blots

The Bio-Rad Image Lab™ software (version 5.1) was used for analyses of Western blot results. The intensities of protein-specific bands were determined and exported to Microsoft Excel. Total protein intensities were also obtained and exported and were used for normalisation of protein-specific results.

2.10 Immunofluorescence

2.10.1 Immunocytochemistry

For immunocytochemistry cells were seeded onto sterile glass microscope coverslips in 6-well cell culture plates. Following treatments the coverslips were removed from the wells and gently washed twice with PBS. Cells were fixed with 100% ice-cold methanol for 5 min and then washed three times with PBS. The coverslips were covered with 200 µl blocking solution (1% BSA, prepared in PBS) and incubated for 1 hr at RT. The blocking solution was then removed and the primary antibody solution was added directly onto the coverslips without washing. All primary antibodies were prepared in blocking solution according to the concentrations listed in table 2.1. Secondary antibody controls (groups not stained with primary antibodies) were covered with PBS. The coverslips were then incubated in a humidified chamber overnight at 4°C. On the following day, the coverslips were washed three times with PBS and then covered with secondary antibody (prepared in blocking solution, table 2.1) and allowed to incubate for 1 hr at RT. The coverslips were washed three times with PBS before being stained with 10 µg/ml Hoechst 33342 for 10 min. Finally, the coverslips were washed three times with PBS and then mounted onto glass microscope slides with Dako Fluorescent Mounting Medium (Dako). The slides were dried for 1 hr at RT, sealed with clear nail polish and then dried for another hour. Slides were stored protected from light at -20°C. Images were acquired with the Zen Imaging software on the Carl Zeiss LSM780 Confocal microscope (Carl Zeiss, Germany) using the 60x oil immersion objective and the 405 nm and 488 nm excitation lasers for Hoechst and FITC, respectively, detected in the emission ranges of 450-490 nm and 520-540 nm, respectively.

2.10.2 Immunohistochemistry

Tumour tissues were sectioned into 10 µm sections with a Leica CM1100 cryostat (Leica Biosystems) and allowed to attach onto glass microscope slides. Three sections of three different internal regions of the tissue were obtained per animal, with a total of three animals per group. Sections were encircled with a water repelling delimiting pen (Dako) to ensure optimal coverage with solutions. Sections were washed once with PBS before being fixed in 100% ice-cold methanol for 5 min. Sections were then washed three times with PBS and blocked in blocking solution (1% BSA, prepared in PBS) for 45 min. After blocking, the solution was removed and sections were covered in primary antibody without washing (prepared in blocking solution, table 2.1). Secondary antibody controls were covered in PBS. Incubation took place overnight in a humidified chamber at 4°C. On the following day, the sections were washed three times with PBS. Secondary antibody (prepared in blocking solution, table 2.1) were added to the sections and incubated for 1 hr at RT. Sections were washed three times in PBS and then stained with 10 µg/ml Hoechst 33342 for 15 min at RT. Lastly, sections were washed again three times with PBS before coverslips were mounted onto the slides with Dako Fluorescent Mounting Medium (Dako). The slides were dried for 1 hr at RT, sealed with clear nail polish and then dried for another hour. Slides were stored protected from light at -20°C.

Images were acquired with the Zen Imaging software on the Carl Zeiss LSM780 Confocal microscope (Carl Zeiss, Germany) using the 60x oil immersion objective and the 405 nm and 488 nm excitation lasers for Hoechst and FITC, respectively, detected in the emission ranges of 450-490 nm and 520-540 nm, respectively.

2.11 *In vivo* study – Tumour-bearing animal model

2.11.1 Mouse strain and tumour cell line

Ethical clearance for the *in vivo* animal study was obtained from the Stellenbosch University Ethical Committee (no. SU-ACUM13-00027). Six-week old female C57BL/6 mice were obtained from the University of Cape Town animal breeding facility. Mice were kept at the Stellenbosch University animal facility under temperature controlled conditions and a reverse dark-light cycle. Standard mouse pellets and tap-water were available ad lib. A total of 48 mice were used in the study and were divided into three groups of 16. The groups were designated as tumour control (TC), low dose DXR (LD-DXR) and high dose DXR (HD-DXR). Mice were routinely monitored and weighed twice a week until experiments were initiated, where after the mice were weighed every second day. Experiments were initiated when mice were 10 weeks old. The murine E0771 breast cancer cell line was used for the establishment of tumours in mice. This particular cell line is syngeneic to the C57BL/6 mice, allowing for a more physiological model.

2.11.2 Tumour establishment

E0771 cells were maintained and cultured under the same conditions described in section 2.2. To prepare the cells for injection, cells were trypsinised, counted and resuspended in Hank's Balanced Salt Solution (HBSS, Sigma-Aldrich). An appropriate amount of cells were added, in a 1:1 ratio, to Corning® Matrigel® Basement Membrane Matrix (9.2 mg/ml protein, BD Biosciences) and kept on ice until injection to prevent the Matrigel® from solidifying. Matrigel® is a basement membrane extract obtained from Engelbreth-Holm-Swarm mouse tumour and consists of a mixture of extracellular matrix proteins such as laminin, collagen IV and heparin sulphate proteoglycans and growth factors such as TGF-β, EGF and FGF. The use of Matrigel® enhances the establishment of tumours and provides an optimal and more physiological environment for tumour growth. A total of 250000 cells in 100 µl was injected subcutaneously with a 23 gauge needle at the fourth mammary fat pad of each mouse. Mice were monitored every second day for tumour growth. Tumour dimensions were obtained with digital callipers where the length was taken as the longest dimension and width as the dimension perpendicular to length. These values were used to calculate tumour volume with the following equation:

$$\frac{length \times width^2}{2} = volume\ (mm^3)$$

2.11.3 DXR treatments

Stock DXR solutions for mice treatments were prepared to a concentration of 2 mg/ml in HBSS. Mice in the LD-DXR group received three doses of 2 mg/kg DXR (cumulative dose of 6 mg/kg) while mice in the HD-DXR group received three doses of 5 mg/kg DXR (cumulative dose of 15 mg/kg). Control mice received injections of HBSS. DXR treatments were initiated once tumours were palpable and were administered every third day by means of intraperitoneal injection with a 25 gauge needle. The weight of the animal was determined before the treatment was prepared. Further dilutions of DXR were performed in HBSS and the finale volume for injection was 100 µl.

2.11.4 Animal sacrifice and tissue harvesting

The endpoint of the study was reached when tumours reached a volume of 400 mm^3. Humane endpoints were established upon the occurrence of bleeding ulcers at the tumour sites or in the event of weight loss larger than 10% of the previous weight measurement. Mice were anaesthetised with isofluorane (Isofor, Safeline Pharmaceuticals) before being sacrificed by means of exsanguination by drawing blood straight from the heart (as part of another study). Tumours were carefully excised and cut into two parts. One part, to be used for Western blot experiments, was snap-frozen in liquid nitrogen and subsequently stored at -80°C. The second part, to be used for immunohistochemistry, was mounted onto a piece of cardboard with tissue freezing medium (Leica Biosystems) and frozen in ice-cold isopentane, and also stored at -80°C.

2.12 Statistical analyses

All statistical analyses were performed in Statistica 13 (Dell Inc.). Data were assessed for normality and the appropriate tests were performed, including paired t-tests, Kaplan-Meier survival analysis, one-and two-way ANOVA's with Fisher's least significance difference test as post hoc test and ANCOVA. Mean values ± standard error of the mean (SEM) are reported and letters were used to indicate significance (i.e. differences in groups with a matching letter are not statistically significant). A value of $p < 0.05$ was taken as the minimum level of significance.

Chapter 3 : Results

3.1 Molecular cloning

3.1.1 Preparation of pGIPZ plasmids

The GIPZ™ Lentiviral shRNA set was selected to contain four plasmids expressing AHNAK-targeting shRNA's and one non-silencing negative control shRNA-expressing plasmid. All four specific shRNA's were confirmed to target both human and mouse AHNAK transcripts by means of sequence alignment. Inoculums of the five pGIPZ plasmids were successfully prepared in competent cells where after maxiprep plasmid extractions were performed to isolate the plasmids. Three elutes, in nuclease-free water, were obtained per plasmid (table 3.1). In all subsequent experiments, pGIPZ-sc were used as the corresponding control.

Table 3.1: pGIPZ plasmid details and Nanodrop results

Plasmid name	***Clone ID***	***Mature antisense sequence***	***Elute***	***[Plasmid] (ng/µl)***	***$A_{260/280}$ value***	***$A_{260/230}$ value***
pGIPZ-AHNAK1	V2LMM_103568	TAAGTCAATATCAGGCATG	1	578.99	1.82	2.00
			2	326.76	1.87	1.92
			3	140.45	1.90	2.10
pGIPZ-AHNAK2	V2LMM_103569	TTAATGTCCACTTTGGGTC	1	819.91	1.85	1.97
			2	410.62	1.87	2.10
			3	229.91	1.88	2.05
pGIPZ-AHNAK3	V2LMM_103572	TTCTAAATCAACTTTAGGC	1	454.17	1.85	2.11
			2	299.12	1.86	2.11
			3	237.88	1.86	2.02
pGIPZ-AHNAK4	V2LMM_103574	TAATGTCCAAGTCGGATCC	1	557.63	1.83	2.06
			2	336.33	1.89	2.10
			3	130.64	1.90	1.97
pGIPZ-sc	Non-silencing	Not supplied	1	435.83	1.86	2.08
			2	291.31	1.88	2.09
			3	127.54	1.87	1.87

3.1.2 Subcloning of AHNAK constructs

The large size of the AHNAK protein does not allow for cloning or transfection of the entire sequence to facilitate overexpression and therefore, constructs coding different regions of the protein were sourced. The pM-DY and pC-DY plasmids (pcDNAI/Amp backbone) expressing regions of the CRU and C-terminal domains of AHNAK (hereafter referred to as the CRU and Cterm constructs, respectively) were generously provided by Prof Silvère van der Maarel (Leiden University Medical Center, Leiden, The Netherlands). The CRU construct covers 510 aa of four complete units of the CRU domain (residue 820-1330) while the Cterm construct corresponds to the entire C-terminal domain (1002 aa) (Huang et al., 2007; Nie et al., 2000). Even though the CRU construct comprises of only four repeated units, the successful use of this particular construct and other similar constructs have been demonstrated in literature (Huang et al., 2007, 2008; Lee et al., 2004).

The plasmids were transformed into competent cells and a diagnostic restriction enzyme digest was performed to verify the presence of a construct with the expected size (fig. 3.1). An empty pcDNAI/Amp plasmid has a size of 4.8 kb while the CRU and Cterm constructs has sizes of 1530 bp and 3006 bp, respectively. The identity of the constructs were also confirmed with sequencing (performed by Inqaba Biotec).

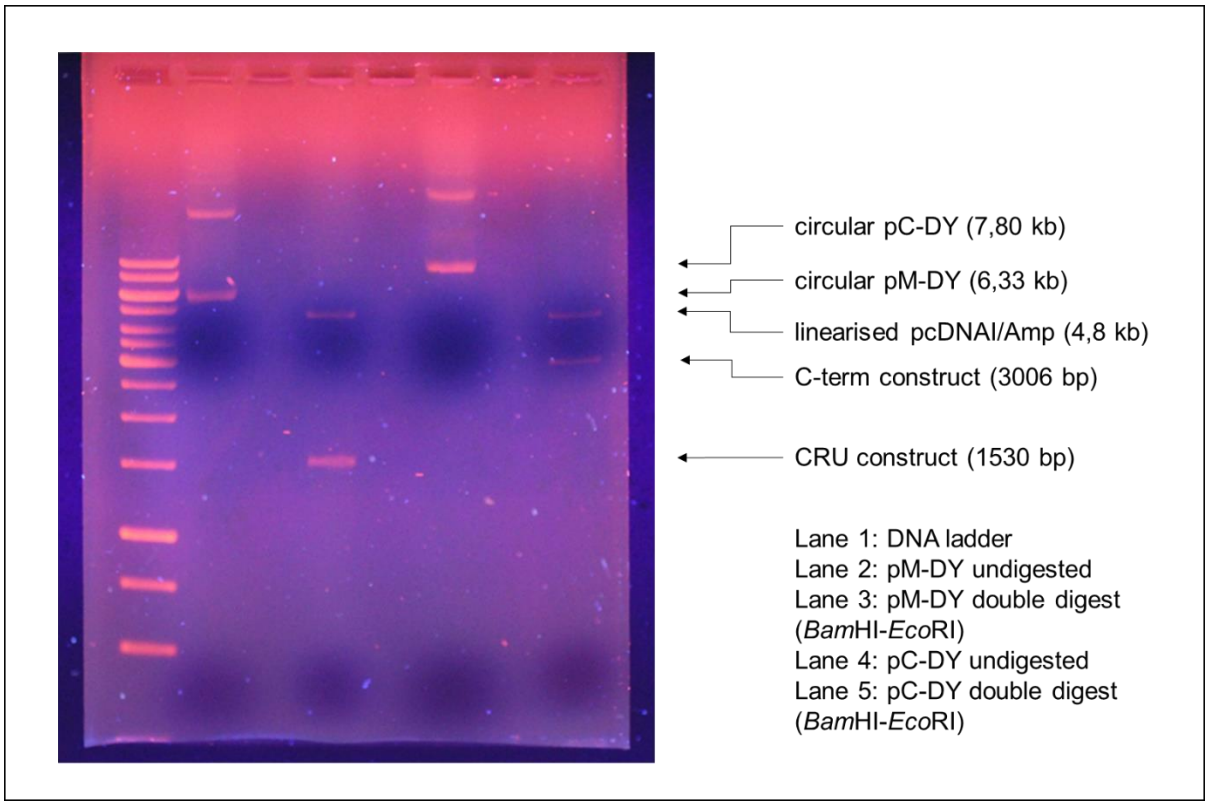

Figure 3.1: Agarose gel showing results from diagnostic restriction enzyme digest. Plasmids contained inserts of the expected size and could be successfully digested with the *Bam*HI and *Eco*RI restriction enzymes

Following positive identification, the CRU and Cterm constructs were subcloned into the pcDNA3.1 (+) plasmid (fig. 3.2). Plasmids pM-DY and pC-DY were digested with *Bam*HI and *Eco*RI restriction enzymes and the products were separated on an agarose gel. Digested CRU and Cterm constructs were then purified from the gel and ligated into linearised pcDNA3.1 (also with *Bam*HI and *Eco*RI). Ligations were transformed into competent cells and colonies were picked to prepare inoculums. The pDNA was extracted with a miniprep extraction and diagnostic restriction enzyme digests with *Bam*HI and *Eco*RI enzymes were performed to screen for positive clones. A digest reaction with a positive clone showed the expected sizes of a linearised pcDNA3.1 plasmid (5.4 kb) and the CRU and Cterm constructs (1530 bp and 3006 bp, respectively). Once identified, a maxiprep plasmid extraction was performed to obtain sufficient pDNA for further experiments (fig. 3.2, table 3.2).

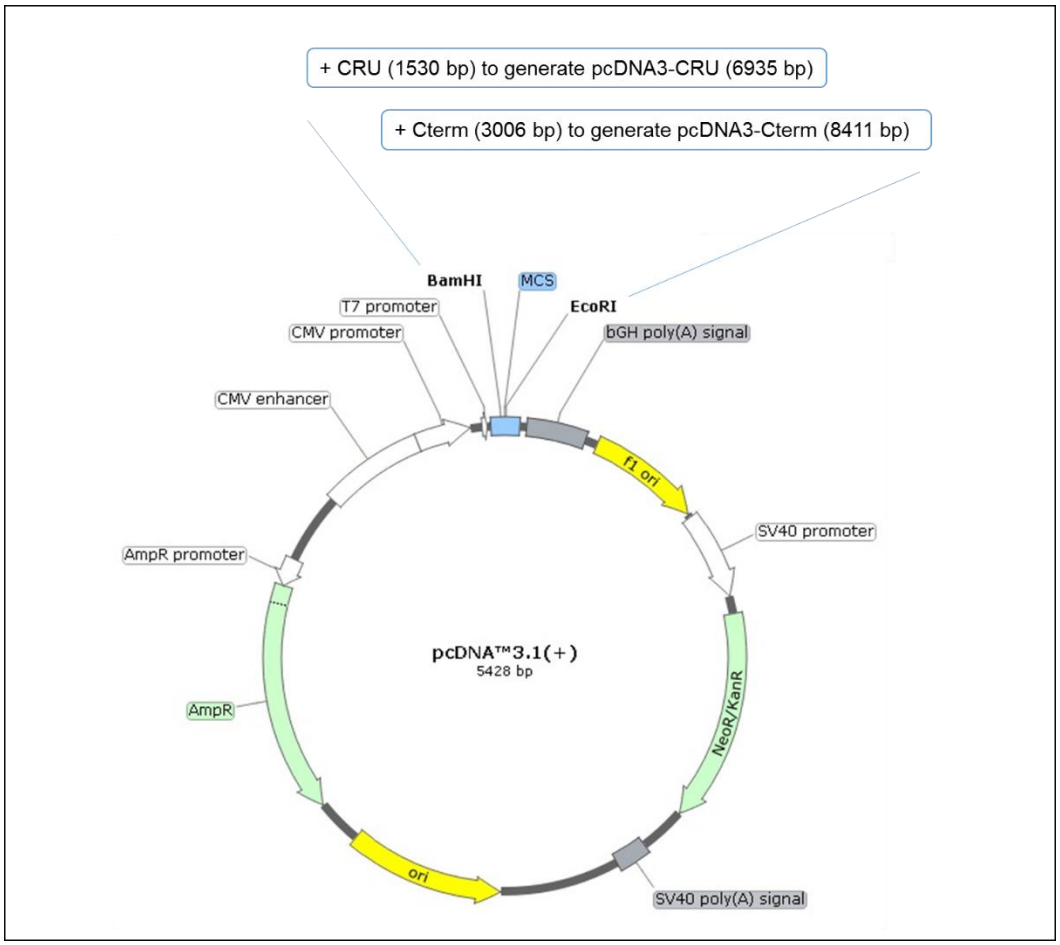

Figure 3.2: Schematic representation of generation of pcDNA3-CRU and pcDNA3-Cterm plasmids. Plasmid map generated with SnapGene™.

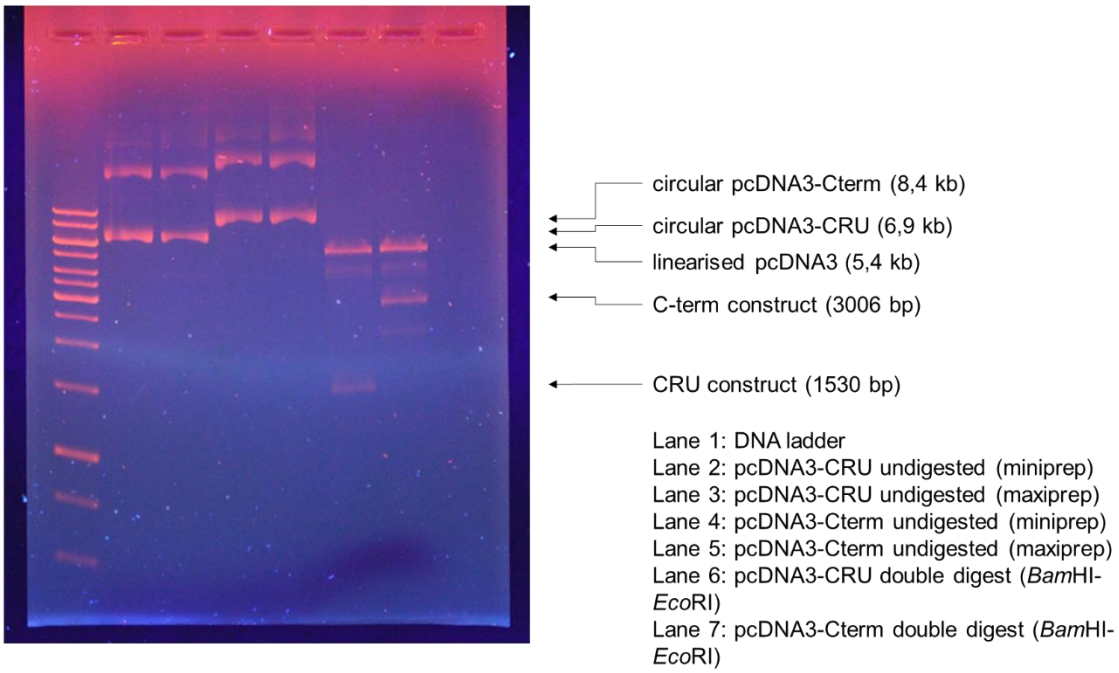

Figure 3.3: Agarose gel showing results of diagnostic restriction enzyme digest. Positive clones with successful ligation of the CRU and Cterm constructs into pcDNA3.1 were identified

Table 3.2: Results for maxiprepped plasmid DNA of subcloned constructs

Plasmid name	***Elute***	***[Plasmid] (ng/µl)***	***$A_{260/280}$ value***	***$A_{260/230}$ value***
pcDNA3-CRU	1	784.48	1.90	2.29
	2	263.45	1.91	2.24
	3	532.80	1.83	2.13
pcDNA3-Cterm	1	820.30	1.90	2.27
	2	357.42	1.90	2.20
	3	165.83	1.90	2.17

To determine whether the subcloned CRU and Cterm constructs could be successfully expressed from the generated plasmids, transfections in an easily transfectable cell line, Cos-7, were performed. Protein extractions were prepared followed by Western blot experiments where the expression of the CRU and Cterm proteins were assessed. Based on literature, the CRU construct produces a protein of 98 kDa while the Cterm construct generates a 170 kDa protein (Nie et al., 2000). Only the KIS AHNAK antibody (recognising CRU) could be sourced from another research group while a commercial antibody designed to recognise the C-terminal domain (AHNAK V16) was purchased. Western blot experiments revealed bands of an appropriate size for CRU in both pM-DY and pcDNA3-CRU transfected samples (fig. 3.4). No bands were however observed for the Cterm

constructs (pC-DY or pcDNA3-Cterm transfected samples), possibly indicating that the purchased antibody was not capable of recognising the Cterm protein. At this point it was decided to continue with only the CRU construct. In all subsequent experiments, an empty pcDNA3.1 plasmid was used as the corresponding control.

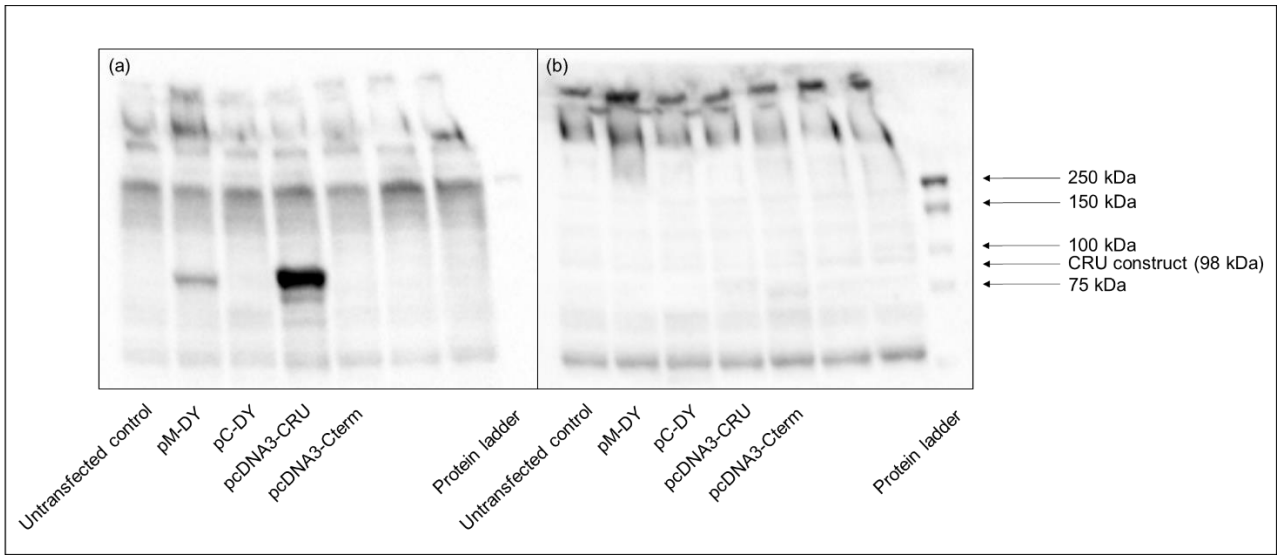

Figure 3.4: Upper section of Western blot for CRU and Cterm constructs in transfected Cos-7 cells. The membrane was probed with the AHNAK KIS antibody to detect the CRU construct (a), stripped and then re-probed with the AHNAK V-16 antibody to detect the Cterm construct (b).

3.2 The effects of DXR on AHNAK

3.2.1 Comparing the MCF-7 and MDA-MB-231 breast cancer cell lines

Dose response curves for the MCF-7 and MDA-MB-231 cells lines were established following treatment with DXR for 24 hrs in order to identify concentrations suitable for further experiments. Mean values of treatments were compared to control values and the results were analysed with a one-way ANOVA. Compared to the control group (100% ± 1.42%) no significant loss of viability was observed in the MCF-7 cells at a dose of 0.1 µM, while further increasing concentrations resulted in significant cell death with viabilities of only 45.09% ± 1.27% ($p < 0.0001$) and 35.51% ± 1.61% ($p < 0.0001$) at higher doses of 5 µM and 10 µM respectively (fig. 3.5). In the MDA-MB-231 cells a significant loss of viability was observed only at the highest dose of 10 µM (80.75% ± 2.08%, $p < 0.0001$) when compared to the control group (100% ± 1.53%) (fig. 3.6). The viability of the 0.1 µM group (106.22% ± 5.10%) was however significantly different from the viability of the 2.5 µM (97.04% ± 1.91%, $p < 0.05$), 5 µM (96.53 ± 2.05%, $p < 0.05$) and 10 µM (80.75% ± 2.08%, $p < 0.0001$) groups. For further experiments, a low dose of 0.1 µM and a high dose of 5 µM was selected. These results also confirm the sensitivity of MCF-7 cells and the resistance of MDA-MB-231 cells to DXR.

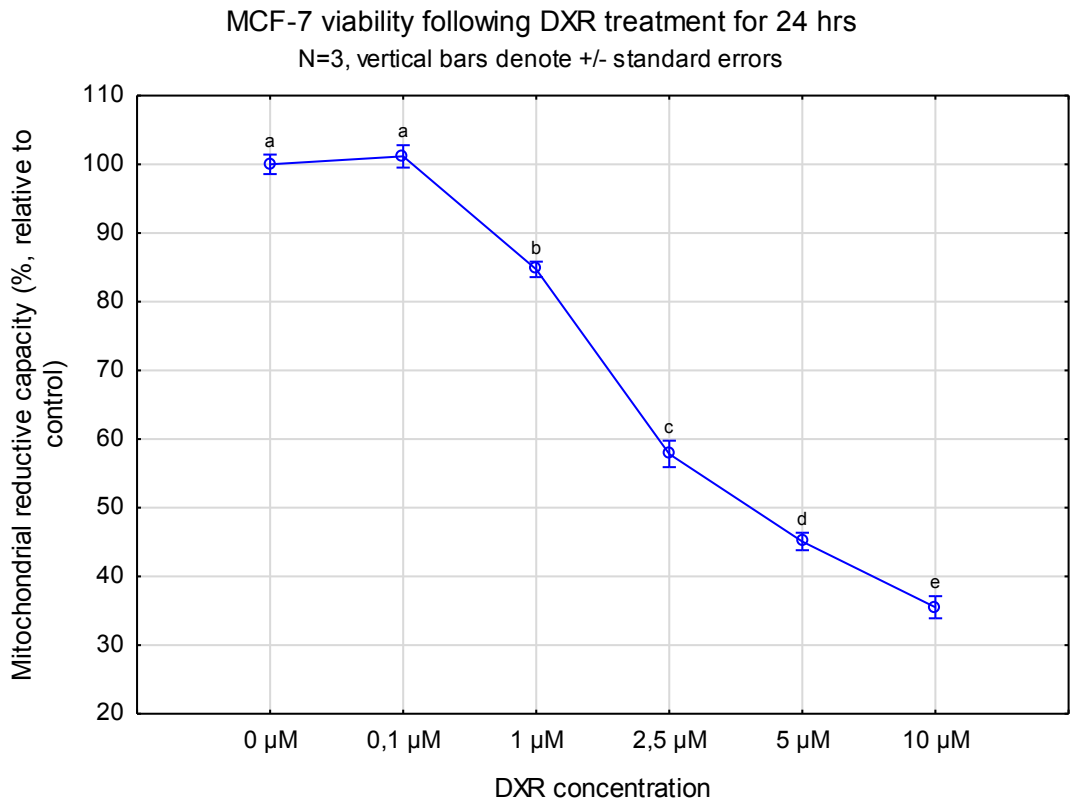

Figure 3.5: Mitochondrial reductive capacity, as a measure of cell viability, of MCF-7 cells following DXR dose response experiments.

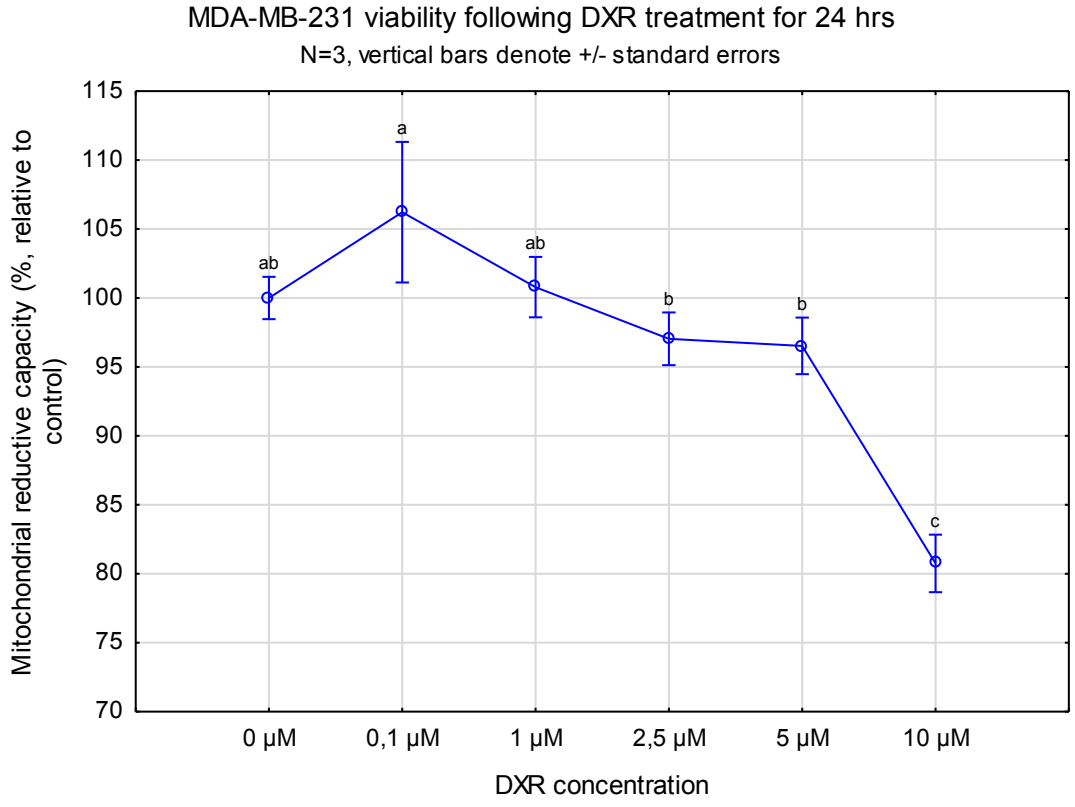

Figure 3.6: Mitochondrial reductive capacity, as a measure of cell viability, for MDA-MB-231 cells following DXR dose response experiments.

To further describe the cytotoxic effect of DXR on these cells protein extractions were performed following treatment with a range of DXR concentrations for 24 hrs. Western blot experiments were performed to assess the protein expression of two markers of apoptosis, namely cleaved caspase 7 (cCasp7) and cleaved PARP (cPARP). Casp7 is an executioner caspase that is active in its cleaved form in the final commitment stage of apoptosis while PARP is a DNA repair protein that is inactivated through cleavage by, amongst others, cCasp7 (Germain et al., 1999). cCasp7 was used as a marker instead of cCasp3, another commonly used caspase marker, as MCF-7 cells are known to not express cCasp3 (Jänicke et al., 1998; Yang et al., 2007). An increase in the cleaved form of both these markers indicate increased levels of apoptosis. After processing data from multiple Western blots, the arbitrary values were analysed with an one-way ANOVA. As expected, DXR treatment induced significant increases in both apoptotic markers in MCF-7 cells at concentrations that resulted in significant cell death (fig. 3.7). Compared to control (0.31 ± 0.05), cPARP showed a significant increase in expression at the 2.5 µM (0.97 ± 0.16, $p < 0.01$) and 5 µM (1.14 ± 0.29, $p < 0.01$) groups (fig. 3.8). Similarly, cCasp7 showed a significant increase in expression at 5 µM when compared to the control group (2.43 ± 0.27 vs. 3.70 ± 0.45, $p < 0.001$) (fig. 3.9). In contrast, significant decreases in protein expression of the apoptotic markers were observed in the MDA-MB-231 cells (fig. 3.7). Compared to the control group cPARP showed a significant decrease at 5 µM DXR (1.29 ± 0.24 vs. 1.01 ± 0.19, $p < 0.05$) (fig. 3.10). Significant decreases in cCasp7 expression was observed even at the lower doses of 0.1 µM (0.35 ± 0.03, $p < 0.0001$), 1 µM (0.31 ± 0.03, $p < 0.0001$) and 2.5 µM (0.34 ± 0.03, $p < 0.0001$) DXR when compared to the control (0.55 ± 0.08) (fig. 3.11). At the high dose of 5 µM cCasp7 did show an increase in expression (0.45 ± 0.05, $p < 0.05$ when compared to lower doses) although it remained significantly lower than the control ($p < 0.05$).

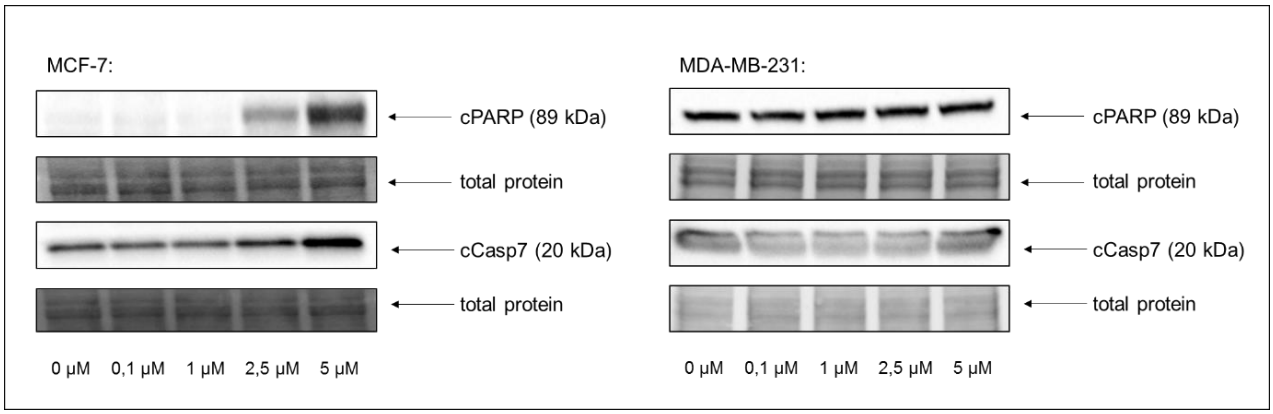

Figure 3.7: Representative images of Western blot experiments for cPARP and cCasp7 in MCF-7 and MDA-MB-231 cells following 24 hrs treatment with increasing concentrations of DXR.

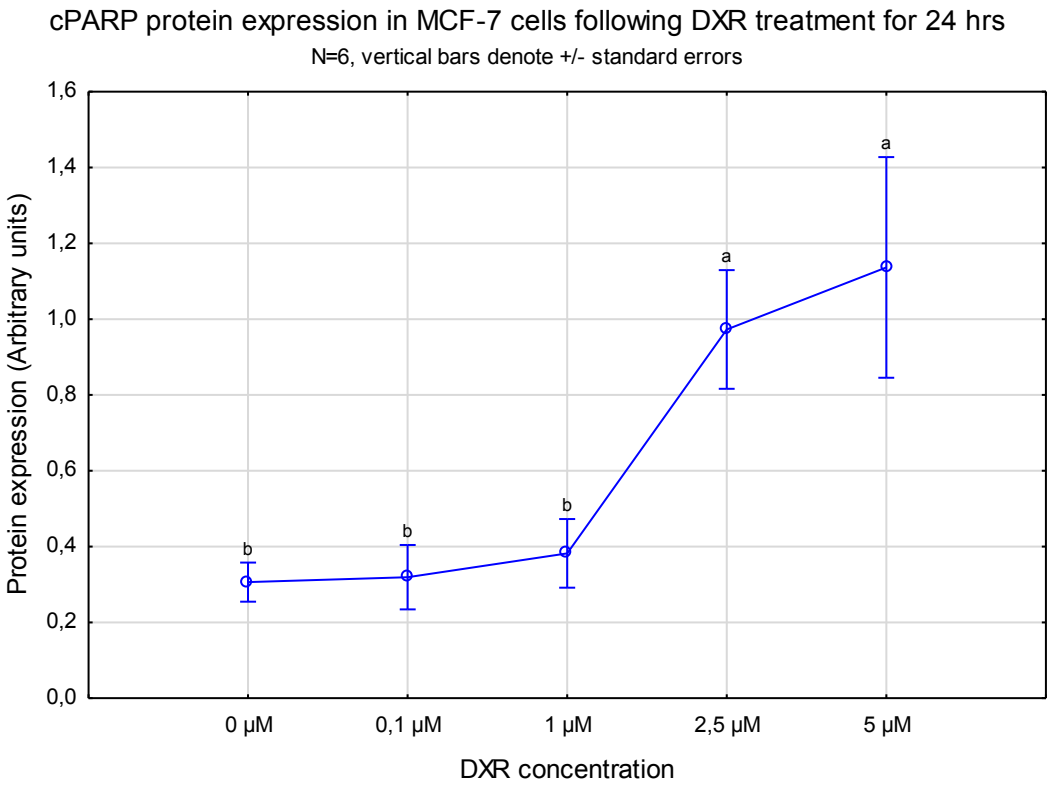

Figure 3.8: Increased cPARP protein expression in MCF-7 cells following 24 hr DXR treatment.

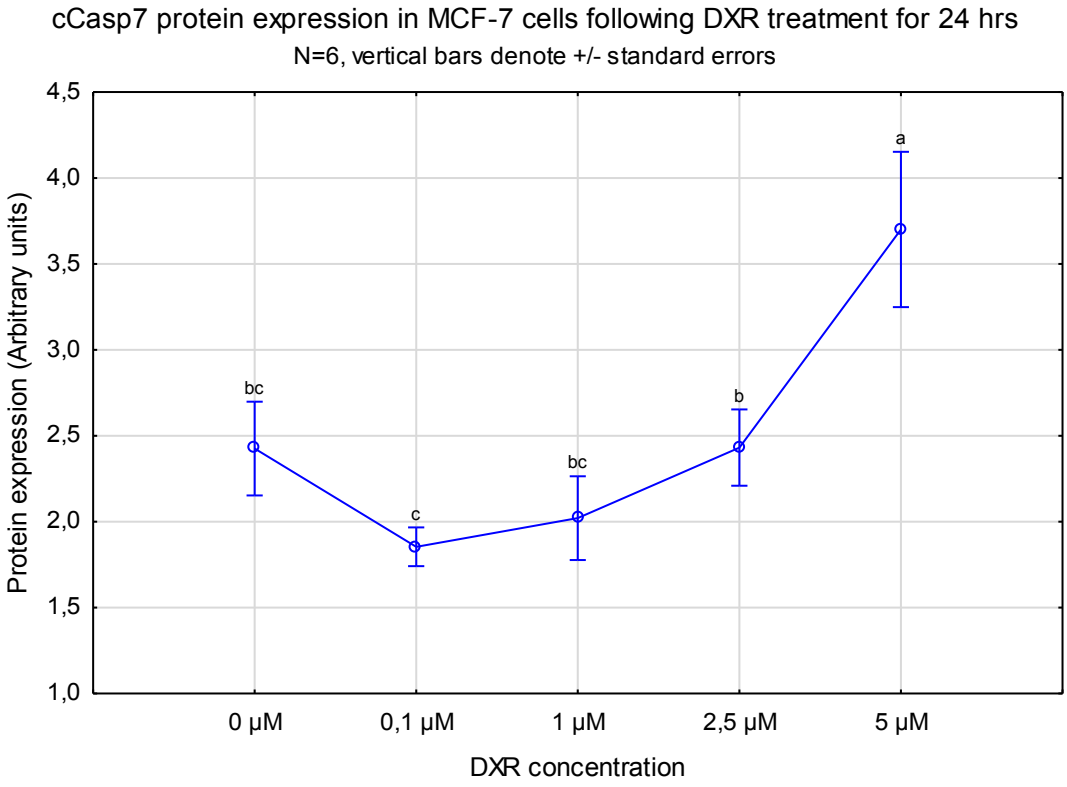

Figure 3.9: Increased cCasp7 protein expression in MCF-7 cells following 24 hr DXR treatment.

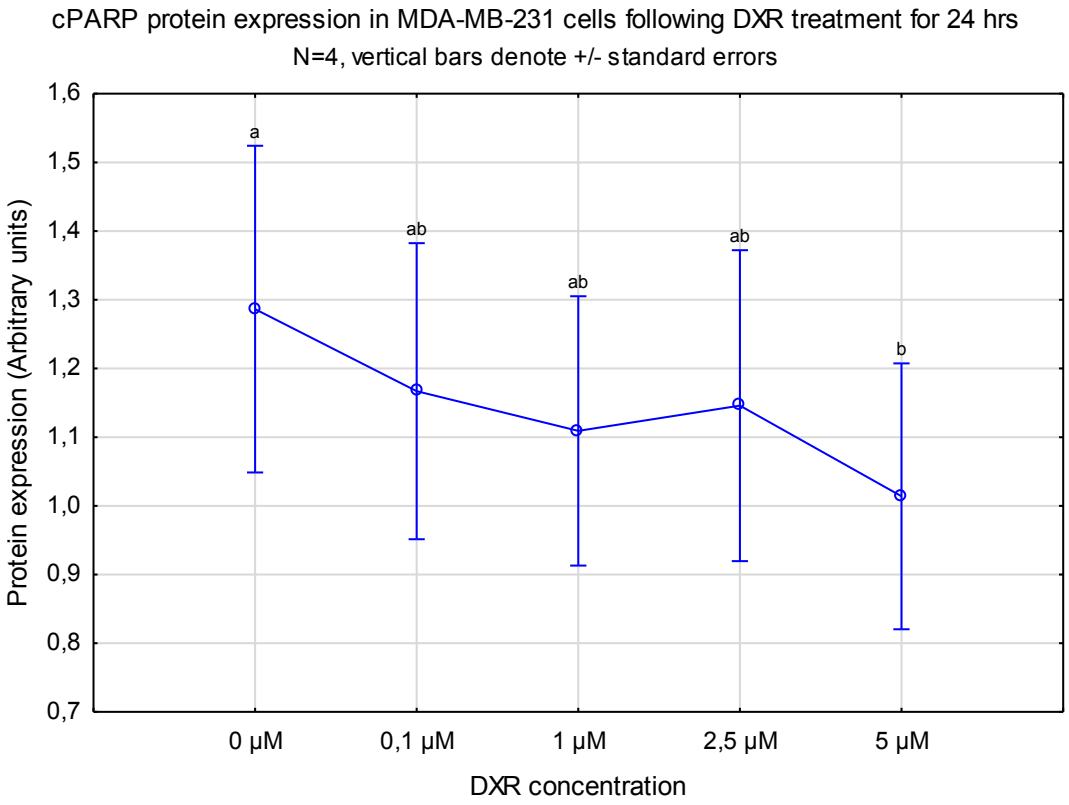

Figure 3.10: Decreased cPARP protein expression in MDA-MB-231 cells following 24 hr DXR treatment.

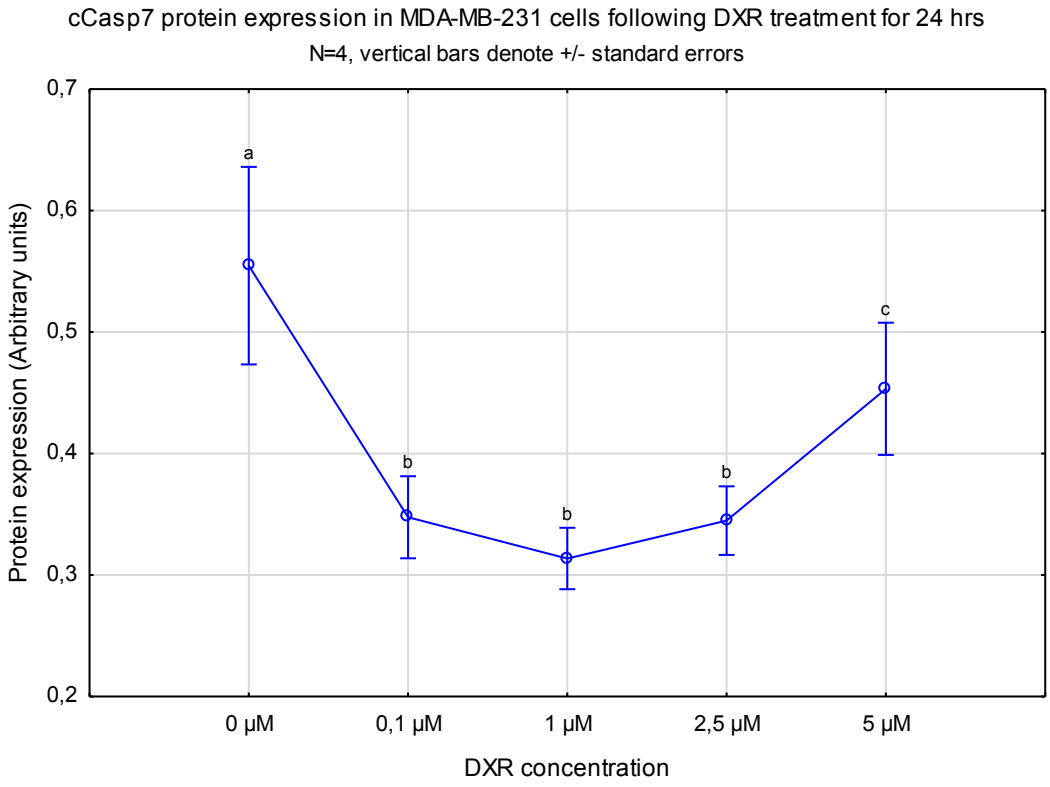

Figure 3.11: Decreased cCasp7 protein expression in MDA-MB-231 cells following 24 hr DXR treatment.

Basal levels of AHNAK protein expression were also compared between the MCF-7 and MDA-MB-231 cell lines. Western blot experiments revealed that AHNAK is expressed at much higher levels in MDA-MB-231 cells than in MCF-7 cells (fig 3.12).

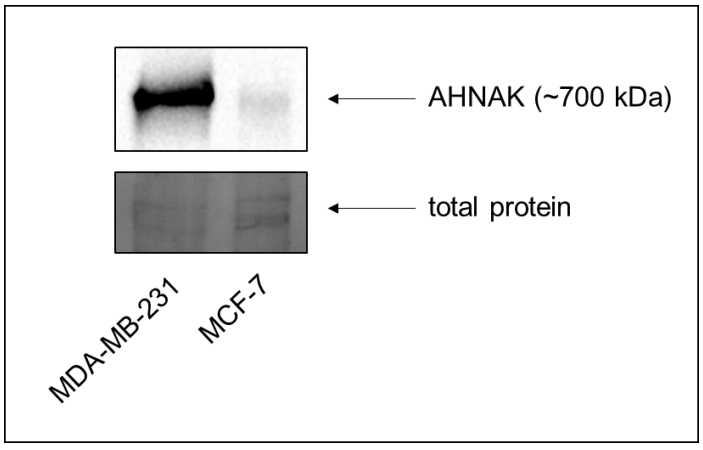

Figure 3.12: Representative image of Western blot experiments for basal AHNAK protein expression in MCF-7 and MDA-MB-231 cells.

3.2.2 DXR affects AHNAK protein expression *in vitro*

Western blot experiments were performed to asses AHNAK protein expression following treatment with DXR for 24 hrs. MCF-7 cells displayed a drastic decrease in AHNAK protein expression across all concentrations of DXR when compared to the control (1.81 ± 0.39 vs. 0.35 ± 0.14 at 0.1 μM, vs. 0.24 ± 0.11 at 1 μM, vs. 0.19 ± 0.09 at 2.5 μM, vs. 0.35 ± 0.13 at 5 μM, all $p < 0.0001$) (fig. 3.13, 3.14). In contrast, MDA-MB-231 cells displayed dose-dependent changes in protein expression (fig. 3.13). Increased protein expression was observed at the low dose of 0.1 μM when compared to the control (2.45 ± 0.31 vs. 2.97 ± 0.40, $p < 0.05$), followed by a decreasing trend in expression with increasing DXR concentrations which reached significance at the high dose of 5 μM (1.56 ± 0.29, $p < 0.01$) (fig. 3.15). AHNAK protein expression was also assessed after 48 hrs of treatment with low and high doses of DXR. MCF-7 cells again exhibited decreased levels of AHNAK protein expression at the low dose of 0.1 μM DXR (1.25 ± 0.26 vs. 0.62 ± 0.10, $p < 0.05$, analysed with t-test) (fig. 3.13, 3.16), however protein expression in these cells could not be assessed following a high dose treatment of 5 μM DXR as the treatment results in almost complete loss of cell viability. In MDA-MB-231 cells, AHNAK protein expression again increased at 0.1 μM (1.65 ± 0.27 vs. 2.42 ± 0.42, $p < 0.01$) and decreased at 5 μM, although this decrease was no longer statistically significant when compared to the control group (fig. 3.13, 3.17).

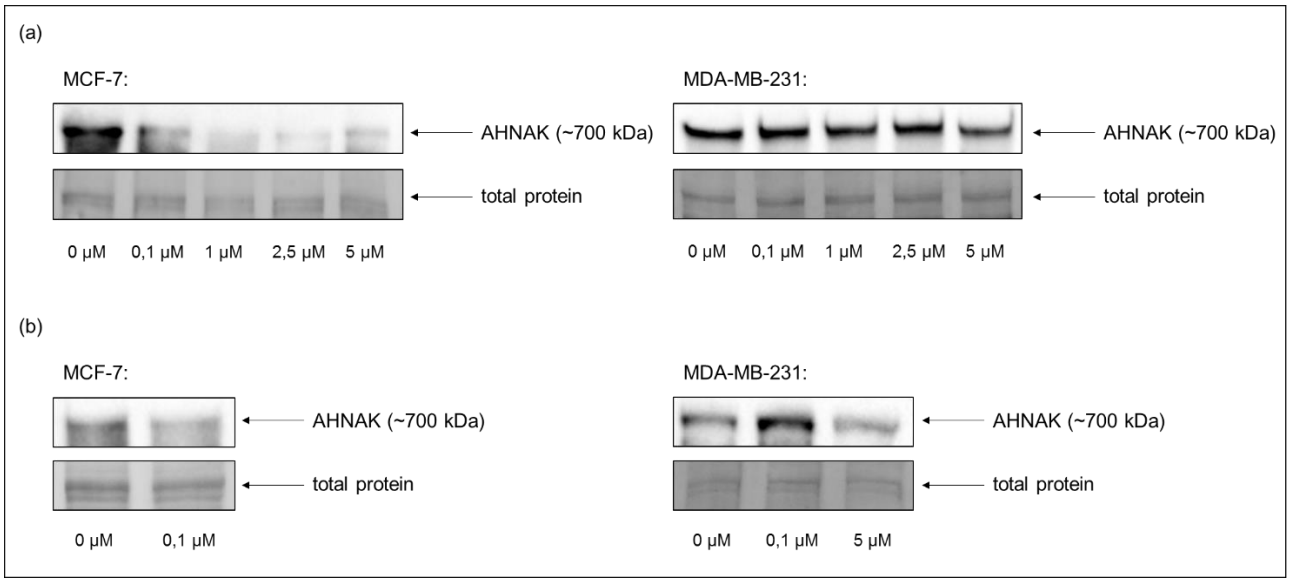

Figure 3.13: Representative images of Western blot experiments for AHNAK following 24 hr (a) and 48 hr (b) DXR treatment in MCF-7 and MDA-MB-231 cells.

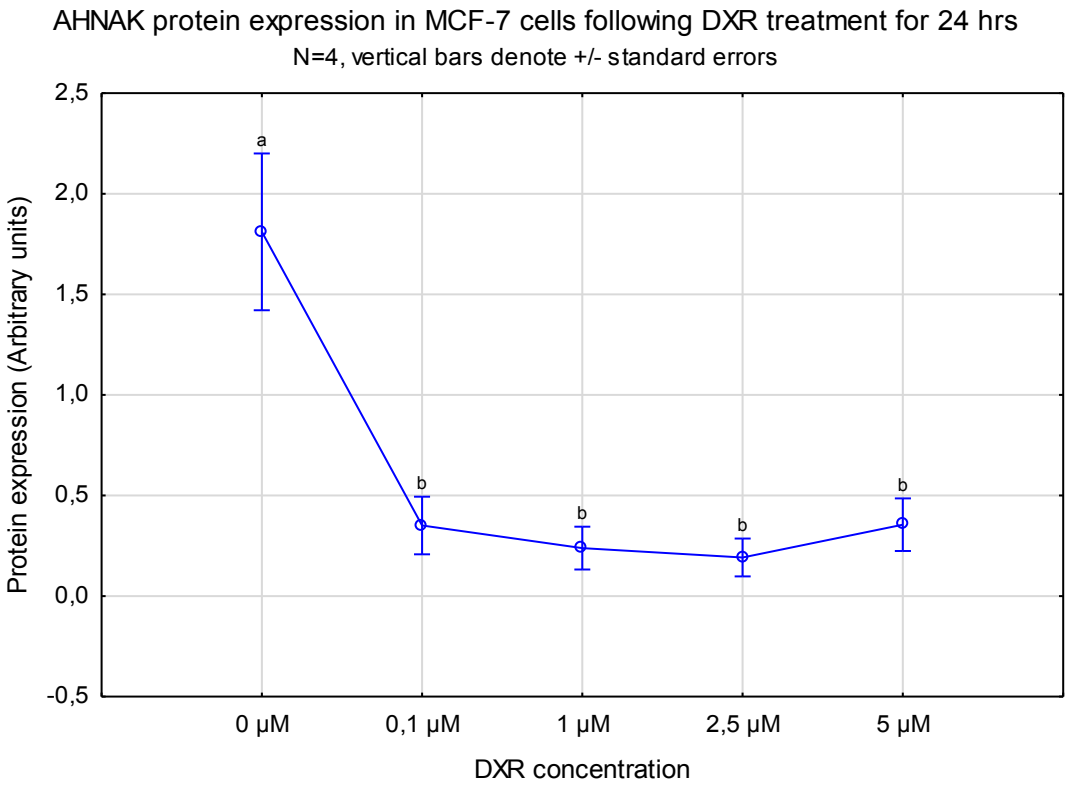

Figure 3.14: Drastic decrease in AHNAK protein expression in MCF-7 cells following 24 hr DXR treatment.

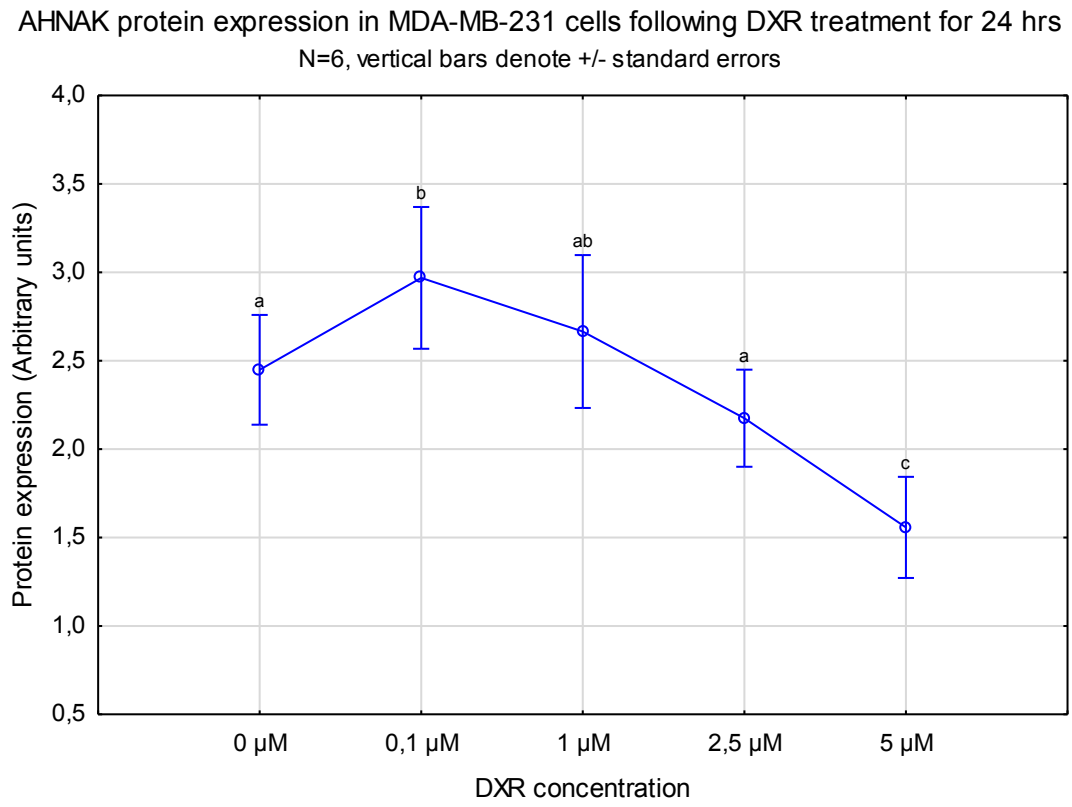

Figure 3.15: Dose-dependent changes in AHNAK protein expression in MDA-MB-231 cells following 24 hr DXR treatment.

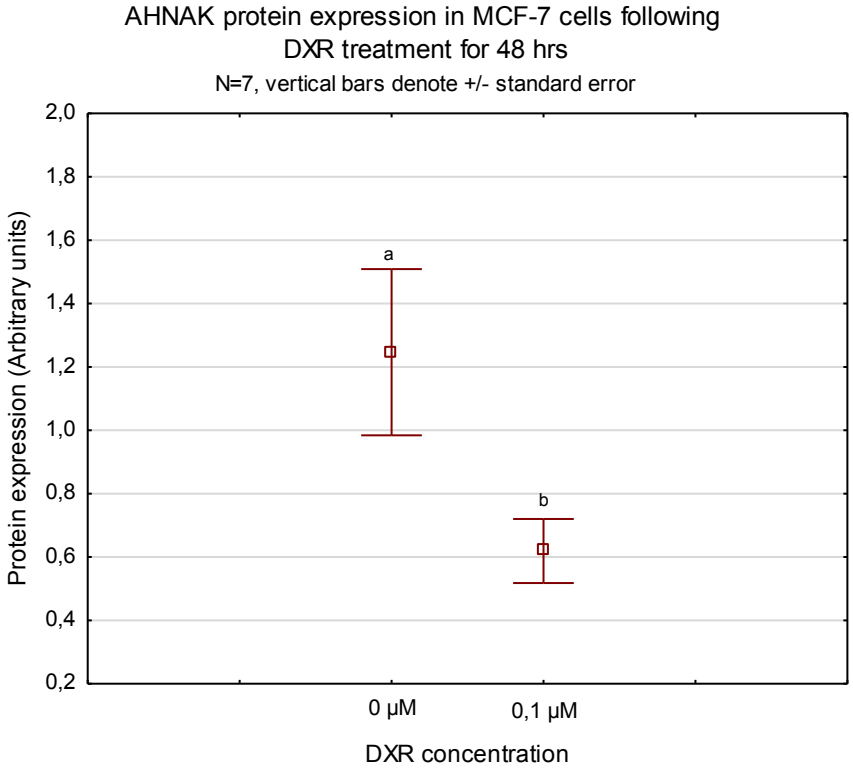

Figure 3.16: Decrease in AHNAK protein expression in MCF-7 cells following 48 hr DXR treatment.

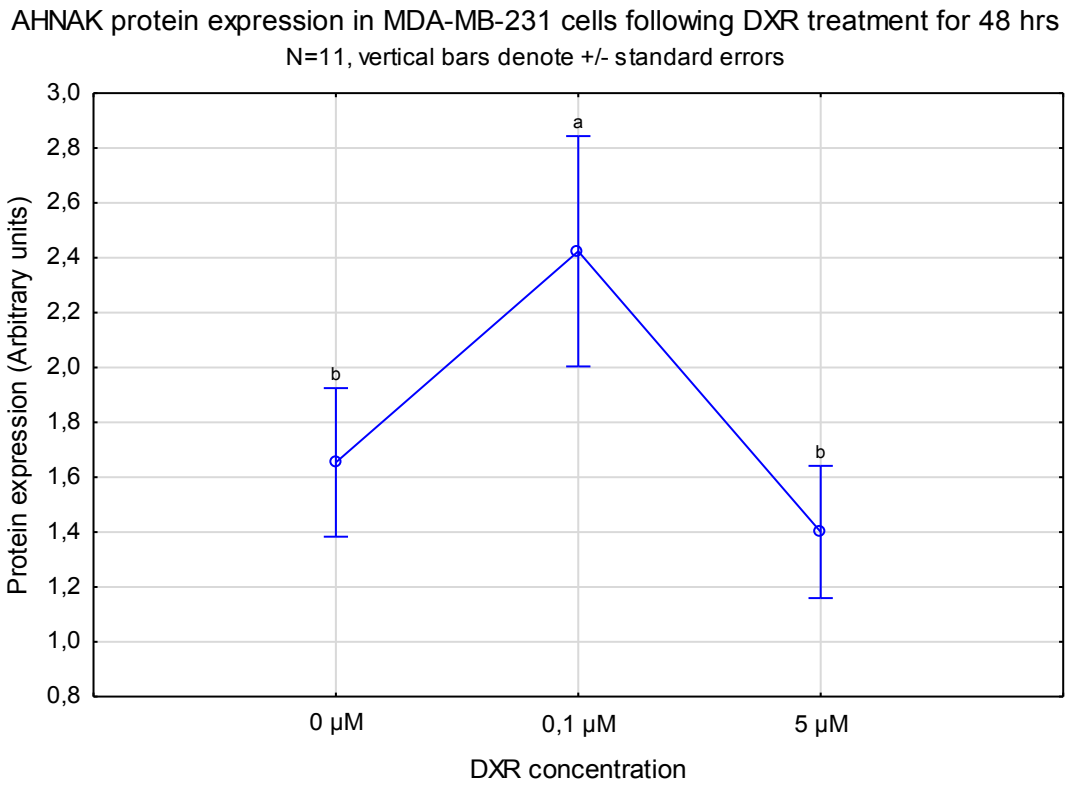

Figure 3.17: Dose-dependent changes in AHNAK protein expression in MDA-MB-231 cells following 48 hr DXR treatment.

3.2.3 DXR does not affect the intracellular localisation of AHNAK

Immunocytochemistry experiments were performed to determine whether DXR treatment can affect the intracellular localisation of AHNAK. Cells were seeded on microscope coverslips and treated with a low and high dose of DXR for 24 and 48 hrs. Following treatment the cells were processed for immunostaining where AHNAK was labelled with FITC (green) and nuclear DNA was stained with Hoechst (blue). All images were assessed qualitatively for changes in localisation only. AHNAK displayed a diffuse cytoplasmic localisation in subconfluent or single MCF-7 cells whereas confluent or cells that have formed cell-cell contacts also displayed an intense plasma membrane-associated pattern (fig. 3.18). No changes in localisation was however observed when cells were treated with DXR for 24 or 48 hrs (a high dose treatment was again not performed for 48 hrs due to almost complete cell death). In MDA-MB-231 cells AHNAK displayed a cytoplasmic localisation with a network-like appearance (fig. 3.19). Localised areas of intense signal were also observed at the plasma membrane as well as what appears to be vesicle-like structures. These structures were mostly located in close proximity to the nucleus. Again, no changes in localisation was observed when cells were treated with DXR for 24 or 48 hrs.

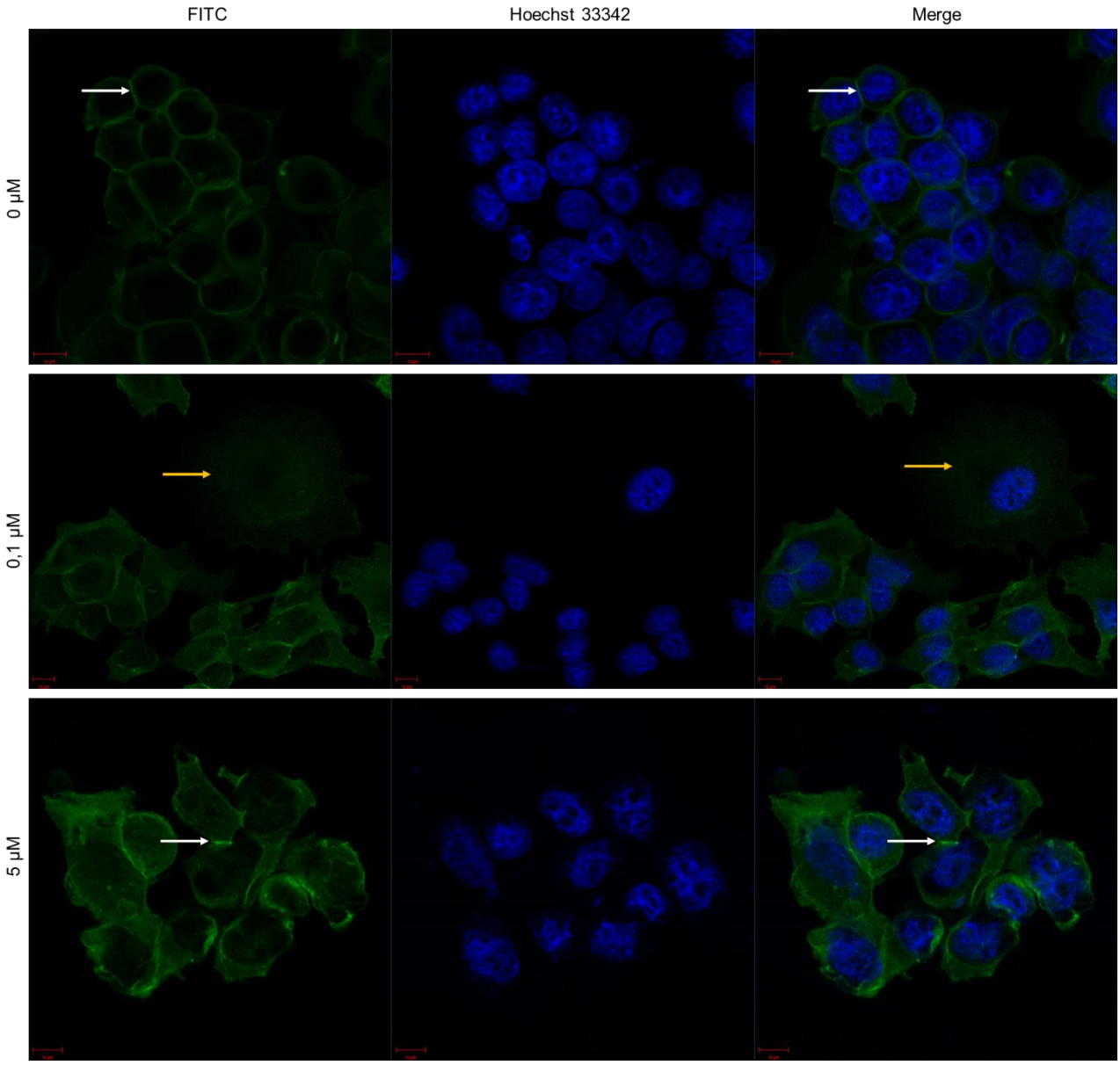

Figure 3.18: Representative immunofluorescent images of AHNAK intracellular localisation in MCF-7 cells following 24 hr DXR treatment. FITC – AHNAK; Hoechst 33342 – nuclear DNA; yellow arrows – cytoplasmic staining of single cell; white arrows – intense plasma membrane-associated staining of cells with cell-cell contacts. Scale = 10 µm, 60x objective.

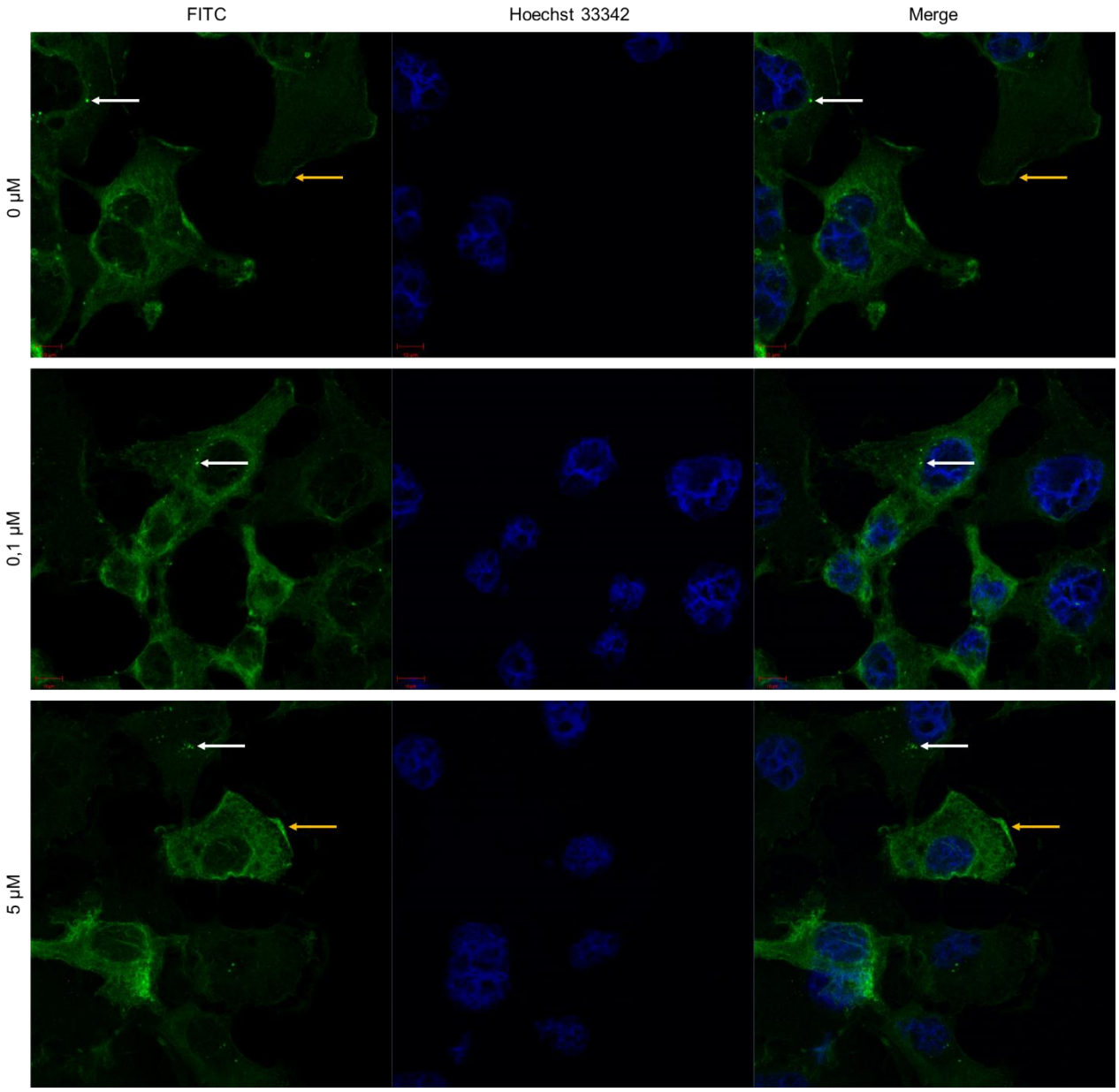

Figure 3.19: Representative immunofluorescent images of AHNAK intracellular localisation in MDA-MB-231 cells following 24 hr DXR treatment. FITC – AHNAK; Hoechst 33342 – nuclear DNA; yellow arrows – localised areas of intense signal at plasma membrane; white arrows – localised areas of intense signal in vesicle structures. Scale = 10 µm, 60x objective.

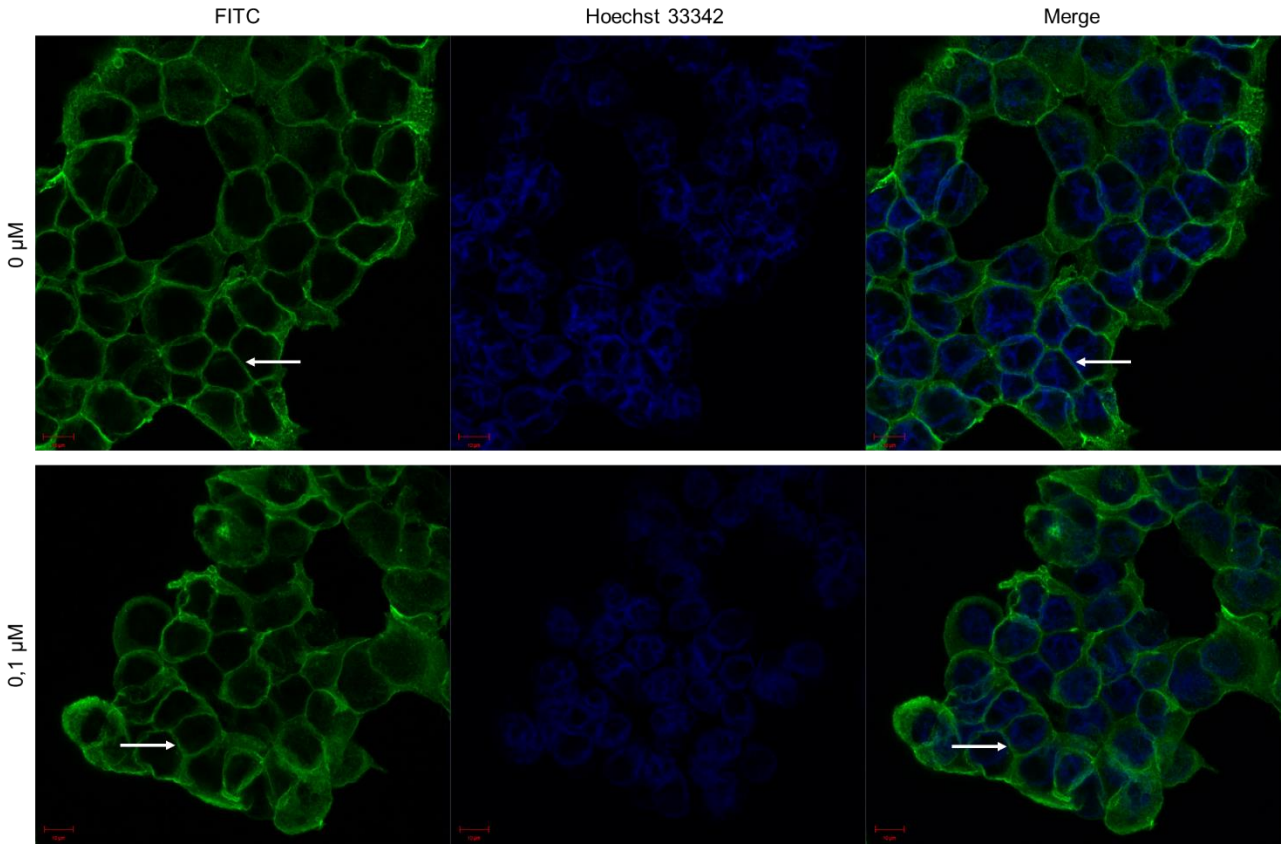

Figure 3.20: Representative immunofluorescent images of AHNAK intracellular localisation in MCF-7 cells following 48 hr DXR treatment. FITC – AHNAK; Hoechst 33342 – nuclear DNA; white arrows – localised areas of intense signal in cells with cell-cell contacts. Scale = 10 µm, 60x objective.

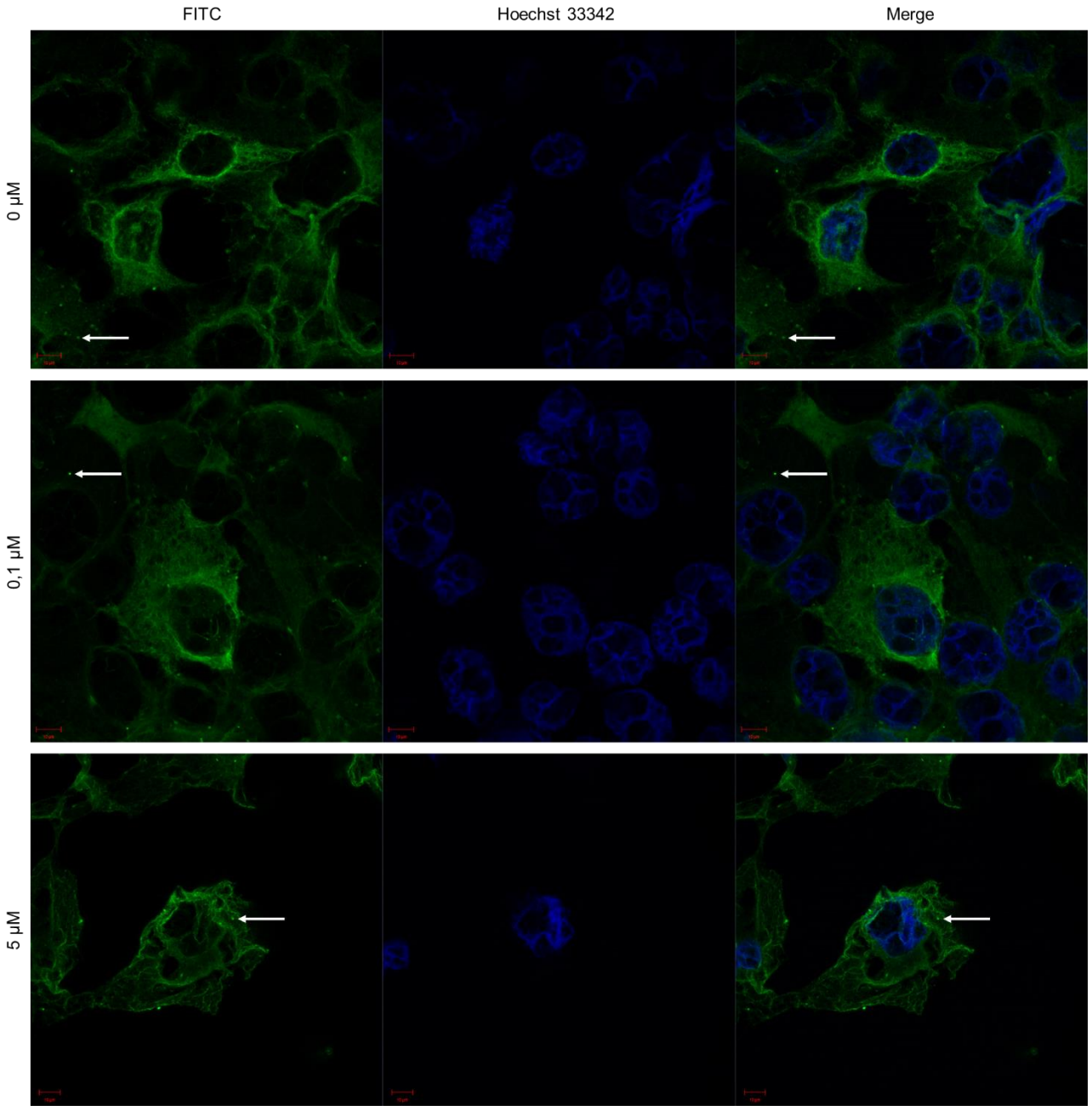

Figure 3.21: Representative immunofluorescent images of AHNAK intracellular localisation in MDA-MB-231 cells following 48 hr DXR treatment. FITC – AHNAK; Hoechst 33342 – nuclear DNA; white arrows – localised intense signal in vesicle-like structures. Scale = 10 µm, 60x objective.

3.2.4 DXR affects AHNAK protein expression *in vivo*

A tumour-bearing mouse model was established to determine the effects of DXR treatment on AHNAK *in vivo*. A total of 48 female C57BL/6 mice was injected with the syngeneic E0771 breast cancer cell line in a 1:1 suspension of HBSS and Matrigel®. Upon the appearance of palpable tumours, the mice received either a low dose (6 mg/kg cumulative, LD-DXR group, N=16) or a high dose (15 mg/kg cumulative, HD-DXR group, N=16) while injections with the treatment vehicle was administered to the control animals (TC group, N=15). Mice were sacrificed once tumours reached a volume of 400 mm^3.

Tumour formation in the mice were successful as 47 out of the 48 mice (97.92%) formed tumours. In addition, palpable tumours were observed from as early as day six after tumour cell injection and by day nine all 47 mice had formed palpable tumours. Measurements of animal weight and tumour volume were taken every second day. Individual animal weights remained mostly steady throughout the study and even though the average weight of the HD-DXR group revealed a decreasing trend, no mice had suffered a weight loss of more than 10% (fig. 3.22). Tumours grew rapidly in size over a period of 30 days with the first group of mice sacrificed 18 days after injection and the last group on day 30 (fig. 3.23). Humane endpoints were enforced for four mice that had developed bleeding ulcers and were thus sacrificed before the required tumour volume was achieved.

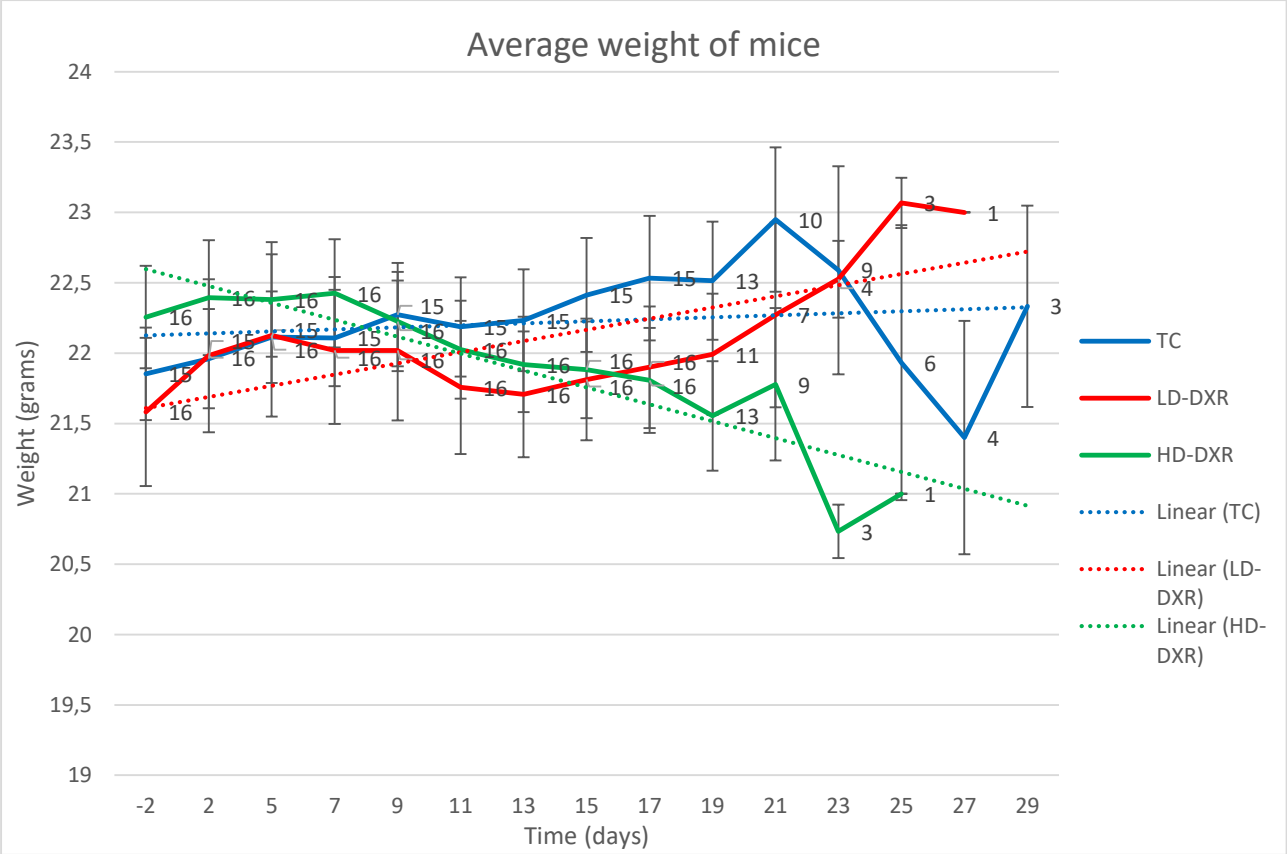

Figure 3.22: Average weight of mice throughout study. Values next to data points indicate number of mice in group on day of measurement. Results presented as mean ± SEM with linear trendlines.

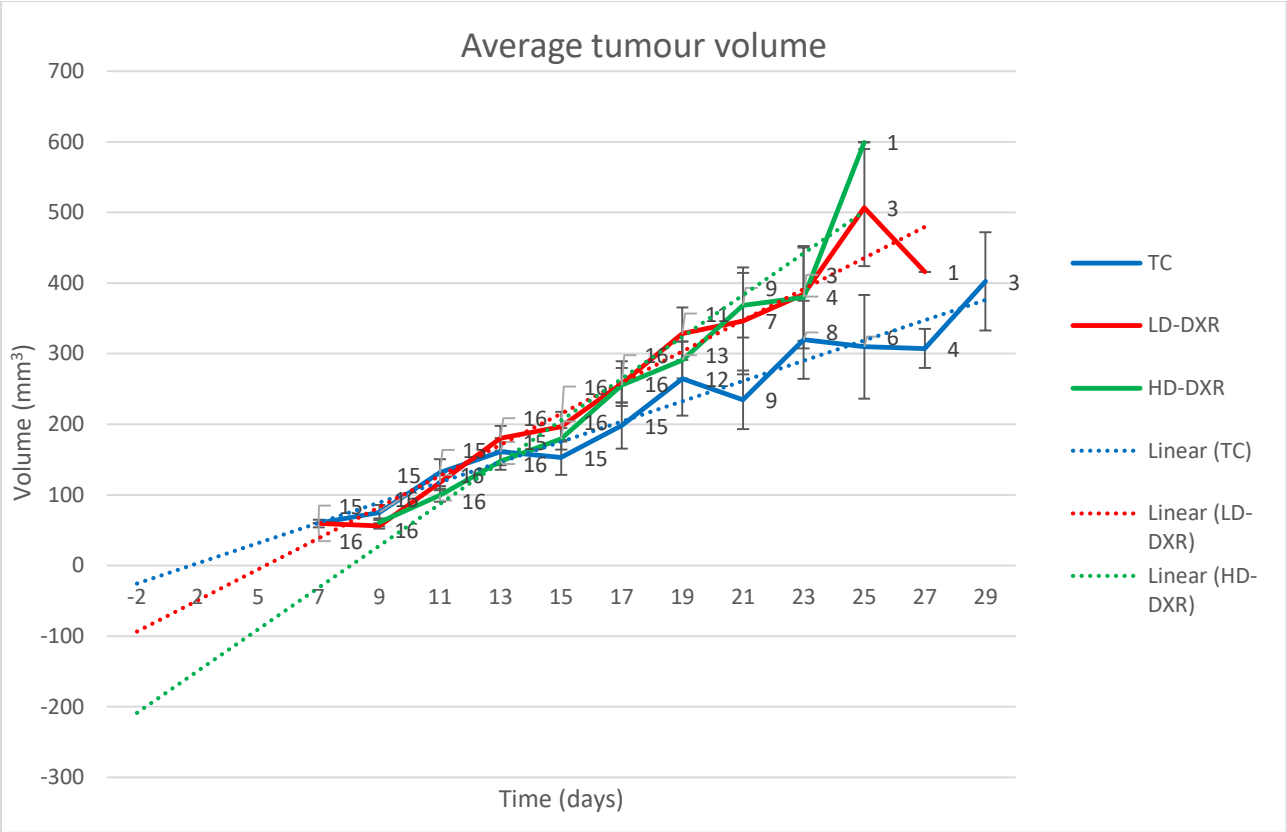

Figure 3.23: Average tumour volume throughout study. Values next to data points indicate number of mice in group on day of measurement. Results presented as mean ± SEM with linear trendlines.

Tumour volumes in all three groups continued to increase throughout the study with trends of increased volumes in the LD-DXR and HD-DXR groups towards the end of the study when compared to the TC group (fig. 3.23). A qualified statistician was employed to perform the appropriate statistical analysis on this data, namely analysis of covariance (ANCOVA). An ANCOVA analysis employs both ANOVA and regression and in this case, determined whether the tumour growth rates between the three groups showed statistically significant differences. Indeed, both the LD-DXR and HD-DXR groups were shown to have significantly increased tumour growth rates when compared to the TC group ($p < 0.05$), as can be seen by the slope of each group's regression line in figure 3.24.

A Kaplan-Meier survival analysis was also performed to determine whether there were any differences between the groups in the time required to reach the desired tumour volume. Even though the curves for each group started to separate towards the end of the study, no statistically significant differences were found between the groups ($p = 0.57$) (fig. 3.25).

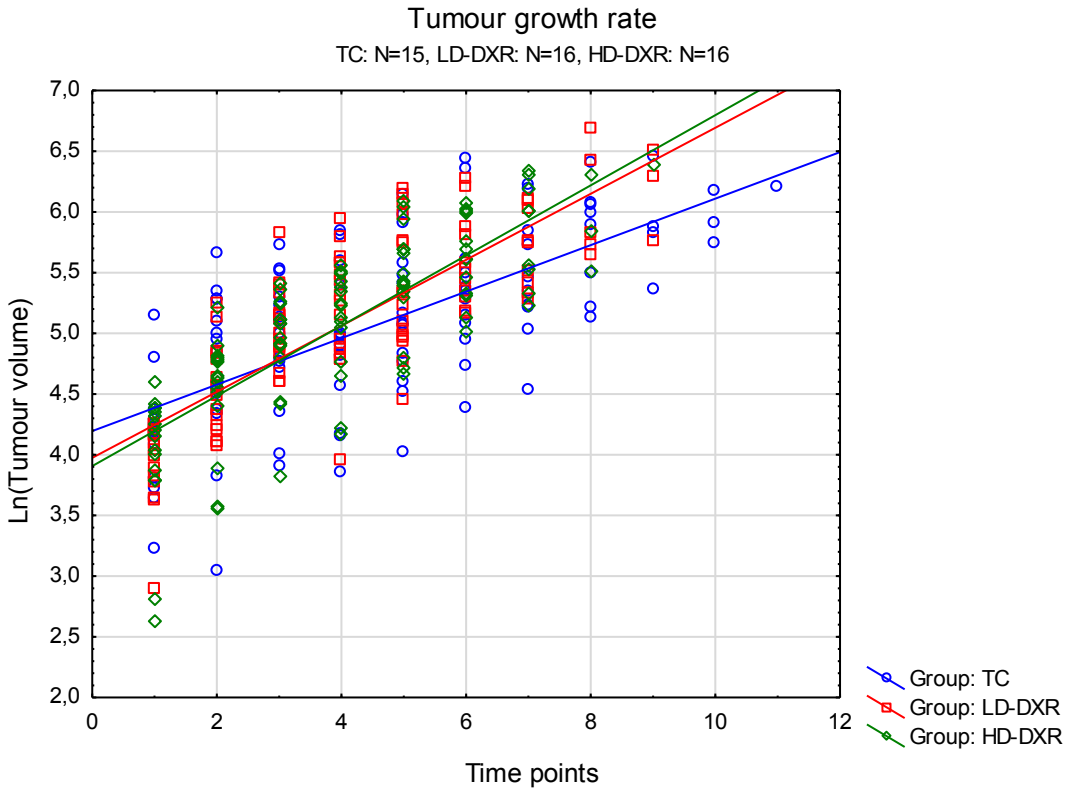

Figure 3.24: Scatterplot fitted with regression lines showing the tumour growth rate for each group.

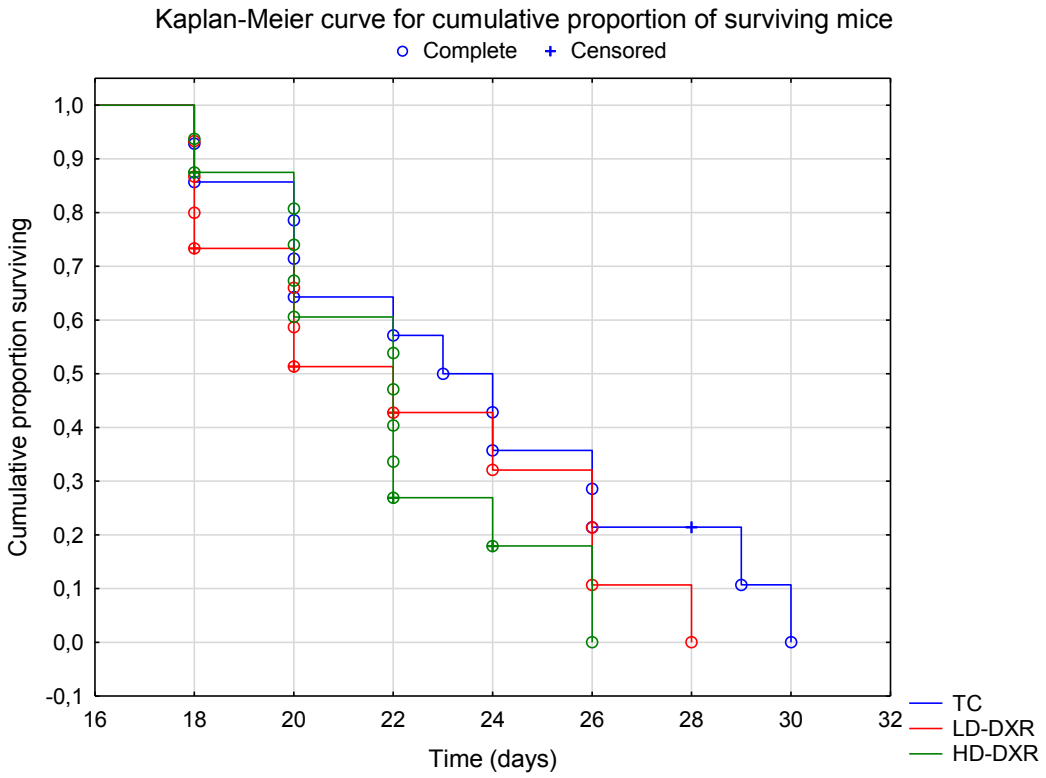

Figure 3.25: Kaplan-Meier survival analysis showing the cumulative proportion of surviving mice throughout the study. Complete – sacrificed due to tumour volume requirement reached; censored – sacrificed due to humane endpoint reached.

Upon sacrifice tumours were harvested from the mice and protein extractions were performed. Western blot experiments were performed to assess protein expression of the apoptotic markers cPARP and cCasp7 and also AHNAK in the tumours. No significant changes were observed in the protein expression of cPARP although cCasp7 showed decreased expression in the LD-DXR group compared to the TC group (1.25 ± 0.26 vs. 0.75 ± 0.11, $p < 0.05$) (fig. 3.26-28). AHNAK showed increased protein expression in the LD-DXR group (1.28 ± 0.34 vs. 1.98 ± 0.32, $p < 0.05$) which decreased back to basal levels in the HD-DXR group (fig. 3.26, 3.29).

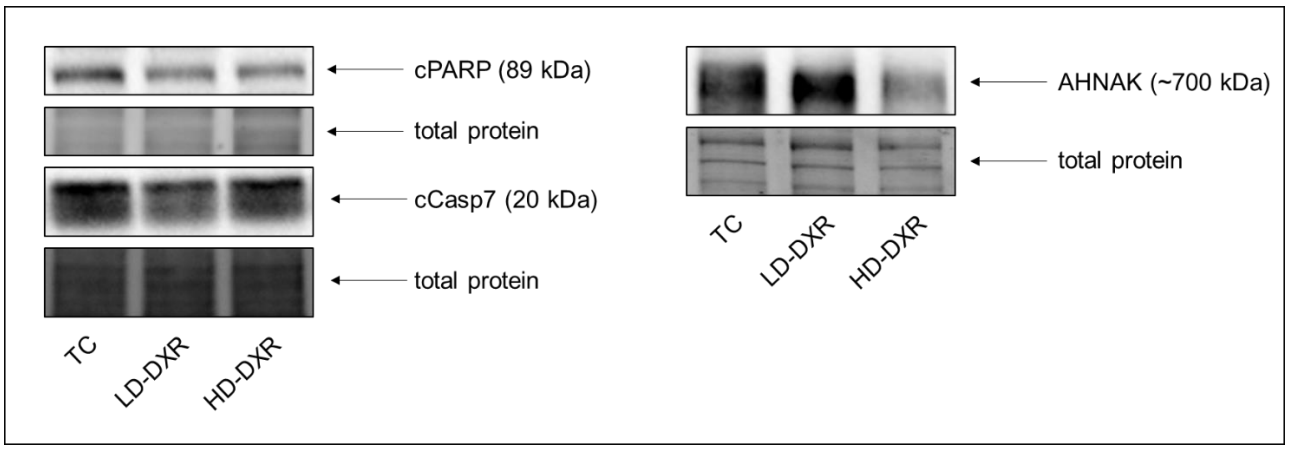

Figure 3.26: Representative images of Western blot experiments for cPARP, cCasp7 and AHNAK protein expression in tumour samples.

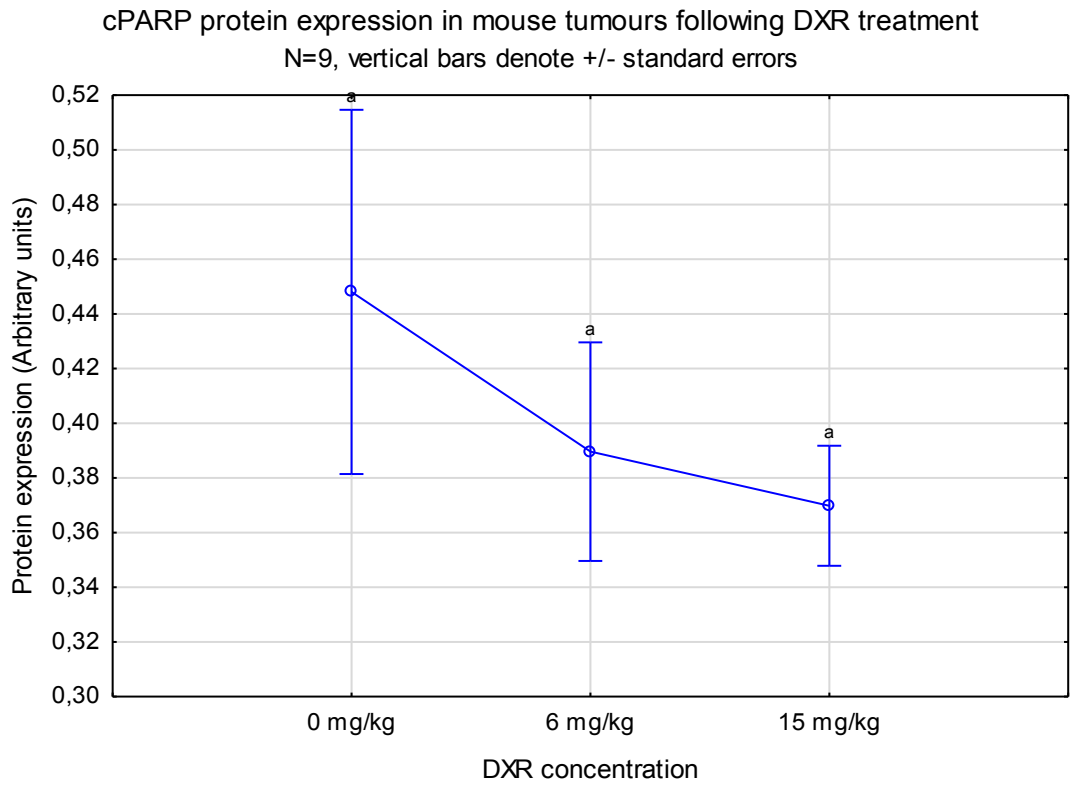

Figure 3.27: cPARP protein expression in mouse tumours.

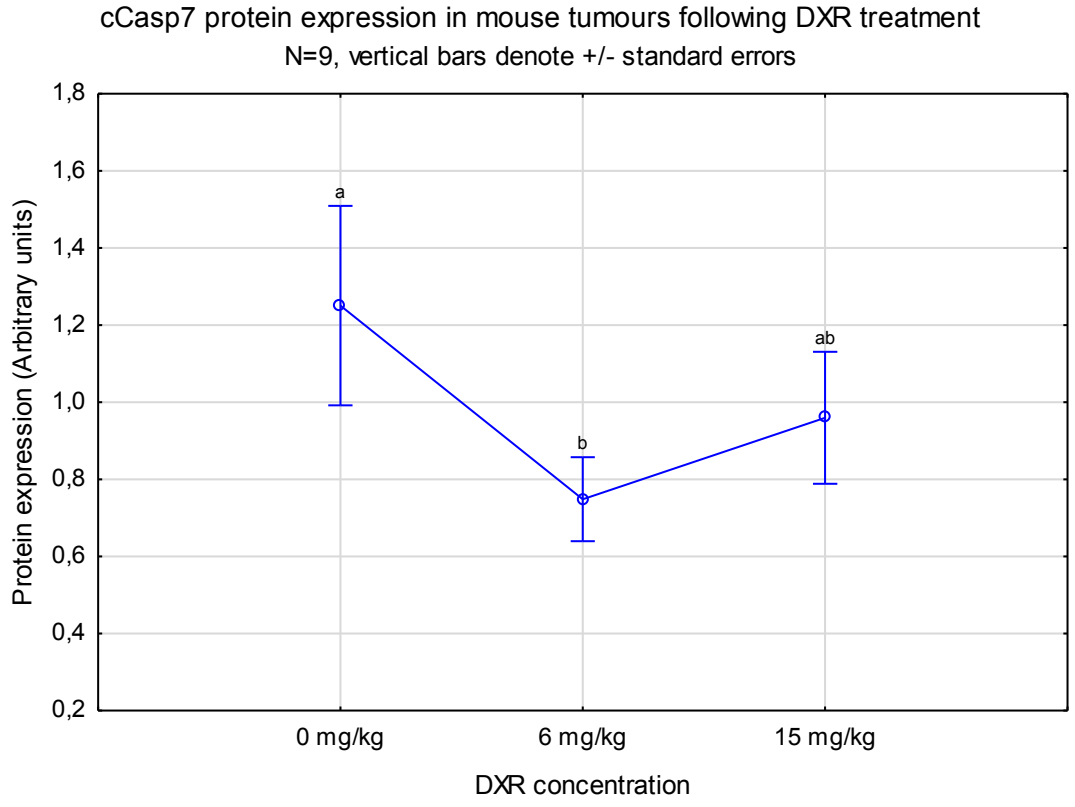

Figure 3.28: Decreased cCasp7 protein expression in mouse tumours.

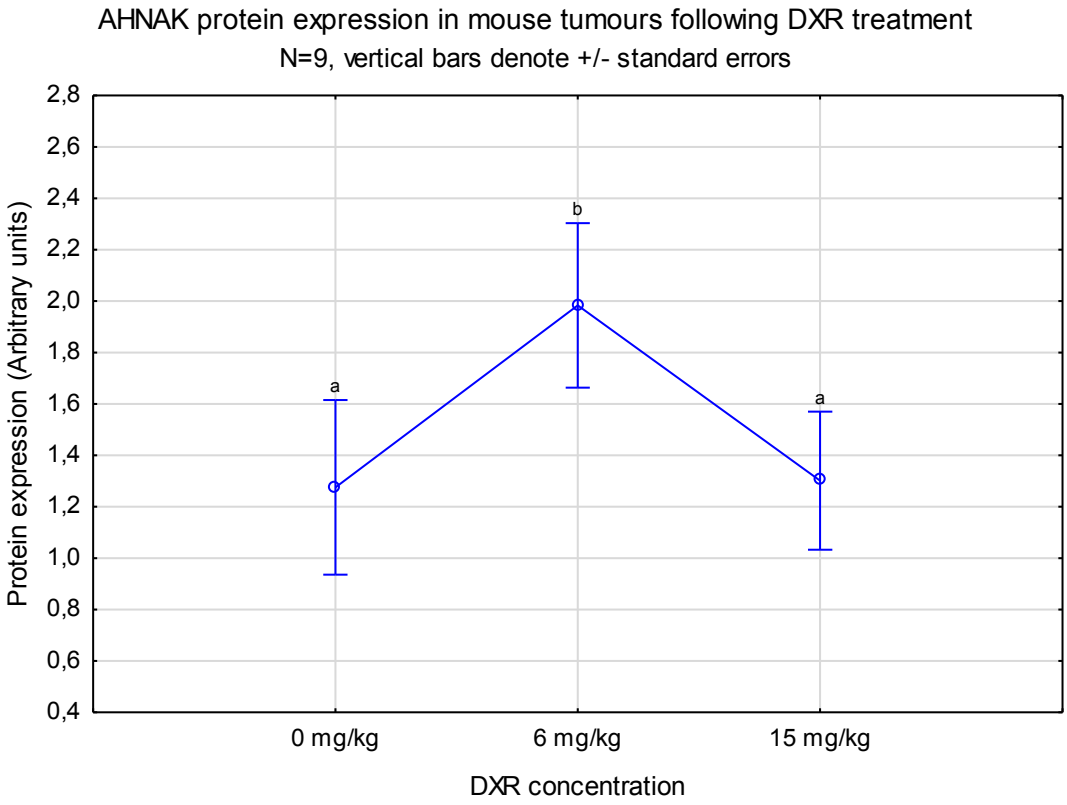

Figure 3.29: Dose-dependent changes in AHNAK protein expression in mouse tumours.

The intracellular localisation of AHNAK in mouse tumours was also determined by means of immunohistochemical staining (fig. 3.30). Nuclear staining (Hoechst) revealed tumours to be highly compact and dense. AHNAK (FITC) displayed a cytoplasmic localisation with localised areas of intense signal that was either perinuclear or plasma membrane-associated, although these areas could not be positively identified due to the compact nature of the tumours. No changes in localisation was however observed with DXR treatment.

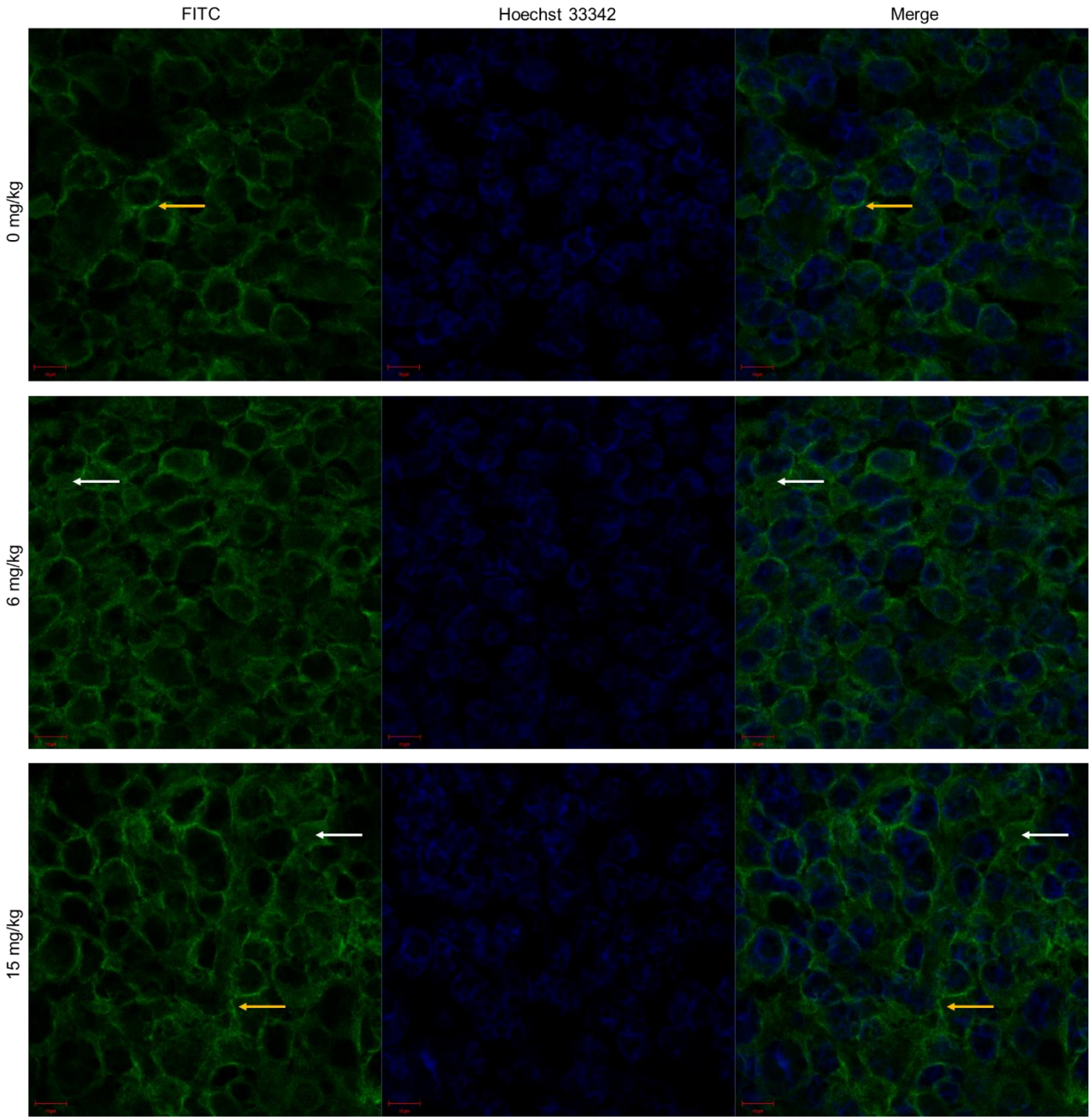

Figure 3.30: Representative immunofluorescent images of AHNAK intracellular localisation in mouse tumours following DXR treatment. FITC – AHNAK; Hoechst 33342 – nuclear DNA; yellow arrows – localised areas of intense signal; white arrows – cytoplasmic staining. Scale = 10 µm, 60x objective.

3.3 The effects of AHNAK on DXR

3.3.1 Optimisation of transfection protocol

Transfection protocols were optimised for the MCF-7 and MDA-MB-231 cell lines. The pGIPZ-sc plasmid was used for this and visualisation of tGFP expression was used to assess transfection efficiency. Representative images of the optimised protocol for each cell line can be seen in figure

3.31. These protocols delivered the highest efficiency together with the least amount of observed cell stress/death (assessed qualitatively).

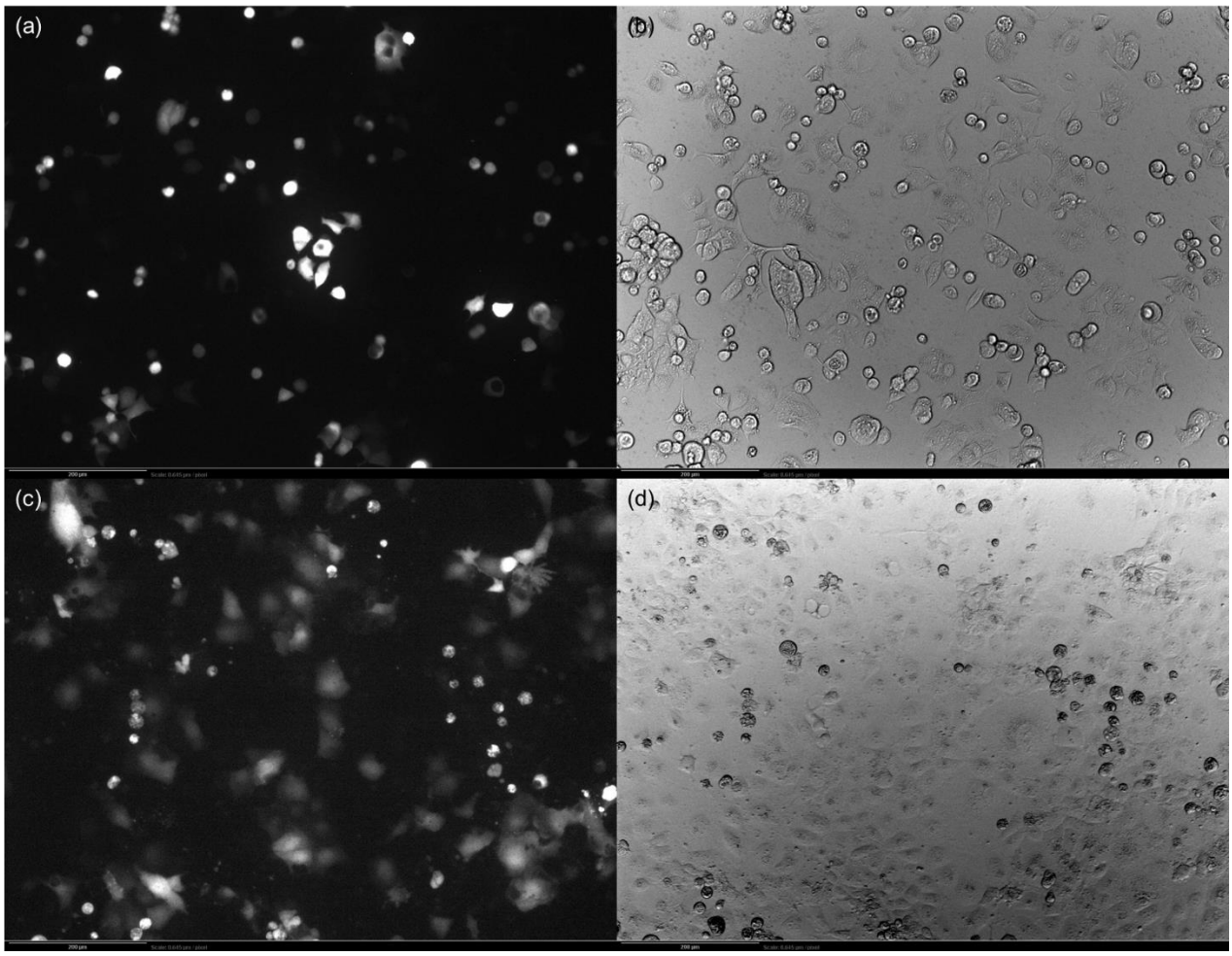

Figure 3.31: Representative images of optimised transfection protocols for MCF-7 and MDA-MB-231 cells. (a) tGFP expression in transfected MCF-7 cells and (b) corresponding brightfield image. (c) tGFP expression in MDA-MB-231 and (d) corresponding brightfield image. Scale = 200 µm, 10x objective.

Next, in order to identify the most suitable pGIPZ plasmid to use for AHNAK knockdown, transfections with all four pGIPZ-AHNAK plasmids, along with pGIPZ-sc as control, were performed. Cellular proteins were extracted and Western blot experiments were performed to assess AHNAK protein expression. In MCF-7 cells, pGIPZ-AHNAK3 resulted in the largest and most consistent decrease in AHNAK expression when compared to pGIPZ-sc (100 ± 12.82 vs. 31.64 ± 5.44, $p < 0.01$) (fig. 3.32, 3.33). In MDA-MB-231 cells pGIPZ-AHNAK2 seemed to be the most suitable plasmid (100 ± 13.08 vs. 60.93 ± 6.68) however statistical significance could not be obtained (fig. 3.32, 3.34). This is attributed to the large amount of variance observed in pGIPZ-AHNAK1 (an ANOVA takes into account the total variance across all groups) and if the analysis was repeated with pGIPZ-AHNAK1

excluded then a statistically significant difference was obtained between pGIPZ-AHNAK2 and pGIPZ-sc ($p < 0.001$).

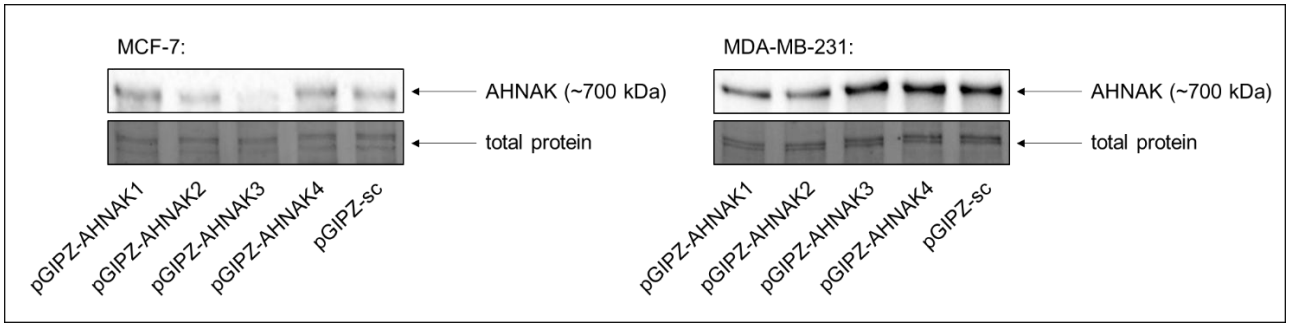

Figure 3.32: Representative images of Western blots for AHNAK protein expression following 48 hr transfection with pGIPZ plasmids in MCF-7 and MDA-MB-231 cells.

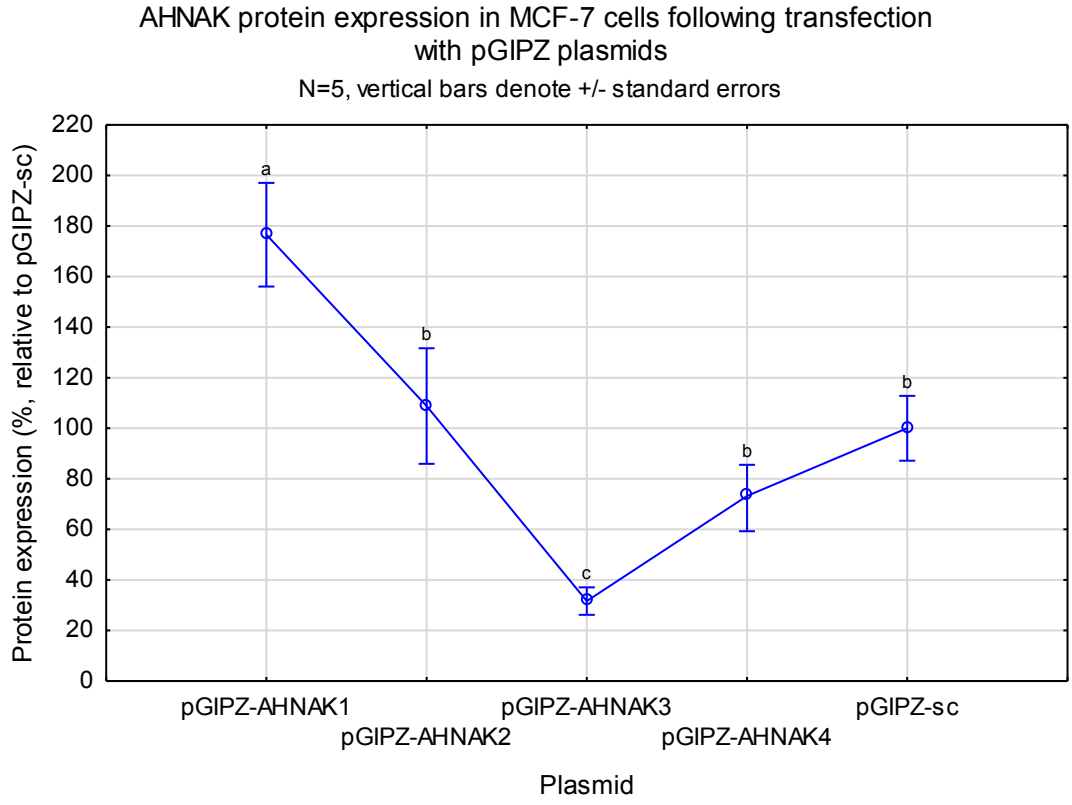

Figure 3.33: Decreased AHNAK protein expression following 48 hr transfection with pGIPZ plasmids.

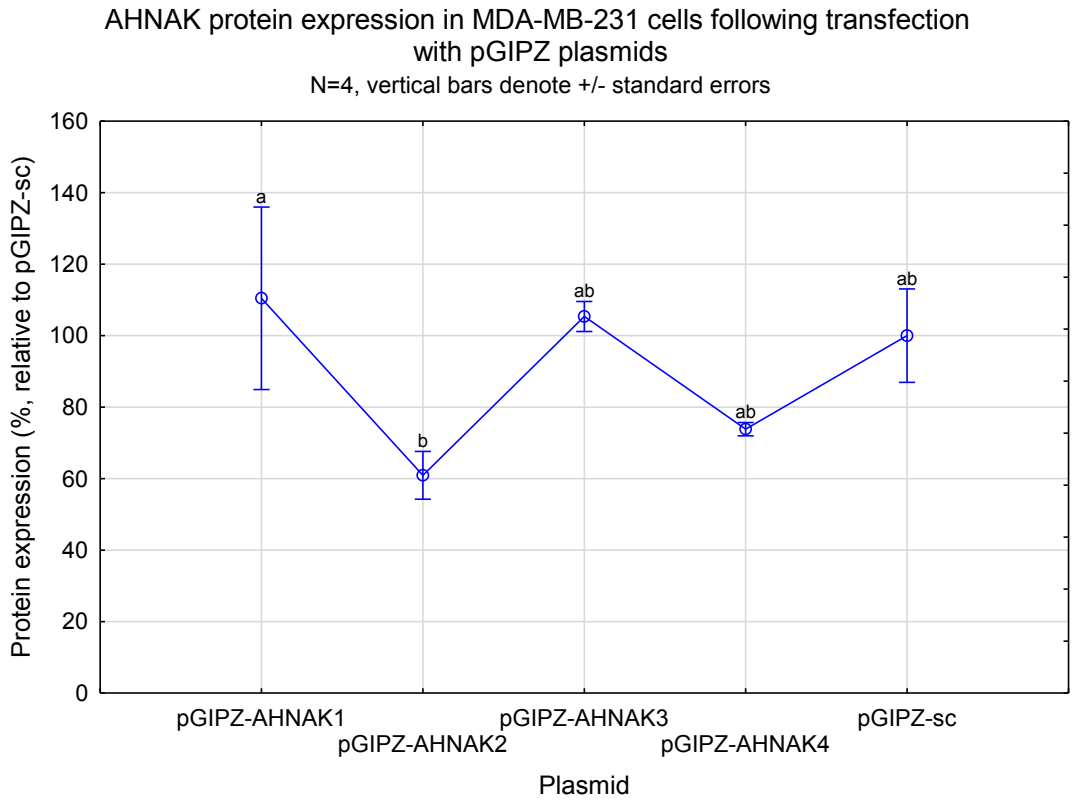

Figure 3.34: Decreased AHNAK protein expression in MDA-MB-231 cells following 48 hr transfection with pGIPZ plasmids.

3.3.2 AHNAK does not influence the cytotoxicity of DXR

In order to determine whether AHNAK has the ability to influence the cytotoxicity of DXR, MTT assays were performed in MCF-7 and MDA-MB-231 cells following knockdown and overexpression of AHNAK. Mean values were compared to the corresponding control (pGIPZ-sc 0 μM and pcDNA3.1 0 μM) and results were analysed with two-way ANOVAs. Knockdown of AHNAK in MCF-7 cells did not affect the cytotoxicity of DXR (fig. 3.35), although it did prevent the DXR-induced increase in viability observed at the low dose of 0.1 μM DXR (100% ± 2.35% at pGIPZ-sc 0 μM vs. 110.92% ± 2.84% at pGIPZ-sc 0.1 μM, $p < 0.05$, no significant change between pGIPZ-AHNAK3 0 μM and pGIPZ-AHNAK3 0.1 μM). In MDA-MB-231 cells knockdown of AHNAK resulted in increased viability across all concentrations of DXR (100% ± 1.03% at pGIPZ-sc 0 μM vs. 125.06% ± 3.96% at pGIPZ-AHNAK2 0 μM, $p < 0.0001$; 107.76% ± 3.45% at pGIPZ-sc 0.1 μM vs. 132.89% ± 5.69% at pGIPZ-AHNAK2 0.1 μM, $p < 0.0001$; 90.94% ± 3.20% at pGIPZ-sc 5 μM vs. 102.46% ± 4.85% at pGIPZ-AHNAK2 5 μM, $p < 0.05$), however the viability of the pGIPZ-AHNAK2 groups followed the same trend with DXR treatment as the pGIPZ-sc groups, indicating that AHNAK knockdown did not have an effect on DXR cytotoxicity (fig. 3.36).

As with AHNAK knockdown, overexpression of the protein also did not affect the cytotoxicity of DXR. In MCF-7 cells AHNAK overexpression slightly decreased viability across all concentrations, with

significant differences at 0.1 µM (105.18% ± 3.12% vs. 92.13% ± 3.37%, $p < 0.01$) and 5 µM (52.70% ± 3.09% vs. 38.10% ± 1.37%, $p < 0.01$) when compared to the respective pcDNA3.1 groups (fig. 3.37). The same viability pattern in response to DXR treatment was however observed between the pcDNA3.1 and pcDNA3-CRU groups. Similarly, overexpression of AHNAK in MDA-MB-231 cells failed to affect DXR cytotoxicity in these cells (fig. 3.38). Instead, as with AHNAK knockdown, overexpression resulted in a general increase in viability across all groups (100% ± 2.14% at pcDNA3.1 0 µM vs. 117.04% ± 4.01% at pcDNA3-CRU 0 µM, $p < 0.01$; 106.96% ± 2.96% at pcDNA3.1 0.1 µM vs. 121.52% ± 3.74% at pcDNA3-CRU 0.1 µM, $p < 0.05$; 87.62% ± 4.07% at pcDNA3.1 5 µM vs. 106.55% ± 5.42% at pcDNA3-CRU 5 µM, $p < 0.01$). Although, where pGIPZ-AHNAK2 5 µM showed a significant decrease in viability when compared to pGIPZ-AHNAK2 0 µM (125.06% ± 3.96% vs. 102.46% ± 4.85%, $p < 0.001$) (fig. 3.36), pcDNA3-CRU 5 µM was not significantly different from pcDNA3-CRU 0 µM.

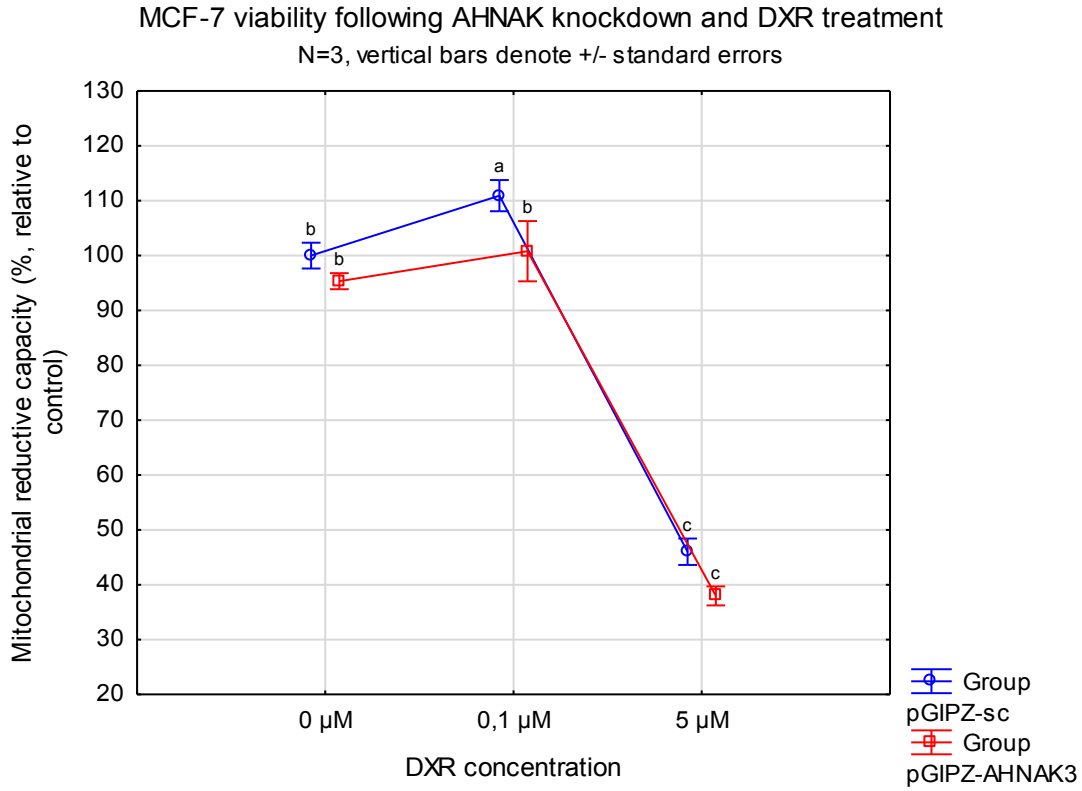

Figure 3.35: Mitochondrial reductive capacity, as a measure of cell viability, of MCF-7 cells following AHNAK knockdown with pGIPZ-AHNAK3 transfection and DXR treatment for 24 hrs.

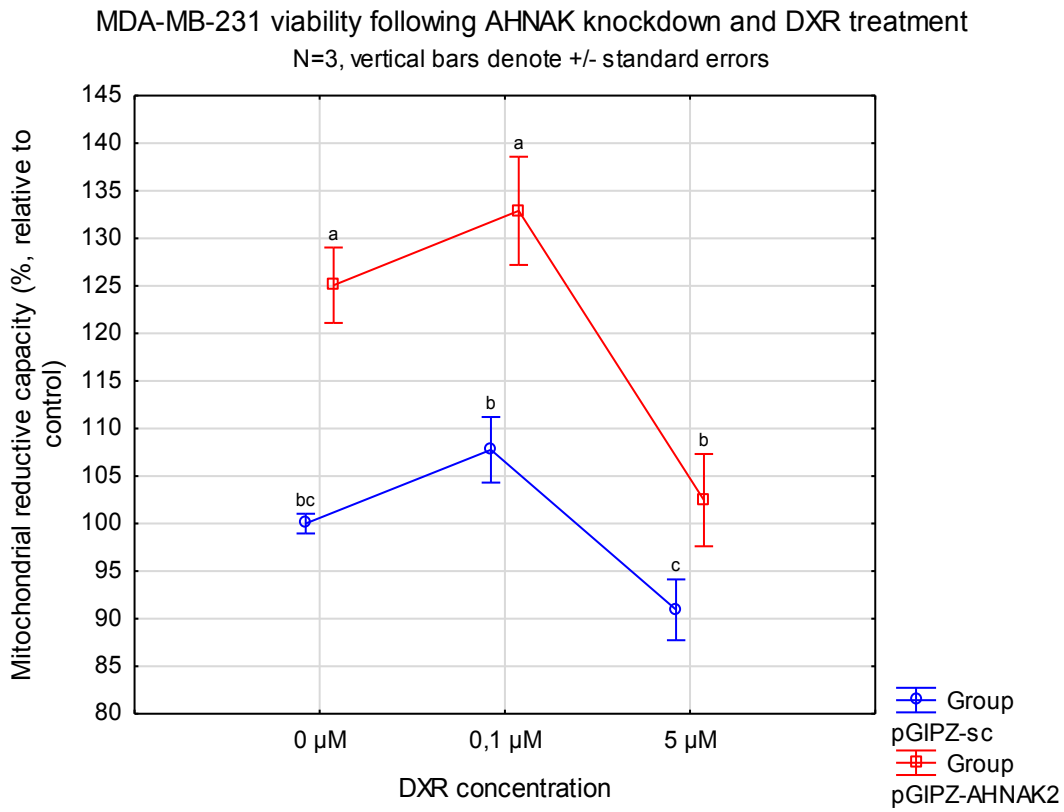

Figure 3.36: Mitochondrial reductive capacity, as a measure of cell viability, of MDA-MB-231 cells following AHNAK knockdown with pGIPZ-AHNAK2 transfection and DXR treatment for 24 hrs.

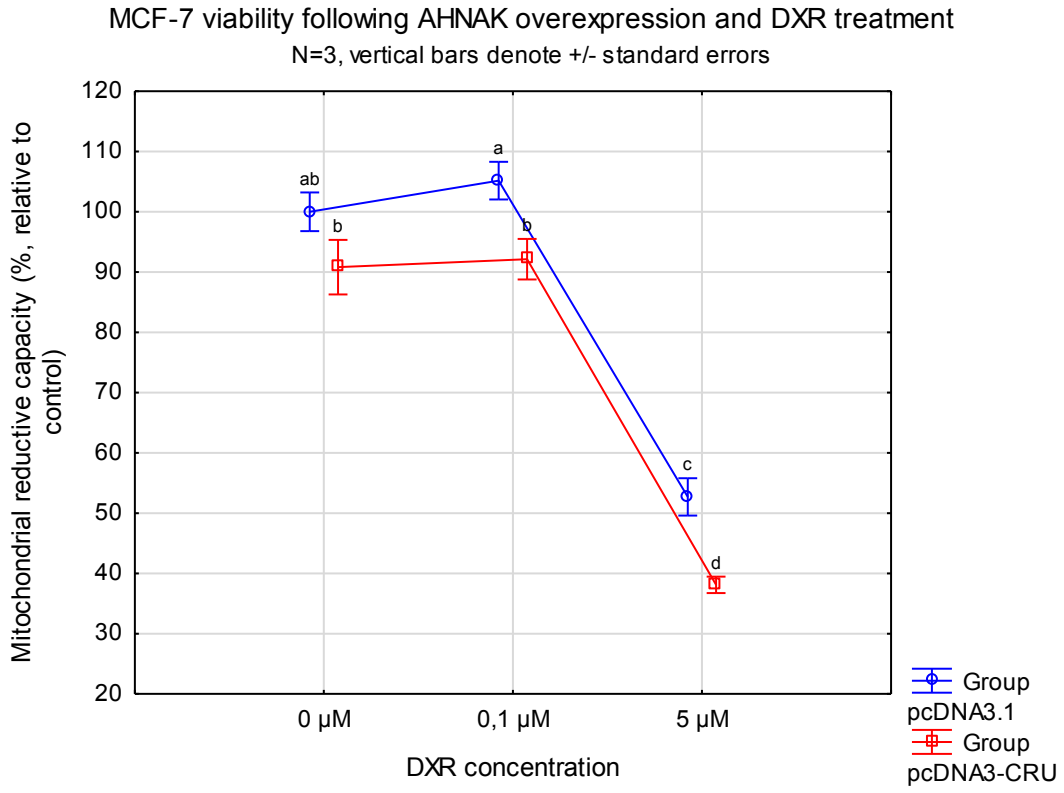

Figure 3.37: Mitochondrial reductive capacity, as a measure of cell viability, of MCF-7 cells following AHNAK overexpression with pcDNA3-CRU transfection and DXR treatment for 24 hrs.

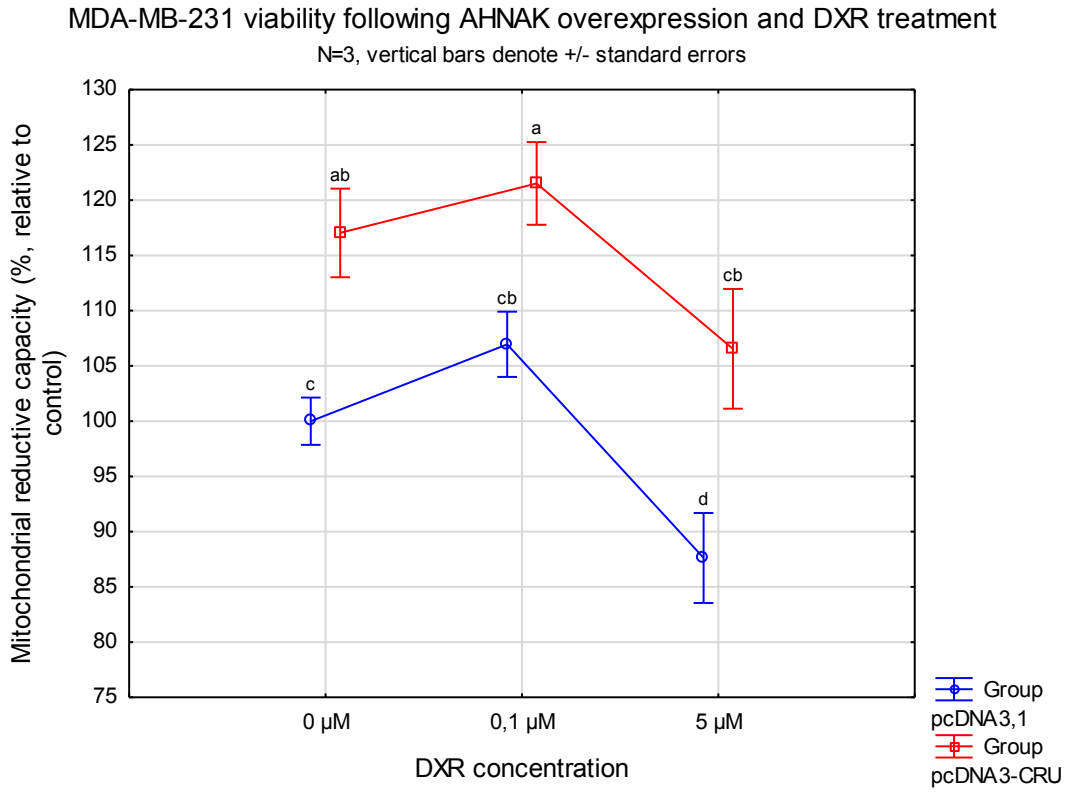

Figure 3.38: Mitochondrial reductive capacity, as a measure of cell viability, of MDA-MB-231 cells following AHNAK overexpression with pcDNA3-CRU transfection and DXR treatment for 24 hrs.

3.3.3 AHNAK partly modulates the activity and expression of apoptotic markers

To determine the effect of AHNAK on apoptotic caspase 3 and 7 activity a Caspase-Glo® 3/7 assay was performed on MCF-7 and MDA-MB-231 cells following AHNAK knockdown and overexpression and DXR treatment. This assay measures the activity of active (or cleaved) caspase 3 and caspase 7 proteins which serves as an indication of the level of apoptosis taking place, i.e. increased activity indicates increased apoptosis. Caspase activity in groups were compared to the corresponding control groups and results were analysed with two-way ANOVAs. Knockdown of AHNAK in MCF-7 cells resulted in increased caspase 3/7 activity (100% ± 2.61% vs. 120.61% ± 4.51%, $p < 0.0001$) but no differences were observed in the presence of DXR (fig. 3.39). Similarly, AHNAK knockdown also resulted in a slight but significant increase in activity in MDA-MB-231 cells at DXR control conditions (100% ± 3.30% vs. 107.16% ± 0.41%, $p < 0.05$) with no further significant differences between the pGIPZ-sc and pGIPZ-AHNAK2 groups (fig. 3.40). Overexpression of AHNAK in MCF-7 cells resulted in increased activity (100% ± 2.73% vs. 115.68% ± 3.76%, $p < 0.01$) and the low dose group (100.92% ± 3.42% vs. 115.12% ± 2.39%, $p < 0.01$) (fig. 3.41). In MDA-MB-231 cells, AHNAK overexpression maintained caspase 3/7 activity at fairly constant levels across all DXR concentrations (fig. 3.42), preventing the increased activity induced by 5 µM DXR in the pcDNA3.1

group (100% ± 1.19% at pcDNA3.1 0 µM vs. 120.34% ± 4.21% at pcDNA3.1 5 µM, $p < 0.0001$). Indeed, where 5 µM DXR induced caspase 3/7 activity in pGIPZ-AHNAK2 (107.16% ± 0.41% vs. 117.96% ± 2.22%, $p < 0.01$), and with pGIPZ-sc 5 µM (100% ± 3.30% vs. 121.25% ± 2.40%, $p < 0.0001$), the same dose failed to do so in pcDNA3-CRU transfected cells.

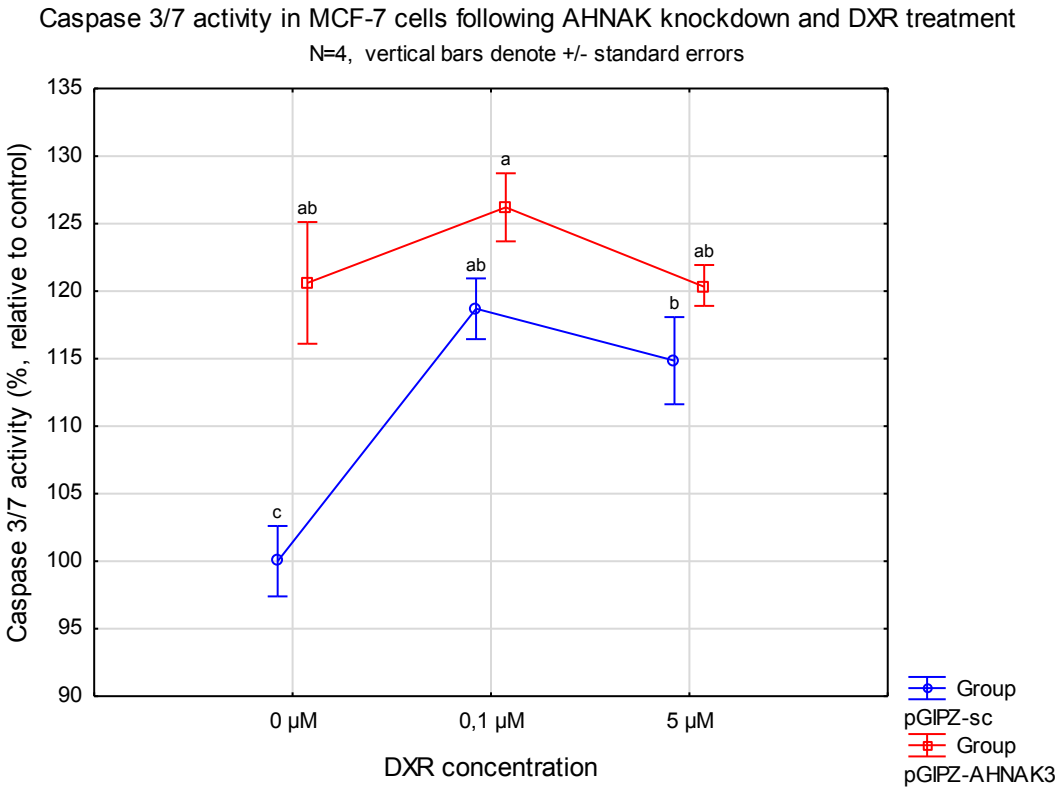

Figure 3.39: Caspase 3/7 activity, as a measure of cell death via apoptosis, in MCF-7 cells following AHNAK knockdown with pGIPZ-AHNAK3 and DXR treatment for 24 hrs.

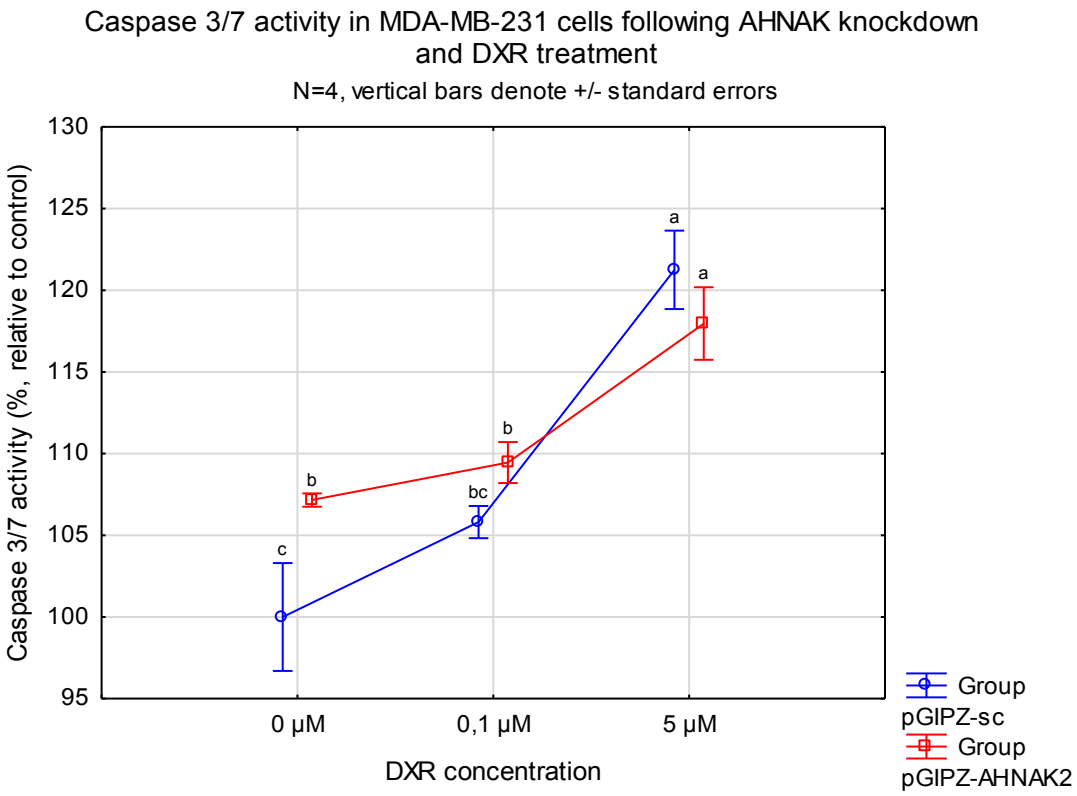

Figure 3.40: Caspase 3/7 activity, as a measure of cell death via apoptosis, in MDA-MB-231 cells following AHNAK knockdown with pGIPZ-AHNAK2 and DXR treatment for 24 hrs.

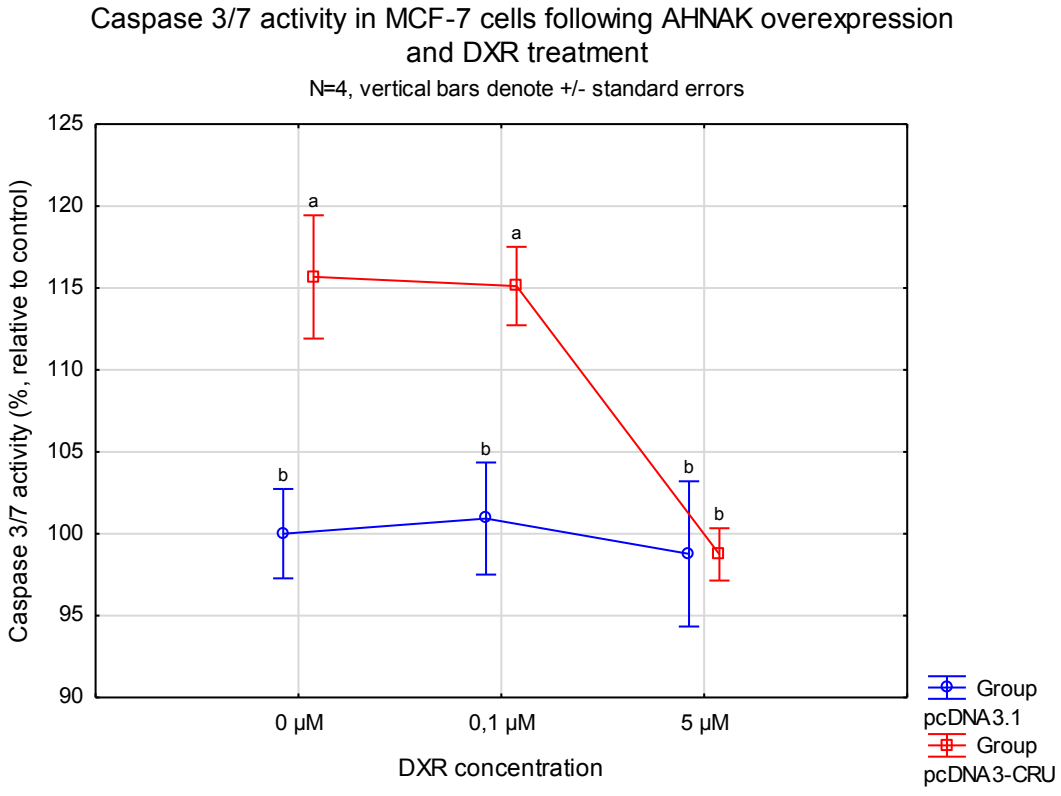

Figure 3.41: Caspase 3/7 activity, as a measure of cell death via apoptosis, in MCF-7 cells following AHNAK overexpression with pcDNA3-CRU and DXR treatment for 24 hrs.

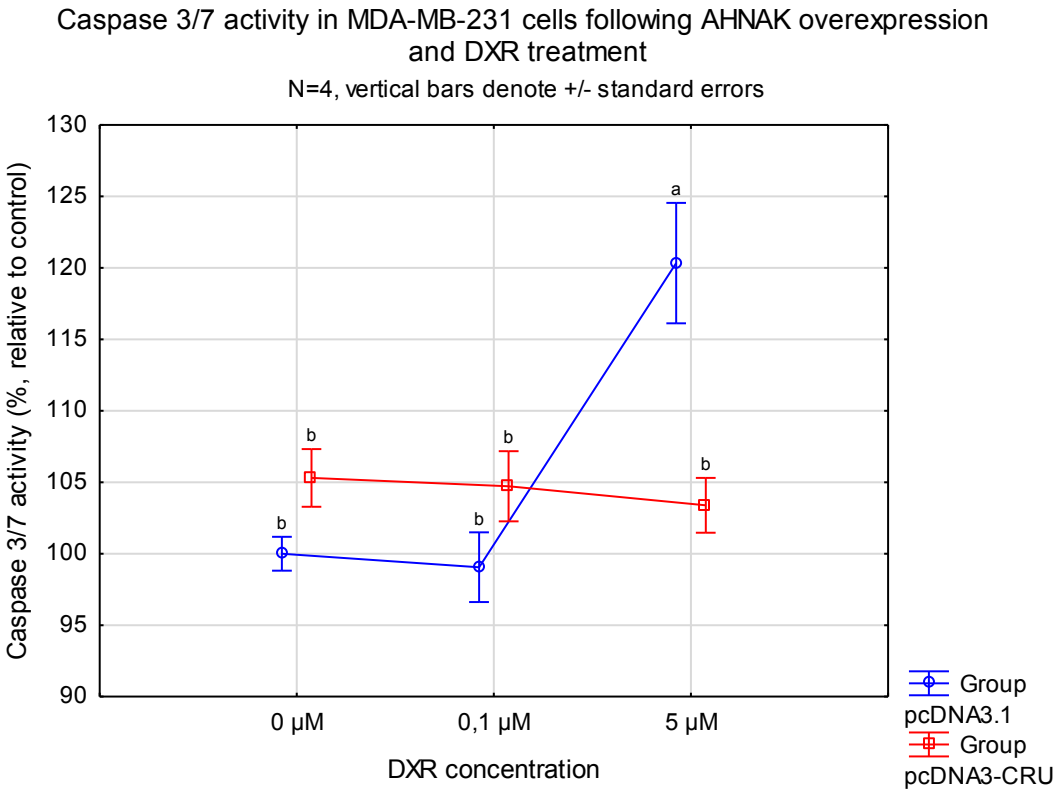

Figure 3.42: Caspase 3/7 activity, as a measure of cell death via apoptosis, in MDA-MB-231 cells following AHNAK overexpression with pcDNA3-CRU and DXR treatment for 24 hrs.

Western blot experiments were also performed to assess the protein expression of apoptotic markers cPARP and cCasp7, as well as to confirm knockdown and overexpression of AHNAK. Decreased AHNAK protein expression following transfection with the pGIPZ-AHNAK3 and pGIPZ-AHNAK2 plasmids were confirmed in knockdown experiments with MCF-7 (1.91 ± 0.35 at pGIPZ-sc 0 µM vs. 0.82 ± 0.19 at pGIPZ-AHNAK3 0 µM, $p < 0.0001$) and MDA-MB-231 (5.72 ± 0.71 at pGIPZ-sc 0 µM vs. 3.54 ± 0.60 at pGIPZ-AHNAK2 0 µM, $p < 0.01$) cells, respectively (fig. 3.43, 3.45, 3.46). The expression of the CRU protein was also confirmed in both cell lines (fig. 3.44).

As expected, 5 µM DXR induced significant increases in cPARP (0.78 ± 0.24 at pGIPZ-sc 0 µM vs. 3.84 ± 1.07 at pGIPZ-sc 5 µM, $p < 0.001$) and cCasp7 (1.99 ± 0.51 at pGIPZ-sc 0 µM vs. 2.75 ± 0.62 at pGIPZ-sc 5 µM, $p < 0.05$) expression in MCF-7 cells (fig. 3.43, 3.47, 3.48). The same response was observed with AHNAK knockdown, where cPARP (0.71 ± 0.28 at pGIPZ-AHNAK3 0 µM vs. 4.29 ± 1.41 at pGIPZ-AHNAK3 5 µM, $p < 0.001$) and cCasp7 (2.02 ± 0.53 at pGIPZ-AHNAK3 0 µM vs. 3.45 ± 1.03 at pGIPZ-AHNAK3 5 µM, $p < 0.001$) was significantly increased when compared to the DXR control group. The high dose DXR treatment resulted in decreased cPARP protein expression in MDA-MB-231 cells (0.19 ± 0.04 at pGIPZ-sc 0 µM vs. 0.11 ± 0.01 at pGIPZ-sc 5 µM, $p < 0.05$) while a similar response was observed with AHNAK knockdown (0.16 ± 0.02 at pGIPZ-AHNAK2 0

μM vs. 0.08 ± 0.02 at pGIPZ-AHNAK2 5 μM, $p < 0.05$) (fig. 3.43, 3.49). A similar decrease in expression with a high dose DXR was observed for cCasp7 (0.34 ± 0.03 at pGIPZ-sc 0 μM vs. 0.25 ± 0.03 at pGIPZ-sc 5 μM, $p < 0.01$) however, here, AHNAK knockdown prevented the DXR-induced decrease and maintained cCasp7 levels at a fairly constant level so that it differed significantly from pGIPZ-sc 5 μM (0.34 ± 0.06 vs. 0.25 ± 0.03, $p < 0.01$) (fig. 3.43, 3.50).

As with the knockdown experiments, a high dose of DXR induced significant increases in cPARP (0.46 ± 0.08 at pcDNA3.1 0 μM vs. 1.70 ± 0.42 at pcDNA3.1 5 μM, $p < 0.0001$) and cCasp7 (1.06 ± 0.15 at pcDNA3.1 0 μM vs. 1.62 ± 0.13 at pcDNA3.1 5 μM, $p < 0.01$) protein expression in control transfected MCF-7 cells while the same response for both cPARP (0.45 ± 0.09 at pcDNA3-CRU 0 μM vs. 1.98 ± 0.36 pcDNA3-CRU 5 μM, $p < 0.0001$) and cCasp7 (1.12 ± 0.04 at pcDNA3-CRU 0 μM vs. 1.83 ± 0.26 at pcDNA3-CRU 5 μM, $p < 0.001$) was observed with overexpression of AHNAK (fig. 3.44, 3.51, 3.52). In MDA-MB-231 cells high dose DXR again resulted in decreased cPARP expression (2.59 ± 0.12 at pcDNA3.1 0 μM vs. 1.41 ± 0.10 at pcDNA3.1 5 μM, $p < 0.0001$), however overexpression of AHNAK also resulted in decreased cPARP expression (2.59 ± 0.12 at pcDNA3.1 0 μM vs.1.78 ± 0.1 at pcDNA3-CRU 0 μM, $p < 0.0001$) which decreased further with 5 μM DXR treatment (1.78 ± 0.1 at pcDNA3-CRU 0 μM vs. 1.49 ± 0.03 at pcDNA3-CRU 5 μM, $p < 0.05$) (3.44, 3.53). While DXR decreased cCasp7 protein expression at both the low and high dose DXR treatments (0.66 ± 0.08 at pcDNA3.1 0 μM vs. 0.30 ± 0.03 at pcDNA3.1 0.1 μM, $p < 0.0001$; vs. 0.28 ± 0.02 at pcDNA3.1 5 μM, $p < 0.0001$), AHNAK overexpression in these cells also decreased cCasp7 expression (0.66 ± 0.08 at pcDNA3.1 0 μM vs. 0.25 ± 0.03 at pcDNA3-CRU 0 μM, $p < 0.0001$) to levels similar to those induced by DXR (fig. 3.44, 3.54).

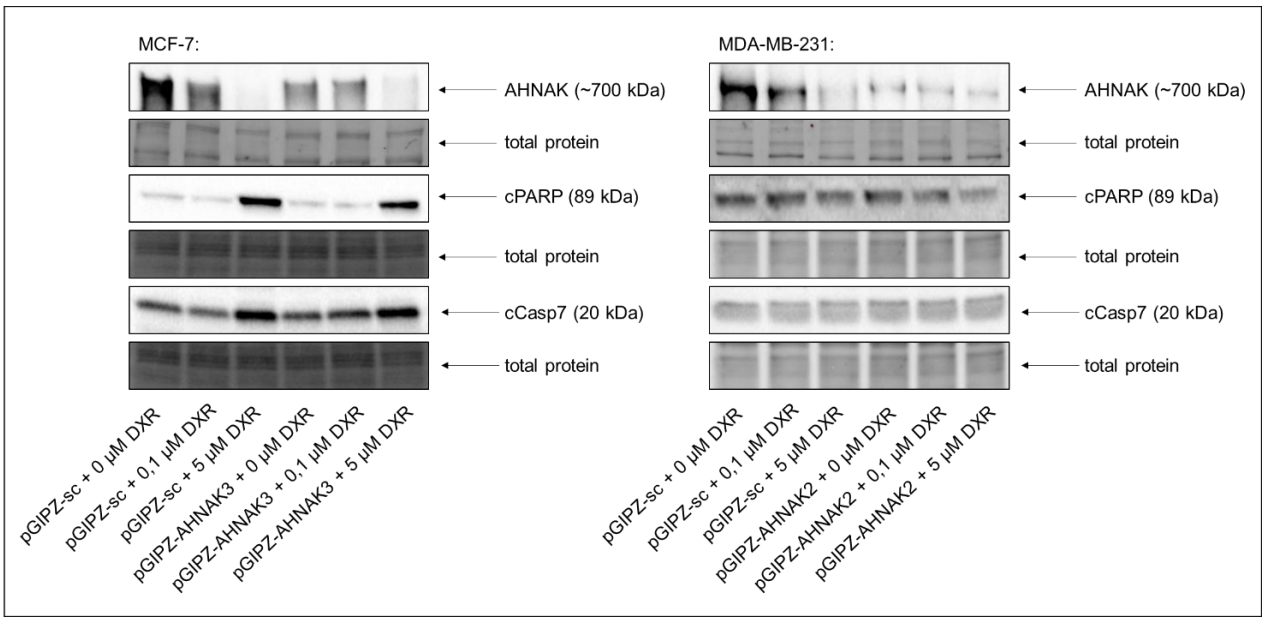

Figure 3.43: Representative images of Western blots for AHNAK, cPARP and cCasp7 protein expression in MCF-7 and MDA-MB-231 cells following AHNAK knockdown and DXR treatment for 24 hrs.

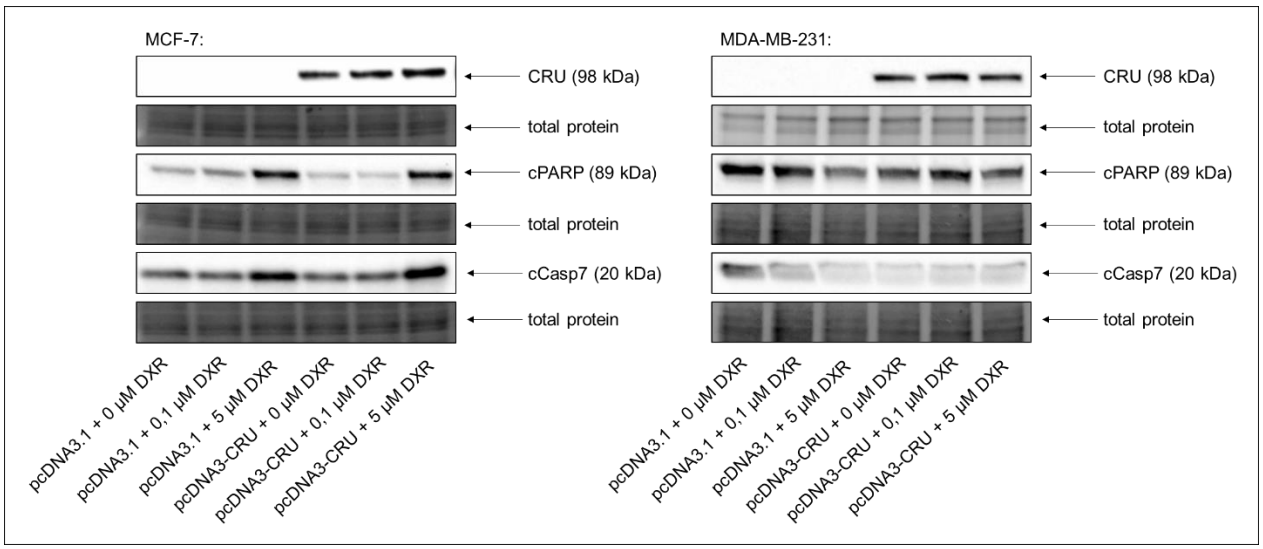

Figure 3.44: Representative images of Western blots for CRU, cPARP and cCasp7 protein expression in MCF-7 and MDA-MB-231 cells following AHNAK overexpression and DXR treatment for 24 hrs.

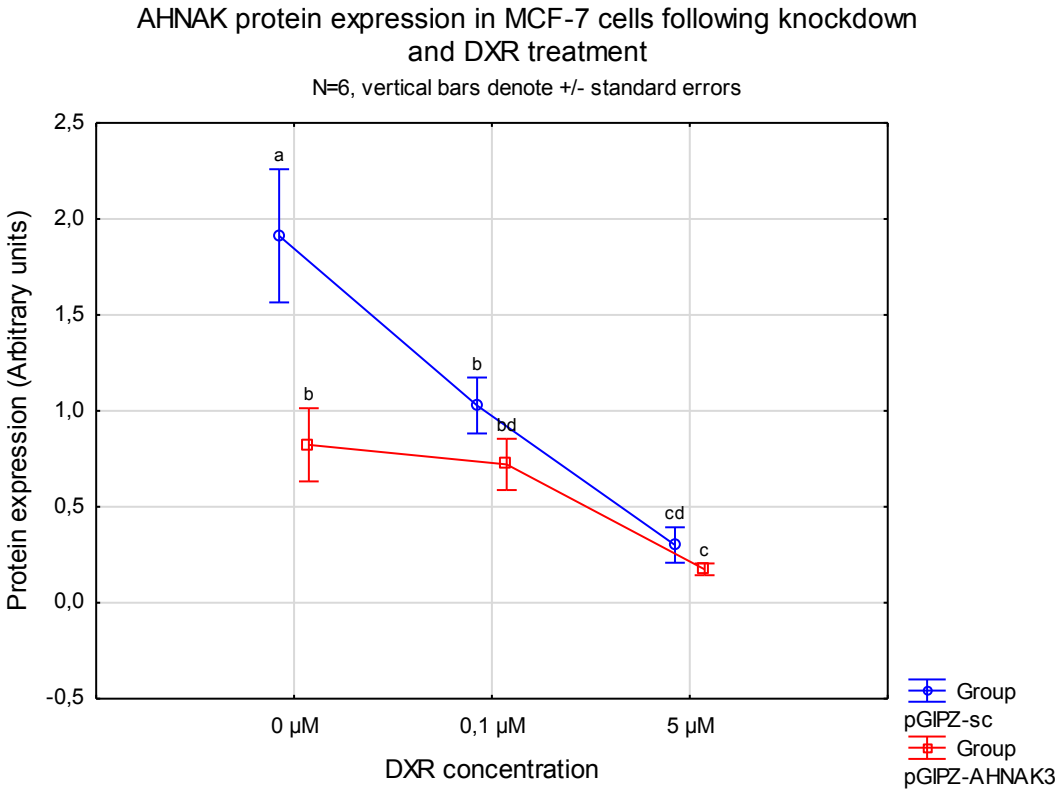

Figure 3.45: Decreased AHNAK protein expression in MCF-cells following knockdown with pGIPZ-AHNAK3 transfection and DXR treatment for 24 hrs.

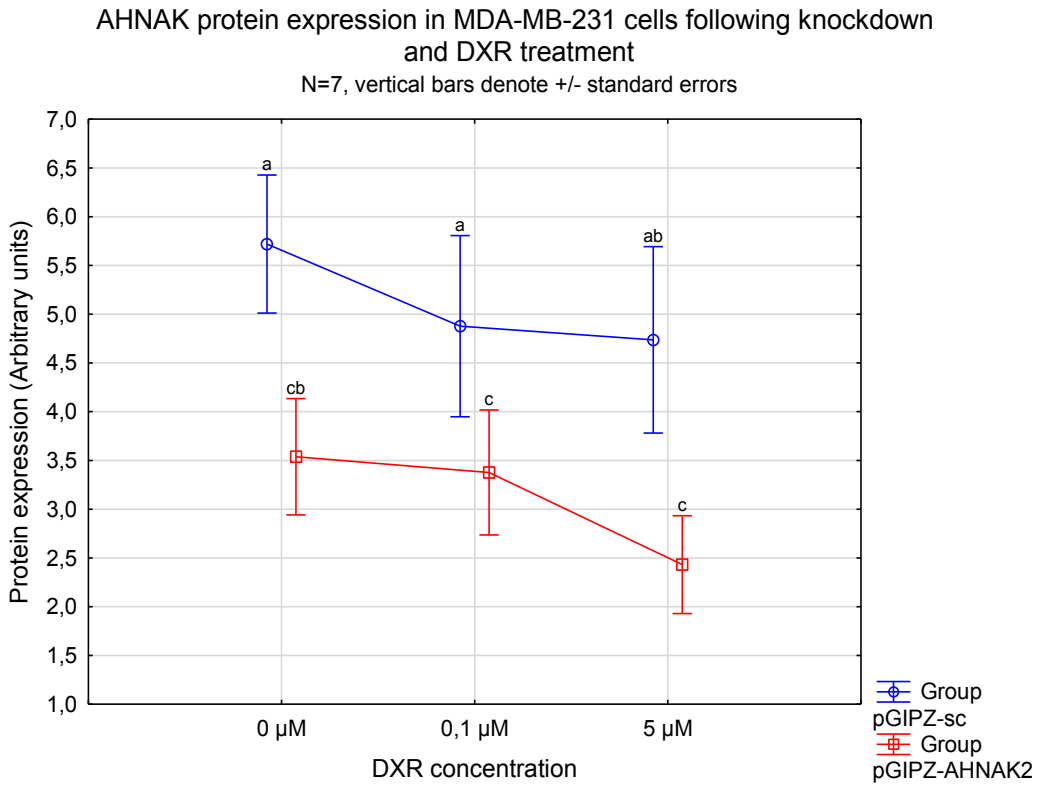

Figure 3.46: Decreased AHNAK protein expression in MDA-MB-231 cells following knockdown with pGIPZ-AHNAK2 transfection and DXR treatment for 24 hrs.

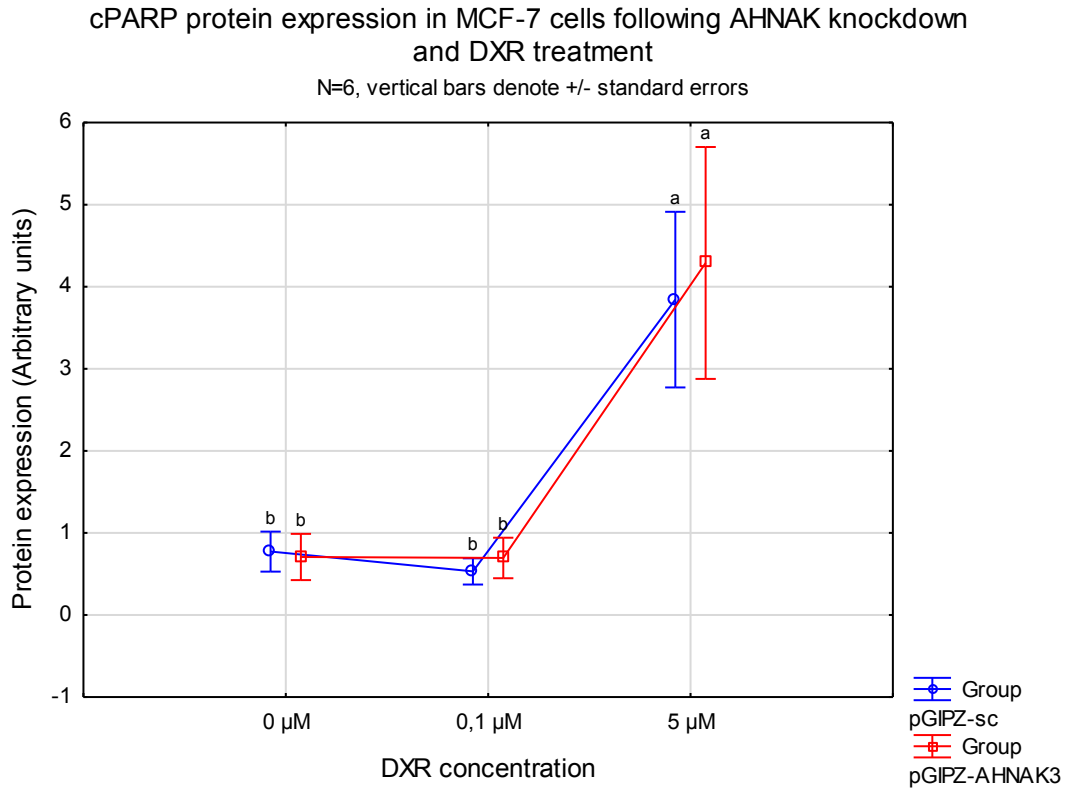

Figure 3.47: cPARP protein expression in MCF-7 cells in response to AHNAK knockdown with pGIPZ-AHNAK3 transfection and DXR treatment for 24 hrs.

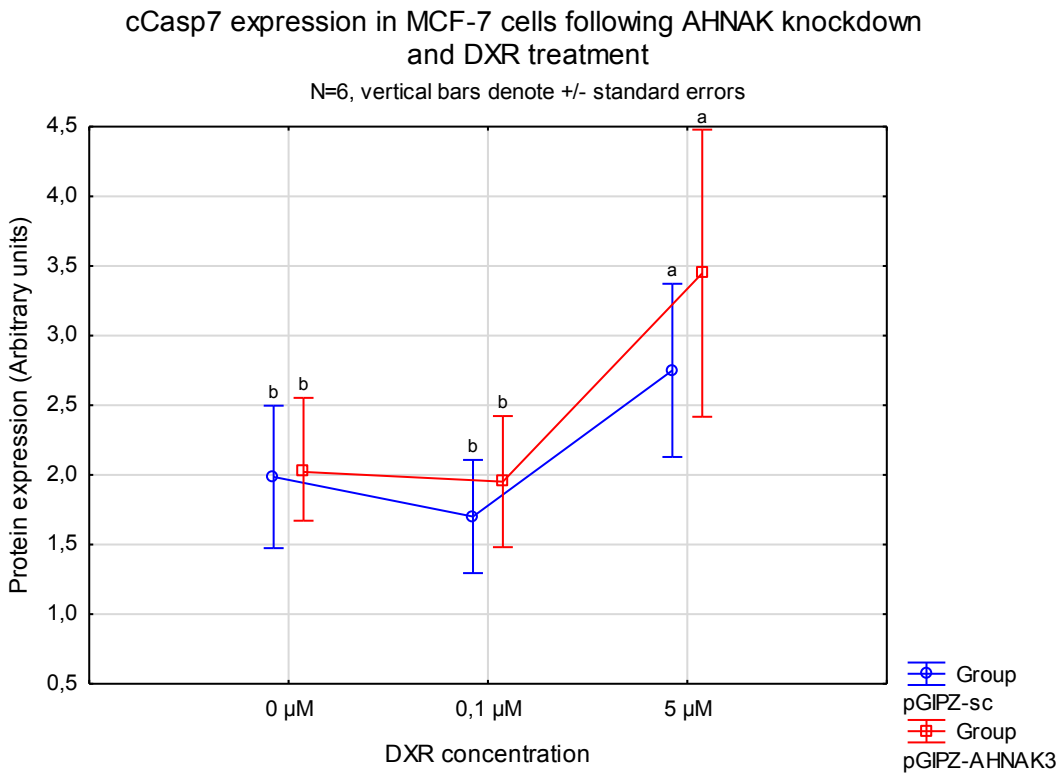

Figure 3.48: cCasp7 protein expression in MCF-7 cells in response to AHNAK knockdown with pGIPZ-AHNAK3 transfection and DXR treatment for 24 hrs.

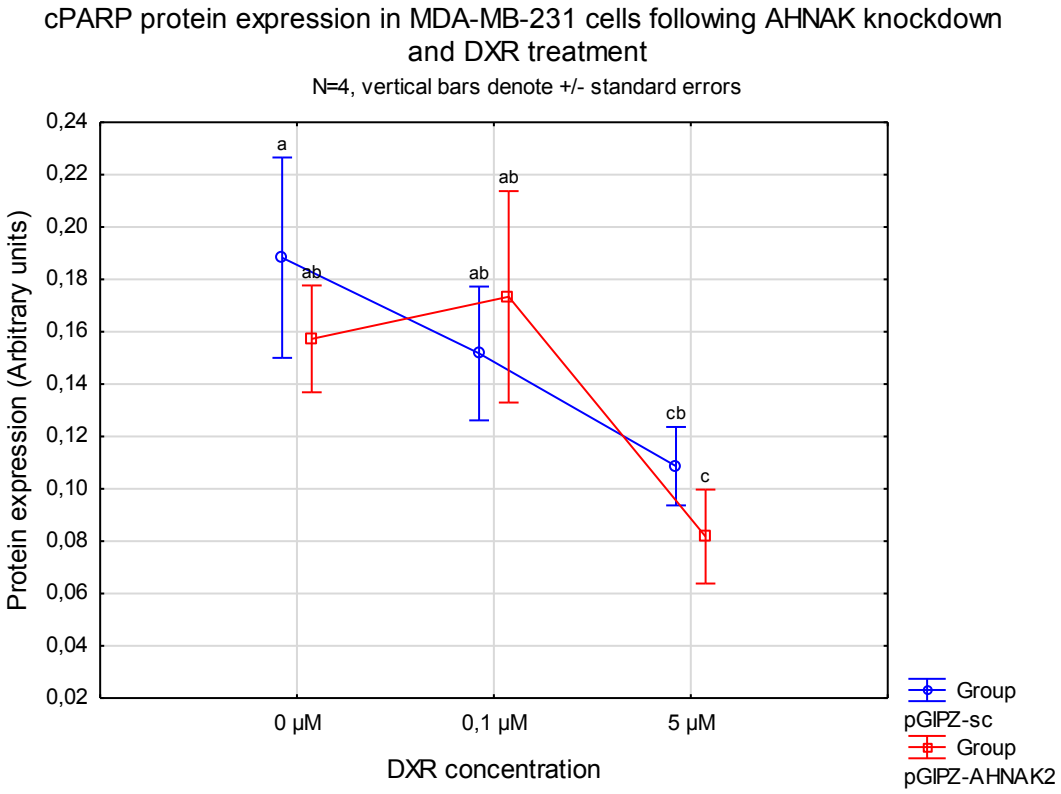

Figure 3.49: cPARP protein expression in MDA-MB-231 cells in response to AHNAK knockdown with pGIPZ-AHNAK2 and DXR treatment for 24 hrs.

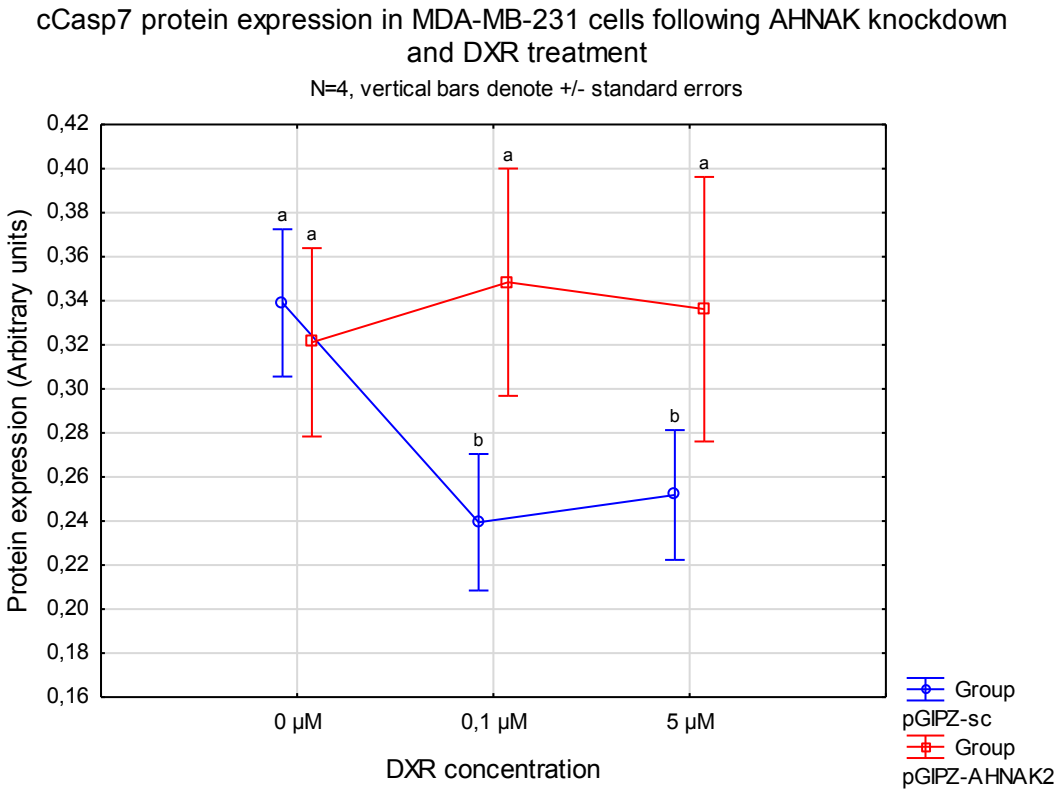

Figure 3.50: cCasp7 protein expression in MDA-MB-231 cells in response to AHNAK knockdown with pGIPZ-AHNAK2 transfection and DXR treatment for 24 hrs.

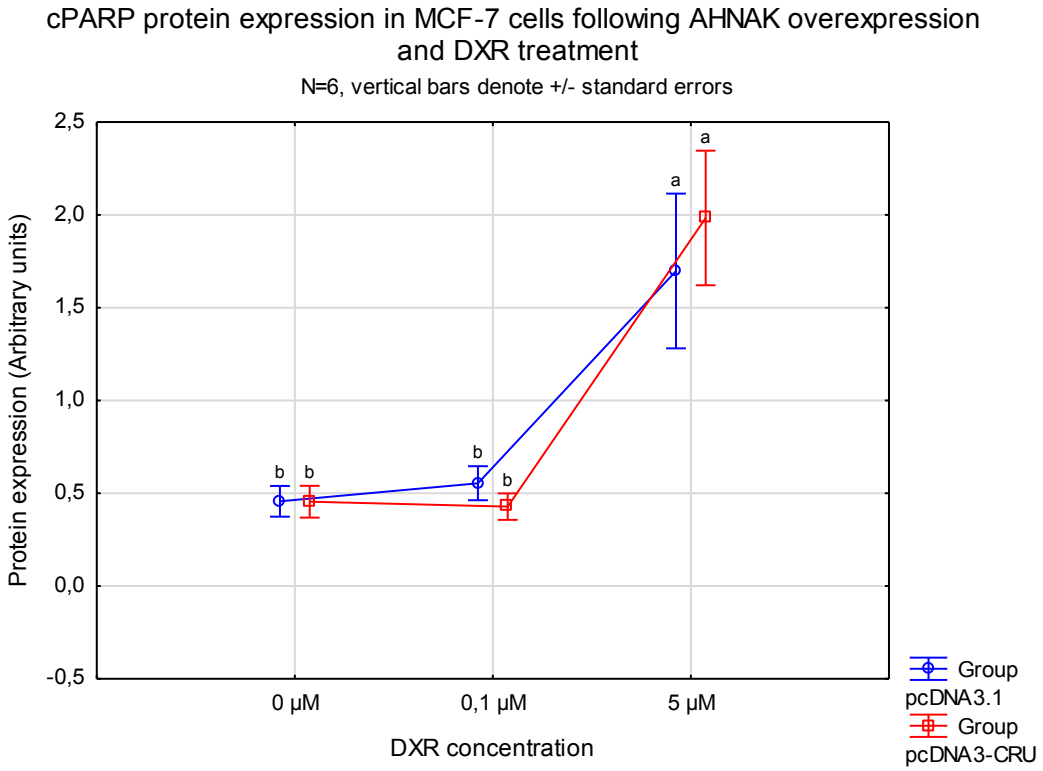

Figure 3.51: cPARP protein expression in MCF-7 cells in response to AHNAK overexpression with pcDNA3-CRU transfection and DXR treatment for 24 hrs.

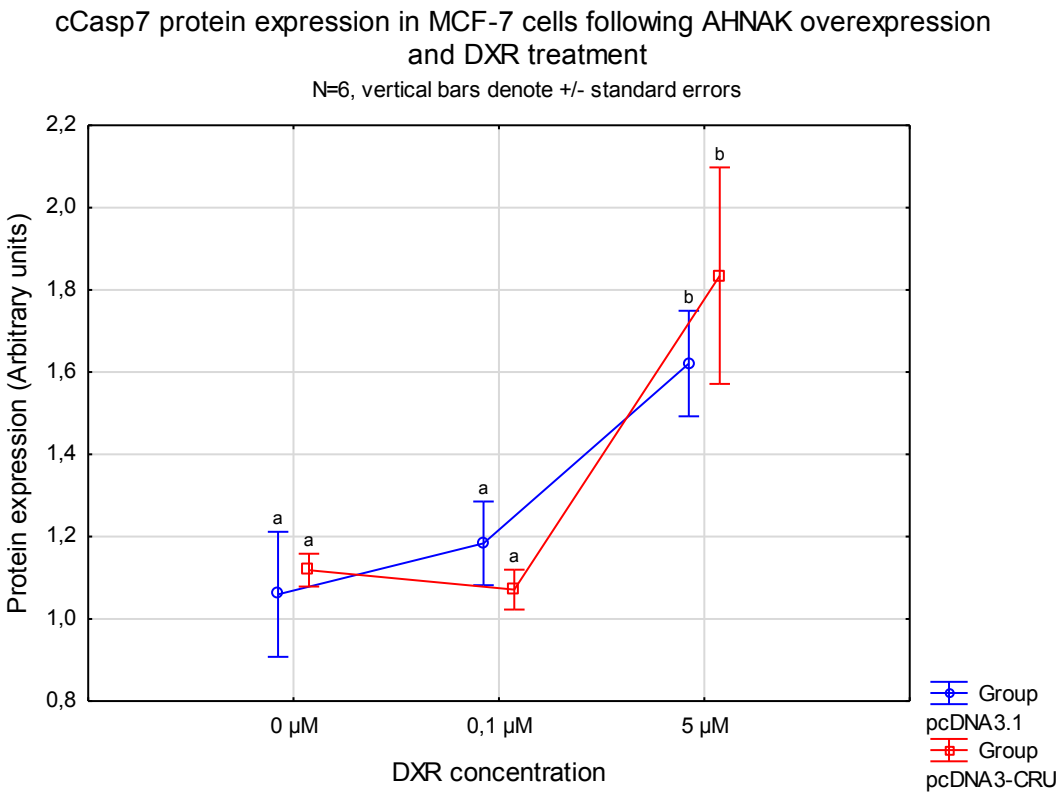

Figure 3.52: cCasp7 protein expression in MCF-7 cells in response to AHNAK overexpression with pcDNA3-CRU transfection and DXR treatment for 24 hrs.

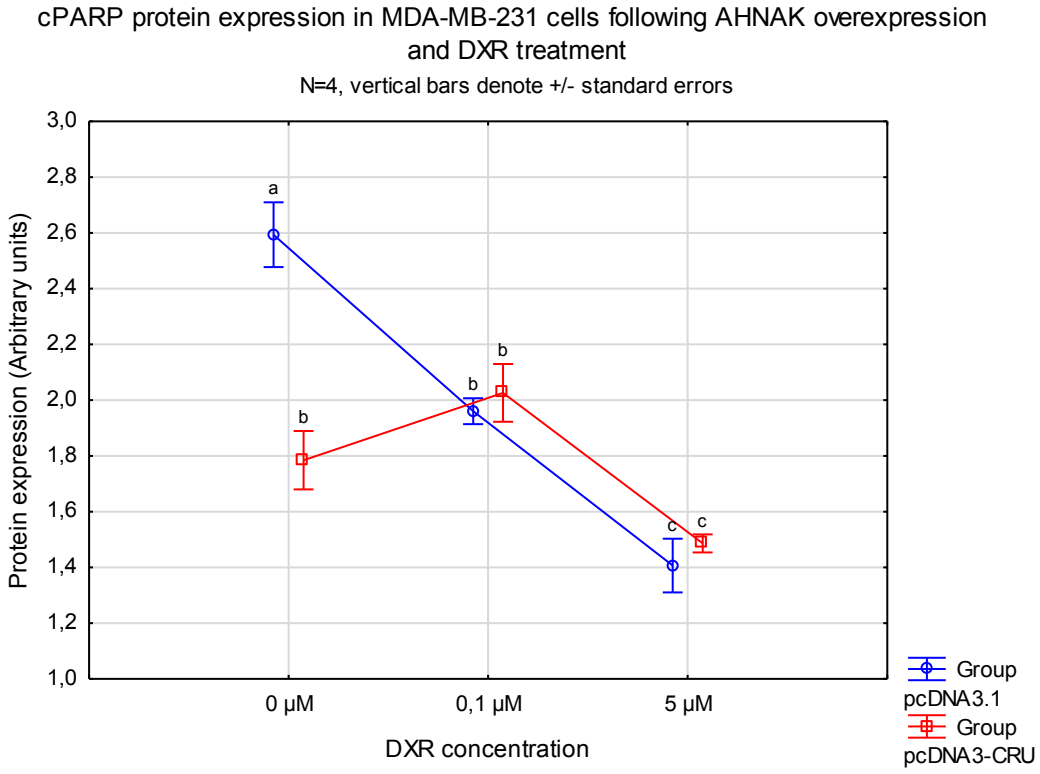

Figure 3.53: cPARP protein expression in MDA-MB-231 cells in response to AHNAK overexpression with pcDNA3-CRU transfection and DXR treatment for 24 hrs.

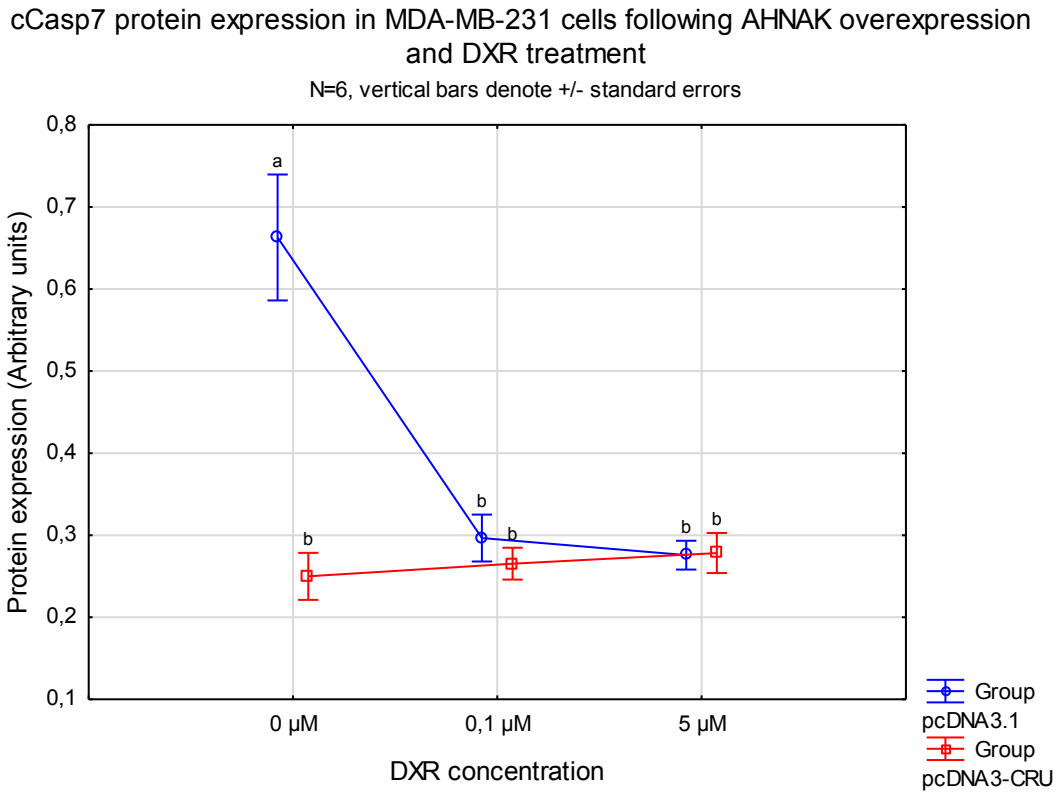

Figure 3.54: cCasp7 protein expression in MDA-MB-231 cells in response to AHNAK overexpression with pcDNA3-CRU transfection and DXR treatment for 24 hrs.

3.3.4 AHNAK is required for DXR-induced cell cycle modulation

In order to determine whether AHNAK can affect the cell cycle, flow cytometry experiments were performed to assess the distribution of the cell cycle phases in a cell population. MCF-7 and MDA-MB-231 cells were transfected and treated with DXR for 24 hrs, where after cells were prepared for flow cytometry. PI was used to measure the DNA content and to identify cells as either in G_0/G_1 (at rest), S (DNA replication) or G_2/M (growth, preparation for mitosis) phase. Statistical analyses (two-way ANOVAs) were performed for each phase separately and phase-specific graphs can be found in the addendum (fig. 7.1-12). Collective graphs for all three phases showing statistical results for each phase are included below.

In MCF-7 cells both the low and high dose DXR treatments significantly decreased the percentage of cells in the G_0/G_1 phase (74.81% ± 0.78% at pGIPZ-sc 0 µM vs. 64.15% ± 1.82% at pGIPZ-sc 0.1 µM, $p < 0.01$; vs. 66.45% ± 1.40% at pGIPZ-sc 5 µM, $p < 0.05$) while increasing the percentage of cells in the S phase (25.19% ± 0.78% at pGIPZ-sc 0 µM vs. 32.06% ± 1.44% at pGIPZ-sc 0.1 µM, $p < 0.05$; vs. 33.13% ± 1.81% at pGIPZ-sc 5 µM, $p < 0.05$) (fig. 3.55, 3.59). Low dose DXR treatment also significantly increased the percentage of cells in the G_2/M phase (0% vs. 3.79% ± 0.45%, $p < 0.0001$). Knockdown of AHNAK had no effect on this and a similar significant decrease and increase in percentage of cells in the G_1/G_0 (70.81% ± 1.75% vs. 64.38% ± 2.38%, $p < 0.05$) and S (29.19%

± 1.75% vs. 35.40% ± 2.38%, $p < 0.05$) phases, respectively, were observed when treated with a 5 µM DXR. In MDA-MB-231 cells 5 µM DXR significantly increased the percentage of cells in the S phase (2.07% ± 1.05% vs. 62.07% ± 6.25%, $p < 0.0001$) with a concomitant slight decrease in G_0/G_1 (40.75% ± 0.36% vs. 31.92% ± 2.33%, $p < 0.01$) and major decrease in G_2/M (57.18% ± 1.25% vs. 6.01% ± 3.95%, $p < 0.0001$) (fig. 3.56, 3.60). Here, knockdown of AHNAK completely prevented the DXR-induced changes in the cell cycle, restoring the percentage of cells in each phase to their respective basal levels and resulting in significant differences between pGIPZ-sc 5 µM and pGIPZ-AHNAK2 5 µM groups in the G_0/G_1 (31.92% ± 2.33% vs. 38.15% ± 3.35%, $p < 0.05$), S (62.07% ± 6.25% vs. 2.98% ± 2.00%, $p < 0.0001$) and G_2/M (6.01% ± 3.95% vs. 58.87% ± 1.37%, $p < 0.0001$) phases.

In pcDNA3.1 transfected MCF-7 cells an increase in the percentage of cells in the G_2/M phase was observed upon treatment with 0.1 µM DXR (0% vs. 6.43% ± 0.78%, $p < 0.01$), similar to that observed in pGIPZ-sc transfected cells, although no further changes with DXR treatment were observed (fig. 3.57, 3.61). However, with overexpression of AHNAK, a significant decrease in the percentage of cells in G_0/G_1 (77.52% ± 0.81% vs. 59.31% ± 0.78%, $p < 0.001$) and a concomitant increase in the S phase (22.45% ± 0.81% vs. 40.44% ± 0.94%, $p < 0.001$) were observed when cells were treated with 5 µM DXR. A similar increase in the G_2/M phase upon 0.1 µM DXR treatment was observed again (0.04% ± 0.03% vs. 5.53% ± 2.19%, $p < 0.01$). Overexpression of AHNAK in MDA-MB-231 cells had a response opposite to that observed with AHNAK knockdown. As with pGIPZ-sc transfected cells, 5 µM DXR treatment of pcDNA3.1 transfected cells resulted in a significant decrease in the percentage of cells in the G_2/M (49.55% ± 2.20% vs. 1.05% ± 0.78%, $p < 0.0001$) phase and a significant increase in the S phase (1.57% ± 0.36% vs. 58.00% ± 3.20%, $p < 0.0001$) (fig. 3.58, 3.62). The overexpression of AHNAK, on its own, induced changes similar to those observed by the high dose treatment of DXR with significant decreases in G_0/G_1 (48.89% ± 2.55% vs. 39.52% ± 1.13%, $p < 0.05$) and G_2/M (49.55% ± 2.20% vs. 2.72% ± 0.39%, $p < 0.0001$) phases along with a significant increase in S phase (1.57% ± 0.36% vs. 57.75% ± 0.96%, $p < 0.0001$) when compared to pcDNA3.1 transfected cells. No significant differences were observed between pcDNA3.1 5 µM, pcDNA3-CRU 0 µM and pcDNA3-CRU 5 µM in any of the three cell cycle phases.

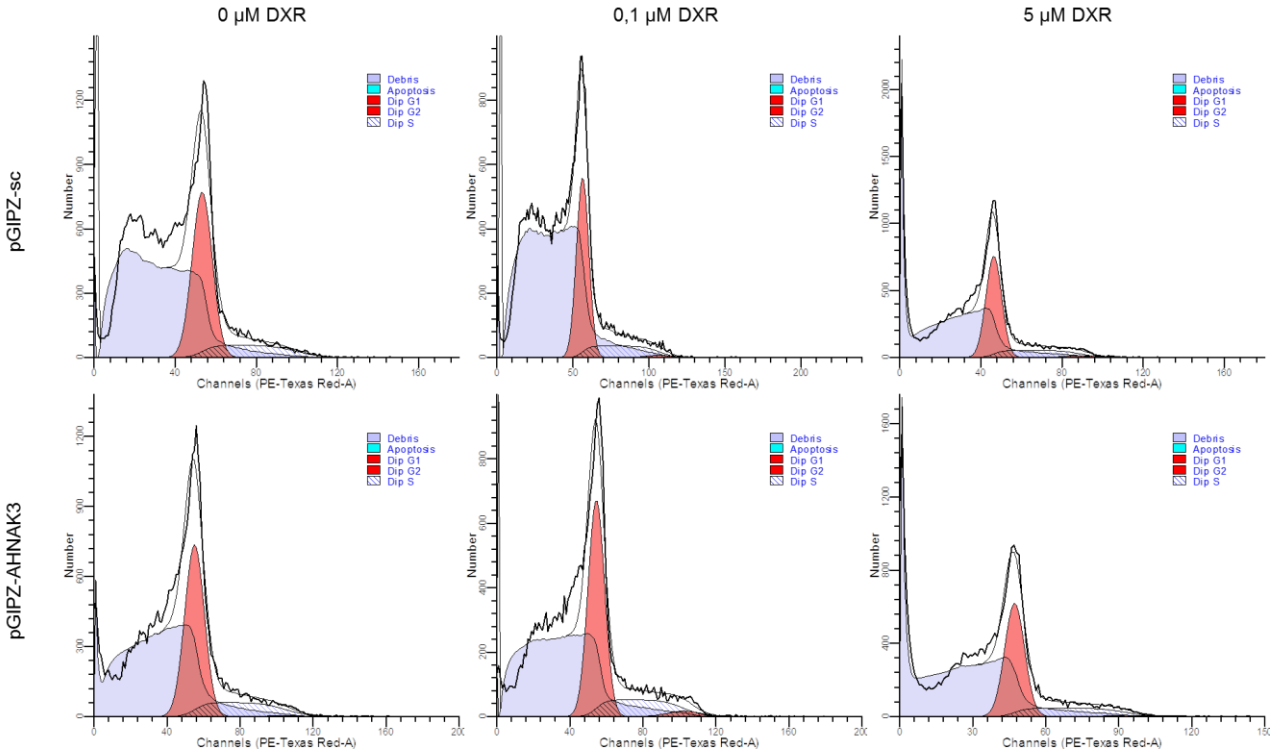

Figure 3.55: Representative images of cell cycle phase peaks in MCF-7 cells following AHNAK knockdown with pGIPZ-AHNAK3 and DXR treatment for 24 hrs.

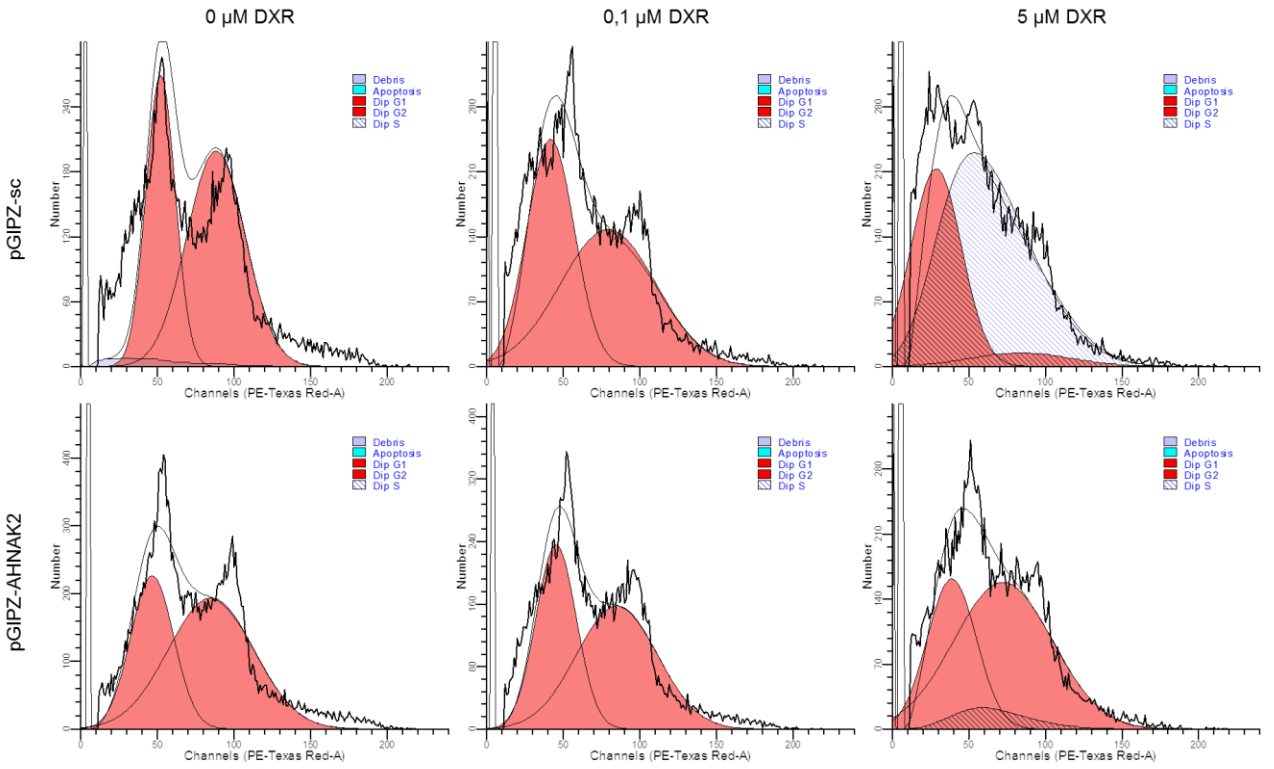

Figure 3.56: Representative images of cell cycle phase peaks in MDA-MB-231 cells following AHNAK knockdown with pGIPZ-AHNAK2 and DXR treatment for 24 hrs.

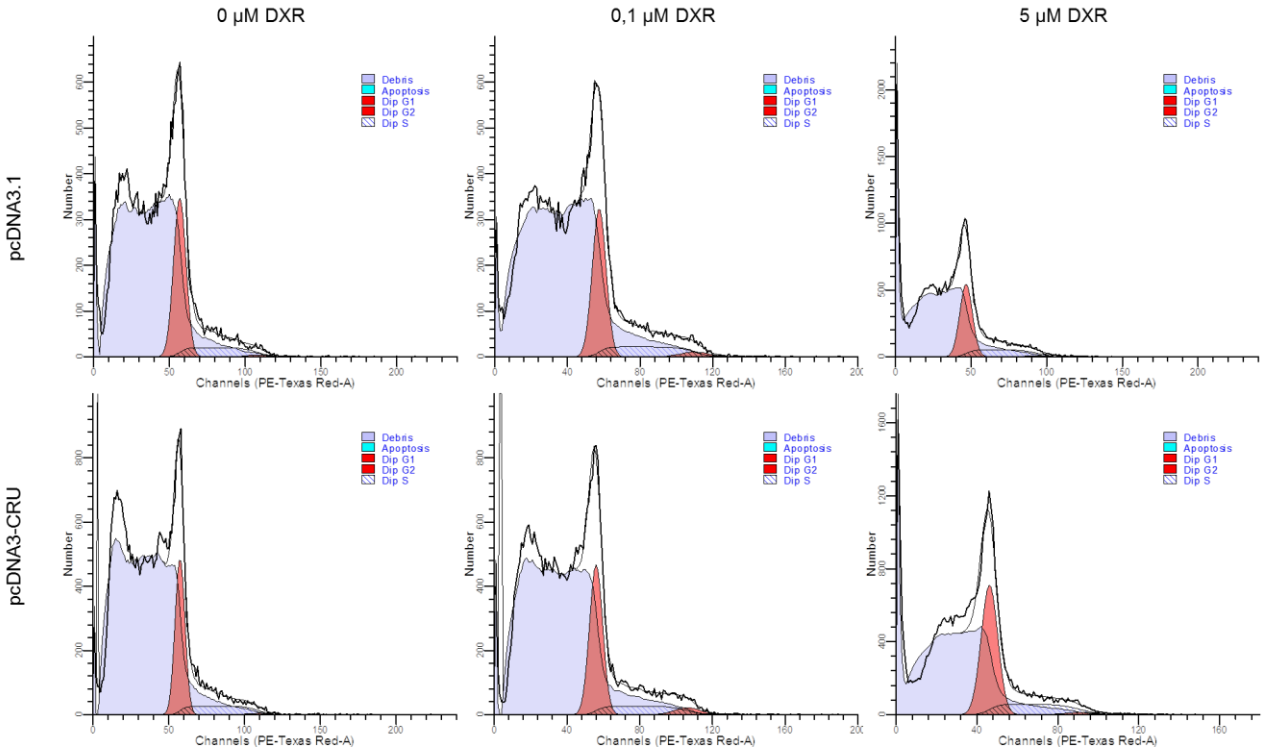

Figure 3.57: Representative images of cell cycle phase peaks in MCF-7 cells following AHNAK overexpression with pcDNA3-CRU and DXR treatment for 24 hrs.

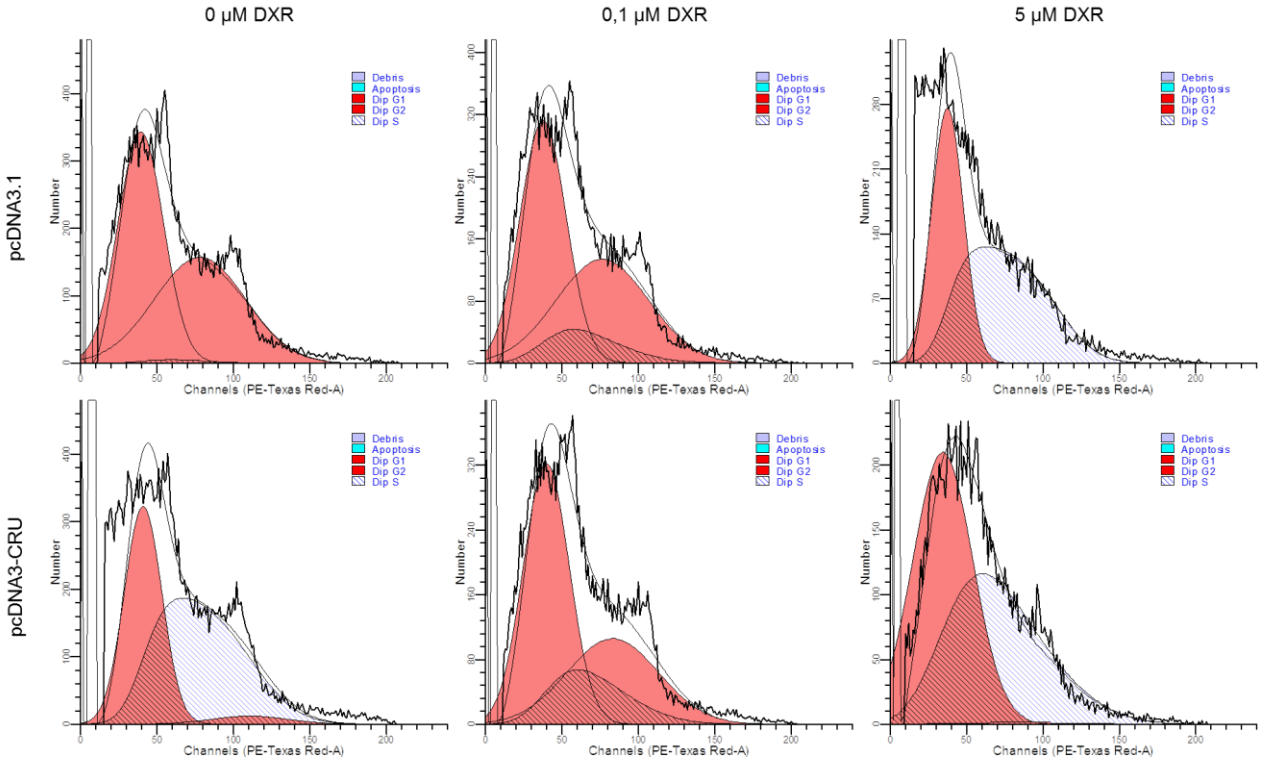

Figure 3.58: Representative images of cell cycle phase peaks in MDA-MB-231 cells following AHNAK overexpression with pcDNA3-CRU and DXR treatment for 24 hrs.

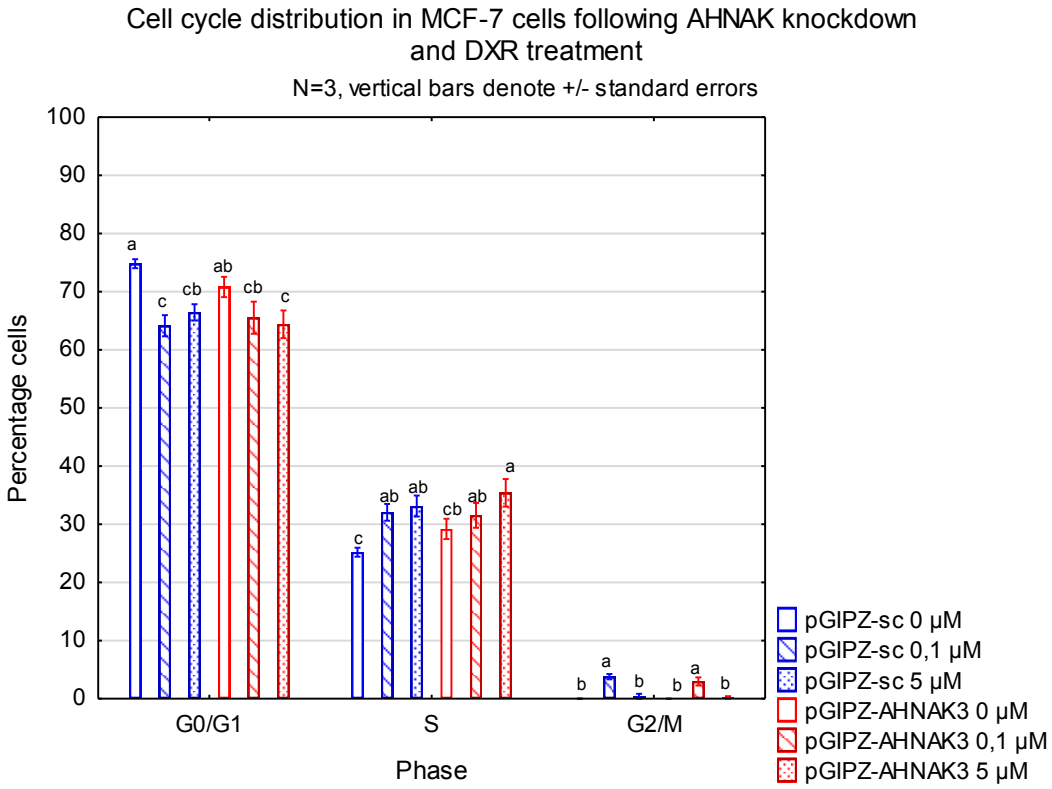

Figure 3.59: Distribution of cell cycle phases in MCF-7 cells following AHNAK knockdown with pGIPZ-AHNAK3 and DXR treatment for 24 hrs.

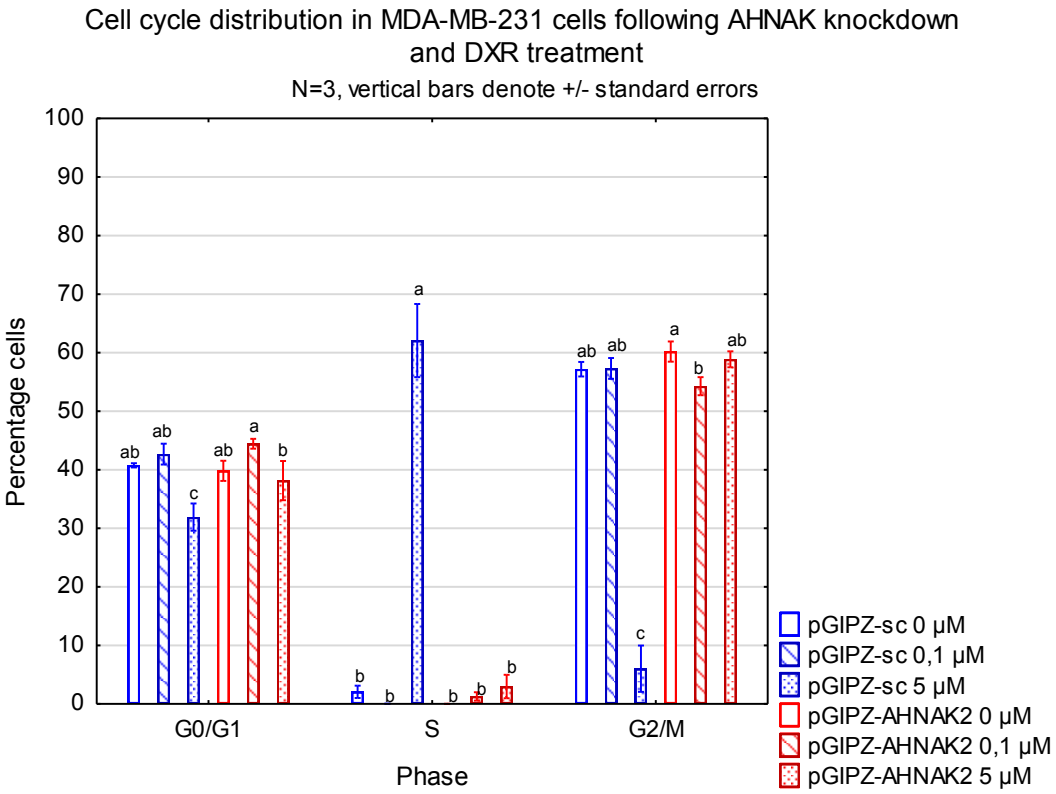

Figure 3.60: Distribution of cell cycle phases in MDA-MB-231 cells following AHNAK knockdown with pGIPZ-AHNAK2 and DXR treatment for 24 hrs.

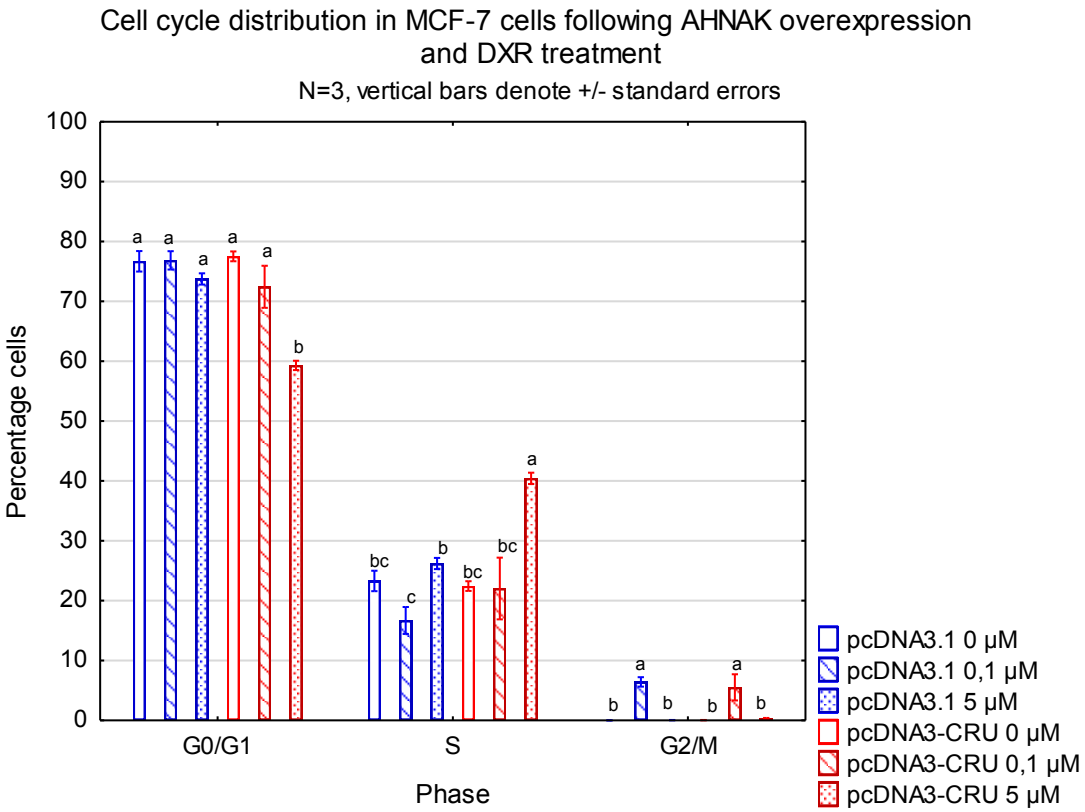

Figure 3.61: Distribution of cell cycle phases in MCF-7 cells following AHNAK overexpression with pcDNA3-CRU and DXR treatment for 24 hrs.

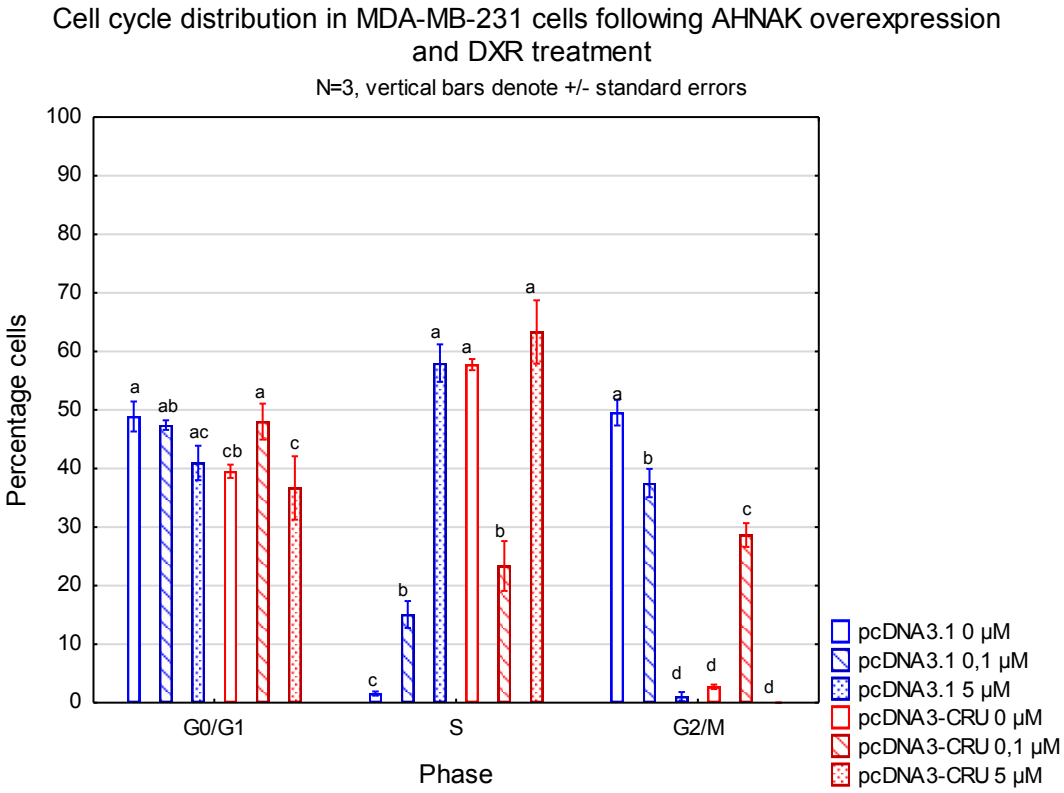

Figure 3.62: Distribution of cell cycle phases in MDA-MB-231 cells following AHNAK overexpression with pcDNA3-CRU and DXR treatment for 24 hrs.

3.4 The effects of AHNAK on cellular migration

3.4.1 AHNAK influences the expression of EMT markers in mesenchymal-like cells

To determine whether AHNAK has a role in the EMT process Western blot experiments were performed for the markers E-cadherin (epithelial state), Snail and Vimentin (mesenchymal state) in MCF-7 (epithelial-like) and MDA-MB-231 (mesenchymal-like) cells following AHNAK knockdown/overexpression and DXR treatment. The expression of these markers were also compared (qualitatively) between the two cell lines to confirm their characteristics (fig. 3.63). A decrease in E-cadherin expression coupled with increased expression of Snail and Vimentin would suggest activation of EMT while the opposite indicates the reverse of EMT, namely MET.

Arbitrary values obtained from processed Western blots were analysed with two-way ANOVAs. A 5 μM DXR treatment in MCF-7 cells induced a significant decrease in E-cadherin protein expression (4.51 ± 1.16 vs. 2.40 ± 0.57, $p < 0.0001$) with a concomitant increase in Snail protein expression (1.08 ± 0.28 vs. 5.43 ± 0.96, $p < 0.0001$), indicative of activation of EMT (fig. 3.64, 3.66, 3.67). Knockdown of AHNAK had no effect on this as pGIPZ-AHNAK3 transfected cells followed the same response with no significant differences when compared to the pGIPZ-sc groups. Expression of the mesenchymal marker Vimentin could not be detected in MCF-7 cells and could not be induced by either DXR treatment or knockdown of AHNAK. In contrast to the MCF-7 cells, no changes was observed in E-cadherin expression in pGIPZ-sc transfected MDA-MB-231 cells upon DXR treatment while 5 μM DXR resulted in a significant decrease in Snail protein expression (1.11 ± 0.13 vs. 0.61 ± 0.11, $p < 0.001$) (fig. 3.64, 3.68, 3.69). Here, knockdown of AHNAK combined with a high dose of DXR resulted in increased E-cadherin expression (0.55 ± 0.12 vs. 0.87 ± 0.26, $p < 0.05$) while the level of Snail protein expression remained fairly similar irrespective of DXR treatment. Knockdown of AHNAK seemed to induce a general trend to increase Vimentin protein expression with significant differences at both the low (0.98 ± 0.11 vs. 1.29 ± 0.12, $p < 0.05$) and high (1.01 ± 0.07 vs. 1.26 ± 0.09, $p < 0.05$) doses of DXR (fig. 3.64, 3.70).

Similar responses were observed in pcDNA3.1 and pcDNA3-CRU transfected MCF-7 cells. A treatment of 5 μM DXR induced a significant decrease in E-cadherin expression (2.78 ± 0.31 at pcDNA3.1 0 μM vs. 1.10 ± 0.10 at pcDNA3.1 5 μM, $p < 0.0001$; 2.47 ± 0.36 at pcDNA3-CRU 0 μM vs. 1.42 ± 0.22 at pcDNA3-CRU 5 μM, $p < 0.0001$) along with a significant increase in Snail expression (0.29 ± 0.08 at pcDNA3.1 0 μM vs. 3.12 ± 0.38 at pcDNA3.1 5 μM, $p < 0.0001$; 0.22 ± 0.06 at pcDNA3-CRU 0 μM vs. 3.15 ± 0.53 at pcDNA3-CRU 5 μM, $p < 0.0001$) in both the pcDNA3.1 and pcDNA3-CRU transfected groups (fig. 3.65, 3.71, 3.72). Again, Vimentin protein expression could not be detected in these cells. In MDA-MB-231 cells E-cadherin expression was again unaffected by DXR while the high dose induced a significant decrease in Snail protein expression (1.74 ± 0.33 vs. 0.62 ± 0.13, $p < 0.0001$) (fig. 3.65, 3.73, 3.74). Overexpression of AHNAK also

induced increased E-cadherin expression when combined with a high dose of DXR (1.22 ± 0.20 vs. 1.67 ± 0.27, $p < 0.0001$) while a decrease in the basal level of Snail expression was observed (1.74 ± 0.33 vs. 1.05 ± 0.19, $p < 0.001$) which decreased further with 5 µM DXR treatment (1.05 ± 0.19 vs. 0.53 ± 0.09, $p < 0.01$). A high dose DXR treatment induced a significant decreased in Vimentin expression (2.55 ± 0.26 vs. 2.20 ± 0.38, $p < 0.05$), while overexpression of AHNAK reduced the basal expression of this protein to levels similar of those induced by DXR (2.55 ± 0.26 vs. 1.94 ± 0.29, $p < 0.01$) (fig. 3.65, 3.75).

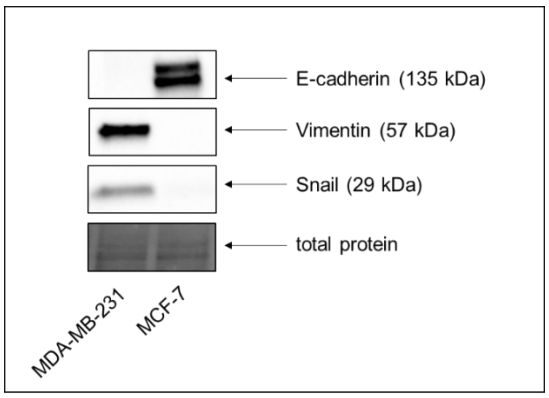

Figure 3.63: Representative of Western blots for E-cadherin, Snail and Vimentin in MCF-7 and MDA-MB-231 cell lines confirming their epithelial-like and mesenchymal-like characteristics.

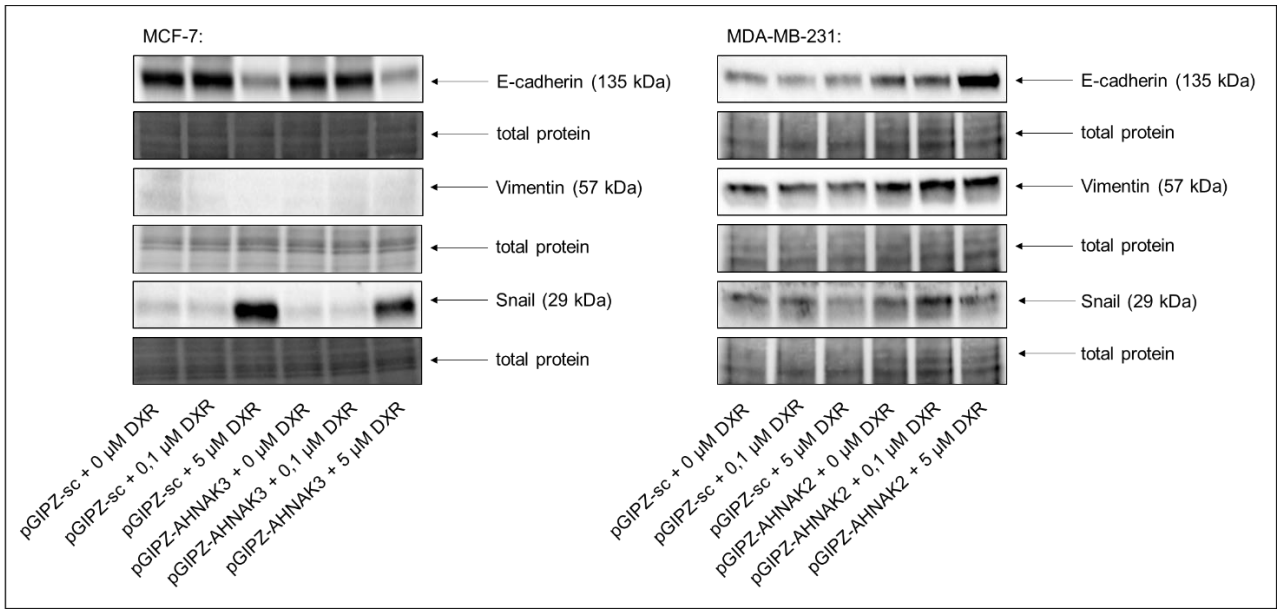

Figure 3.64: Representative images of Western blot experiments for EMT markers E-cadherin, Snail and Vimentin in MCF-7 and MDA-MB-231 cells following AHNAK knockdown with pGIPZ-AHNAK3 and pGIPZ-AHNAK2, respectively, and DXR treatment for 24 hrs.

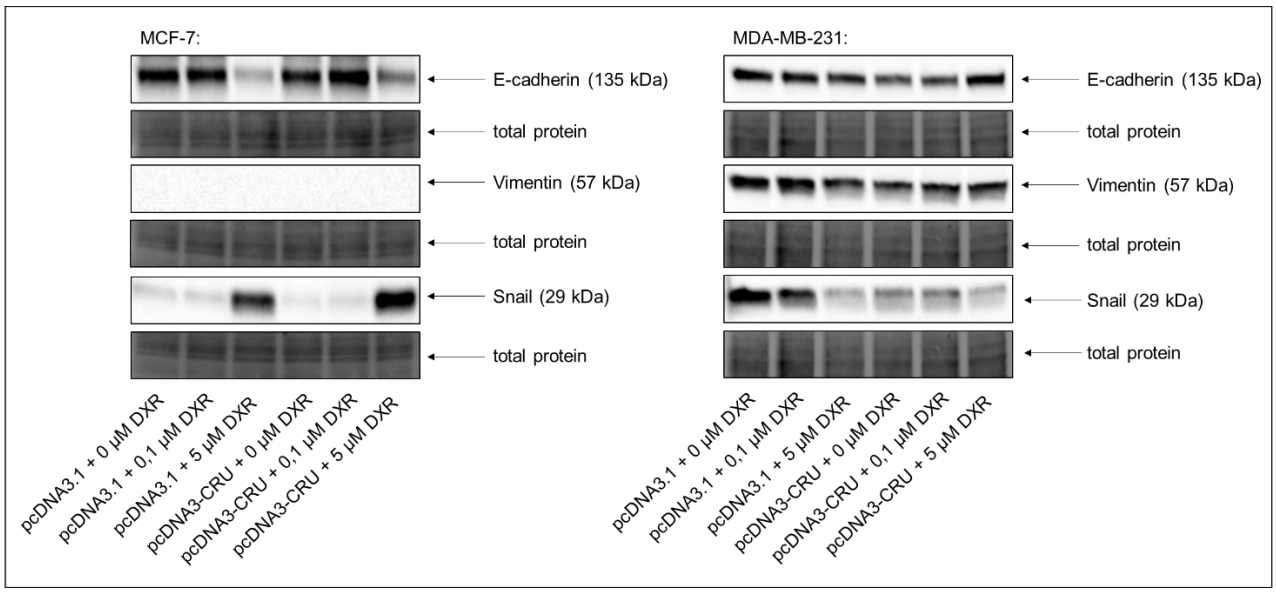

Figure 3.65: Representative images of Western blot experiments for EMT markers E-cadherin, Snail and Vimentin in MCF-7 and MDA-MB-231 cells following AHNAK overexpression with pcDNA3-CRU and DXR treatment for 24 hrs.

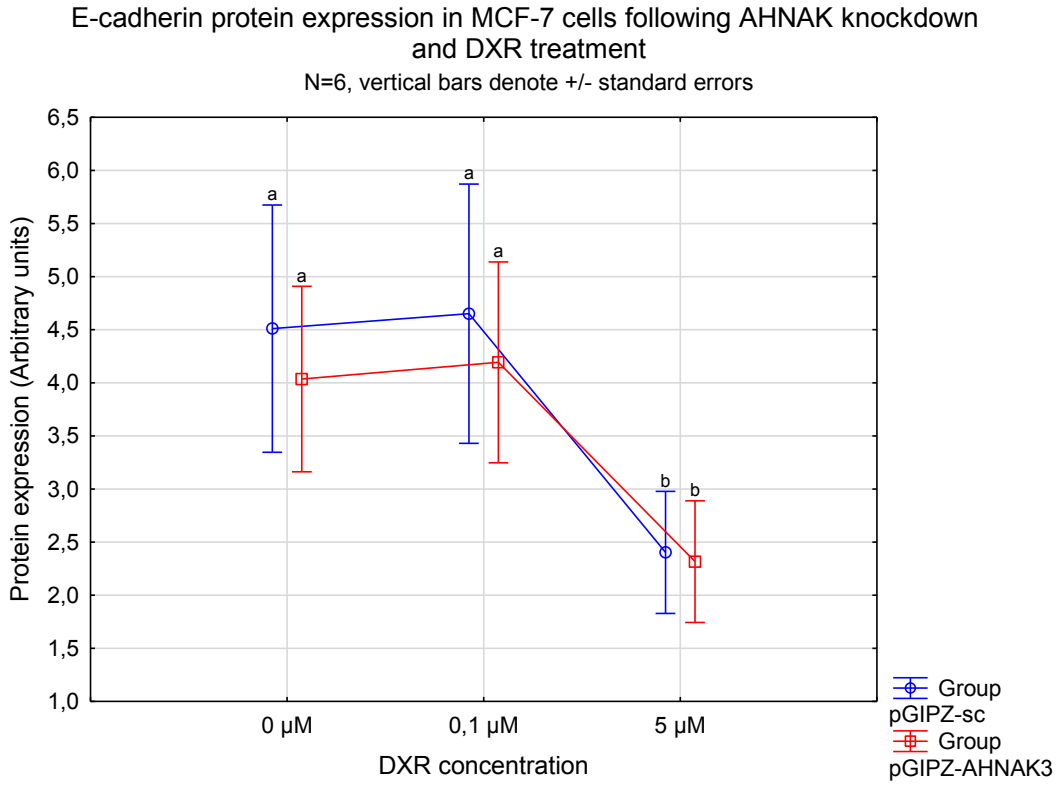

Figure 3.66: E-cadherin protein expression in MCF-7 cells following AHNAK knockdown with pGIPZ-AHNAK3 and DXR treatment for 24 hrs.

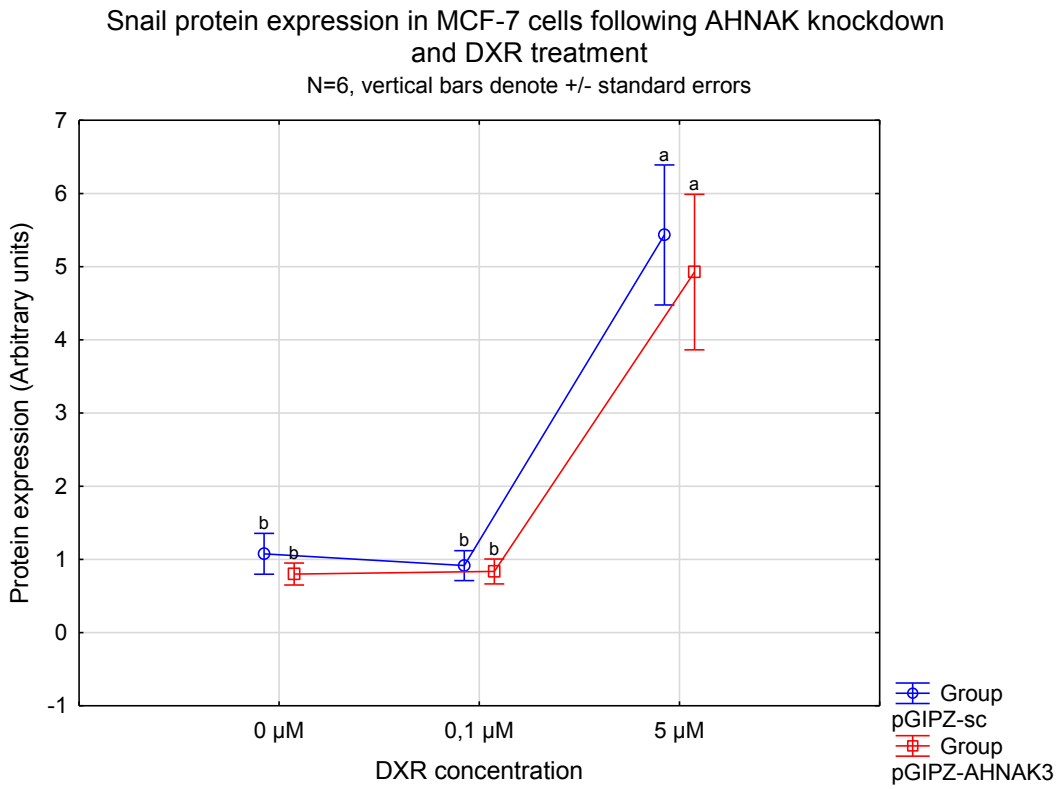

Figure 3.67: Snail protein expression in MCF-7 cells following AHNAK knockdown with pGIPZ-AHNAK3 and DXR treatment for 24 hrs.

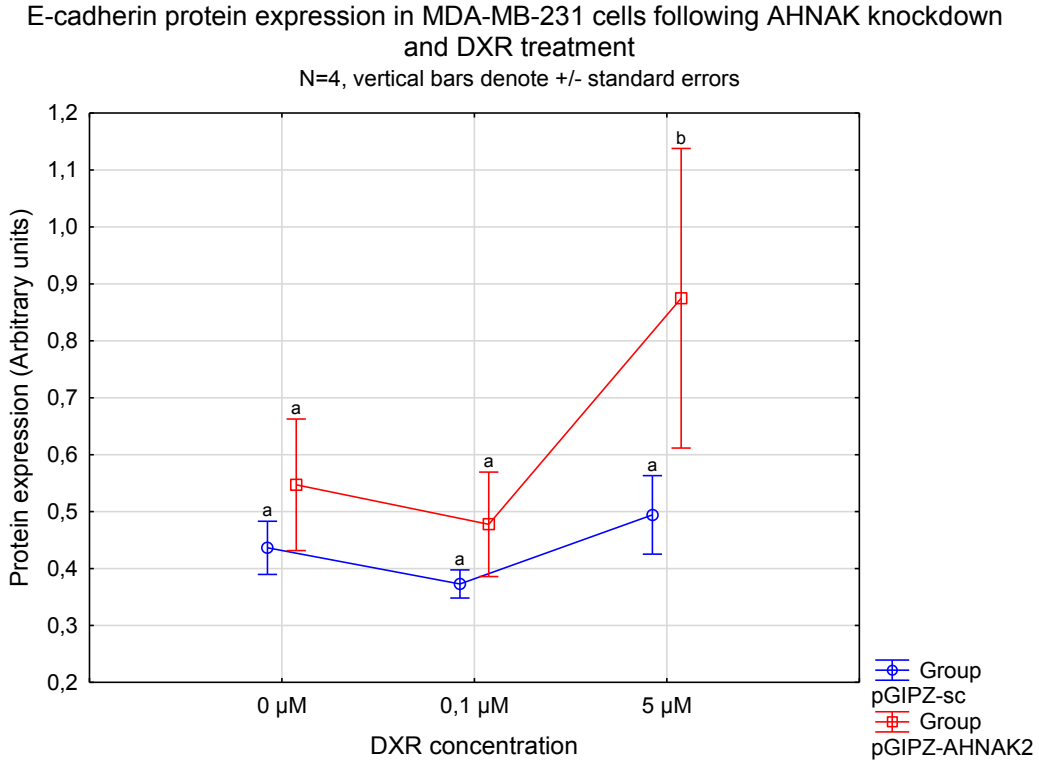

Figure 3.68: E-cadherin protein expression in MDA-MB-231 cells following AHNAK knockdown with pGIPZ-AHNAK2 and DXR treatment for 24 hrs.

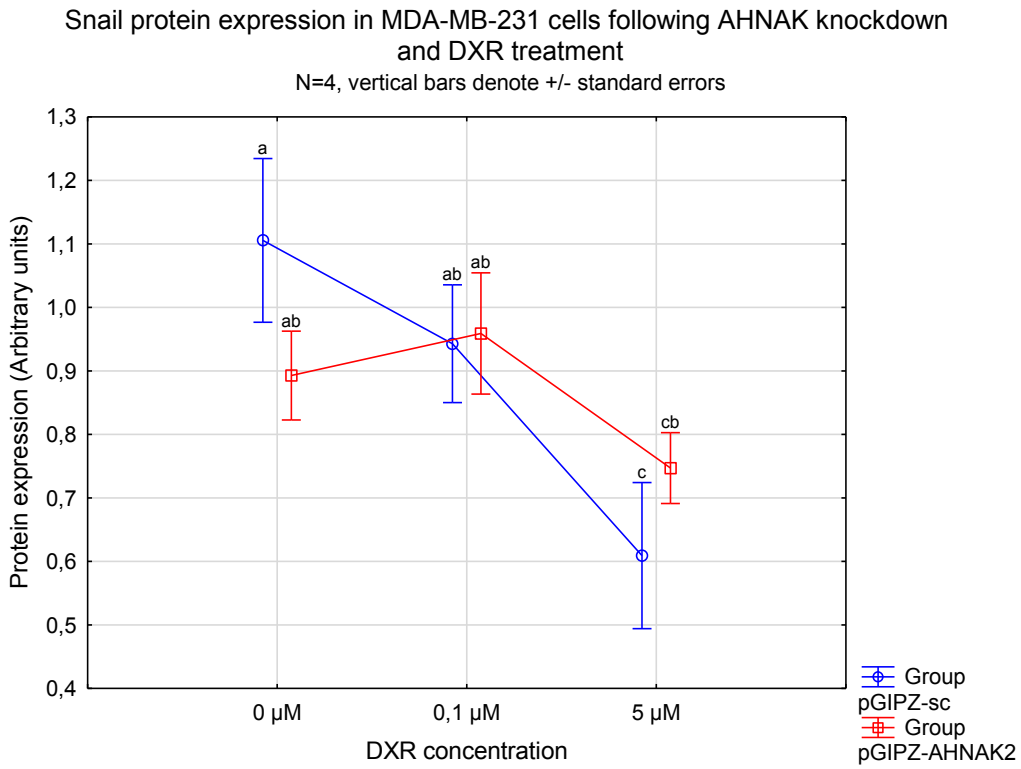

Figure 3.69: Snail protein expression in MDA-MB-231 cells following AHNAK knockdown with pGIPZ-AHNAK2 and DXR treatment for 24 hrs.

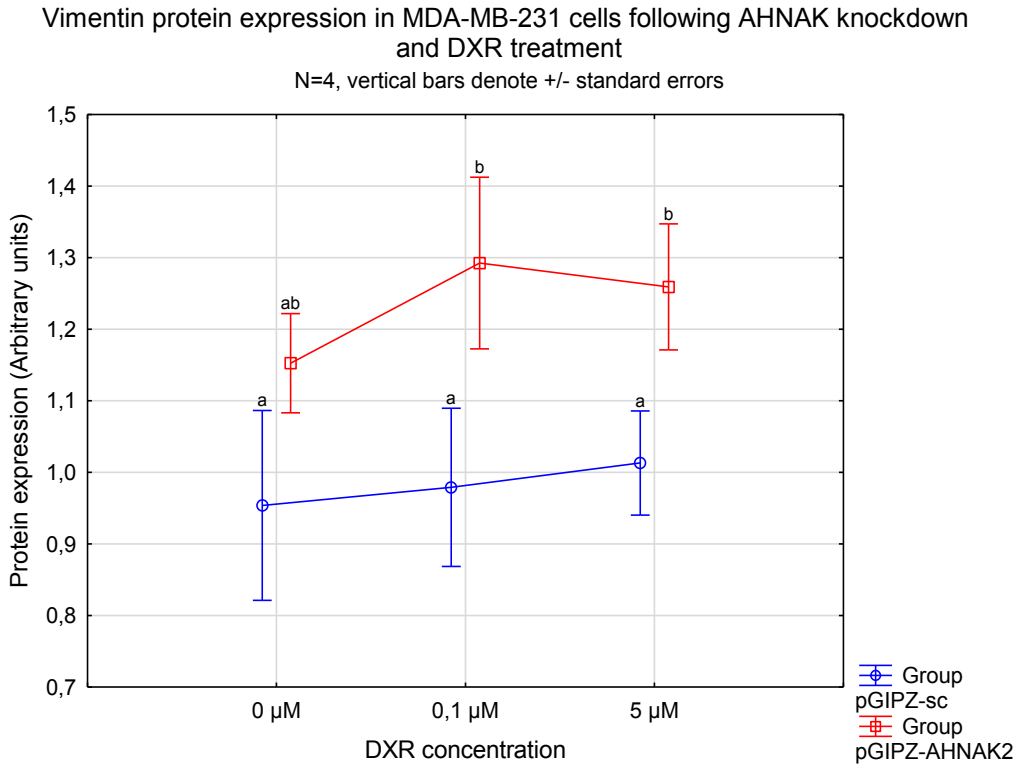

Figure 3.70: Vimentin protein expression in MDA-MB-231 cells following AHNAK knockdown with pGIPZ-AHNAK2 and DXR treatment for 24 hrs.

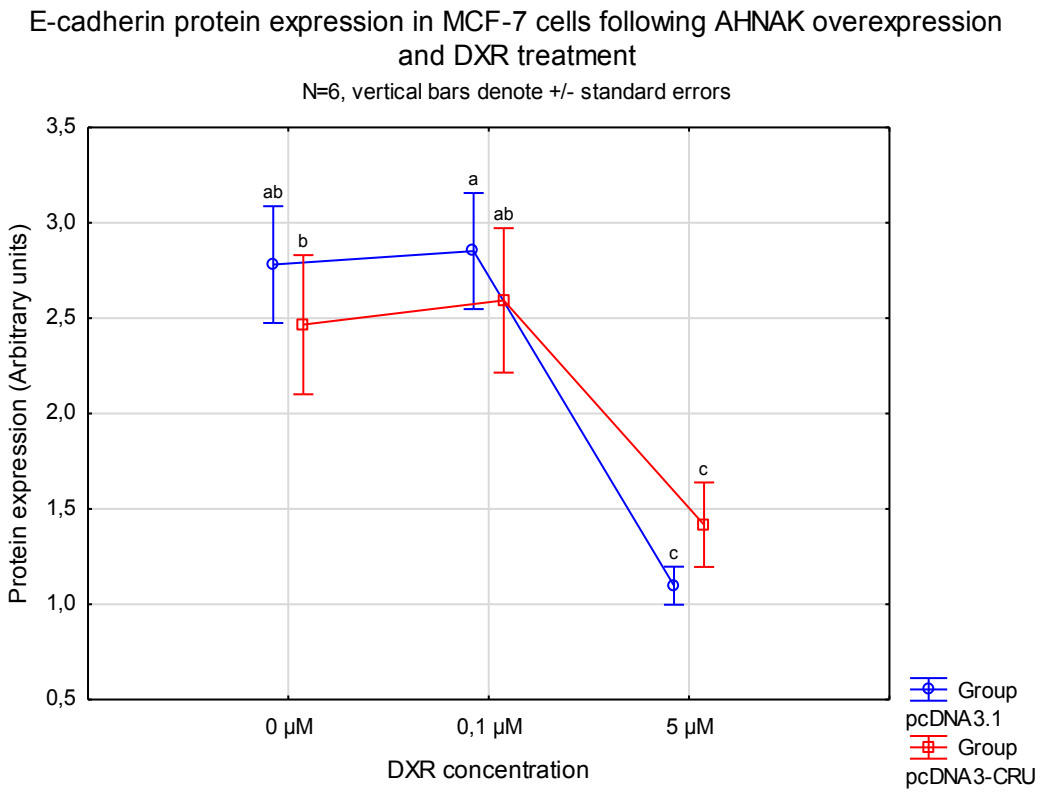

Figure 3.71: E-cadherin protein expression in MCF-7 cells following AHNAK overexpression with pcDNA3-CRU and DXR treatment for 24 hrs.

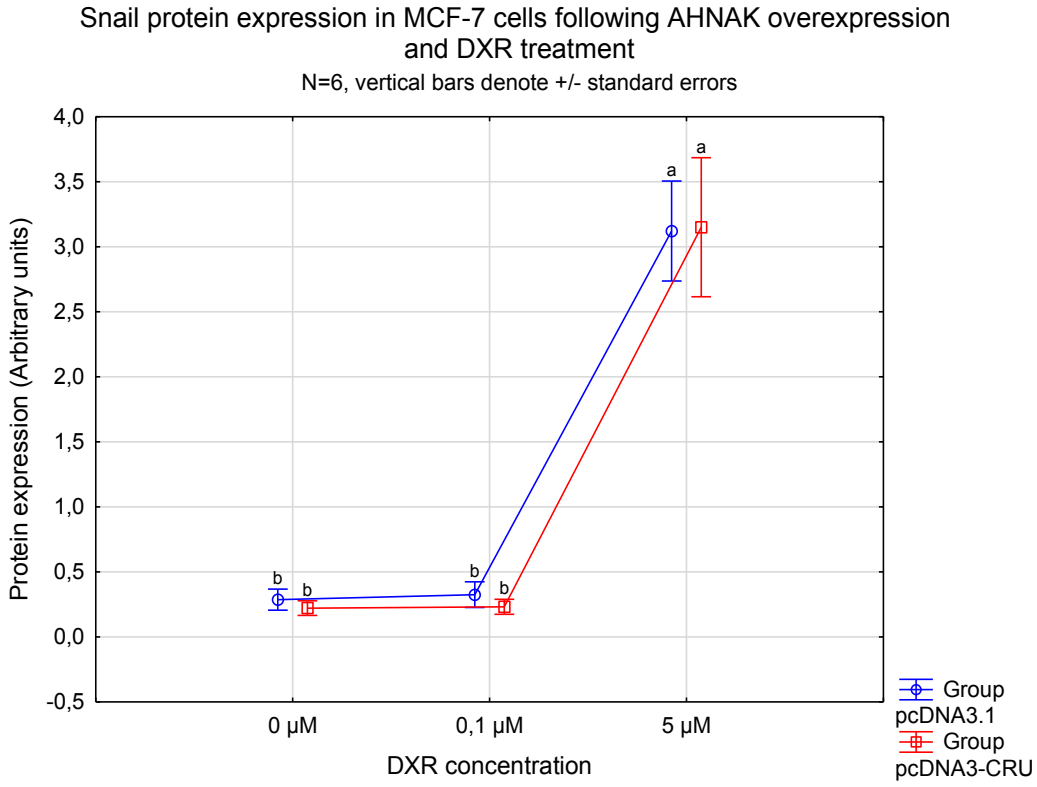

Figure 3.72: Snail protein expression in MCF-7 cells following AHNAK overexpression with pcDNA3-CRU and DXR treatment for 24 hrs.

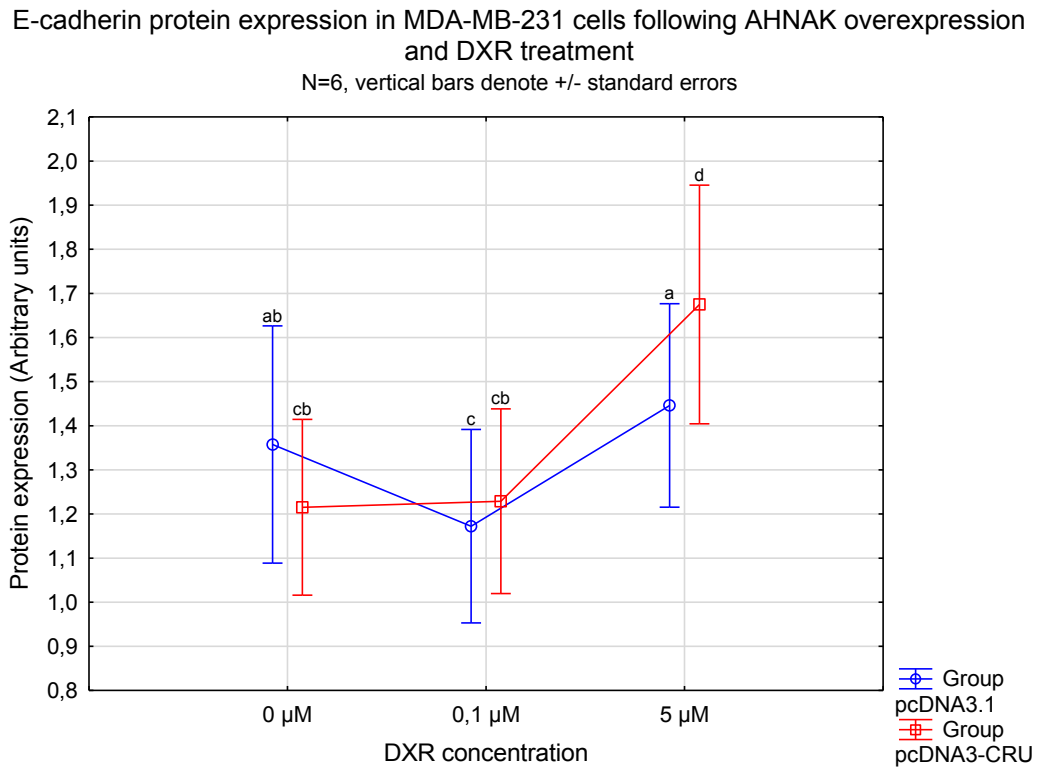

Figure 3.73: E-cadherin protein expression in MDA-MB-231 cells following AHNAK overexpression with pcDNA3-CRU and DXR treatment for 24 hrs.

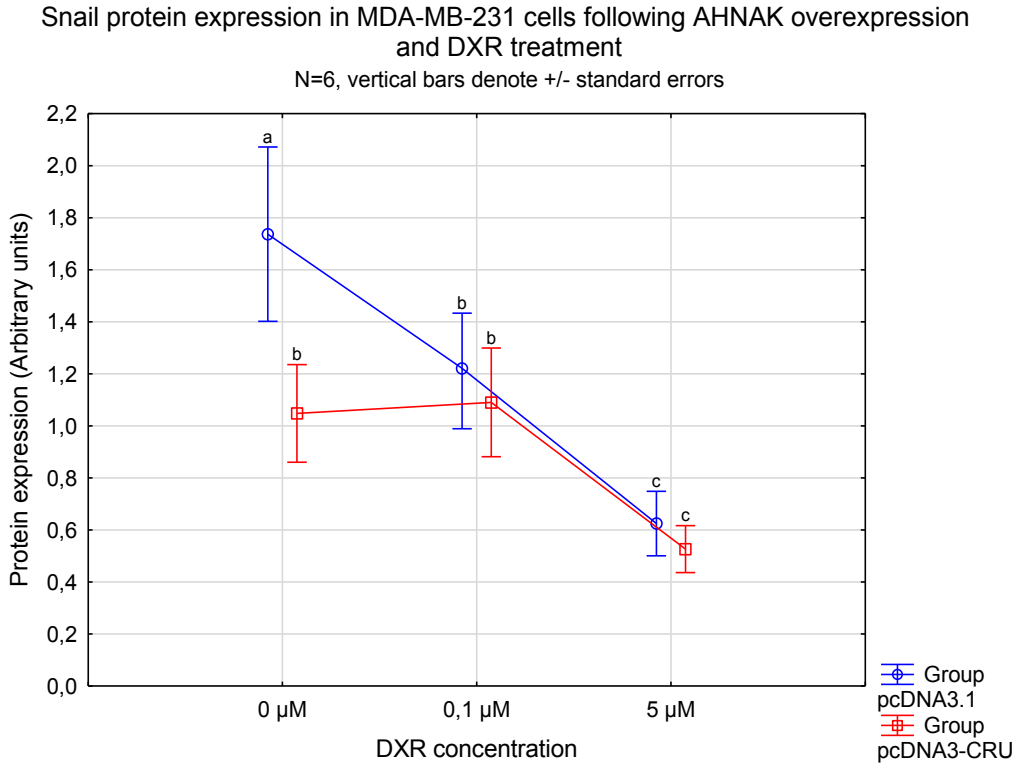

Figure 3.74: Snail protein expression in MDA-MB-231 cells following AHNAK overexpression with pcDNA3-CRU and DXR treatment for 24 hrs.

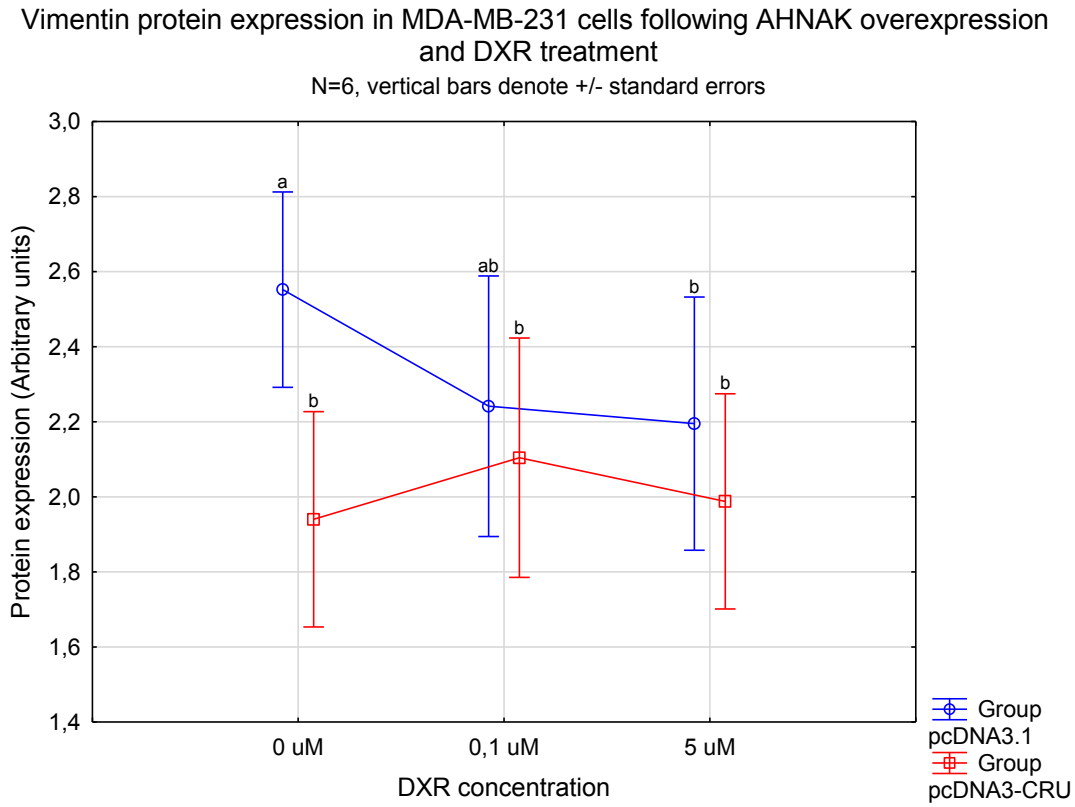

Figure 3.75: Vimentin protein expression in MDA-MB-231 cells following AHNAK overexpression with pcDNA3-CRU and DXR treatment for 24 hrs.

3.4.2 Overexpression of AHNAK affects cellular migration

Wound healing assays were performed following AHNAK knockdown/overexpression to determine whether the protein can influence cellular migration. To exclude the effects of cellular proliferation cells were treated with MMC.

Initial treatments with MMC were performed to determine the optimal concentration required for inhibition of cellular proliferation. MCF-7 and MDA-MB-213 cells were treated with a range of concentrations for 24 hrs where after cells were fixed and stained with the nuclear dye Hoechst. Nuclear counts revealed treatments of 1 µg/ml and 5 µg/ml to be most suitable for the MCF-7 and MDA-MB-231 cell lines, respectively, since in each case, lower doses showed signs of cellular proliferation and higher doses showed signs of cell death (table 3.3).

Table 3.3: Nuclear counts during MMC optimisation

MCF-7						
Group (time point)	Control (0 hrs)	Control (24 hrs)	1 µg/ml (24 hrs)	2 µg/ml (24 hrs)	5 µg/ml (24 hrs)	10 µg/ml (24 hrs)
Average count (N=9)	280.22	426.56	278.44	277.11	47.44	11.00
Total count	2522	3839	2506	2494	427	99
MDA-MB-231						
Group (time point)	Control (0 hrs)	Control (24 hrs)	1 µg/ml (24 hrs)	2 µg/ml (24 hrs)	5 µg/ml (24 hrs)	10 µg/ml (24 hrs)
Average count (N=9)	119.22	247.22	168.44	183.67	109.89	52
Total count	1073	2225	1516	1653	989	468

MMC – mitomycin C

Wound healing assays were performed with both the MCF-7 and MDA-MB-231 cell lines and with DXR treatment for 24 hrs, although MCF-7 cells were not treated with the high dose DXR since the amount of cell death observed in this group does not allow for accurate determination of the wound area. Images of the wound areas were acquired during the 24 hr DXR treatment at time points 6, 12, 18 and 24 hrs and were used to assess the ability of cells to close/re-fill the wound over time. Statistical analyses (two-way ANOVAs) were performed for each time point separately. Collective graphs for all time points showing statistical results for each separate time point are included below. Representative images of wound closure in the MCF-7 and MDA-MB-231 cells across the time-points can be found in the addendum (fig. 7.13-36). As expected, the MMC control groups (not treated with MMC) in each experiment showed significantly higher percentages of wound closure when compared to the other groups, which is most likely due to the fact that wound closure in these groups can be attributed to both cell migration and cell proliferation. A clear difference in the migratory abilities of MCF-7 and MDA-MB-231 cells were also observed; where the percentage of wound closure ranged between 0.04% and 13.42% for MCF-7 cells, a range between 1.25% and 56.56% was observed for the MDA-MB-231 cells. The migration of MCF-7 cells in all groups remained fairly similar and only the pGIPZ-sc 0.1 µM group showed significantly decreased percentage of wound closure after 24 hrs (11.02% ± 1.46% vs. 8.04% ± 1.14%, $p < 0.05$) (fig. 3.77, 3.81). In MDA-MB-231 cells AHNAK knockdown resulted in increased percentage of wound closure but only at the 6 hr time point (7.17% ± 1.19% vs. 10.64% ± 1.10%, $p < 0.05$) (fig. 3.78, 3.82). All groups exhibited fairly similar migration at 12-24 hr time points. Overexpression of AHNAK in MCF-7 cells revealed a general trend of decreased migration (fig. 3.79, 3.83). At both the 12 and 18 hr

time points, pcDNA3-CRU cells displayed decreased percentage wound closure when compared to pcDNA3-CRU cells treated with a low dose DXR (3.98% ± 0.82% vs. 2.00% ± 0.45%, $p < 0.05$ at 12 hrs; 5.79% ± 0.88% vs. 2.86% ± 0.51%, $p < 0.05$ at 18 hrs). At the 18 and 24 hr time points, pcDNA3-CRU cells also displayed decreased percentage wound closure when compared to pcDNA3.1 cells (6.73% ± 1.25% vs. 2.86% ± 0.51%, $p < 0.01$ at 18 hrs; 8.99% ± 1.62% vs. 4.49% vs. 0.73%, $p < 0.05$). Similar results were obtained with the MDA-MB-231 cells (fig. 3.80, 3.84). At the 6 and 12 hr time points, pcDNA3-CRU cells treated with 0.1 µM DXR showed decreased percentage wound closure when compared to pcDNA3.1 0.1 µM DXR group (8.72% ± 1.14% vs. 4.73% ± 0.91%, $p < 0.05$ at 6 hrs; 13.37% ± 0.93% vs. 9.14% ± 1.78%, $p < 0.05$ at 12 hrs). At the 12, 18 and 24 hr time points, pcDNA3-CRU cells treated with 5 µM DXR showed a decreased percentage wound closure compared to the pcDNA3.1 5 µM group (12.15% ± 1.47% vs. 7.29% ± 1.34%, $p < 0.05$ at 12 hrs; 16.20% ± 2.05% vs. 9.39% ± 1.82%, $p < 0.05$ at 18 hrs; 21.51% ± 1.66 vs. 10.40% ± 1.96%, $p < 0.05$). Treatment with a high dose of DXR further slowed down the migration of pcDNA3-CRU transfected cells, since the pcDNA3-CRU 5 µM group showed a significantly decreased percentage wound closure when compared to the pcDNA3-CRU 0 µM group after 24 hrs (18.74% ± 2.25% vs. 10.40% ± 1.96%, $p < 0.05$).

In each experiment the rate of wound closure was also calculated. In both cell lines, and with both AHNAK knockdown and overexpression, these rates stayed fairly constant across time. Significant differences were observed between individual groups at different time points and these mirrored the significant differences obtained when the percentage of wound closure was calculated. Figures 7.37-40 in the addendum shows the collective results for each group across time.

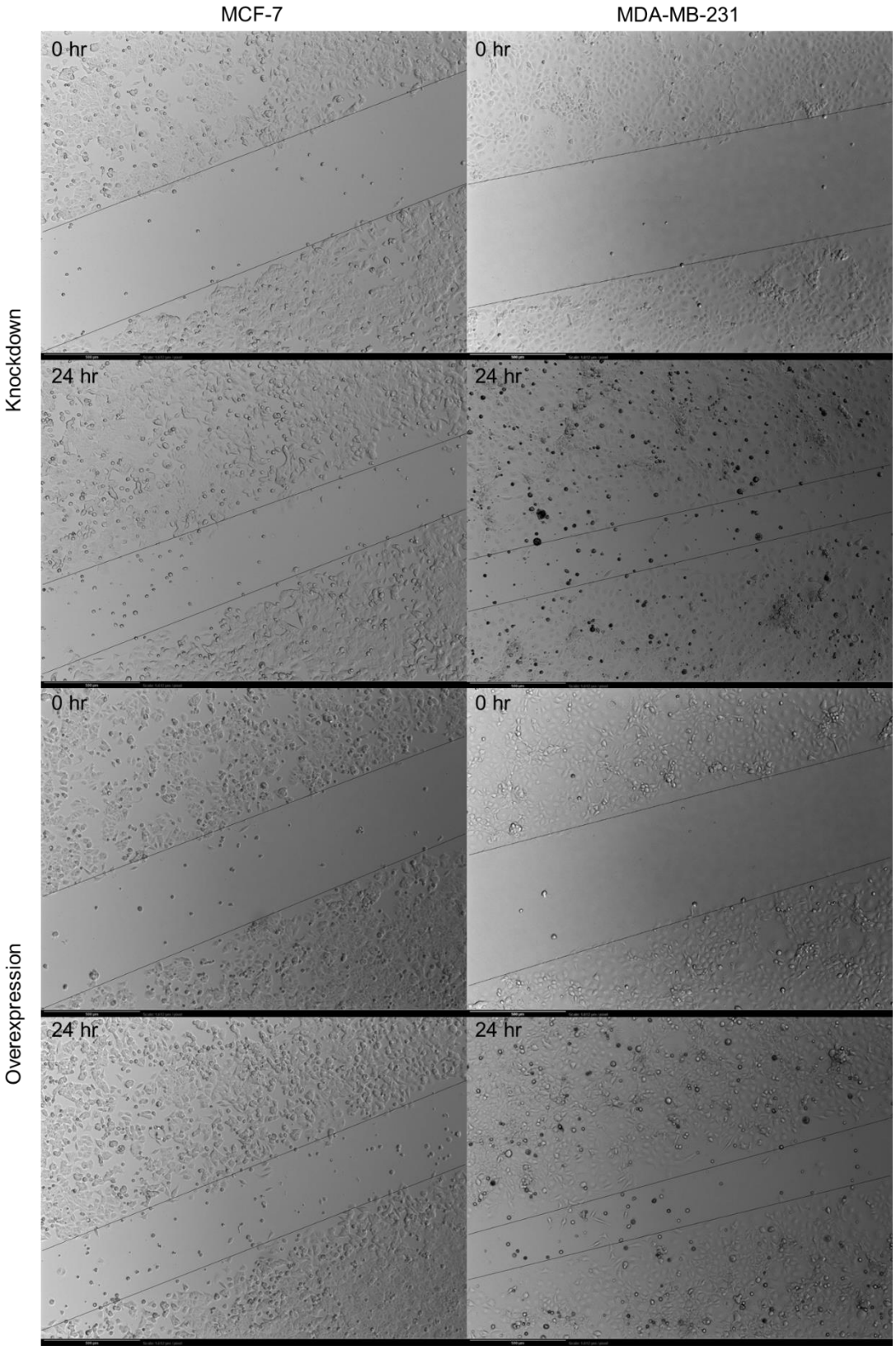

Figure 3.76: Representative brightfield microscopy images of MMC control groups at 0 and 24 hrs for MCF-7 and MDA-MB-231 cell lines in AHNAK knockdown and overexpression experiments. Lines serve as indication of wound area and where drawn to fit the general migration front across the imaged area. Scale = 500 µm, 4x objective.

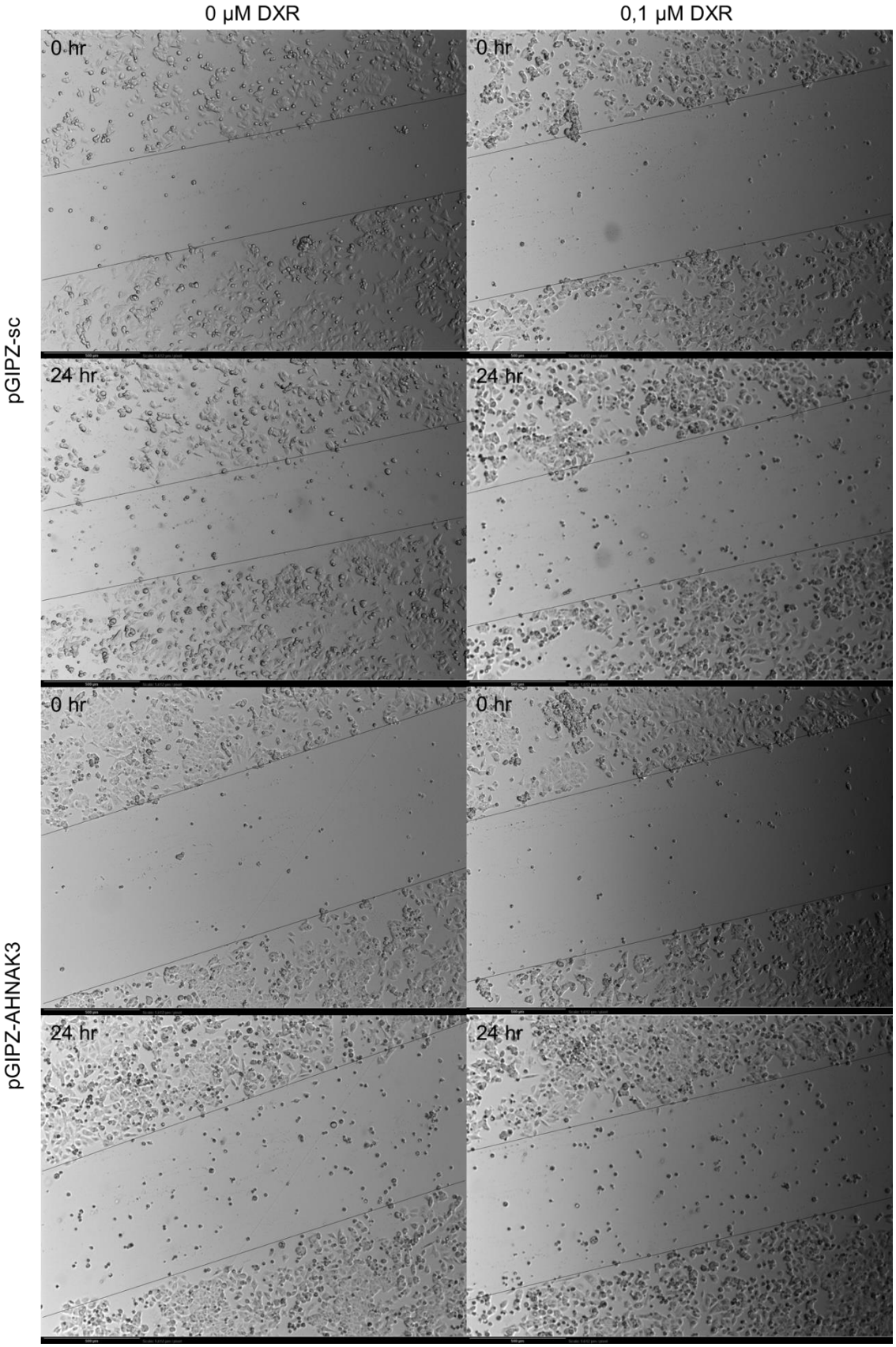

Figure 3.77: Representative brightfield microscopy images of wound closure at 0 and 24 hrs in MCF-7 cells following AHNAK knockdown and DXR treatment. Lines serve as indication of wound area and where drawn to fit the general migration front across the imaged area. Scale = 500 µm, 4x objective.

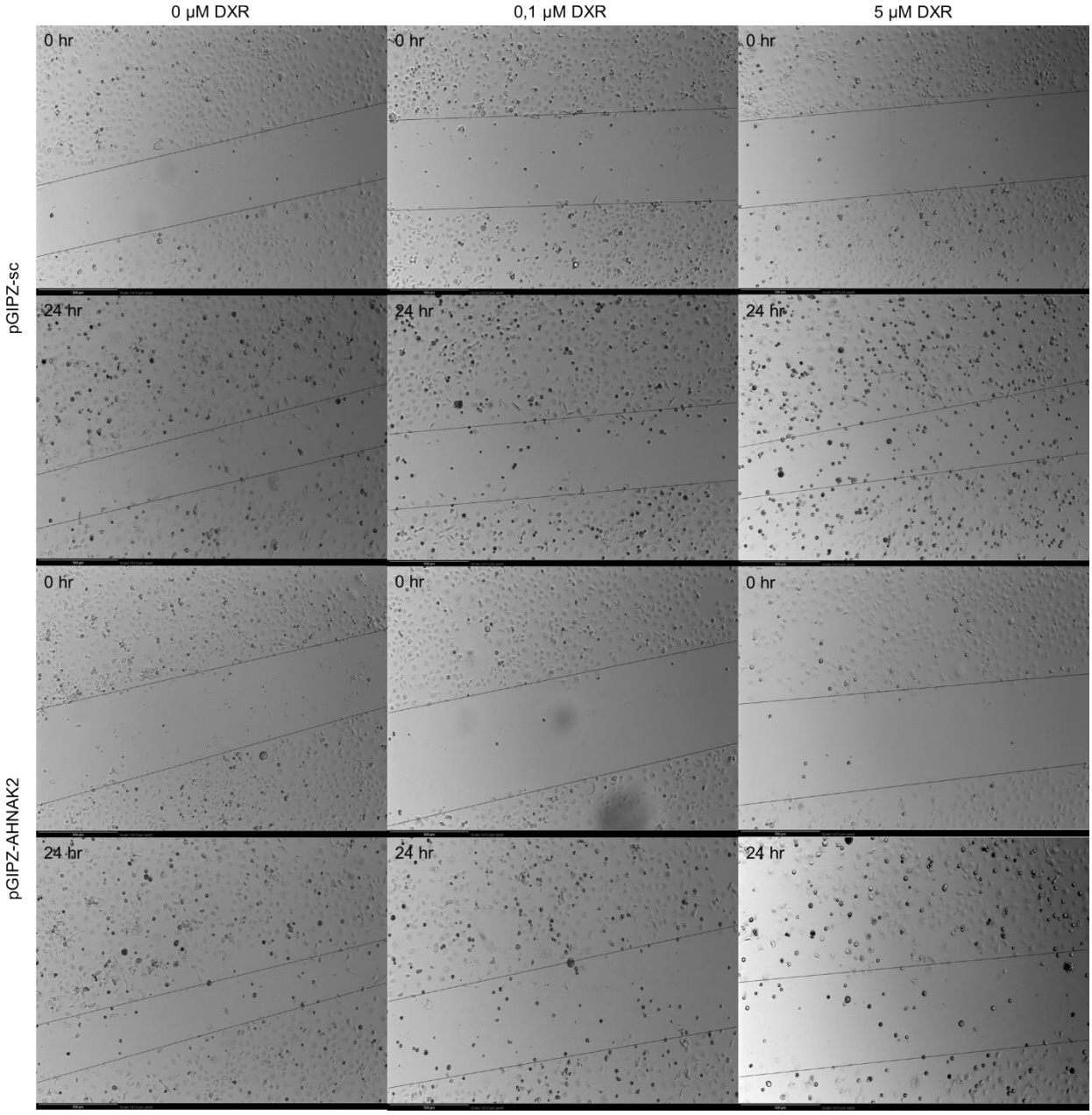

Figure 3.78: Representative brightfield microscopy images of wound closure at 0 and 24 hrs in MDA-MB-231 cells following AHNAK knockdown and DXR treatment. Lines serve as indication of wound area and where drawn to fit the general migration front across the imaged area. Scale = 500 µm, 4x objective.

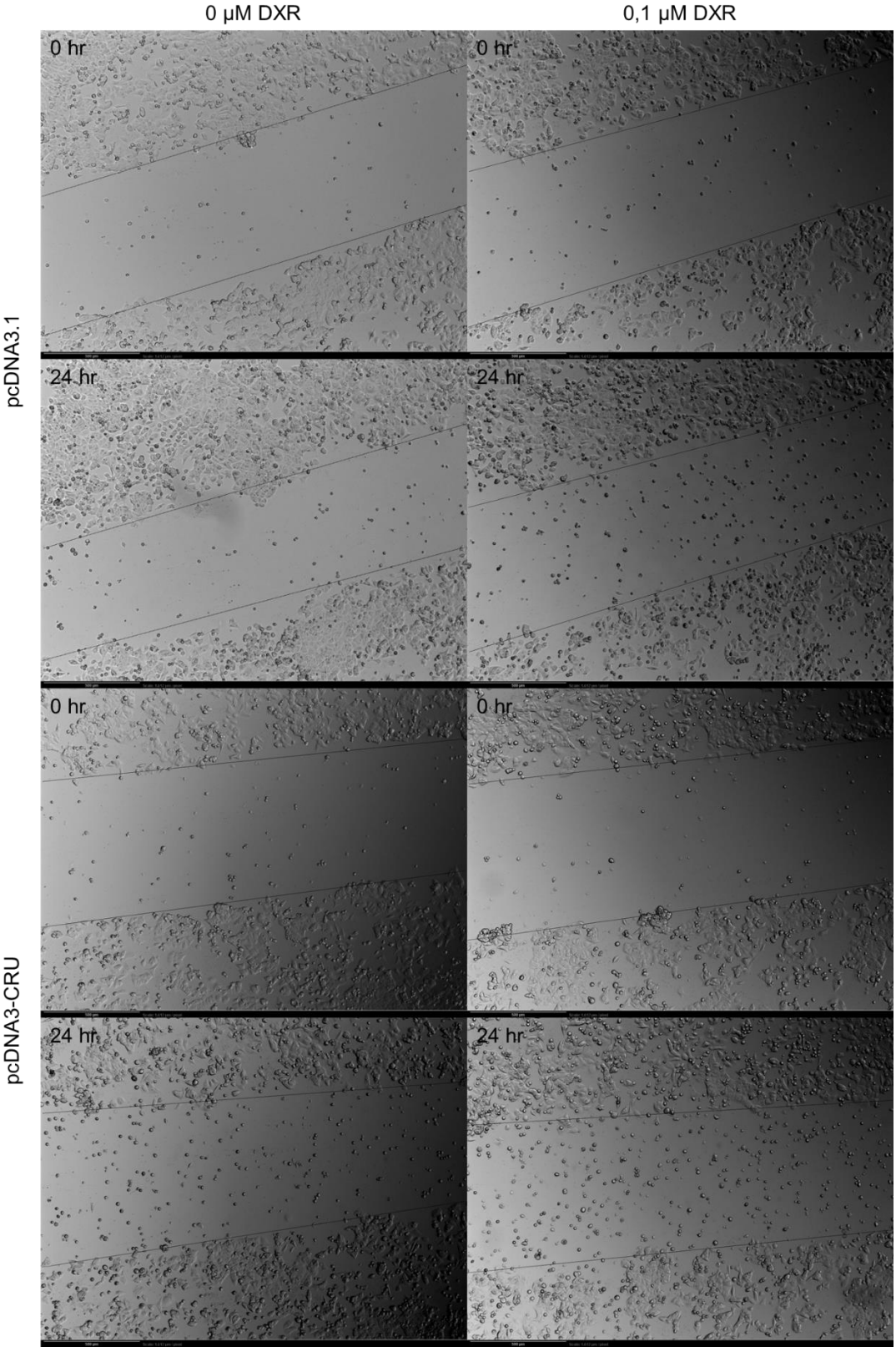

Figure 3.79: Representative brightfield microscopy images of wound closure at 0 and 24 hrs in MCF-7 cells following AHNAK overexpression and DXR treatment. Lines serve as indication of wound area and where drawn to fit the general migration front across the imaged area. Scale = 500 µm, 4x objective.

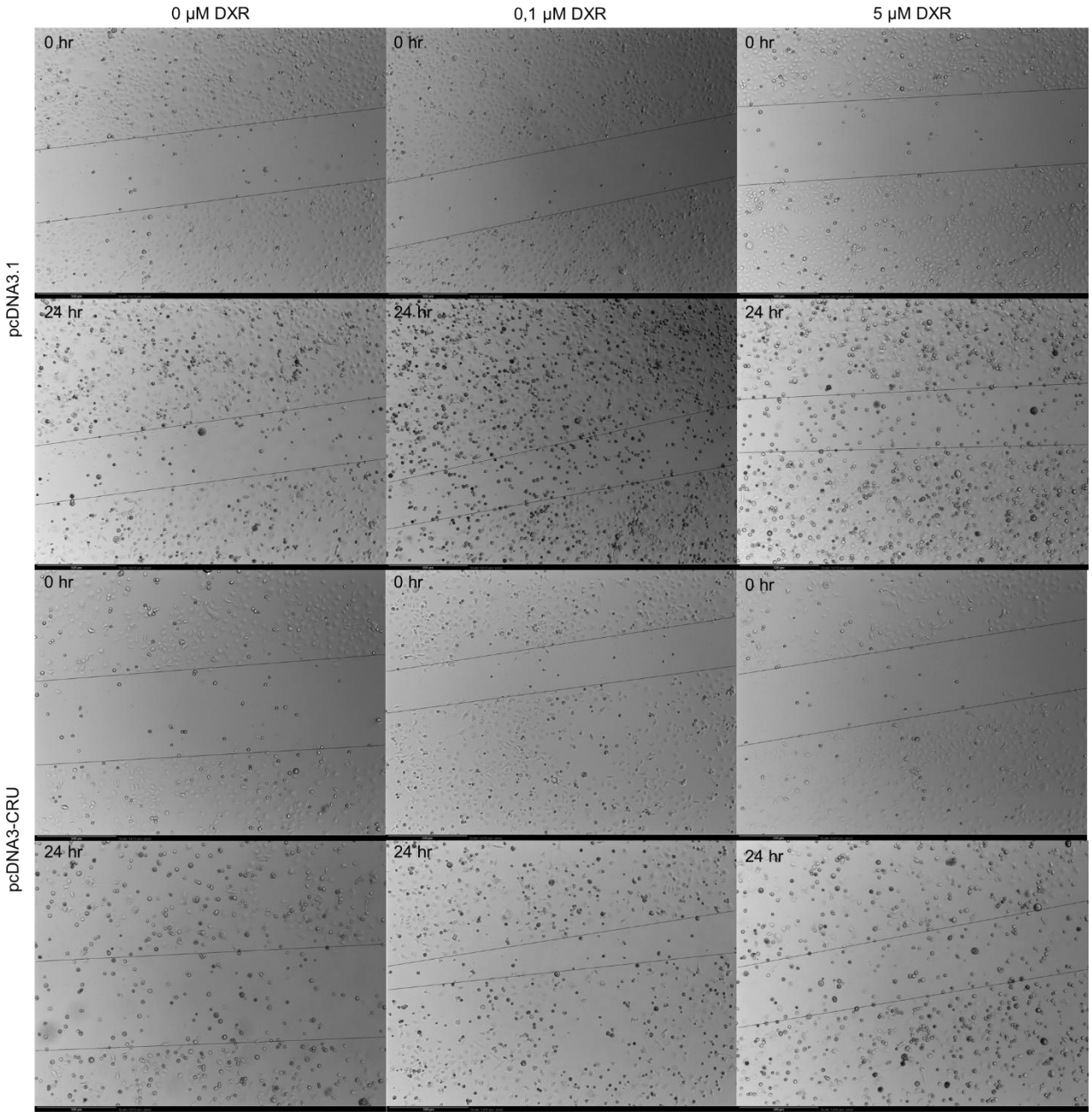

Figure 3.80: Representative brightfield microscopy images of wound closure at 0 and 24 hrs in MDA-MB-231 cells following AHNAK overexpression and DXR treatment. Lines serve as indication of wound area and where drawn to fit the general migration front across the imaged area. Scale = 500 µm, 4x objective.

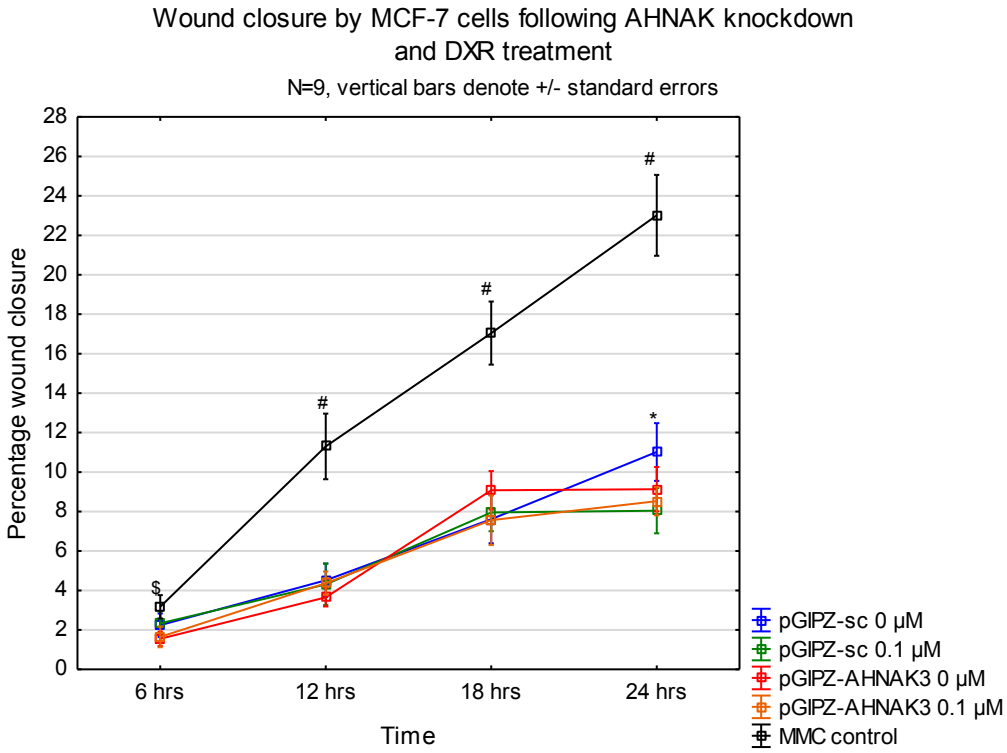

Figure 3.81: Percentage wound closure by MCF-7 cells following AHNAK knockdown and DXR treatment. Statistical significance between groups per time point is indicated by symbols. $ - MMC control vs. pGIPZ-AHNAK3 0 µM, $p < 0.05$; # - MMC control group vs. all other groups, $p < 0.0001$; * - pGIPZ-sc 0 µM vs. pGIPZ-sc 0.1 µM, $p < 0.05$.

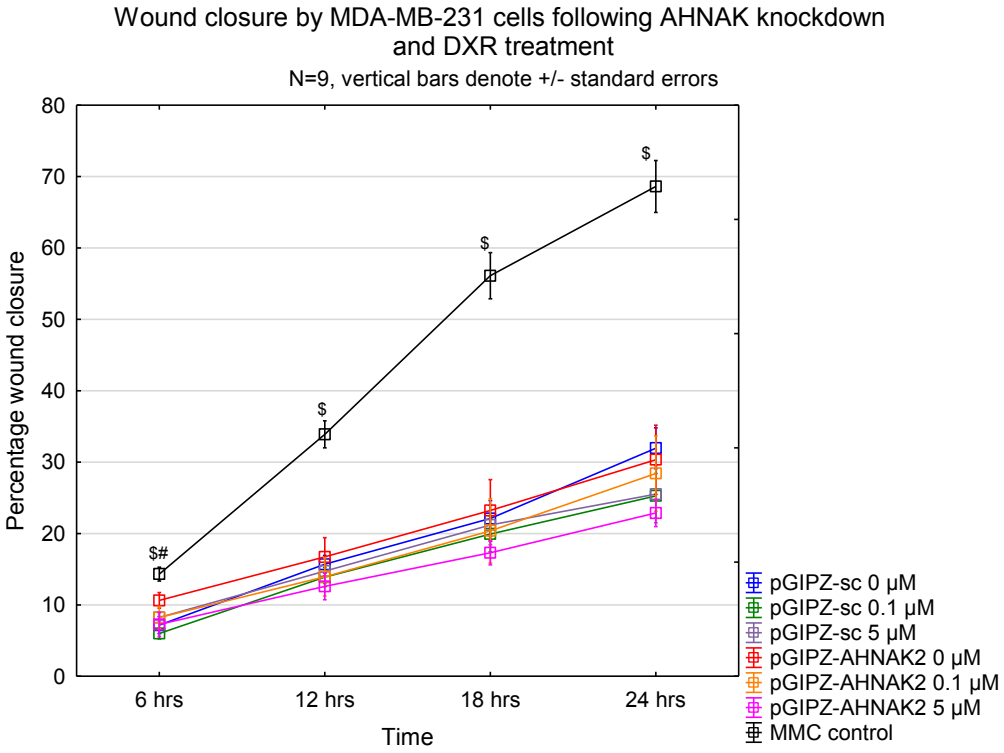

Figure 3.82: Percentage wound closure by MDA-MB-231 cells following AHNAK knockdown and DXR treatment. Statistical significance between groups per time point is indicated by symbols. $ - MMC control vs. all other groups, $p < 0.05$ at 6 hrs, $p < 0.0001$ at 12-24 hrs; # - pGIPZ-sc 0 µM vs. pGIPZ-AHNAK2 0 µM, $p < 0.05$.

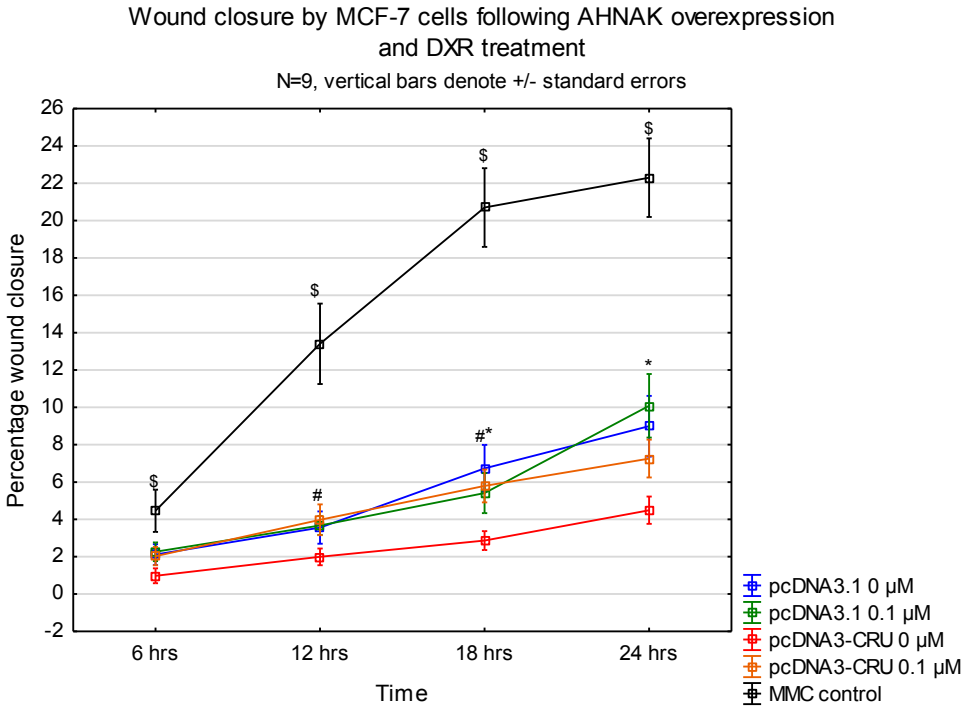

Figure 3.83: Percentage wound closure by MCF-7 cells following AHNAK overexpression and DXR treatment. Statistical significance between groups per time point is indicated by symbols. $ - MMC control vs. all other groups, $p < 0.05$ at 6 hrs, $p < 0.0001$ at 12-18 hrs; # - pcDNA3-CRU 0 µM vs. pcDNA3-CRU 0.1 µM, $p < 0.05$; * - pcDNA3.1 0 µM vs. pcDNA3-CRU 0 µM, $p < 0.05$.

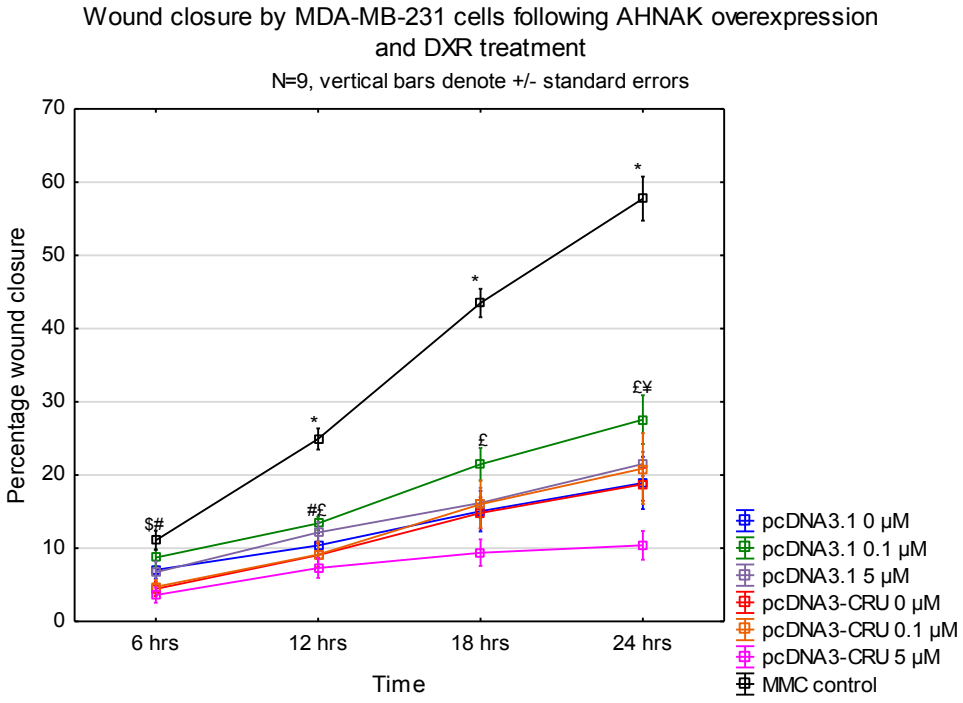

Figure 3.84: Percentage wound closure by MDA-MB-231 cells following AHNAK overexpression and DXR treatment. Statistical significance between groups per time point is indicated by symbols. $ - MMC control vs. all other groups except pcDNA3.1 0.1 µM, $p < 0.05$; # - pcDNA3.1 0.1 µM vs. pcDNA3-CRU 0.1 µM, $p < 0.05$; * - MMC control vs. all other groups, $p < 0.0001$; £ - pcDNA3.1 5 µM vs. pcDNA3-CRU 5 µM, $p < 0.05$; ¥ - pcDNA3-CRU 0 µM vs. pcDNA3-CRU 5 µM, $p < 0.05$.

Chapter 4 : Discussion

4.1 The effects of DXR on AHNAK *in vitro*

The cellular response elicited by a cancer cell following exposure to an anti-cancer agent is crucial for determining its fate. There are two main types of responses; surrender and die, or fight back and become resistant. A clear relationship exists between a cancer cell's genetic background and the outcome of its response, and this is well reflected in cases of intrinsic resistance. Mutational loss of PTEN can promote Akt-mediated pro-survival signalling and has been associated with resistance to Erlotinib (Sos et al., 2009). Mutant p53, the most frequently mutated tumour-suppressor protein, has also been associated with resistance to certain therapies such as 5-fluorouracil and cisplatin, but not paclitaxel (Bunz et al., 1999; Keshelava et al., 2001; Rantanen et al., 2002). Acquired resistance also represents a "fight back" situation although it involves adaptations such as changes in transcriptomic and proteomic profiles, and is almost reminiscent of evolution. Increased expression of the *MDR1* gene and encoded protein, P-gp, has been shown to mediate chemotherapeutic resistance *in vitro* and *in vivo* following exposure to drugs, including mitoxantrone, docetaxel, cisplatin and DXR (Abolhoda et al., 1999; Sánchez et al., 2009). Compensatory upregulation of alternative RTKs following exposure to receptor-targeting therapies has also been reported. Human breast cancer cells, overexpressing the HER2 receptor, induced expression of EGFR as well as heterodimerisation with HER2, which facilitated resistance to trastuzumab treatment (Ritter et al., 2007). Understanding how a cancer cell responds to an anti-cancer drug is crucial when designing a therapeutic strategy. It can determine whether certain modifications are needed, such as dosage or the use of adjuvant therapies, or even if certain drugs should be avoided completely.

We observed differential responses to DXR in MCF-7 and MDA-MB-231 cells, with MCF-7 cells being sensitive to DXR treatment compared to MDA-MB-231 cells which were resistant. This was evident in both the cell viability data (fig. 3.5 and 3.6) and expression of apoptotic markers (fig. 3.7-3.11) following DXR treatment. The sensitivity of these cell lines to DXR is well-known in literature (Aroui et al., 2009b; Kim et al., 2014; Mussi et al., 2014). The DXR response in these cell lines may be linked to their characteristics; MDA-MB-231 cells are known to express P-gp and mutant p53, while MCF-7 cells express wild-type p53 (Gartel et al., 2003; Kim et al., 2014; Neve et al., 2006). Increased sensitivity to DXR has been observed in p53 wild-type, compared to p53 mutant, acute lymphoblastic leukaemia cell lines and tumour xenografts, while a poor response to DXR correlated with a mutant p53 status in advanced breast cancer patients (Dart et al., 2004; Geisler et al., 2001; Lam et al., 1999). In addition, anthracyclines, including DXR, are known to be exported by the P-gp transporters (Szakács et al., 2006). Furthermore, decreased expression of apoptotic markers following DXR treatment in MDA-MB-231 cells may also represent an apoptosis-resistant phenotype. It has been reported that DXR can induce different types of cell death in tumour cells, which are

dose-dependent and possibly also cell line-dependent (Di et al., 2009; Rebbaa et al., 2003; Roninson et al., 2001). Where a medium dose of DXR induced apoptotic cell death, characterised by increased cleaved caspase 3 expression, a high dose of DXR induced a type of necrosis characterised by a lack of cleaved caspase 3 but increased phosphorylated Akt (Rebbaa et al., 2003). In another study it was shown that, while P-gp expression facilitated apoptosis resistance, radiation-induced cell death was facilitated by mitotic catastrophe and senescence (Ruth and Roninson, 2000). Cell death programs are known to be compensatory, and inhibition of apoptosis can also upregulate autophagic cell death (Di et al., 2009). The decreased expression of apoptotic markers at the highest dose of DXR in MDA-MB-231 cells observed in our study coincided with a minor decrease in viability (approximately 19%) which suggests that an alternative cell death mechanism was involved. It is however clear that therapeutic resistance is a multifactorial process (Broxterman et al., 2009). MCF-7 and MDA-MB-231 cells differ significantly in their transcriptomes, which includes differences in active signalling pathways, and it is very likely that several of these differences contribute to their respective DXR-responses (Kenny et al., 2007; Nagaraja et al., 2005).

We also observed that MCF-7 and MDA-MB-231 cells differ with regards to AHNAK protein expression under control conditions as well as when exposed to DXR. Compared to MCF-7 cells, MDA-MB-231 cells expressed substantially higher levels of AHNAK protein under control conditions (fig. 3.12). This was also observed in a recent study (Silva et al., 2016). In addition, increased expression of phosphorylated AHNAK has also been detected, by means of spectrometry, in MDA-MB-231 cells when compared to MCF-7 cells (Kabir et al., 2012). Unfortunately we were unable to assess the expression of phosphorylated AHNAK since a commercially available antibody specific for the phosphorylated form was not available.

Furthermore, AHNAK protein expression decreased in both cell lines in response to DXR, but to different extents. Changes independent of the DXR dose was observed in MCF-7 cells compared to dose-dependent changes in MDA-MB-231 cells (fig. 3.13-3.15). The effect of DXR on AHNAK protein expression in MCF-7 cells has not been investigated before. Decreased AHNAK expression has previously been reported in MDA-MB-231 cells following a treatment regime of DXR (10 µM, 4 hrs) and TRAIL, however it was unclear whether the changes were induced by DXR or TRAIL (Leong et al., 2012). Our results suggest that DXR was responsible for the observed changes. We have shown that DXR-induced changes in AHNAK protein expression can differ between breast cancer cell lines but the cell-specific response is not universal since the effect is also therapy-dependent. Where DXR induced only minor reductions in AHNAK protein expression in MDA-MB-231 cells in our study, treatment with 1 µM staurosporine for 24 hrs almost completely inhibited AHNAK protein expression (Silva et al., 2016). In addition, radiation therapy has been shown to increase AHNAK protein expression in MDA-MB-231 cells (Kim et al., 2015).

It has been noted during some of its other functions that AHNAK can localise to different intracellular regions and also translocate between them (Huang et al., 2007; Lee et al., 2014; Sussman et al.,

2001). Through qualitative assessment of AHNAK's localisation patterns, we investigated whether DXR can affect its intracellular distribution. In both MCF-7 and MDA-MB-231 cells, no changes in AHNAK localisation were observed following 24 or 48 hrs treatments with either low or high DXR doses (fig. 3.18-3.21). AHNAK displayed a diffuse cytoplasmic localisation in single/sub-confluent MCF-7 cells while confluent cells also displayed intense signal at the plasma membrane (fig. 3.18 and 3.20). This localisation pattern has been shown before in MCF-7 cells, as well as in the epithelial cell lines HeLa and MDCK, and is associated with AHNAK's function in the formation of cell-cell contacts (Benaud et al., 2004; Silva et al., 2016; Sussman et al., 2001). In MDA-MB-231 cells, AHNAK displayed a network-like cytoplasmic localisation with areas of intense signal at the plasma membrane and in what appears to be vesicle-like structures (fig. 3.19 and 3.21). Similar patterns of localisation have been observed before in these cells (Leong et al., 2012; Shankar et al., 2010; Silva et al., 2016).

Localised areas of intense signal at the plasma membrane, especially at pseudopodial protrusions, were suggested to be associated with AHNAK's function in the migration of metastatic cancer cells (Shankar et al., 2010). We also observed vesicle-like structures in the MDA-MB-231 cells which were mostly localised in close proximity to the nucleus. Based on their location, these vesicles could potentially originate from the endoplasmic reticulum since AHNAK has been reported to be present in this organelle (Leong et al., 2012). However, a recent study also provides a plausible explanation. AHNAK was identified as the major component in microvesicles released from MDA-MB-231 cells in a co-culture with non-transformed mammary fibroblasts (Silva et al., 2016). Direction of microvesicle transfer was confirmed to predominantly originate from the cancer cells and thus the authors suggested that the cancer cells release the vesicles to modulate fibroblast activity. However, whether the presence of fibroblasts are required for the production of these vesicles is unclear, therefore the precise identification of the vesicles observed in our study would require further investigation. This could be achieved by performing vesicle size analyses coupled with co-localisation experiments with AHNAK and markers for the endoplasmic reticulum and microvesicles, such as GRP94 and flotillin-1, respectively.

Based on the results obtained, we propose that AHNAK is indeed involved in the response of breast cancer cells to DXR with regards to its expression but not localisation. It is clear that MCF-7 and MDA-MB-231 cells respond differently to DXR and we also observed differences in AHNAK's basal expression and the DXR-induced changes in its expression in these cells. These findings provide, for the first time, a link between AHNAK protein expression and DXR-response in breast cancer cells.

4.2 The effects of DXR on AHNAK *in vivo*

The mouse model established in the study was designed to represent a more physiological model of breast cancer treated with either a suboptimal or optimal dose of DXR. Syngeneic E0771 breast cancer cells, suspended in HBSS and Corning® Matrigel®, were injected subcutaneously into female C57BL/6 mice at the mammary fat pad. Matrigel® was used to promote the formation of tumours and provide a physiological tumour microenvironment. Dosage for the HD-DXR group was based on a previously performed study where a reduction in tumour volume was observed following DXR treatment, although this study did not make use of Matrigel® for tumour cell injection (Sishi et al., 2013). It was decided that dosage for the LD-DXR group should be at least half of that for the HD-DXR group. A reduction in tumour volume for this group was not expected but it was hypothesised that the suboptimal DXR dose might promote tumour growth. From the tumour volume data (fig. 3.23), it is clear that there was no reductions in volume following treatment with either the low or high dose of DXR. Indeed, a Kaplan-Meier analysis revealed no significant differences in survival between the groups (fig. 3.25). In addition, an ANCOVA analysis of the tumour volumes showed that the DXR-treated groups had significantly higher tumour growth rates when compared to the control group (fig. 3.24). These results support our hypothesis for the LD-DXR group, but is unexpected for the HD-DXR group. Since no differences were observed between the two DXR doses, it suggests that the presence of DXR alone had an effect on tumour growth rate. Also, since the high dose of DXR was based on a previous study where Matrigel® was not used, it is likely that the use of this extracellular matrix for tumour cell injection contributed to these unexpected findings.

Matrigel® is widely used in *in vivo* tumour models to ensure tumour formation and is known to promote tumour growth (Bao et al., 1994; Kleinman and Martin, 2005; Noël et al., 1993). *In vitro* experiments have also shown that tumour cells cultured in basement membrane extracts displayed altered three-dimensional organisation when compared to normal cells (Wang et al., 2002; Weaver et al., 2002). This was also accompanied by increased growth and therapeutic resistance. Cellular interactions with the ECM, such as interactions between α6β4 integrin and laminin, and the activation of signalling pathways, such as the PI3K and MAPK pathways, were shown to mediate these changes and that inhibition of these interactions and signalling pathways were sufficient to revert the altered tumour organisation to that of normal cells. Findings from a recent study further support the role of signalling pathways in the cellular response to the microenvironment when the PI3K and Rac pathways were shown to mediate mechanotransduction and a malignant phenotype based on the ECM composition and stiffness (Chaudhuri et al., 2014). Indeed, the ECM is well-known to play a crucial role in regulating and maintaining normal tissue homeostasis however, increasing research in this field have recognised that the tumour-associated ECM also plays a crucial role in tumour progression and therapeutic response (Pickup et al., 2014). Furthermore, DXR on its own is also capable of acting on signalling pathways. Activation of signalling pathways capable of promoting cellular growth and therapeutic resistance, such as the PI3K, MAPK and JNK pathways, have been reported to occur following exposure to DXR in both non-transformed and tumour cells (Lee et al., 2006; Li et al., 2005; Shukla et al., 2010). In particular, DXR was shown to increase the expression

and phosphorylation of the ERK1/2 proteins and knockdown of these proteins in combination with DXR treatment resulted in increased tumour cell death *in vitro* and decreased tumour growth rates *in vivo* (Shukla et al., 2010).

Based on the data available in literature, we propose that Matrigel® advanced tumour progression to a more aggressive and resistant phenotype, most likely involving growth-associated signalling pathways and that DXR further acted on these pathways to promote tumour growth. Although a complete investigation of the underlying molecular mechanisms associated with these findings were outside the scope of the current study, a separate study is currently being performed to identify the mechanisms of DXR-induced tumour growth in this model. Our results also emphasise the significance of the tumour microenvironment in therapeutic efficacy. Careful considerations should be made when assessing the anti-cancer properties of a drug. The role of the tumour microenvironment is often neglected in *in vitro* studies where a reconstituted basement membrane extract is only utilised when anti-invasive, anti-angiogenic or anti-metastatic properties are investigated. Furthermore, the use of these extracts may also be limited to *in vivo* studies involving xenograft models with known difficulties in tumour establishment. Our results, and the increasing evidence in literature, suggests that the role of the tumour microenvironment should be considered more regularly in drug efficacy studies, especially since it could help explain the disparity between results obtained in *in vitro* and *in vivo* experiments, as well as between *in vivo* experiments and clinical trials.

Expression of apoptotic markers in the tumours also supported the observations that there were no decreases in tumour volume since apoptosis induction following DXR treatment did not take place. Instead, cPARP showed a non-significant trend of decreased expression, while cCasp7 showed decreased expression in the LD-DXR group which increased slightly in the HD-DXR group (fig. 3.26-3.28). These changes in expression are similar to those observed in the MDA-MB-231 cells following DXR exposure; cPARP expression also decreased reaching significance only at the highest dose of DXR while cCasp7 expression decreased and increased again towards the highest dose (fig. 3.10 and 3.11). These results also confirm the resistance of the tumour cells to apoptosis.

AHNAK's protein expression was assessed in the tumours to determine whether DXR could influence its expression *in vivo*. Indeed, we observed increased expression in the LD-DXR group which returned back to basal levels in the HD-DXR group (fig. 3.29). These changes in protein expression were dose-dependent and again, similar to those observed in the MDA-MB-231 cells after both 24 (comparing the low dose of 0.1 μM and the higher dose of 2.5 μM) and 48 hrs DXR treatment. We also assessed the intracellular localisation of AHNAK in the tumours and while co-localisation studies would have to be performed to confirm the identity of the localised areas of intense signal (for instance with a cell membrane marker such as the sodium potassium ATPase pump), we observed no changes in localisation following DXR treatment.

Studies investigating the role of AHNAK *in vivo* are limited. Lee *et al.* made use of AHNAK$^{-/-}$ mice displaying spontaneous breast cancer formation to show that AHNAK possesses tumour-suppressive capabilities, whereas Sudo *et al.* showed that AHNAK is expressed at different intracellular locations in sarcomatoid and epitheliod mesothelioma mouse xenograft tumours (Lee et al., 2014; Sudo et al., 2014). We present the first data reporting the tumour-associated protein expression of AHNAK in a murine breast cancer model following chemotherapeutic treatment. Our *in vivo* results support the results obtained in the *in vitro* experiments, both with regards to the changes in AHNAK's protein expression and localisation, and thus further supports our hypothesis that AHNAK is involved in the cellular response to DXR.

Based on both the *in vitro* and *in vivo* results obtained in this study we propose a correlation between AHNAK, DXR response and DXR resistance. MDA-MB-231 cells, a DXR-resistant cell line, expressed high levels of AHNAK and maintained its expression fairly well following exposure to DXR while MCF-7 cells, a DXR-sensitive cell line, expressed much less AHNAK that was significantly susceptible to further downregulation following DXR treatment. Previous correlations between AHNAK expression and drug resistance have been suggested. Increased AHNAK expression was reported in cisplatin-resistant versus cisplatin-sensitive ovarian and neuroblastoma cell lines (Cheng et al., 2006; Piskareva et al., 2015). Furthermore, positive correlations between AHNAK expression and resistance to tubulin-binding drugs such as paclitaxel, docetaxel, vinblastine and vincristine were also reported (Hsu et al., 2013). Increased AHNAK expression is however not universally correlated with drug resistance since negative correlations were also reported with resistance to targeted therapies such as everolimus, dasatinib and erlotinib. In addition, based on the findings from Lee *et al.* (2014) that suggests that AHNAK functions as a tumour suppressor, one can speculate that any correlations between its expression and drug response may also be cancer-type dependent. These earlier studies only reveal correlations between AHNAK's basal expression and drug resistance; our results now provide an additional level of information, that is, the changes in AHNAK expression elicited by the drug. With the aim of further characterising the relationship between AHNAK expression and the therapeutic drug response, it will be worthwhile to investigate whether similar changes in its expression exist in sensitive and resistant cancer cells treated with cisplatin (which functions similarly to DXR) and tubulin-binding therapies as those observed here in MCF-7 and MDA-MB-231 cells treated with DXR.

4.3 The effects of AHNAK on DXR-induced cellular responses

Through several excellent studies AHNAK has been shown to function as a scaffold protein active in several cellular processes in different cell types (Davis et al., 2014). The protein's role in cancer remains however undefined as its potential roles in tumour metastasis, chemoresponse and, in

contrast, as a tumour suppressor, have been reported in only a few separate studies (Lee et al., 2014; Leong et al., 2012; Shankar et al., 2010). To further investigate the role of AHNAK in breast cancer cell response to DXR and to determine the specific effect of AHNAK on DXR, we generated *in vitro* models of AHNAK knockdown and overexpression by means of plasmid transfection.

We first investigated whether AHNAK could influence DXR cytotoxicity. Knockdown and overexpression of AHNAK did not have any significant effects on MCF-7 viability under basal conditions (fig. 3.35 and 3.37). Furthermore, MCF-7 cells also displayed a similar sensitivity to DXR following both knockdown and overexpression of AHNAK, although overexpression of the protein did result in a slight increase in cell death after treatment with 5 µM DXR. Significant differences in viability were observed in the 0.1 µM DXR group in both the knockdown and overexpression experiments, with the control transfected group displaying higher viability in both instances. In MDA-MB-231 cells, both AHNAK knockdown and overexpression resulted in a general increase in viability (fig. 3.36 and 3.38). This is unexpected and the reason why opposing conditions would have the same effect is unclear. The same trends in cell viability were however observed following treatment with DXR. When comparing the results obtained from the knockdown and overexpression experiments, we observed that the knockdown 5 µM DXR group showed significantly decreased viability when compared to the control transfected group treated with the same dose, but this significant difference was not observed in the overexpression experiments. However, the representative control transfected groups in the knockdown and overexpression experiments do not replicate each other, making it challenging to indicate whether AHNAK knockdown or overexpression results in more or less cell death, respectively, when treated with a high dose of DXR. Overall, our results suggest that AHNAK does not influence the extent of cytotoxicity brought about by DXR.

The effect of AHNAK on the cytotoxicity of DXR, or any other chemotherapeutic drug, have not been investigated before and only a few studies have reported on the effect of AHNAK on cell proliferation in general. In two studies it was found that knockdown of AHNAK had no effect on breast cancer cell proliferation or viability (Shankar et al., 2010; Silva et al., 2016). In contrast, results from another two studies reveal opposing effects on cell proliferation; whereas knockdown of AHNAK resulted in increased hippocampal cell proliferation, it resulted in decreased cell proliferation in PDGF-stimulated aortic smooth muscle cells (Lim et al., 2013; Shin et al., 2015b). In a more extensive investigation, AHNAK was suggested to function as a tumour suppressor based on the findings that a loss of AHNAK increased the proliferation of MEF cells while overexpression of the protein in SiHa cells (cervical cancer) reduced colony forming activity and tumour growth (Lee et al., 2014). Our results obtained following AHNAK knockdown in MDA-MB-231 cells support the role of AHNAK as a tumour suppressor, however, since the same effect was observed following overexpression of the protein, we can not fully support this role. Contrasting findings surrounding the role of AHNAK in cellular proliferation suggests a possible dependency on cell type and the specific function of AHNAK within the particular cell type. AHNAK is known to exhibit different functions in different cell types

and thus in each case a loss of its expression may or may not have a direct or even indirect impact on cellular proliferation. This is supported by our findings where knockdown and overexpression of AHNAK had an effect on MDA-MB-231 cells but not on MCF-7 cells.

Next we investigated whether AHNAK could influence apoptosis induced by DXR by performing Caspase-Glo® 3/7 assays (which measures caspase 3 and 7 activity) and Western blots for markers of apoptosis (measuring cPARP and cCasp7 expression). In MCF-7 cells, knockdown of AHNAK increased basal levels of caspase activity and prevented any further increase following DXR treatment (fig. 3.39). Overexpression of AHNAK also resulted in increased basal levels, which decreased following treatment with DXR (fig. 3.41). However, in these experiments, no increase in caspase activity was observed in the control transfected group treated with 5 µM DXR which is not consistent with the expected results. In MDA-MB-231 cells, knockdown of AHNAK resulted in a basal increase in caspase activity but followed the same trend of increasing activity as the control transfected groups during DXR treatment (fig. 3.40). In contrast, overexpression of AHNAK maintained caspase activity at a constant level and prevented any further increase in activity at 5 µM DXR (fig. 3.42). These results support the lack of significant differences obtained in the MTT assay between the control transfected and overexpressed 5 µM DXR groups.

Western blot experiments revealed significant increases in both cPARP and cCasp7 protein expression when MCF-7 cells were treated with 5 µM DXR which is indicative of a significant increase in apoptosis (fig. 3.43, 3.44, 3.47, 3.48, 3.51 and 3.52). These findings support the significant decrease in MCF-7 viability at the same DXR concentration and suggests that cell death occurred mainly through apoptosis. Knockdown or overexpression of AHNAK however had no effect on the expression of these proteins at basal conditions or with DXR treatment. In contrast, AHNAK knockdown and overexpression did influence the expression of apoptotic markers in MDA-MB-231 cells (fig. 3.43, 3.44, 3.49, 3.50, 3.53 and 3.54). While no differences were observed in cPARP expression between control transfected and AHNAK knockdown groups, AHNAK knockdown prevented the DXR-induced decrease in cCasp7 expression. Overexpression of AHNAK had the opposite effect; decreased cPARP expression was observed under basal conditions which decreased further with 5 µM DXR treatment while AHNAK overexpression maintained cCasp7 expression at reduced levels comparable to that induced by 5 µM DXR. These results would suggest that, in MDA-MB-231 cells, overexpression of AHNAK is capable of promoting a similar apoptosis-resistant phenotype that is observed in these cells when treated with DXR. This effect is prevented when AHNAK is knocked down, as seen with the opposite response in cCasp7 results. This effect is more clearly observed in cCasp7 expression data than with cPARP, which is intriguing since the cleavage of PARP normally occurs after cleavage of Casp7. These findings would also support the correlations observed in the previous sections, where increased expression of AHNAK was associated with DXR resistance (fig. 3.5-6, 3.12 and Cheng et al., 2006, Piskareva et al., 2015 and Hsu et al., 2013). These effects are however not observed in MCF-7 cells and even overexpression

of AHNAK in these cells was not capable of conferring resistance to DXR, although this is not completely unexpected. In several of AHNAK's other described functions, the protein forms interactions with other proteins (such annexin 2 and S100A10) and often takes part in the formation of a multiprotein complex that is required for a certain function (establishing cell-cell contacts). In this scenario it could be reasonable to assume that other protein components, which may also be lacking in MCF-7 cells, are required for AHNAK to fulfil its role in apoptosis/DXR resistance.

Even though changes in apoptotic marker expression, in the presence or absence of DXR treatment, was observed in the MDA-MB-231 cells following knockdown and overexpression of AHNAK, no changes were observed in cell viability data. This supports our earlier hypothesis that the decrease in cell viability observed in these cells was most likely brought about by an alternative cell death mechanism. In addition, although knockdown of AHNAK prevented the decrease in cCasp7 expression, it wasn't sufficient to increase it above the basal level, which further supports no increased cytotoxicity. AHNAK knockdown prevented the DXR-induced apoptosis-resistant phenotype (as seen in the apoptotic marker expression data) without an increase in sensitivity (as seen in the MTT assay data) and this could be explained in one of two ways, or perhaps a combination of both; 1) more than one mechanism of DXR resistance exists and is it possible that an alternative mechanism prevented cell death in these conditions, such as export of DXR through P-gp, and 2) that a threshold is required in the loss of AHNAK expression in order to achieve increased sensitivity, especially since we only achieved a reduction of approximately 50% in AHNAK protein expression in our knockdown experiments.

Several contradicting findings were identified when comparing the results obtained from the Caspase-Glo® assays with those from the Western blots. Apart from the control transfected groups in the MCF-7 overexpression experiments, all other control transfected groups showed increased caspase activity, and thus apoptosis, when treated with 5 µM DXR. However, the level of increased activity is similar between the MCF-7 and MDA-MB-231 cells. This does not correlate with the cell viability results obtained with the MTT assays, where a lot more death was observed in the MCF-7 than in the MDA-MB-231 cells, and also in the Western blot results where it is clear that cPARP and cCasp7 expression in MCF-7 cells increased by much more than a mere ±20%. In general, results obtained with the Caspase-Glo® assay for the MDA-MB-231 cells do not correlate with the Western blot data which showed a decrease in the expression of the apoptotic markers and correlated with the cPARP and cCasp7 Western blot data obtained with the DXR dose response curve. Furthermore, caspase activity in the MCF-7 cells following AHNAK overexpression was increased when compared to the control transfected group and decreased when treated with 5 µM DXR, which also does not correlate with the other caspase activity data. Based on these inconsistencies we are inclined to disregard the results obtained with the Caspase-Glo® assays.

Apoptosis is a highly controlled cell death process mediated by multiple pro-apoptotic proteins (Ola et al., 2011). Members of the main protein family responsible for the phenotypic outcome of

apoptosis, the caspases, are classified as either initiator or executioner caspases. As the names suggests, initiator caspases receive the signals to induce apoptosis and initiates the process while the executioner caspases are responsible for the final outcome that is cell death. Apoptosis inhibition is not only common during therapeutic resistance, but is also a hallmark of cancer in general (Hanahan and Weinberg, 2011). Inhibition of the apoptotic pathway is achieved by multiple anti-apoptotic proteins that act in on different levels between the initiator and executioner caspases and are commonly regulated by pro-survival signalling pathways, such as the PI3K pathway. For example, phosphorylated Akt can negatively regulate pro-apoptotic Bad and caspase 9, as well as upregulate inhibitor of apoptosis proteins (IAPs) to suppress apoptosis through caspase inhibition (Seol, 2008). In particular, Akt was shown to facilitate caspase inhibition through XIAP (a member of the IAP family) following DXR treatment in DXR-resistant but not DXR-sensitive uterine cancer cells (Gagnon et al., 2008). To our knowledge, we present here the first evidence that implicate AHNAK in the modulation of apoptosis-related proteins. Based on our results, we speculate that AHNAK might function downstream of Akt in the inhibition of caspases during DXR treatment in DXR-resistant breast cancer cell lines. AHNAK has indeed previously been shown to be phosphorylated by Akt (Sussman et al., 2001). In this scenario, knockdown of AHNAK would then interrupt the DXR-induced signal to decrease the expression of caspase proteins, which was observed in our results. Overexpression of AHNAK is sufficient to promote this phenotype, possibly by promoting the activation of Akt in a manner similar to XIAP which is also capable of feedback promotion of Akt phosphorylation (Gagnon et al., 2008). The associations between AHNAK expression and chemoresponse may be drug-dependent but it would be interesting to determine whether AHNAK can have the same effect with other DNA-damaging chemotherapeutic drugs. In particular, a similar scenario has been reported in ovarian cancer cells where treatment with cisplatin induced Akt phosphorylation and apoptosis inhibition in cisplatin-resistant but not cisplatin-sensitive cells (Stronach et al., 2011).

AHNAK has previously been shown to modulate the cell cycle (Lee et al., 2014). Since DXR has also been shown to affect the cell cycle (Reinhardt et al., 2007), we investigated whether AHNAK knockdown or overexpression could influence the cell cycle during DXR treatment. DXR treatment induced a slight decrease in the G_0/G_1 phase with a concomitant increase in the S phase in MCF-7 cells (fig. 3.55, 3.57, 3.59 and 3.61). In contrast, DXR induced a significant increase in the S phase with a concomitant decrease in the G_2/M phase in MDA-MB-231 cells (fig. 3.56, 3.58, 3.60 and 3.62). Knockdown of AHNAK in MCF-7 cells did not influence the DXR-induced changes in the cell cycle, although the overexpression of AHNAK together with 5 µM DXR treatment induced a significant increase in the S phase which coincided with a decrease in the G_0/G_1 phase. Here, the effects of AHNAK on DXR-induced changes were again more pronounced in the MDA-MB-231 cells. Knockdown of AHNAK completely prevented the DXR-induced increase and decrease in S- and G_2/M phase, respectively, in MDA-MB-231 cells. Overexpression of AHNAK had the opposite effect and was, on its own, sufficient to induce changes similar to those induced by 5 µM DXR, that is,

AHNAK overexpression induced a significant increase in the S phase along with a significant decrease in the G_2/M phase. There were no significant differences between the control transfected 5 µM DXR group and overexpression 5 µM DXR group.

As part of the physiological response following DNA damage, cells activate complex signalling pathways to ensure genomic integrity and that only undamaged DNA is passed on to daughter cells during mitosis (Reinhardt and Yaffe, 2009). Depending on the extent of damage, the cell undergoes either cell cycle arrest, providing sufficient time for DNA repair mechanisms, or cell death via apoptosis. This important decision is predominantly made by the p53 tumour suppressor protein (Reinhardt et al., 2007; Xiao et al., 2003). To control progression through the cell cycle, certain checkpoints are enforced after the G_0/G_1 phase, within the S-phase and in the G_2/M phase (Reinhardt and Yaffe, 2009; Xiao et al., 2003). In the event of minor DNA damage in non-cancerous cells, p53 is activated to induce p21-mediated inhibition of the cell cycle, resulting in the arrest of damaged cells at the G_1/S checkpoint (Reinhardt and Yaffe, 2009; Reinhardt et al., 2007; Xiao et al., 2003). Tumour cells may also induce cell cycle arrest to allow for DNA repair in an attempt to maintain viability following genotoxic stress induced by DNA-damaging drugs, such as DXR, camptothecin and cisplatin. However, tumour cells often contain disrupting mutations within the *TP53* gene and are thus deficient in p21-mediated G_1/S arrest. Instead, these cells rely on alternative pathways to facilitate arrest at either the S or G_2/M checkpoints (fig. 4.1) (Reinhardt and Yaffe, 2009; Reinhardt et al., 2007; Xiao et al., 2003).

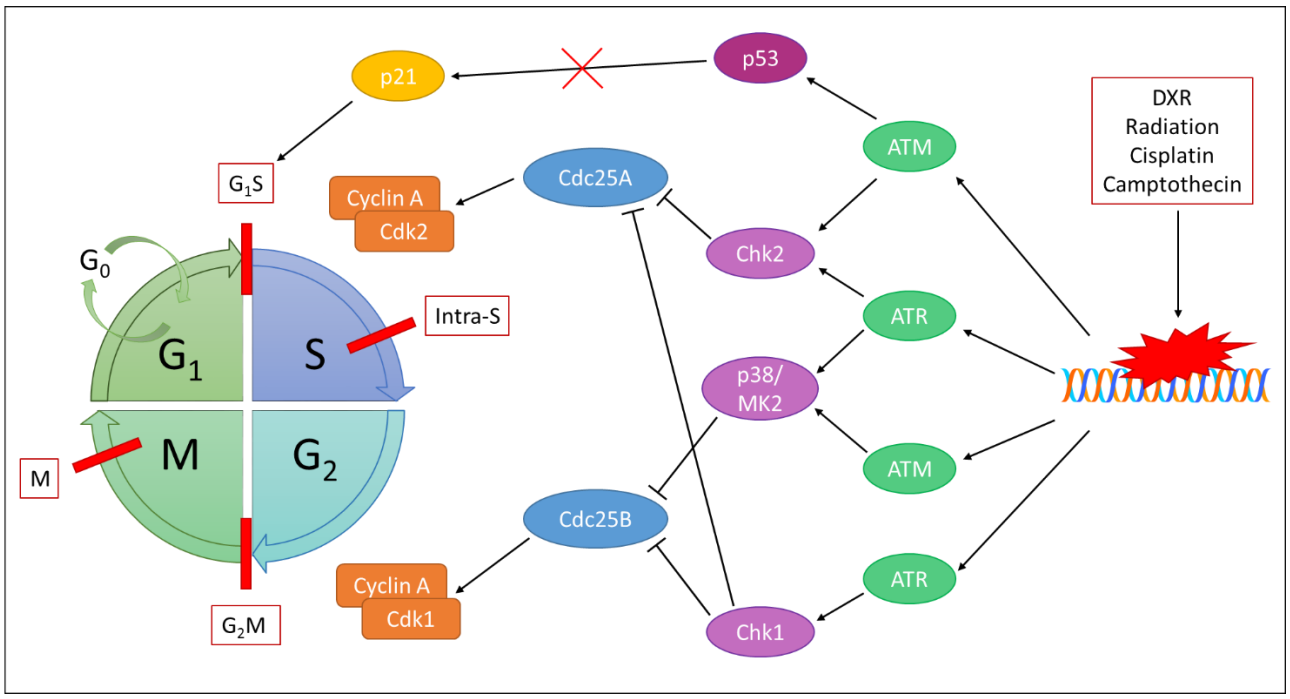

Figure 4.1: Pathways activated in p53-deficient cancer cells leading to cell cycle arrest following genotoxic stress.

DXR induces DNA damage by binding and inhibiting TOP2, an enzyme responsible for DNA unwinding during replication and transcription (Palchaudhuri and Hergenrother, 2007; Tacar et al., 2013). Through binding, DXR stabilises the TOP2-DNA complex, preventing the DNA from re-annealing and resulting in double-strand DNA breaks. We observed a significant increase in the percentage of cells in S phase upon treatment with 5 μM DXR, suggesting that DXR arrested the cells in S phase during DNA replication (fig. 3.60). Knockdown of AHNAK prevented the DXR-induced cell cycle arrest, suggesting that AHNAK is required in the signalling pathway that facilitates arrest in the S phase following DXR-induced DNA damage. In contrast, overexpression of AHNAK was sufficient to induce cell cycle arrest on its own. Cell cycle arrest following AHNAK overexpression has previously been reported in a recent study, although in contrast, arrest occurred at the G_1/S checkpoint in normal p53-wildtype NIH3T3 cells (Lee et al., 2014). Here, AHNAK was shown to be required for TGF-β-induced cell cycle arrest by promoting Smad-mediated transcriptional activities. The different outcomes of AHNAK overexpression in our study compared with the previous study could be explained by the difference in p53 status, as MDA-MB-231 cells are p53 mutant, as well as the specific requirement of TGF-β stimulation for the proposed role of AHNAK in the previous study, suggesting that the particular pathway may not have contributed to the results obtained in our study. In addition, the TGF-β-induced role of AHNAK involved translocation of the protein to the nucleus and we did not observe any nuclear expression of AHNAK with or without DXR treatment. Since overexpression of AHNAK in the MDA-MB-231 cells exhibited the same response as when the cells were treated with a high dose of DXR, we searched for mechanisms of DXR-induced cell cycle arrest to identify possible additional roles for AHNAK in cell cycle arrest.

DXR is capable of inducing DNA-damage-induced cell cycle arrest through a pathway involving the p38 and MK2 (MAP kinase-activated protein kinase 2) proteins in p53-deficient cells (Reinhardt et al., 2007; Xiao et al., 2003). DXR was shown to induce specific phosphorylation and activation of p38 and MK2 which resulted in the cytoplasmic sequestration and inactivation of Cdc25B. Cdc25B regulates the cell cycle by dephosphorylating and activating Cdk1/Cyclin B which in turn drives cell cycle progression. The outcome of the DXR-induced pathway was G_2/M arrest. Similarly, treatment of p53-deficient cells with cisplatin also activated the p38 and MK2 proteins, which facilitated Cdc25A degradation and cell cycle arrest in the S phase. Depletion of MK2 prevented cell cycle arrest leading to mitotic catastrophe through apoptotic cell death. The pathway was shown to require the upstream cell cycle regulators ataxia-telangiectasia mutated (ATM) and ATM and Rad-3-related (ATR) when treated with DXR, and ATR when treated with cisplatin, although the specific link between these proteins and p38 and MK2 is unclear. Overexpression of the MK2 homologue in *Schizosaccharomyces pombe*, Srk1, has been shown to induce cell cycle arrest at G_2/M through Cdc25 inhibition (López-Avilés et al., 2005). The DXR-induced p38/MK2 pathway is also independently paralleled by the ATR/Chk1 pathway which mediates Cdc25A degradation and cell

cycle arrest at the S phase (when p53 deficient cells are treated with cisplatin and camptothecin) as well as G_2/M arrest (when treated with DXR) (Xiao et al., 2003). Furthermore, an additional ATM/Chk2 pathway also converges onto the Cdc25A protein to promote S-phase arrest following radiation-induced DNA damage (Falck et al., 2002). Overexpression of Chk1 on its own is also sufficient to induce cell cycle arrest while knockdown induces mitotic catastrophe and apoptosis (Syljuasen et al., 2006; Xiao et al., 2003). Similarly, overexpression of Chk2 can result in auto-activation in the absence of DNA damage, which could result in cell cycle arrest (Reinhardt and Yaffe, 2009; Schwarz et al., 2003).

In our *in vitro* model it is possible that the p38/MK2 pathway (and possibly the ATM/Chk2 or ATR/Chk1 pathways) was activated in the p53-deficient MDA-MB-231 cells following DXR treatment. Since knockdown of AHNAK showed that the protein is required for one (or more) of these pathways, we propose that AHNAK participates in the ATM- and ATR-mediated cell cycle arrest pathways induced in p53-mutant cancer cells following DNA damage. Similar to MK2 and Chk1, and possibly Chk2, overexpression of AHNAK promoted cell cycle arrest on its own. Since we did not observe a nuclear localisation for AHNAK during DXR treatment, it is unlikely that the protein functions downstream of p38/MK2, or Chk1 and Chk2. These pathways do however rely on the upstream activation of ATM and ATR. ATM has a nuclearplasmic localisation but upon DNA damage relocates to intense nuclear foci characterised by a build-up of DNA-repair proteins at the sites of damage (Lavin and Kozlov, 2007). The relocalisation of ATM to damaged DNA as well as its activation requires an interaction with the MRN complex, which consists of the Mre11, Rad50 and Nibrin proteins (Cerosaletti et al., 2006; Lavin and Kozlov, 2007). This complex is formed in the cytoplasm and upon binding of Nibrin to Mre11-Rad50 is translocated to the nucleus. The interaction between ATM and MRN is crucial for the downstream pathways following DNA damage since MRN-deficient colorectal cancer cells were defective in Chk2 phosphorylation and S phase arrest following treatment with camptothecin (Takemura et al., 2006). Furthermore, ATM can promote the activation of ATR which may also require the MRN complex (Reinhardt and Yaffe, 2009; Yoo et al., 2009). In accordance with AHNAK's other functions, we propose that AHNAK may function as a scaffold protein that facilitates the formation of the MRN complex within the cytoplasm before being translocated to the nucleus (fig. 4.2). Further studies are however required to assess the ability of AHNAK to interact with components of the MRN complex, possibly with co-immunoprecipitation experients.

In the studies described above, DXR induced G_2/M arrest, while cisplatin and camptothecin induced arrest at the S phase (Reinhardt et al., 2007; Xiao et al., 2003). In contrast, we observed S phase arrest with DXR treatment. Is it possible that in our model DXR primarily induced either the ATM/Chk2 or ATR/Chk1 pathways which converge on Cdc25A, since inhibition of this regulator plays a major role in intra-S phase arrest (Reinhardt & Yaffe, 2009). However, cisplatin-induced S phase arrest has been shown to be a transient event before arrest in G_2/M (Lundholm et al., 2013; Shapiro

and Harper, 1999; Tanida et al., 2012). In addition, G_2/M arrest induced by DXR was achieved with a treatment of 10 µM DXR for 30 hrs (compared to our treatment with 5 µM DXR for 24 hrs) (Reinhardt et al., 2007). It is thus also possible that the S phase arrest we observed in our study with the treatment of a high dose DXR or with overexpression of AHNAK was a transient event and may have led to a final G_2/M arrest under different conditions. Furthermore, we also observed an increase in the expression of the apoptotic markers during AHNAK knockdown but the expression levels increased only to match control levels without any additional loss of cell viability. Thus, with a longer treatment (or with a higher dose) we may have obtained the same mitotic catastrophe and apoptotic cell death as observed in the studies where MK2 and Chk1 were knocked down.

As an alternative to the proposed role described above, AHNAK may also function in a separate pathway activated by DXR and involving Akt. Akt is a well-established regulator of the cell cycle capable of either directly or indirectly regulating multiple proteins involved in the cell cycle (Liang and Slingerland, 2003). In particular, Maddika *et al.* reported on the cyclic activation of Akt during cell cycle progression; Akt activity increased during G_1-, decreased during S- and increased again during the G_2 phase (Maddika et al., 2008). In addition, activated Akt also translocated between the cytoplasm (G_0 and G_1) and nucleus (G_2), while showing a dispersed localisation among both locations during S phase. Searching for novel Akt substrates, the group reported that Cdk2 phosphorylation and translocation were dependent on Akt. During G_1 phase, Cdk2 was mainly nuclear while a cytoplasmic localisation was observed during the G_2 phase. Similarly to Akt, Cdk2 was present in both the cytoplasm and nucleus during the S phase. The group suggested that active Akt translocates to the nucleus, phosphorylates Cdk2, and together the proteins shuffle back to cytoplasm. The pathway was required for the progression of cells from S- to G_2 phase while Akt or Cdk2 mutants lead to S phase arrest. These experiments were however performed in non-cancerous cells. Interestingly, when cancer cells were treated with either methotrexate, docetaxel or DXR, Akt showed constitutive activation and nuclear localisation. This coincided with constitutive Cdk2 phosphorylation and cytoplasmic relocalisation. In a separate study, Chen *et al.* reported similar findings following treatment with pemetrexed in non-small-cell lung carcinoma cells (Chen et al., 2014). Pemetrexed, like DXR, causes DNA damage through inhibition of DNA replication and induction of double-stranded DNA breaks. Similarly to Maddika *et al.*, Chen *et al.* reported that treatment of cancer cells with pemetrexed resulted in constitutive Akt activation and nuclear accumulation. Increased Cyclin A/Cdk2 activity and S phase arrest was also reported while inhibition of the pathway blocked all effects. The ability of Akt to translocate to the nucleus is however unclear, and as Maddika *et al.* pointed out, Akt does not have a nuclear localisation signal which suggests that Akt requires an interaction with a nuclear targeting protein. Since it was reported in an earlier study that AHNAK contains a nuclear localisation signal as well as being phosphorylated by Akt (Sussman et al., 2001), we speculate that under constitutive activation by DXR in cancer cells, active Akt phosphorylated and associated with AHNAK in the cytoplasm and that AHNAK assisted Akt with translocation to the nucleus where Cdk2 is phosphorylated, resulting in S phase arrest (fig. 4.2).

Since we did not observe a nuclear localisation for AHNAK it suggests that the Akt/AHNAK association was lifted upon reaching the nuclear membrane. One caveat to this proposed role is however that with chemotherapeutic treatment in both studies, the constitutive activation of the Akt/Cdk2 pathway was also associated with increased apoptotic death, which we did not observe in our study.

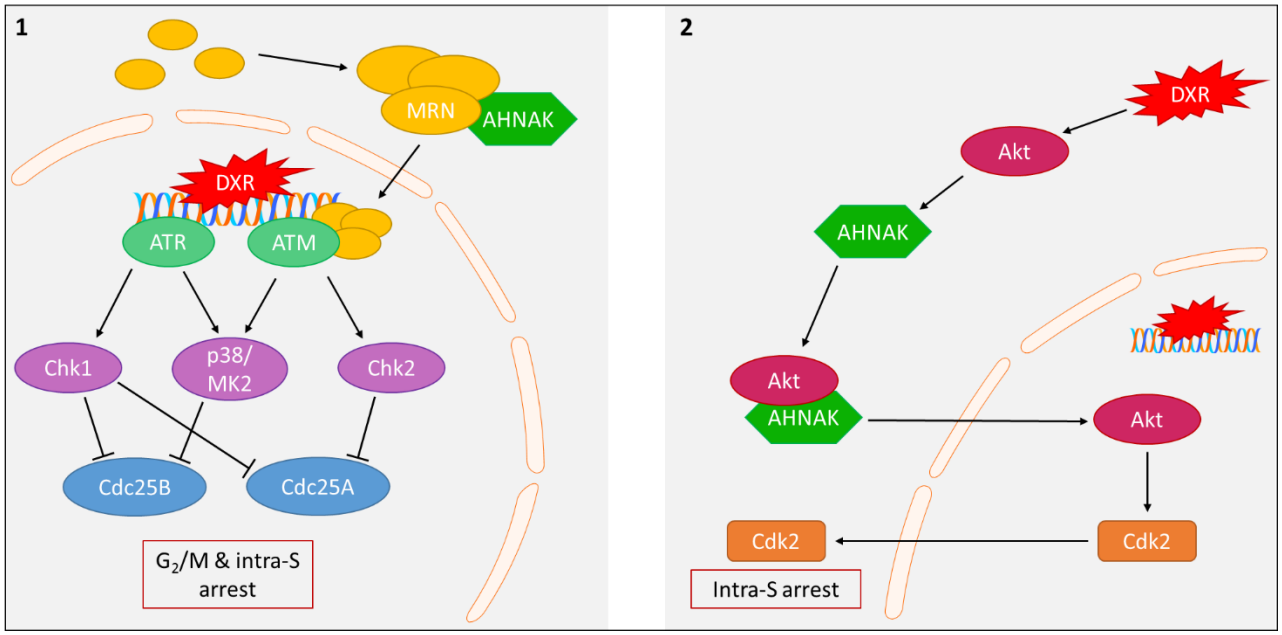

Figure 4.2: Proposed possible roles for AHNAK in cell cycle arrest

In contrast to the results obtained in the MDA-MB-231 cells, we did not observe such a role for AHNAK in the MCF-7 cells, and it is likely that the p53 status of these cells is involved. Depending on the degree of DNA damage, a functional p53 can induce either cell cycle arrest or apoptosis. Since we observed significant apoptosis induction during DXR treatment in MCF-7 cells, it is likely that the induction of apoptosis was favoured upon severe DNA damage rather than cell cycle arrest to attempt DNA repair. The combination of AHNAK overexpression and DXR treatment did however result in an increase in the S phase, indicating that the decreased levels of AHNAK protein expression in MCF-7 cells may have contributed to the lack of DXR-induced DNA-damage response in these cells. In comparison to the MDA-MB-231 cells, the extent of S phase arrest in MCF-7 was to a lesser degree, indicating that other required factors may also be lacking in these cells.

4.4 Linking AHNAK and DXR

Considering the results obtained while determining the effect of DXR on AHNAK and vice versa, we propose that AHNAK plays a role in mediating the intracellular response to DXR in DXR-resistant p53-mutant breast cancer cells. This is achieved through a role in modulating the expression of apoptotic markers as well as a role in cell cycle arrest. The expression of AHNAK has been shown to correlate with the cellular response to chemotherapeutic drugs before and our results now suggest that, at least in breast cancer cells, its expression also correlates with DXR resistance. However, whether the correlation exists because AHNAK causes DXR resistance or because its expression merely coincides with resistance remains to be confirmed.

Resistance to chemotherapeutic drugs is achieved through multiple mechanisms. In our study we observed two mechanisms, namely the downregulation of apoptosis-related proteins and cell cycle arrest. The purpose of cell cycle arrest is to repair damaged DNA following a therapeutic insult, thus promoting cell survival and is a common response observed in cancer cells (Xiao et al., 2003). Our intra-S phase arrest coincided well with DXR's mechanism of action as most damage would occur in this phase. In addition, we also observed decreased cPARP expression. Not only does this represent decreased apoptotic conversion of PARP to cPARP, thus reduced apoptotic cell death, but it may also contribute to the repair of damaged DNA during arrest. In particular, PARP has been shown to be important for the detection of stalled DNA replication forks, the recruitment of the MRN complex and replication restart following DNA repair (Bryant et al., 2009). In the MDA-MB-231 cells we observed that cell viability and AHNAK expression was maintained fairly well during DXR treatment with only a minor decrease in viability at higher DXR doses which coincided with decreased AHNAK protein expression. We also observed that, during DXR treatment, AHNAK decreased the expression of apoptotic markers (which started to increase again at the higher doses) and that AHNAK was required for DXR-induced cell cycle arrest during the S phase. Considering these results it is possible that AHNAK facilitated the DXR response while its protein expression was maintained. After a 24 hr treatment with a high dose of DXR, the treatment may have started to overcome the resistance exhibited by the cells, indicated by the minor degree of cell death, decreased AHNAK expression and comparative increase in cCasp7 expression. Cell cycle arrest was yet to be effected and may represent the last aspect to be lost especially since the proposed roles of AHNAK are of an indirect nature. It would be interesting to compare AHNAK expression, apoptosis induction and cell cycle arrest between our high DXR dose and an even higher dose capable of promoting more significant cell death in MDA-MB-231 cells.

The dual role of AHNAK in DXR response may however be mediated by a central pro-survival signalling protein, namely Akt. As we described previously, Akt is known to suppress apoptosis and to regulate the cell cycle. Given our proposed mechanisms for AHNAK's involvement in cell cycle arrest described above, it is possible that Akt phosphorylates AHNAK as part of its pro-survival functions.

It also clear that AHNAK has different functions in MCF-7 and MDA-MB-231 cells. The protein is significantly differentially expressed and the majority of the results obtained differ between the two cell lines, where mostly none of the effects observed in MDA-MB-231 cells were seen in MCF-7 cells. We propose that AHNAK is differentially regulated in the two breast cancer cell lines, leading to different expression levels, localisation and function. When considering the other functions of AHNAK, the role of possible protein-protein interactions in its function in these two cell lines should not be overlooked. The MCF-7 and MDA-MB-231 cell lines differ not only with regards to their p53 status, DXR sensitivity, and breast cancer-related molecular characteristics, but have widely different transcriptomic and proteomic profiles. Since AHNAK forms protein interactions in almost every other function it would be reasonable to propose that protein interactions form part of the function(s) of AHNAK in these cells too. Furthermore, since the partners required for AHNAK function in MDA-MB-231 cells may not be available to the same extent in MCF-7 cells it is possible that the protein can have different functions.

4.4 The effects of AHNAK on EMT and breast cancer cell migration

Epithelial-mesenchymal transition (EMT) is a physiological process that allows for phenotypical adjustments of cells to acquire certain characteristics, such as migration, that would enable them to fulfil a certain function. Just as cancer cells have “hijacked” other physiological processes to promote their own survival and growth, EMT represents another “stolen” process that is now associated with advanced tumour progression, metastasis and invasion (Spano et al., 2012). Tumour resistance and metastasis often goes hand in hand and it is estimated that approximately 90% of cancer deaths are due to metastases (Chen, 2012; Christofori, 2006). The physical adaptations that a cell goes through in order to have migratory properties are immense, and many of these are regulated by or acquired through the EMT process (Polyak and Weinberg, 2009). Changes in genomic profiles drive these adaptations which is mediated by countless signalling and effector proteins. Therapeutics have been designed to target many of these proteins in the hope of preventing the spread of tumour cells throughout the body. This includes matrix metalloproteinase inhibitors to limit tumour invasion and antibodies that target the vascular endothelial growth factor to prevent tumour angiogenesis (Gialeli et al., 2011; Van der Veldt et al., 2012). However, similar to cytotoxic agents, these agents are also plagued by problems such as therapeutic failure, resistance and adverse effects. Thus patients diagnosed with metastatic cancer are often given a poor and terminal prognosis (Sleeman and Steeg, 2010).

It is suggested in previous studies that AHNAK is required for the EMT process which thus implicated the protein in tumour metastasis (Shankar et al., 2010; Sudo et al., 2014). We investigated the role of AHNAK in cellular migration by assessing the protein expression of three markers for EMT with

Western blots and determining the rate of cellular migration by means of scratch assays following AHNAK knockdown and overexpression. With EMT activation loss of the epithelial marker E-cadherin is expected, while the mesenchymal markers Snail and Vimentin are expected to increase. The opposite is expected for EMT reversion, or MET (mesenchymal-epithelial transition). Since DXR has also been previously shown to be capable of inducing EMT (Li et al., 2009a), we included DXR treatments in these experiments to determine whether a possible link between AHNAK, DXR and EMT exists.

In MCF-7 cells, a treatment of 5 µM DXR induced a significant decrease in E-cadherin expression which coincided with a significant increase in Snail expression. MCF-7 cells are known to be epithelial-like and we also confirmed this (fig. 3.63). These changes in protein expression however suggest the activation of EMT and thus a shift toward a mesenchymal-like state. MCF-7 cells are also known to express very little Vimentin during basal conditions (Mendez et al., 2010), but interestingly we did not observe an induction of Vimentin with the activation of EMT. Two possible scenarios could explain this; firstly, it may have been too early to detect Vimentin. Snail is an important transcription factor during the activation of EMT and one of its primary functions is to negatively regulate the expression of E-cadherin (Guarino, 2007). Vimentin expression can be induced by multiple transcription factors (Sánchez-Tilló et al., 2012) and it could have been that in our scenario, other transcription factors, which may not have been activated yet, were required for the induction of Vimentin expression. As another possibility, it has been shown before that not all EMT markers are present during the activation of EMT and in several studies the activation of EMT was reported with only a subset of known markers (Kalluri and Weinberg, 2009; Micalizzi et al., 2010).

Regarding the activation of EMT in MCF-7 cells, we expected these findings for the low dose DXR but not for the high dose, although it seems that in our experiments the low dose may not have been sufficient for the induction of EMT. DXR has previously been shown to induce EMT at low concentrations, even as low as 0.025 µM DXR (Bandyopadhyay et al., 2010; Han et al., 2013). It is also possible that EMT could have been induced by a dose between 0.1 µM and 5 µM. In our experiments, 5 µM DXR induced apoptosis in the majority of MCF-7 cells (most likely approximately 54%, the percentage representing the decrease in cell viability measured by the MTT assay) while the remaining (approximately 46%) underwent activation of EMT. Li *et al.* reported similar results, where DXR induced either apoptosis or EMT in MCF-7 cells (Li et al., 2009a). The knockdown and overexpression of AHNAK however had no effect on these DXR-induced changes and thus AHNAK is most likely not involved in DXR-induced EMT activation in MCF-7 cells.

DXR treatment in MDA-MB-231 cells resulted in a significant decrease in Snail protein expression (fig. 3.69 and 3.74). Whether this decrease signals EMT reversion is however unclear since E-cadherin protein expression remained mostly constant during DXR treatment and the only change observed was a decrease in expression in the 0.1 µM DXR control transfected group during AHNAK

overexpression experiments (fig. 3.73). A decrease in Vimentin expression was however observed in the 5 µM DXR control transfected group during AHNAK overexpression experiments, which would support MET. Knockdown of AHNAK did not seem to induce any major changes in the expression of EMT markers. Together with both a low and high dose of DXR, AHNAK knockdown increased Vimentin expression, which could be an indication of EMT. However, no changes in Snail expression were observed and at the high DXR dose an increase E-cadherin was also detected, which would be inconsistent with EMT activation. Overexpression of AHNAK appeared to induce MET under basal conditions which is indicated by a decrease in both Snail and Vimentin protein expression (fig. 3.74-75). No increase in E-cadherin expression was however observed. These changes are similar to those induced by a treatment of 5 µM DXR and interestingly, overexpression of AHNAK together with a treatment of 5 µM DXR lead to an increase in E-cadherin expression, which is consistent with MET (fig. 3.73).

Our results suggest that AHNAK is capable of promoting EMT reversion, or MET. The lack of opposite findings in the knockdown of AHNAK could be due to the fact that MDA-MB-231 cells are already mesenchymal and thus a further activation of EMT may not have occurred. We did observe an increase in Vimentin expression and since we only achieved approximately 50% knockdown, with higher levels of knockdown we may have observed an increase in Snail expression too.

Assessing the protein expression of EMT markers represents a molecular but indirect assessment of cellular migratory capacity. As a more direct measurement we performed scratch assays to assess the ability of cells to migrate into and re-fill a wound following AHNAK knockdown and overexpression and during DXR treatment.

Knockdown of AHNAK did not seem to have a major effect on the migratory capacity of MCF-7 and MDA-MB-231 cells. Significant changes were only detected between the 0.1 µM control transfected and 0.1 µM knockdown groups (24 hrs) in MCF-7 cells, and between the control transfected and knockdown groups (6 hrs) in MDA-MB-231 cells. In both instances, knockdown of AHNAK resulted in increased percentage of wound closure, and is thus indicative of increased migratory capacity. However, since these significant changes are limited and only briefly encountered at certain time points, a further investigation is needed to confirm the effect of AHNAK knockdown in cellular migration. In contrast, the overexpression of AHNAK revealed more significant changes. In MCF-7 cells, AHNAK overexpression decreased the percentage wound closure when compared to control transfected groups, both without (at 12 and 18 hrs) and with a low dose DXR treatment (at 18 and 24 hrs). In the MDA-MB-231 cells, overexpression of AHNAK also decreased the percentage wound closure when compared to the control transfected groups during both the low (6 and 12 hrs) and high (12-24 hrs) DXR treatments, while the high dose DXR treatment cooperated with AHNAK overexpression to decrease the percentage wound closure even further. These results, obtained from both MCF-7 and MDA-MB-231 cells, suggests that AHNAK overexpression decreased the migratory capacity of cells.

A limited number of studies have investigated the role of AHNAK in cellular migration and metastasis, however, for the most part, our results contradict those studies. Shankar *et al.* also investigated the effect of AHNAK knockdown on the expression of EMT markers but found that this resulted in increased E-cadherin and decreased Vimentin (as well as decreased N-cadherin, an additional mesenchymal marker, in various cancer cells), indicating that AHNAK was required for EMT (Shankar et al., 2010). However, similar to our results, Sheppard *et al.* also reported contrasting results and found that not only did AHNAK negatively correlate with metastasis but it was also required for E-cadherin expression in melanoma cancer cells (Sheppard et al., 2015). Even though we did not observe increased E-cadherin expression with AHNAK overexpression, we did observe decreased Snail expression, which could indicate that E-cadherin levels were still to increase, or the suppression was maintained by another transcription factors, such as Slug. Sudo *et al*. also reported results that contradict our scratch assay results. They assessed cellular migration and invasion by means of transwell inserts and found that AHNAK knockdown decreased the number of migrating and invasive mesothelioma cells (Sudo et al., 2014).

When considering the results obtained from both the Western blot experiments and the scratch assays, there seems to be a consensus that AHNAK overexpression negatively affects cellular migration. Since the knockdown of AHNAK did not induce the opposite effect, it would indicate that AHNAK may not function as a negative regulator directly involved in the migration process but rather that the protein has a different function that indirectly affects migration. That is, overexpression of AHNAK stimulates a separate process, which in turn would oppose migration. When taking into account the cell cycle results obtained during AHNAK overexpression, this may indeed be the case.

It is suggested that proliferative and migratory states in cells are mutually exclusive and that processes such as EMT serve to uncouple the cell from one state before transitioning into the other. Evdokimova *et al.* reported on the ability of the YB-1 protein to induce both EMT and inhibition of cellular proliferation (Evdokimova et al., 2009). This was achieved through activation of EMT-inducing transcription factors and suppression of cyclin B and D1/D2, both positive regulators of the cell cycle. Svensson *et al.* elegantly showed that tumour-infiltrating regions located at the edges of tumours showed decreased proliferative markers and increased expression of the cell cycle inhibitor $p16^{INK4a}$, while the centre areas showed the opposite (Svensson et al., 2003). Hoek *et al.* distinguished between a proliferative and invasive signature in melanoma cells through DNA microarray experiments and showed in *in vitro* and *in vivo* studies that these signatures resulted in significant differences in terms of proliferation and motility (Hoek et al., 2008). Furthermore, Vega *et al.* reported that while Snail overexpression induced EMT in MDCK cells, it also decreased cellular proliferation by increasing the expression of p21, resulting in arrest at the G_1/S checkpoint (Vega et al., 2004).

The separation of proliferative and migratory states also supports the most recent ideas regarding the origins of secondary tumours during metastasis, which suggests that cancer cells acquire the

mutational requirements for invasion and disseminate early to establish micrometastases at secondary sites (Bernards and Weinberg, 2002; Coghlin and Murray, 2010). The disseminated cells would be inefficient at proliferation and thus, it is reasonable that these micrometastases would take longer to form noticeable secondary tumours than the primary tumour where mutated cells providing proliferative advantages would have been selected for. The rationale behind this separation may be simple and logical; through this restriction, the cell is allowed to focus on only one state at a time, thus ensuring resource availability and proper control.

We speculate that a similar phenomenon may have occurred in our study. The overexpression of AHNAK activated signalling pathways that promoted cell cycle arrest. Even though this is not necessarily associated with a proliferative state, it still represents an important process and may still have directed some of the focus of the cell to that response rather than migration. Indeed, we only observed decreased migration and EMT and not a complete inhibition, which indicates that the focus of the cell was shifted only slightly. In keeping with this theory, since DXR treatment induced the same response in terms of cell cycle arrest, it is expected that a similar effect would be observed in migration. Indeed, we observed decreased Snail and Vimentin expression (fig. 3.69, 3.74 and 3.75) and also decreased migration (fig. 3.84) following DXR treatment.

We did not observe any changes in EMT marker expression when overexpressing AHNAK in MCF-7 cells, which further supports our theory since we did not observe the same response in cell cycle modulation in these cells. We did however observe two instances in the scratch assays where AHNAK overexpression decreased cellular migration compared to the control transfected group (at 12 and 18 hrs) and compared to the overexpression group treated with low dose DXR (at 18 and 24 hrs). These effects may have stemmed from AHNAK's role in the formation of cell-cell contacts, especially since MCF-7 cells were one of the cell lines used during the identification of this role (Sussman et al., 2001; Benaud et al., 2004). In addition, we also observed the same localisation patterns reported in these studies. Increased AHNAK expression would then promote the establishment of adherens junctions, which, interestingly, was suggested as a function of AHNAK by Sheppard *et al.* (2015). Nonetheless, the contrasting results presented here and by previous studies in literature regarding the role of AHNAK in cellular migration emphasises the need for further investigation.

Chapter 5 : Conclusions

The cancer cell response to chemotherapeutic drugs represents a complex but vital process in determining the therapeutic efficacy of anti-cancer therapies. The significant amount of cancer-associated deaths continues to have a devastating impact on society and emphasises the urgent need to fully understand the response elicited by cancer cells during treatment. The human AHNAK protein is a diverse scaffold protein involved in multiple cellular processes. In recent years new roles for AHNAK in cancer have been suggested, including tumour metastasis and chemoresponse. However, due to limited information and several contradicting reports, the precise role of AHNAK in cancer remains unclear. To clarify the role of AHNAK in cancer, especially with regards to chemotherapeutic treatment, we have utilised a well-designed *in vitro* model as well as a physiological *in vivo* breast cancer model. The cell lines used for the *in vitro* experiments had opposing characteristics, such DXR sensitivity, p53 status and capacity for migration, which contributed meaningfully towards identifying a role for AHNAK in the DXR-response.

We observed several differences between the MCF-7 and MDA-MB-231 cell lines with regards to AHNAK, primarily associated with changes in protein expression and its role in apoptosis inhibition and cell cycle arrest. This is likely associated with the differential DXR-responses, possibly influenced by their respective p53 statuses exhibited by these cells, although their differential metastatic abilities can not be ignored. Confirming our results with a cell line pair that differs in only one phenotype will clarify this, however one should keep in mind that these two characteristics often go hand-in-hand. Rather, it may be more appropriate to propose that AHNAK is associated with a more malignant and aggressive phenotype than just one specific functional characteristic. Results obtained with the tumour-bearing mouse model also reflected an aggressive and resistant phenotype and supported our *in vitro* results. Notably, it is cancers exhibiting this particular phenotype that contribute the most to the current mortality rate and thus our results have the potential to be of real consequence.

We present here convincing evidence that AHNAK plays an important role in DXR-response in breast cancer cells. We have shown that AHNAK's protein expression is affected by DXR, but not its localisation. Furthermore, we also show that AHNAK can affect DXR-induced changes in apoptosis inhibition and cell cycle modulation in breast cancer cells. Based on these findings we propose an interesting and novel association between AHNAK, DXR and DXR response/resistance. Identifying the exact molecular mechanisms involved requires further investigation, although we provide a suitable starting point with regards to the possible involvement of Akt. With regards to the role of AHNAK in cellular migration and EMT, our results do not support a direct involvement of the protein

in these processes. However, one can not ignore the results obtained from the earlier studies, and thus further investigation into this potential role is needed.

We experienced some limitations during the study. Firstly, increased knockdown efficiency may have revealed more information regarding the effect of AHNAK knockdown in mitigating DXR-induced apoptosis inhibition and also cellular migration. Even though we selected key proteins involved in EMT, the use of different, or perhaps additional, EMT markers may have provided clearer results with regards to AHNAK's role in EMT. A phospho-specific antibody for AHNAK was not commercially available, although generating such an antibody would have been of great value in determining the role of AHNAK in cancer.

It is recommended that further studies be performed to clarify the molecular mechanisms of AHNAK's role in DXR-induced apoptosis inhibition and cell cycle modulation. Furthermore, on several occasions we noted the possibility of cell-type or drug-dependent effects. It would be advisable to confirm the role of AHNAK identified here in other cell lines, especially in pairs of cell lines resistant and sensitive to DXR. In addition, it would also be useful to explore the role of AHNAK with other chemotherapeutic drugs, those with a similar mechanism of action than DXR but also those that have previously been shown to be positively correlated with AHNAK and, importantly, negatively correlated as well. A central aspect that warrants further investigation is the regulation of AHNAK and this would surely also be of benefit to future studies aimed at identifying the molecular mechanisms of AHNAK's function. Here, the use of a phospho-specific AHNAK antibody would be especially useful. Also, AHNAK is known to form multiple protein interactions therefore co-immunoprecipitation and co-localisation studies to identify interacting protein partners are also needed.

To conclude, we have shown for the first time that AHNAK plays an important part in the DXR-response of breast cancer cells. Our study has contributed considerably to obtaining a better understanding of AHNAK in cancer, especially with regards to its involvement in therapeutic responses where there was previously a gap in the available literature. Our results have potential therapeutic implications, especially with regards to the modulation of DXR response to ensure improved treatment efficacy. However, much research is needed before any clinical benefits can be achieved.

Chapter 6 : References

Abolhoda, A., Wilson, A.E., Ross, H., Danenberg, P.V., Burt, M., and Scotto, K.W. (1999). Rapid Activation of MDR1 Gene Expression in Human Metastatic Sarcoma after in Vivo Exposure to Doxorubicin. Am. Assoc. Cancer Res. *5*, 3352–3356.

Abreu-Blanco, M.T., Watts, J.J., Verboon, J.M., and Parkhurst, S.M. (2012). Cytoskeleton responses in wound repair. Cell. Mol. Life Sci. *69*, 2469–2483.

Agadjanian, H., Chu, D., Hwang, J., Wachsmann-Hogiu, S., Rentsendorj, A., Song, L., Valluripalli, V., Lubow, J., Ma, J., Sharifi, B., et al. (2012). Chemotherapy targeting by DNA capture in viral protein particles. Nanomed. *7*, 335–352.

Alexander, N.R., Tran, N.L., Rekapally, H., Summers, C.E., Glackin, C., and Heimark, R.L. (2006). N-cadherin gene expression in prostate carcinoma is modulated by integrin-dependent nuclear translocation of Twist1. Cancer Res. *66*, 3365–3369.

Al-Lazikani, B., Banerji, U., and Workman, P. (2012). Combinatorial drug therapy for cancer in the post-genomic era. Nat. Biotechnol. *30*, 679–692.

Alvarez, J., Hamplova, J., Hohaus, A., Morano, I., Haase, H., and Vassort, G. (2004). Calcium Current in Rat Cardiomyocytes Is Modulated by the Carboxyl-terminal Ahnak Domain. J. Biol. Chem. *279*, 12456–12461.

Amagai, M. (2004). A mystery of AHNAK/desmoyokin still goes on. J. Invest. Dermatol. *123*, xiv–xv.

American Cancer Soceity (2014). The History of Cancer. http://www.cancer.org/cancer/cancerbasics/thehistoryofcancer/index?sitearea. Accessed: 06/09/2016.

Araki, K., Shimura, T., Suzuki, H., Tsutsumi, S., Wada, W., Yajima, T., Kobayahi, T., Kubo, N., and Kuwano, H. (2011). E/N-cadherin switch mediates cancer progression via TGF-β-induced epithelial-to-mesenchymal transition in extrahepatic cholangiocarcinoma. Br. J. Cancer *105*, 1885–1893.

Arcamone, F., Cassinelli, G., Fantini, G., Grein, A., Orezzi, P., Pol, C., and Spalla, C. (2000). Adriamycin, 14-Hydroxydaunomycin, a new antitumor antibiotic from S. peucetius var. caesius. Biotechnol. Bioeng. *67*, 704–713.

Aroui, S., Brahim, S., De Waard, M., Bréard, J., and Kenani, A. (2009a). Efficient induction of apoptosis by doxorubicin coupled to cell-penetrating peptides compared to unconjugated doxorubicin in the human breast cancer cell line MDA-MB 231. Cancer Lett. *285*, 28–38.

Aroui, S., Ram, N., Appaix, F., Ronjat, M., Kenani, A., Pirollet, F., and De Waard, M. (2009b). Maurocalcine as a Non Toxic Drug Carrier Overcomes Doxorubicin Resistance in the Cancer Cell Line MDA-MB 231. Pharm. Res. *26*, 836–845.

Aroui, S., Brahim, S., Waard, M. De, and Kenani, A. (2010). Cytotoxicity, intracellular distribution and uptake of doxorubicin and doxorubicin coupled to cell-penetrating peptides in different cell lines: a comparative study. Biochem. Biophys. Res. Commun. *391*, 419–425.

Ballabh, P., Braun, A., and Nedergaard, M. (2004). The blood–brain barrier: an overview. Neurobiol. Dis. *16*, 1–13.

Bandyopadhyay, A., Wang, L., Agyin, J., Tang, Y., Lin, S., Yeh, I.-T., De, K., and Sun, L.-Z. (2010). Doxorubicin in combination with a small TGFbeta inhibitor: a potential novel therapy for metastatic breast cancer in mouse models. PloS One *5*, e10365.

Bansal, D., Miyake, K., Vogel, S.S., Groh, S., Chen, C.-C., Williamson, R., McNell, P.L., and Campbell, K.P. (2003). Defective membrane repair in dysferlin-deficient muscular dystrophy. Nature *423*, 168–172.

Bao, L., Matsumura, Y., Baban, D., Sun, Y., and Tarin, D. (1994). Effects of inoculation site and Matrigel on growth and metastasis of human breast cancer cells. Br. J. Cancer *70*, 228–232.

Barraud, L., Merle, P., Soma, E., Lefrançois, L., Guerret, S., Chevallier, M., Dubernet, C., Couvreur, P., Trépo, C., and Vitvitski, L. (2005). Increase of doxorubicin sensitivity by doxorubicin-loading into nanoparticles for hepatocellular carcinoma cells in vitro and in vivo. J. Hepatol. *42*, 736–743.

Baruthio, F., Quadroni, M., Rüegg, C., and Mariotti, A. (2008). Proteomic analysis of membrane rafts of melanoma cells identifies protein patterns characteristic of the tumor progression stage. Proteomics *8*, 4733–4747.

Beavon, I.R. (2000). The E-cadherin–catenin complex in tumour metastasis. Eur. J. Cancer *36*, 1607–1620.

Benaud, C., Gentil, B.J., Assard, N., Court, M., Garin, J., Delphin, C., and Baudier, J. (2004). AHNAK interaction with the annexin 2/S100A10 complex regulates cell membrane cytoarchitecture. J. Cell Biol. *164*, 133–144.

Bernards, R., and Weinberg, R.A. (2002). A progression puzzle. Nature *418*, 823.

Bers, D.M. (2000). Calcium Fluxes Involved in Control of Cardiac Myocyte Contraction. Circ. Res. *87*, 275–281.

Berthiaume, J.M., and Wallace, K.B. (2007). Adriamycin-induced oxidative mitochondrial cardiotoxicity. Cell Biol. Toxicol. *23*, 15–25.

Bhowmick, N.A, Ghiassi, M., Bakin, A., Aakre, M., Lundquist, C.A., Engel, M.E., Arteaga, C.L., and Moses, H.L. (2001). Transforming growth factor-beta1 mediates epithelial to mesenchymal transdifferentiation through a RhoA-dependent mechanism. Mol. Biol. Cell *12*, 27–36.

Bi, G.Q., Morris, R.L., Liao, G., Alderton, J.M., Scholey, J.M., and Steinhardt, R. a. (1997). Kinesin- and myosin-driven steps of vesicle recruitment for Ca2+- regulated exocytosis. J. Cell Biol. *138*, 999–1008.

Bindels, S., Mestdagt, M., Vandewalle, C., Jacobs, N., Volders, L., Noël, A., van Roy, F., Berx, G., Foidart, J.-M., and Gilles, C. (2006). Regulation of vimentin by SIP1 in human epithelial breast tumor cells. Oncogene *25*, 4975–4985.

Bolós, V., Peinado, H., Pérez-Moreno, M.A., Fraga, M.F., Esteller, M., and Cano, A. (2003). The transcription factor Slug represses E-cadherin expression and induces epithelial to mesenchymal transitions: a comparison with Snail and E47 repressors. J. Cell Sci. *116*, 499–511.

Borgonovo, B., Cocucci, E., Racchetti, G., Podini, P., Bachi, A., and Meldolesi, J. (2002). Regulated exocytosis: a novel, widely expressed system. Nat. Cell Biol. *4*, 955–962.

El Bounkari, O., and Bernhagen, J. (2012). MIF and autophagy: a novel link beyond “eating.” Cell Res. *22*, 950–953.

Boveri, M., Kinsner, A., Berezowski, V., Lenfant, A-M., Draing, C., Cecchelli, R., Dehouck, M.-P., Hartung, T., Prieto, P., and Bal-Price, a (2006). Highly purified lipoteichoic acid from gram-positive bacteria induces in vitro blood-brain barrier disruption through glia activation: role of pro-inflammatory cytokines and nitric oxide. Neuroscience *137*, 1193–1209.

von Boxberg, Y., Salim, C., Soares, S., Baloui, H., Alterio, J., Ravaille-Veron, M., and Nothias, F. (2006). Spinal cord injury-induced up-regulation of AHNAK, expressed in cells delineating cystic cavities, and associated with neoangiogenesis. Eur. J. Neurosci. *24*, 1031–1041.

von Boxberg, Y., Soares, S., Féréol, S., Fodil, R., Bartolami, S., Taxi, J., Tricaud, N., and Nothias, F. (2014). Giant scaffolding protein AHNAK1 interacts with β-dystroglycan and controls motility and mechanical properties of schwann cells. Glia 1–15.

Boyer, B., Tucker, G.C., Vallés, A.M., Franke, W.W., and Thiery, J.P. (1989). Rearrangements of desmosomal and cytoskeletal proteins during the transition from epithelial to fibroblastoid organization in cultured rat bladder carcinoma cells. J. Cell Biol. *109*, 1495–1509.

Broxterman, H.J., Gotink, K.J., and Verheul, H.M.W. (2009). Understanding the causes of multidrug resistance in cancer: a comparison of doxorubicin and sunitinib. Drug Resist. Updat. *12*, 114–126.

Bryant, H.E., Petermann, E., Schultz, N., Jemth, A.-S., Loseva, O., Issaeva, N., Johansson, F., Fernandez, S., McGlynn, P., and Helleday, T. (2009). PARP is activated at stalled forks to mediate Mre11-dependent replication restart and recombination. EMBO J. *28*, 2601–2615.

Bunz, F., Hwang, P.M., Torrance, C., Waldman, T., Zhang, Y., Dillehay, L., Williams, J., Lengauer, C., Kinzler, K.W., and Vogelstein, B. (1999). Disruption of p53 in human cancer cells alters the responses to therapeutic agents. J. Clin. Invest. *104*, 263–269.

Bussemakers, M.J.G., and Schalken, J.A. (2000). Cadherin Switching in Human Prostate Cancer Progression. Urology 3650–3654.

Cano, A., Pérez-Moreno, M.A., Rodrigo, I., Locascio, A., Blanco, M.J., del Barrio, M.G., Portillo, F., and Nieto, M. (2000). The transcription factor snail controls epithelial-mesenchymal transitions by repressing E-cadherin expression. Nat. Cell Biol. *2*, 76–83.

Cardoso, F., Harbeck, N., Fallowfield, L., Kyriakides, S., and Senkus, E. (2012). Locally recurrent or metastatic breast cancer: ESMO Clinical Practice Guidelines for diagnosis, treatment and follow-up. Ann. Oncol. *23*, vii11-vii19.

Carlson, S.S., Valdez, G., and Sanes, J.R. (2010). Presynaptic calcium channels and α3-integrins are complexed with synaptic cleft laminins, cytoskeletal elements and active zone components. J. Neurochem. *115*, 654–666.

Caruso, J.A., and Stemmer, P.M. (2011). Proteomic profiling of lipid rafts in a human breast cancer model of tumorigenic progression. Clin Exp Metastasis *28*, 529–540.

Catterall, W., Perez-Reyes, E., Snutch, T.P., and Striessnig, J. (2005). International Union of Pharmacology. XLVIII. Nomenclature and structure-function relationships of voltage-gated calcium channels. Pharmacol. Rev. *57*, 411–425.

Cenacchi, G., Fanin, M., De Giorgi, L.B., and Angelini, C. (2005). Ultrastructural changes in dysferlinopathy support defective membrane repair mechanism. J. Clin. Pathol. *58*, 190–195.

Cerosaletti, K., Wright, J., and Concannon, P. (2006). Active Role for Nibrin in the Kinetics of Atm Activation. Mol. Cell. Biol. *26*, 1691–1699.

Chabner, B., and Roberts, T.G. (2005). Timeline: Chemotherapy and the war on cancer. Nat. Rev. Cancer *5*, 65–72.

Chaudhuri, O., Koshy, S.T., Branco da Cunha, C., Shin, J.-W., Verbeke, C.S., Allison, K.H., and Mooney, D.J. (2014). Extracellular matrix stiffness and composition jointly regulate the induction of malignant phenotypes in mammary epithelium. Nat. Mater. *13*, 970–978.

Chekhun, V.F., Kulik, G.I., Yurchenko, O. V., Tryndyak, V.P., Todor, I.N., Luniv, L.S., Tregubova, N. a., Pryzimirska, T. V., Montgomery, B., Rusetskaya, N. V., et al. (2006). Role of DNA hypomethylation in the development of the resistance to doxorubicin in human MCF-7 breast adenocarcinoma cells. Cancer Lett. *231*, 87–93.

Chen, E.I. (2012). Mitochondrial dysfunction and cancer metastasis. J. Bioenerg. Biomembr. *44*, 619–622.

Chen, H., Pimienta, G., Gu, Y., Sun, X., Hu, J., Kim, M.-S., Chaerkady, R., Gucek, M., Cole, R.N., Sukumar, S., et al. (2010). Proteomic characterization of Her2/neu-overexpressing breast cancer cells. Proteomics *10*, 3800–3810.

Chen, H.-C., Chu, R.Y., Hsu, P.-N., Hsu, P.-I., Lu, J.-Y., Lai, K.-H., Tseng, H.-H., Chou, N.-H., Huang, M.-S., Tseng, C.-J., et al. (2003). Loss of E-cadherin expression correlates with poor differentiation and invasion into adjacent organs in gastric adenocarcinomas. Cancer Lett. *201*, 97–106.

Chen, K.-C., Yang, T.-Y., Wu, C.-C., Cheng, C.-C., Hsu, S.-L., Hung, H.-W., Chen, J.-W., and Chang, G.-C. (2014). Pemetrexed Induces S-Phase Arrest and Apoptosis via a Deregulated Activation of Akt Signaling Pathway. PLoS ONE *9*, e97888.

Chen, W.-C., Lai, Y.-A., Lin, Y.-C., Ma, J.-W., Huang, L.-F., Yang, N.-S., Ho, C.-T., Kuo, S.-C., and Way, T.-D. (2013). Curcumin suppresses doxorubicin-induced epithelial-mesenchymal transition via the inhibition of TGF-β and PI3K/AKT signaling pathways in triple-negative breast cancer cells. J. Agric. Food Chem. *61*, 11817–11824.

Chen, Y.-R., Juan, H., Huang, H.-C., Huang, H., Lee, Y., Liao, M., Tseng, C., Lin, L., Chen, J.-Y., Wang, M., et al. (2006). Quantitative proteomic and genomic profiling reveals metastasis-related protein expression patterns in gastric cancer cells. J. Proteome Res. *5*, 2727–2742.

Cheng, W.W.K., and Allen, T.M. (2008). Targeted delivery of anti-CD19 liposomal doxorubicin in B-cell lymphoma: A comparison of whole monoclonal antibody, Fab′ fragments and single chain Fv. J. Controlled Release *126*, 50–58.

Cheng, T.C., Manorek, G., Samimi, G., Lin, X., Berry, C.C., and Howell, S.B. (2006). Identification of genes whose expression is associated with cisplatin resistance in human ovarian carcinoma cells. Cancer Chemother. Pharmacol. *58*, 384–395.

Chiaretti, S., Li, X., Gentleman, R., Vitale, A., Vignetti, M., Mandelli, F., Ritz, J., and Foa, R. (2004). Gene expression profile of adult T-cell acute lymphocytic leukemia identifies distinct subsets of patients with different response to therapy and survival. Blood *103*, 2771–2778.

Chien, A.J., Zhao, X., Shirokov, R.E., Puri, T.S., Chang, C.F., Sun, D., Rios, E., and Hosey, M.M. (1995). Roles of a membrane-localized β-subunit in the formation and targeting of functional L-type Ca2+ channels. J. Biol. Chem. *270*, 30036–30044.

Chieregatti, E., and Meldolesi, J. (2005). Regulated exocytosis: new organelles for non-secretory purposes. Nat. Rev. Mol. Cell Biol. *6*, 181–187.

Chou, C.-H., Cheng, Y.-F., Siow, T.Y., Kumar, A., Peck, K., and Chang, C. (2013). SCUBE3 regulation of early lung cancer angiogenesis and metastatic progression. Clin. Exp. Metastasis *30*, 741–752.

Christofori, G. (2006). New signals from the invasive front. Nature *441*, 444–450.

Cocucci, E., Racchetti, G., Rupnik, M., and Meldolesi, J. (2008). The regulated exocytosis of enlargeosomes is mediated by a SNARE machinery that includes VAMP4. J. Cell Sci. *121*, 2983–2991.

Coghlin, C., and Murray, G.I. (2010). Current and emerging concepts in tumour metastasis. J. Pathol. *222*, 1–15.

Cohen, C.J., Gartner, J.J., Horovitz-fried, M., Shamalov, K., Trebska-Mcgowan, K., Bliskovsky, V. V, Parkhurst, M.R., Ankri, C., Prickett, T.D., Crystal, J.S., et al. (2015). Isolation of neoantigen-specific T cells from tumor and peripheral lymphocytes. J. Clin. Invest. *125*, 3981–3991.

Colognato, H., Galvin, J., Wang, Z., Relucio, J., Nguyen, T., Harrison, D., Yurchenco, P.D., and Ffrench-Constant, C. (2007). Identification of dystroglycan as a second laminin receptor in oligodendrocytes, with a role in myelination. Dev. Camb. Engl. *134*, 1723–1736.

Comijn, J., Berx, G., Vermassen, P., Verschueren, K., Van Grunsven, L., Bruyneel, E., Mareel, M., Huylebroeck, D., and Van Roy, F. (2001). The two-handed E box binding zinc finger protein SIP1 downregulates E-cadherin and induces invasion. Mol. Cell *7*, 1267–1278.

Connell, P.P., and Hellman, S. (2009). Advances in Radiotherapy and Implications for the Next Century: A Historical Perspective. Cancer Res. *69*, 383–392.

Connolly, E.C., van Doorslaer, K., Rogler, L.E., and Rogler, C.E. (2010). Overexpression of miR-21 promotes an *in vitro* metastatic phenotype by targeting the tumor suppressor RHOB. Mol. Cancer Res. *8*, 691-700.

Cortés-Funes, H., and Coronado, C. (2007). Role of anthracyclines in the era of targeted therapy. Cardiovasc. Toxicol. *7*, 56–60.

De Craene, B., and Berx, G. (2013). Regulatory networks defining EMT during cancer initiation and progression. Nat. Rev. Cancer *13*, 97–110.

Cummings, J., Anderson, L., Willmott, N., and Smyth, J.F. (1991). The molecular pharmacology of doxorubicin in vivo. Eur. J. Cancer *27*, 532–535.

Cutts, S., Nudelman, A., Rephaeli, A., and Phillips, D. (2005). The Power and Potential of Doxorubicin-DNA Adducts. IUBMB Life Int. Union Biochem. Mol. Biol. Life *57*, 73–81.

Dart, D.A., Picksley, S.M., Cooper, P.A., Double, J.A., and Bibby, M.C. (2004). The role of p53 in the chemotherapeutic responses to cisplatin, doxorubicin and 5-fluorouracil treatment. Int. J. Oncol. *24*, 115–125.

Davis, T.A., Loos, B., and Engelbrecht, A.-M. (2014). AHNAK: The giant jack of all trades. Cell. Signal. *26*, 2683–2693.

Defour, A., Van der Meulen, J.H., Bhat, R., Bigot, A., Bashir, R., Nagaraju, K., and Jaiswal, J.K. (2014). Dysferlin regulates cell membrane repair by facilitating injury-triggered acid sphingomyelinase secretion. Cell Death Dis. *5*, e1306.

Dempsey, B.R., Rezvanpour, A., Lee, T.-W., Barber, K.R., Junop, M.S., and Shaw, G.S. (2012). Structure of an Asymmetric Ternary Protein Complex Provides Insight for Membrane Interaction. Structure *20*, 1737–1745.

DeVita, V.T., and Chu, E. (2008). A History of Cancer Chemotherapy. Cancer Res. *68*, 8643–8653.

Devita, V.T., Young, R.C., and Canellos, G.P. (1975). Combination versus single agent chemotherapy: A review of the basis for selection of drug treatment of cancer. Cancer *35*, 98–110.

Di, X., Shiu, R.P., Newsham, I.F., and Gewirtz, D. a (2009). Apoptosis, autophagy, accelerated senescence and reactive oxygen in the response of human breast tumor cells to adriamycin. Biochem. Pharmacol. *77*, 1139–1150.

Disatnik, M.H., Hernandez-Sotomayor, S.M., Jones, G., Carpenter, G., and Mochly-Rosen, D. (1994). Phospholipase C-gamma 1 binding to intracellular receptors for activated protein kinase C. Proc. Natl. Acad. Sci. U. S. A. *91*, 559–563.

Du, J., Du, X., Mao, C., and Wang, J. (2011). Tailor-Made Dual pH-Sensitive Polymer- Doxorubicin Nanoparticles for Efficient Anticancer Drug Delivery. J Am Chem Soc 17560–175633.

Duffy, M.J., McGowan, P.M., and Gallagher, W.M. (2008). Cancer invasion and metastasis: changing views. J. Pathol. *214*, 283–293.

Dumitru, C.A., Bankfalvi, A., Gu, X., Zeidler, R., Brandau, S., and Lang, S. (2013). AHNAK and Inflammatory Markers Predict Poor Survival in Laryngeal Carcinoma. PLoS ONE *8*, e56420.

Eger, A., Aigner, K., Sonderegger, S., Dampier, B., Oehler, S., Schreiber, M., Berx, G., Cano, A., Beug, H., and Foisner, R. (2005). DeltaEF1 is a transcriptional repressor of E-cadherin and regulates epithelial plasticity in breast cancer cells. Oncogene *24*, 2375–2385.

Evdokimova, V., Tognon, C., Ng, T., and Sorensen, P.H.B. (2009). Reduced proliferation and enhanced migration: Two sides of the same coin? Molecular mechanisms of metastatic progression by YB-1. Cell Cycle *8*, 2901–2906.

Falck, J., Petrini, J.H.J., Williams, B.R., Lukas, J., and Bartek, J. (2002). The DNA damage-dependent intra–S phase checkpoint is regulated by parallel pathways. Nat. Genet. *30*, 290–294.

Ferlay, J., Soerjomataram, I., Ervik, M., Dikshit, R., Eser, S., Mathers, C., Rebelo, M., Parkin, D.M., Forman, D., and Bray, F. (2013). GLOBOCAN 2012 v1.0, Cancer Incidence and Mortality Worldwide: IARC CancerBase No. 11.

Finetti, F., Terzuoli, E., Giachetti, A., Santi, R., Villari, D., Hanaka, H., Radmark, O., Ziche, M., and Donnini, S. (2015). mPGES-1 in prostate cancer controls stemness and amplifies epidermal growth factor receptor-driven oncogenicity. Endocr. Relat. Cancer *22*, 665–678.

Friesen, C., Fulda, S., and Debatin, K. (1999). Induction of CD 95 ligand and apoptosis by doxorubicin is modulated by the redox state in chemosensitive- and drug-resistant tumor cells. Cell Death Differ. *6*, 471–480.

Gagnon, V., Van Themsche, C., Turner, S., Leblanc, V., and Asselin, E. (2008). Akt and XIAP regulate the sensitivity of human uterine cancer cells to cisplatin, doxorubicin and taxol. Apoptosis *13*, 259–271.

Galli, A., and DeFelice, L.J. (1994). Inactivation of L-type Ca channels in embryonic chick ventricle cells: dependence on the cytoskeletal agents colchicine and taxol. Biophys. J. *67*, 2296–2304.

Gartel, A.L., Feliciano, C., and Tyner, A.L. (2003). A New Method for Determining the Status of p53 in Tumor Cell Lines of Different Origin. Oncol. Res. Featur. Preclin. Clin. Cancer Ther. *13*, 405–408.

Geisler, S., Lønning, P.E., Aas, T., Johnsen, H., Fluge, Ø., Haugen, D.F., Lillehaug, J.R., Akslen, L.A., and Børresen-Dale, A.-L. (2001). Influence of TP53 Gene Alterations and c-erbB-2 Expression on the Response to Treatment with Doxorubicin in Locally Advanced Breast Cancer. Cancer Res. *61*, 2505–2512.

Gentil, B.J., Benaud, C., Delphin, C., Remy, C., Berezowski, V., Cecchelli, R., Feraud, O., Vittet, D., and Baudier, J. (2005). Specific AHNAK expression in brain endothelial cells with barrier properties. J. Cell. Physiol. *203*, 362–371.

Gerke, V., Creutz, C.E., and Moss, S.E. (2005). Annexins: linking Ca2+ signalling to membrane dynamics. Nat. Rev. Mol. Cell Biol. *6*, 449–461.

Germain, M., Affar, E.B., D'Amours, D., Dixit, V.M., Salvesen, G.S., and Poirier, G.G. (1999). Cleavage of Automodified Poly(ADP-ribose) Polymerase during Apoptosis EVIDENCE FOR INVOLVEMENT OF CASPASE-7. J. Biol. Chem. *274*, 28379–28384.

Gewirtz, D.A. (1999). A critical evaluation of the mechanisms of action proposed for the antitumor effects of the anthracycline antibiotics adriamycin and daunorubicin. Biochem. Pharmacol. *57*, 727–741.

Gialeli, C., Theocharis, A.D., and Karamanos, N.K. (2011). Roles of matrix metalloproteinases in cancer progression and their pharmacological targeting: MMPs as potential targets in malignancy. FEBS J. *278*, 16–27.

Gilles, C., Polette, M., Piette, J., Delvigne, A.C., Thompson, E.W., Foidart, J.M., and Birembaut, P. (1996). Vimentin expression in cervical carcinomas: Association with invasive and migratory potential. J. Pathol. *180*, 175–180.

Gilles, C., Polette, M., Mestdagt, M., Nawrocki-Raby, B., Ruggeri, P., Birembaut, P., and Foidart, J.-M. (2003). Transactivation of vimentin by beta-catenin in human breast cancer cells. Cancer Res. *63*, 2658–2664.

Gilman, A. (1963). The initial clinical trial of nitrogen mustard. Am. J. Surg. *105*, 574-578.

Goel, P.N., and Gude, R.P. (2011). Unravelling the antimetastatic potential of pentoxifylline, a methylxanthine derivative in human MDA-MB-231 breast cancer cells. Mol. Cell. Biochem. *358*, 141-151.

Goldhirsch, A., Winer, E., Coates, A., Gelber, R., Piccart-Gebhart, M., Thürlimann, B., and Senn, H.-J. (2013). Personalizing the treatment of women with early breast cancer: highlights of the St Gallen International Expert Consensus on the Primary Therapy of Early Breast Cancer 2013. Ann. Oncol. *24*, 2206–2223.

Goonesekere, N.C.W., Wang, X., Ludwig, L., and Guda, C. (2014). A Meta Analysis of Pancreatic Microarray Datasets Yields New Targets as Cancer Genes and Biomarkers. PLoS ONE *9*, e93046.

Gottesman, M.M. (2002). Mechanisms of Cancer Drug Resistance.

Gottesman, M.M., Fojo, T., and Bates, S.E. (2002). Multidrug Resistance in Cancer: Role of Atp-Dependent Transporters. Nat. Rev. Cancer *2*, 48–58.

Gravdal, K., Halvorsen, O.J., Haukaas, S.A., and Akslen, L.A. (2007). A Switch from E-Cadherin to N-Cadherin Expression Indicates Epithelial to Mesenchymal Transition and Is of Strong and Independent Importance for the Progress of Prostate Cancer. Clin. Cancer Res. *13*, 7003–7011.

Gridelli, C., Perrone, F., Gallo, C., Cigolari, S., Rossi, A., Piantedosi, F., Barbera, S., Ferraù, F., Piazza, E., Rosetti, F., et al. (2003). Chemotherapy for elderly patients with advanced non-small-cell lung cancer: the Multicenter Italian Lung Cancer in the Elderly Study (MILES) phase III randomized trial. J. Natl. Cancer Inst. *95*, 362–372.

Grieve, A.G., Moss, S.E., and Hayes, M.J. (2012). Annexin A2 at the Interface of Actin and Membrane Dynamics: A Focus on Its Roles in Endocytosis and Cell Polarization. Int. J. Cell Biol. *2012*, 1–11.

Grünwald, V., DeGraffenried, L., Russel, D., Friedrichs, W.E., Ray, R.B., and Hidalgo, M. (2002). Inhibitors of mTOR reverse doxorubicin resistance conferred by PTEN status in prostate cancer cells. Cancer Res. *62*, 6141–6145.

Guarino, M. (2007). Epithelial-mesenchymal transition and tumour invasion. Int. J. Biochem. Cell Biol. *39*, 2153–2160.

Gulhati, P., Bowen, K.A., Liu, J., Stevens, P.D., Rychahou, P.G., Chen, M., Lee, E.Y., Weiss, H.L., O'Connor, K.L., Gao, T., et al. (2011). mTORC1 and mTORC2 Regulate EMT, Motility, and

Metastasis of Colorectal Cancer via RhoA and Rac1 Signaling Pathways. Cancer Res. *71*, 3246–3256.

Guo, G., Gui, Y., Gao, S., Tang, A., Hu, X., Huang, Y., Jia, W., Li, Z., He, M., Sun, L., et al. (2011). Frequent mutations of genes encoding ubiquitin-mediated proteolysis pathway components in clear cell renal cell carcinoma. Nat. Genet. *44*, 17–19.

Haase, H., Podzuweit, T., Lutsch, G., Hohaus, A., Kostka, S., Lindschau, C., Kott, M., Kraft, R., and Morano, I. (1999). Signaling from beta-adrenoceptor to L-type calcium channel: identification of a novel cardiac protein kinase A target possessing similarities to AHNAK. FASEB J. Off. Publ. Fed. Am. Soc. Exp. Biol. *13*, 2161–2172.

Haase, H., Alvarez, J., Petzhold, D., Doller, A., Behlke, J., Erdmann, J., Hetzer, R., Regitz-Zagrosek, V., Vassort, G., and Morano, I. (2005). Ahnak is critical for cardiac Ca(V)1.2 calcium channel function and its beta-adrenergic regulation. FASEB J. Off. Publ. Fed. Am. Soc. Exp. Biol. *19*, 1969–1977.

Han, H., and Kursula, P. (2014). Periaxin and AHNAK nucleoprotein 2 form intertwined homodimers through domain swapping. J. Biol. Chem. *289*, 14121–14131.

Han, R., Xiong, J., Xiao, R., Altaf, E., Wang, J., Liu, Y., Xu, H., Ding, Q., and Zhang, Q. (2013). Activation of β-catenin signaling is critical for doxorubicin-induced epithelial-mesenchymal transition in BGC-823 gastric cancer cell line. Tumour Biol. J. Int. Soc. Oncodevelopmental Biol. Med. *34*, 277–284.

Han, W.-Q., Xia, M., Xu, M., Boini, K.M., Ritter, J.K., Li, N.-J., and Li, P.-L. (2012). Lysosome fusion to the cell membrane is mediated by the dysferlin C2A domain in coronary arterial endothelial cells. J. Cell Sci. *125*, 1225–1234.

Hanahan, D., and Weinberg, R.A. (2011). Hallmarks of Cancer: The Next Generation. Cell *144*, 646–674.

Hansen, M.D.H. (2002). Molecular Mechanism for Orienting Membrane and Actin Dynamics to Nascent Cell-Cell Contacts in Epithelial Cells. J. Biol. Chem. *277*, 45371–45376.

Hashimoto, T., Amagai, M., Parry, D. a, Dixon, T.W., Tsukita, S., Tsukita, S., Miki, K., Sakai, K., Inokuchi, Y., and Kudoh, J. (1993). Desmoyokin, a 680 kDa keratinocyte plasma membrane-associated protein, is homologous to the protein encoded by human gene AHNAK. J. Cell Sci. *105 (Pt 2*, 275–286.

Hashimoto, T., Gamou, S., Shimizu, N., Kitajima, Y., and Nishikawa, T. (1995). Regulation of translocation of the desmoyokin/AHNAK protein to the plasma membrane in keratinocytes by protein kinase C. Exp. Cell Res. *217*, 258–266.

Hayes, M.J., Shao, D., Bailly, M., and Moss, S.E. (2006). Regulation of actin dynamics by annexin 2. EMBO J. *25*, 1816–1826.

Heldin, C.-H., Landström, M., and Moustakas, A. (2009). Mechanism of TGF-β signaling to growth arrest, apoptosis, and epithelial–mesenchymal transition. Curr. Opin. Cell Biol. *21*, 166–176.

Hoek, K.S., Eichhoff, O.M., Schlegel, N.C., Döbbeling, U., Kobert, N., Schaerer, L., Hemmi, S., and Dummer, R. (2008). In vivo Switching of Human Melanoma Cells between Proliferative and Invasive States. Cancer Res. *68*, 650–656.

Hohaus, A., Person, V., Behlke, J., Schaper, J., Morano, I., and Haase, H. (2002). The carboxyl-terminal region of ahnak provides a link between cardiac L-type Ca2+ channels and the actin-based cytoskeleton. FASEB J. *16*, 1205–1216.

Hollenbeck, P.J. (2005). The axonal transport of mitochondria. J. Cell Sci. *118*, 5411–5419.

Hsu, Y.-C., Chen, H.-Y., Yuan, S., Yu, S.-L., Lin, C.-H., Wu, G., Yang, P.-C., and Li, K.-C. (2013). Genome-wide analysis of three-way interplay among gene expression, cancer cell invasion and anti-cancer compound sensitivity. BMC Med. *11*, 106.

Hu, Q.-D., Chen, W., Yan, T.-L., Ma, T., Chen, C.-L., Liang, C., Zhang, Q., Xia, X.-F., Liu, H., Zhi, X., et al. (2012). NSC 74859 enhances doxorubicin cytotoxicity via inhibition of epithelial-mesenchymal transition in hepatocellular carcinoma cells. Cancer Lett. *325*, 207–213.

Huang, Y., Laval, S.H., van Remoortere, A., Baudier, J., Benaud, C., Anderson, L.V.B., Straub, V., Deelder, A., Frants, R.R., den Dunnen, J.T., et al. (2007). AHNAK, a novel component of the dysferlin protein complex, redistributes to the cytoplasm with dysferlin during skeletal muscle regeneration. FASEB J. Off. Publ. Fed. Am. Soc. Exp. Biol. *21*, 732–742.

Huang, Y., de Morrée, A., van Remoortere, A., Bushby, K., Frants, R.R., Dunnen, J.T., and van der Maarel, S.M. (2008). Calpain 3 is a modulator of the dysferlin protein complex in skeletal muscle. Hum. Mol. Genet. *17*, 1855–1866.

Huggins, C., and Hodges, C.V. (1941). Studies on prostatic cancer: I. The effect of castration, of estrogen and of androgen injection on serum phosphatases in metastatic carcinoma of the prostate. Cancer Res. *1*, 293-297.

Hunt, N.C., Douglas-Jones, A.G., Jasani, B., Morgan, J.M., and Pignatelli, M. (1997). Loss of E-cadherin expression associated with lymph node metastases in small breast carcinomas. Virchows Arch *430*, 285–289.

Hwang, J.Y., Park, J., Kang, B.J., Lubow, D.J., Chu, D., Farkas, D.L., Shung, K.K., and Medina-Kauwe, L.K. (2012). Multimodality imaging in vivo for preclinical assessment of tumor-targeted doxorubicin nanoparticles. PloS One *7*, e34463.

Ikenouchi, J., Matsuda, M., Furuse, M., and Tsukita, S. (2003). Regulation of tight junctions during the epithelium-mesenchyme transition: direct repression of the gene expression of claudins/occludin by Snail. J. Cell Sci. *116*, 1959–1967.

Jänicke, R.U., Sprengart, M.L., Wati, M.R., and Porter, A.G. (1998). Caspase-3 is required for DNA fragmentation and morphological changes associated with apoptosis. J. Biol. Chem. *273*, 9357–9360.

Jia, Z. (2005). Tumor Cell Pseudopodial Protrusions: Localized signalling domains coordinating cytoskeleton remodeling, cell adhesion, glycolysis, RNA translocation, and protein translation. J. Biol. Chem. *280*, 30564–30573.

Jolly, C., Winfree, S., Hansen, B., and Steele-Mortimer, O. (2013). The Annexin A2/p11 complex is required for efficient invasion of Salmonella Typhimurium in epithelial cells. Cell Microbiol *16*, 64–77.

Kabir, M.H., Suh, E.J., and Lee, C. (2012). Comparative phosphoproteome analysis reveals more ERK activation in MDA-MB-231 than in MCF-7. Int. J. Mass Spectrom. *309*, 1–12.

Kalluri, R., and Weinberg, R. a (2009). The basics of epithelial-mesenchymal transition. J. Clin. Invest. *119*, 1420–1428.

Kalyanaraman, B., Joseph, J., Kalivendi, S., Wang, S., Konorev, E., and Kotamraju, S. (2002). Doxorubicin-induced apoptosis: Implications in cardiotoxicity. Mol. Cell. Biochem. *234–235*, 119–124.

Kamp, T.J., and Hell, J.W. (2000). Regulation of cardiac L-type calcium channels by protein kinase A and protein kinase C. Circ. Res. *87*, 1095–1102.

Kenny, P.A., Lee, G.Y., Myers, C.A., Neve, R.M., Semeiks, J.R., Spellman, P.T., Lorenz, K., Lee, E.H., Barcellos-Hoff, M.H., Petersen, O.W., et al. (2007). The morphologies of breast cancer cell lines in three-dimensional assays correlate with their profiles of gene expression. Mol. Oncol. *1*, 84–96.

Kerr, J.P., Ziman, A.P., Mueller, A.L., Muriel, J.M., Kleinhans-Welte, E., Gumerson, J.D., Vogel, S.S., Ward, C.W., Roche, J.A., and Bloch, R.J. (2013). Dysferlin stabilizes stress-induced Ca2+ signaling in the transverse tubule membrane. Proc. Natl. Acad. Sci. *110*, 20831–20836.

Keshamouni, V.G., Michailidis, G., Grasso, C.S., Anthwal, S., Strahler, J.R., Walker, A., Arenberg, D. a., Reddy, R.C., Akulapalli, S., Thannickal, V.J., et al. (2006). Differential protein expression profiling by iTRAQ-2DLC-MS/MS of lung cancer cells undergoing epithelial-mesenchymal transition reveals a migratory/invasive phenotype. J. Proteome Res. *5*, 1143–1154.

Keshelava, N., Zuo, J.J., Chen, P., Waidyaratne, S.N., Luna, M.C., Gomer, C.J., Triche, T.J., and Reynolds, C.P. (2001). Loss of p53 Function Confers High-Level Multidrug Resistance in Neuroblastoma Cell Lines. Cancer Res. *61*, 6185–6193.

Kim, I.Y., Jung, J., Jang, M., Ahn, Y.G., Shin, J.H., Choi, J.W., Sohn, M.R., Shin, S.M., Kang, D.-G., Lee, H.-S., et al. (2010). 1H NMR-based metabolomic study on resistance to diet-induced obesity in AHNAK knock-out mice. Biochem. Biophys. Res. Commun. *403*, 428–434.

Kim, M., Jung, S., Ahn, J., Hwang, S., Woo, H., An, S., Nam, S., Lim, D.-S., and Song, J.-Y. (2015). Quantitative proteomic analysis of single or fractionated radiation-induced proteins in human breast cancer MDA-MB-231 cells. Cell Biosci. *5*, 2.

Kim, T.H., Shin, Y.J., Won, A.J., Lee, B.M., Choi, W.S., Jung, J.H., Chung, H.Y., and Kim, H.S. (2014). Resveratrol enhances chemosensitivity of doxorubicin in multidrug-resistant human breast cancer cells via increased cellular influx of doxorubicin. Biochim. Biophys. Acta BBA - Gen. Subj. *1840*, 615–625.

Kirov, A., Kacer, D., Conley, B.A., Vary, C.P.H., and Prudovsky, I. (2015). AHNAK2 Participates in the Stress-Induced Nonclassical FGF1 Secretion Pathway. J. Cell. Biochem. *116*, 1522–1531.

Klein, C.A. (2008). The Metastasis Cascade. Geochem. Geophys. Geosystems *9*, n/a-n/a.

Klein, C.A. (2009). Parallel progression of tumour and metastases. Nat. Rev. Cancer *9*, 302–312.

Kleinman, H.K., and Martin, G.R. (2005). Matrigel: Basement membrane matrix with biological activity. Semin. Cancer Biol. *15*, 378–386.

Kluza, J., Marchetti, P., Gallego, M.-A., Lancel, S., Fournier, C., Loyens, A., Beauvillain, J.-C., and Bailly, C. (2004). Mitochondrial proliferation during apoptosis induced by anticancer agents: effects of doxorubicin and mitoxantrone on cancer and cardiac cells. Oncogene *23*, 7018–7030.

Kokkinos, M.I., Wafai, R., Wong, M.K., Newgreen, D.F., Thompson, E.W., and Waltham, M. (2007). Vimentin and epithelial-mesenchymal transition in human breast cancer - Observations in vitro and in vivo. Cells Tissues Organs *185*, 191–203.

Komuro, A., Masuda, Y., Kobayashi, K., Babbitt, R., Gunel, M., Flavell, R.A., and Marchesi, V.T. (2004). The AHNAKs are a class of giant propeller-like proteins that associate with calcium channel proteins of cardiomyocytes and other cells. Proc. Natl. Acad. Sci. U. S. A. *101*, 4053–4058.

Kouno, M., Kondoh, G., Horie, K., Komazawa, N., Ishii, N., Takahashi, Y., Takeda, J., and Hashimoto, T. (2004). Ahnak/desmoyokin is dispensable for proliferation, differentiation, and maintenance of integrity in mouse epidermis. J. Invest. Dermatol. *123*, 700–707.

Kudoh, J., Wang, Y., Minoshima, S., Hashimoto, T., Amagai, M., Nishikawa, T., Shtivelman, E., Bishop, J.M., and Shimizu, N. (1995). Localization of the human AHNAK/desmoyokin gene (AHNAK) to chromosome band 11q12 by somatic cell hybrid analysis and fluorescence in situ hybridization. Cytogenet. Genome Res. *70*, 218–220.

Kuznetsov, A. V., Margreiter, R., Amberger, A., Saks, V., and Grimm, M. (2011). Changes in mitochondrial redox state, membrane potential and calcium precede mitochondrial dysfunction in doxorubicin-induced cell death. Biochim. Biophys. Acta - Mol. Cell Res. *1813*, 1144–1152.

Lader, A.S., Kwiatkowski, D.J., and Cantiello, H.F. (1999). Role of gelsolin in the actin filament regulation of cardiac L-type calcium channels. Am. J. Physiol. *277*, C1277–C1283.

Lam, V., McPherson, J.P., Salmena, L., Lees, J., Chu, W., Sexsmith, E., Hedley, D.W., Freedman, M.H., Reed, J.C., Malkin, D., et al. (1999). p53 gene status and chemosensitivity of childhood acute lymphoblastic leukemia cells to adriamycin. Leuk. Res. *23*, 871–880.

Lamouille, S., Xu, J., and Derynck, R. (2014). Molecular mechanisms of epithelial-mesenchymal transition. Nat. Rev. Mol. Cell Biol. *15*, 178–196.

Lang, S.H., Hyde, C., Reid, I.N., Hitchcock, I.S., Hart, C. a., Bryden, a. a G., Villette, J.M., Stower, M.J., and Maitland, N.J. (2002). Enhanced expression of vimentin in motile prostate cell lines and in poorly differentiated and metastatic prostate carcinoma. Prostate *52*, 253–263.

Lavin, M.F., and Kozlov, S. (2007). ATM Activation and DNA Damage Response. Cell Cycle *6*, 931–942.

Lee, E.-R., Kim, J.-Y., Kang, Y.-J., Ahn, J.-Y., Kim, J.-H., Kim, B.-W., Choi, H.-Y., Jeong, M.-Y., and Cho, S.-G. (2006). Interplay between PI3K/Akt and MAPK signaling pathways in DNA-damaging drug-induced apoptosis. Biochim. Biophys. Acta BBA - Mol. Cell Res. *1763*, 958–968.

Lee, E.S., Na, K., and Bae, Y.H. (2005). Doxorubicin loaded pH-sensitive polymeric micelles for reversal of resistant MCF-7 tumor. J. Controlled Release *103*, 405–418.

Lee, I.H., You, J.O., Ha, K.S., Bae, D.S., Suh, P.-G., Rhee, S.G., and Bae, Y.S. (2004). AHNAK-mediated activation of phospholipase C-gamma1 through protein kinase C. J. Biol. Chem. *279*, 26645–26653.

Lee, I.H., Lim, H.J., Yoon, S., Seong, J.K., Bae, D.S., Rhee, S.G., and Bae, Y.S. (2008). Ahnak protein activates protein kinase C (PKC) through dissociation of the PKC-protein phosphatase 2A complex. J. Biol. Chem. *283*, 6312–6320.

Lee, I.H., Sohn, M., Lim, H.J., Yoon, S., Oh, H., Shin, S., Shin, J.H., Oh, S.-H., Kim, J., Lee, D.K., et al. (2014). Ahnak functions as a tumor suppressor via modulation of TGFβ/Smad signaling pathway. Oncogene *33*, 4675–4684.

Lemjabbar-Alaoui, H., Hassan, O., Yang, Y., and Buchanan, P. (2015). Lung cancer: Biology and treatment options. Biochim. Biophys. Acta BBA - Rev. Cancer *1856*, 189–210.

Lennon, N.J., Kho, A., Bacskai, B.J., Perlmutter, S.L., Hyman, B.T., and Brown, R.H. (2003). Dysferlin Interacts with Annexins A1 and A2 and Mediates Sarcolemmal Wound-healing. J. Biol. Chem. *278*, 50466–50473.

Leong, S., Nunez, A.C., Lin, M.Z., Crossett, B., Christopherson, R.I., and Baxter, R.C. (2012). iTRAQ-Based Proteomic Profiling of Breast Cancer Cell Response to Doxorubicin and TRAIL. J. Proteome Res. *11*, 3561–3572.

Li, F., Wang, W., Gu, M., Gyoneva, S., Zhang, J., Huang, S., Traynelis, S.F., Cai, H., Guggino, S.E., and Zhang, X. (2011). L-type calcium channel activity in osteoblast cells is regulated by the actin cytoskeleton independent of protein trafficking. J. Bone Miner. Metab. *29*, 515–525.

Li, H., Lin, J., Wang, X., Yao, G., Wang, L., Zheng, H., Yang, C., Jia, C., and Liu A. (2012). Targeting of mTORC2 prevents cell migration and promotes apoptosis in breast cancer. Breast Cancer Res. Treat. *134*, 1057-1066.

Li, J., Liu, H., Yu, J., and Yu, H. (2015). Chemoresistance to doxorubicin induces epithelial-mesenchymal transition via upregulation of transforming growth factor Kβ signaling in HCT116 colon cancer cells. Mol. Med. Rep. 192–198.

Li, Q.-Q., Xu, J.-D., Wang, W.-J., Cao, X.-X., Chen, Q., Tang, F., Chen, Z.-Q., Liu, X.-P., and Xu, Z.-D. (2009a). Twist1-Mediated Adriamycin-Induced Epithelial-Mesenchymal Transition Relates to Multidrug Resistance and Invasive Potential in Breast Cancer Cells. Clin. Cancer Res. *15*, 2657–2665.

Li, X., Lu, Y., Liang, K., Liu, B., and Fan, Z. (2005). Differential responses to doxorubicin-induced phosphorylation and activation of Akt in human breast cancer cells. Breast Cancer Res. BCR *7*, R589-597.

Li, X., Ding, L., Xu, Y., Wang, Y., and Ping, Q. (2009b). Targeted delivery of doxorubicin using stealth liposomes modified with transferrin. Int. J. Pharm. *373*, 116–123.

Liang, J., and Slingerland, J.M. (2003). Multiple Roles of the PI3K/PKB (Akt) Pathway in Cell Cycle Progression. Cell Cycle *2*, 336–342.

Lim, H.J., Kang, D.M.H., Lim, J.M., Kang, D.M.H., Seong, J.K., Kang, S.W., and Bae, Y.S. (2013). Function of Ahnak protein in aortic smooth muscle cell migration through Rac activation. Cardiovasc. Res. *97*, 302–310.

Lim, H.J., Kim, J., Park, C.-H., Lee, S.A., Lee, M.R., Kim, K.-S., Kim, J., and Bae, Y.S. (2015). Regulation of c-Myc expression by Ahnak promotes iPSC generation. J. Biol. Chem. *291*, jbc.M115.659276.

Liu, Q.-Y., and Tan, B.K. (2003). Relationship between anti-oxidant activities and doxorubicin-induced lipid peroxidation in P388 tumour cells and heart and liver in mice. Clin. Exp. Pharmacol. Physiol. *30*, 185–188.

Lopes-Ramos, C., Koyama, F.C., Habr-Gama, A., Salim, A.C.M., Bettoni, F., Asprino, P.F., França, G.S., Gama-Rodrigues, J., Parmigiani, R.B., Perez, R.O., et al. (2015). Comprehensive evaluation of the effectiveness of gene expression signatures to predict complete response to neoadjuvant chemoradiotherapy and guide surgical intervention in rectal cancer. Cancer Genet. *208*.

López-Avilés, S., Grande, M., González, M., Helgesen, A.-L., Alemany, V., Sanchez-Piris, M., Bachs, O., Millar, J.B.A., and Aligue, R. (2005). Inactivation of the Cdc25 Phosphatase by the Stress-Activated Srk1 Kinase in Fission Yeast. Mol. Cell *17*, 49–59.

Lorusso, A., Covino, C., Priori, G., Bachi, A., Meldolesi, J., and Chieregatti, E. (2006). Annexin2 coating the surface of enlargeosomes is needed for their regulated exocytosis. EMBO J. *25*, 5443–5456.

Lowery, A., Onishko, H., Hallahan, D.E., and Han, Z. (2011). Tumor-targeted delivery of liposome-encapsulated doxorubicin by use of a peptide that selectively binds to irradiated tumors. J. Controlled Release *150*, 117–124.

Lu, J., Wu, Y., Sousa, N., and Almeida, O.F.X. (2005). SMAD pathway mediation of BDNF and TGF beta 2 regulation of proliferation and differentiation of hippocampal granule neurons. Dev. Camb. Engl. *132*, 3231–3242.

Lugassy, C., Lazar, V., Dessen, P., van den Oord, J.J., Winnepenninckx, V., Spatz, A., Bagot, M., Bensussan, A., Janin, A., Eggermont, A.M., et al. (2011). Gene expression profiling of human angiotropic primary melanoma: Selection of 15 differentially expressed genes potentially involved in extravascular migratory metastasis. Eur. J. Cancer *47*, 1267–1275.

Lundholm, L., Hååg, P., Zong, D., Juntti, T., Mörk, B., Lewensohn, R., and Viktorsson, K. (2013). Resistance to DNA-damaging treatment in non-small cell lung cancer tumor-initiating cells involves reduced DNA-PK/ATM activation and diminished cell cycle arrest. Cell Death Dis. *4*, e478.

Maddika, S., Ande, S.R., Wiechec, E., Hansen, L.L., Wesselborg, S., and Los, M. (2008). Akt-mediated phosphorylation of CDK2 regulates its dual role in cell cycle progression and apoptosis. J. Cell Sci. *121*, 979–988.

Marklund, S.L., Westman, N.G., Lundgren, E., Dismutase, S., Peroxidase, G., and Roos, G. (1982). Manganese-containing Superoxide Dismutase, Catalase, and Glutathione Peroxidase in Normal and Neoplastic Human Cell Lines and Normal Human Tissues Copper- and Zinc-containing. Am. Assoc. Cancer Res. *42*, 1955–1961.

Masunaga, T., Shimizu, H., Ishiko, A., Fujiwara, T., Hashimoto, T., and Nishikawa, T. (1995). Desmoyokin/AHNAK protein localizes to the non-desmosomal keratinocyte cell surface of human epidermis. J. Invest. Dermatol. *104*, 941–945.

Matza, D., and Flavell, R. a. (2009). Roles of Cav channels and AHNAK1 in T cells: The beauty and the beast. Immunol. Rev. *231*, 257–264.

Matza, D., Badou, A., Kobayashi, K.S., Goldsmith-Pestana, K., Masuda, Y., Komuro, A., McMahon-Pratt, D., Marchesi, V.T., and Flavell, R. a. (2008). A Scaffold Protein, AHNAK1, Is Required for Calcium Signaling during T Cell Activation. Immunity *28*, 64–74.

Matza, D., Badou, A., Jha, M.K., Willinger, T., Antov, A., Sanjabi, S., Kobayashi, K.S., Marchesi, V.T., and Flavell, R. a (2009). Requirement for AHNAK1-mediated calcium signaling during T lymphocyte cytolysis. Proc. Natl. Acad. Sci. U. S. A. *106*, 9785–9790.

McDade, J.R., and Michele, D.E. (2014). Membrane damage-induced vesicle-vesicle fusion of dysferlin-containing vesicles in muscle cells requires microtubules and kinesin. Hum. Mol. Genet. *23*, 1677–1686.

Mechetner, E., Kyshtoobayeva, A., Zonis, S., Kim, H., Stroup, R., Garcia, R., Parker, R., and Fruehauf, J. (1998). Levels of Multidrug Resistance (MDR1) P-glycoprotein Expression by Human Breast Cancer Correlate with in Vitro Resistance to Taxol and Doxorubicin. Clin. Cancer Res. *4*, 389–398.

Mendez, M.G., Kojima, S.I., and Goldman, R.D. (2010). Vimentin induces changes in cell shape, motility, and adhesion during the epithelial to mesenchymal transition. FASEB J. *24*, 1838–1851.

Merrifield, C.J., Rescher, U., Almers, W., Proust, J., Gerke, V., Sechi, A.S., and Moss, S.E. (2001). Annexin 2 has an essential role in actin-based macropinocytic rocketing. Curr. Biol. *11*, 1136–1141.

Micalizzi, D.S., Farabaugh, S.M., and Ford, H.L. (2010). Epithelial-Mesenchymal Transition in Cancer: Parallels Between Normal Development and Tumor Progression. J. Mammary Gland Biol. Neoplasia *15*, 117–134.

Miettinen, P.J., Ebner, R., Lopez, A.R., and Derynck, R. (1994). TGF-beta induced transdifferentiation of mammary epithelial cells to mesenchymal cells: involvement of type I receptors. J. Cell Biol. *127*, 2021–2036.

Miyake, K., McNeil, P.L., Suzuki, K., Tsunoda, R., and Sugai, N. (2001). An actin barrier to resealing. J. Cell Sci. *114*, 3487–3494.

Mochly-Rosen, D., Khaner, H., and Lopez, J. (1991). Identification of intracellular receptor proteins for activated protein kinase C. Proc. Natl. Acad. Sci. U. S. A. *88*, 3997–4000.

Mok, C.C., and Lau, C.S. (2003). Pathogenesis of systemic lupus erythematosus. J. Clin. Pathol. *56*, 481–490.

Monteiro, J., and Fodde, R. (2010). Cancer stemness and metastasis: Therapeutic consequences and perspectives. Eur. J. Cancer *46*, 1198–1203.

Morel, E., Parton, R.G., and Gruenberg, J. (2009). Annexin A2-Dependent Polymerization of Actin Mediates Endosome Biogenesis. Dev. Cell *16*, 445–457.

de Morrée, A., Hensbergen, P.J., van Haagen, H.H.H.B.M., Dragan, I., Deelder, A.M., 't Hoen, P.A.C., Frants, R.R., and van der Maarel, S.M. (2010). Proteomic analysis of the dysferlin protein complex unveils its importance for sarcolemmal maintenance and integrity. PloS One *5*, e13854.

de Morrée, A., Droog, M., Grand Moursel, L., Bisschop, I.J.M., Impagliazzo, A., Frants, R.R., Klooster, R., and van der Maarel, S.M. (2012). Self-regulated alternative splicing at the AHNAK locus. FASEB J. Off. Publ. Fed. Am. Soc. Exp. Biol. *26*, 93–103.

Mukhopadhyay, P., Rajesh, M., Bátkai, S., Kashiwaya, Y., Haskó, G., Liaudet, L., Szabó, C., and Pacher, P. (2009). Role of superoxide, nitric oxide, and peroxynitrite in doxorubicin-induced cell death in vivo and in vitro. Am. J. Physiol. Heart Circ. Physiol. *296*, H1466–H1483.

Müller, I., Jenner, A., Bruchelt, G., Niethammer, D., and Halliwell, B. (1997). Effect of concentration on the cytotoxic mechanism of doxorubicin--apoptosis and oxidative DNA damage. Biochem. Biophys. Res. Commun. *230*, 254–257.

Mussi, S.V., Sawant, R., Perche, F., Oliveira, M.C., Azevedo, R.B., Ferreira, L.A.M., and Torchilin, V.P. (2014). Novel Nanostructured Lipid Carrier Co-Loaded with Doxorubicin and Docosahexaenoic Acid Demonstrates Enhanced in Vitro Activity and Overcomes Drug Resistance in MCF-7/Adr Cells. Pharm. Res. *31*, 1882–1892.

Nagaraja, G.M., Othman, M., Fox, B.P., Alsaber, R., Pellegrino, C.M., Zeng, Y., Khanna, R., Tamburini, P., Swaroop, A., and Kandpal, R.P. (2005). Gene expression signatures and biomarkers of noninvasive and invasive breast cancer cells: comprehensive profiles by representational difference analysis, microarrays and proteomics. Oncogene *25*, 2328–2338.

Nakamura, M., Sunagawa, M., Kosugi, T., and Sperelakis, N. (2000). Actin filament disruption inhibits L-type Ca(2+) channel current in cultured vascular smooth muscle cells. Am. J. Physiol. Cell Physiol. *279*, C480-7.

Neve, R.M., Chin, K., Fridlyand, J., Yeh, J., Baehner, F.L., Fevr, T., Clark, L., Bayani, N., Coppe, J.-P., Tong, F., et al. (2006). A collection of breast cancer cell lines for the study of functionally distinct cancer subtypes. Cancer Cell *10*, 515–527.

Newton, A.C. (2010). Protein kinase C: poised to signal. Am. J. Physiol. Endocrinol. Metab. *298*, E395–E402.

Nie, Z., Ning, W., Amagai, M., and Hashimoto, T. (2000). C-terminus of desmoyokin/AHNAK protein is responsible for its translocation between the nucleus and cytoplasm. J. Invest. Dermatol. *114*, 1044–1049.

Nishimune, H., Sanes, J.R., and Carlson, S.S. (2004). A synaptic laminin-calcium channel interaction organizes active zones in motor nerve terminals. Nature *432*, 580–587.

Nitiss, J.L. (2009). Targeting DNA topoisomerase II in cancer chemotherapy. Nat. Rev. Cancer *9*, 338–350.

Noël, A., De Pauw-Gillet, M.C., Purnell, G., Nusgens, B., Lapiere, C.M., and Foidart, J.M. (1993). Enhancement of tumorigenicity of human breast adenocarcinoma cells in nude mice by matrigel and fibroblasts. Br. J. Cancer *68*, 909–915.

Nourry, C., Grant, S.G.N., and Borg, J. (2003). PDZ domain proteins: plug and play! Sci. STKE Signal Transduct. Knowl. Environ. *2003*, RE7.

Octavia, Y., Tocchetti, C.G., Gabrielson, K.L., Janssens, S., Crijns, H.J., and Moens, A.L. (2012). Doxorubicin-induced cardiomyopathy: From molecular mechanisms to therapeutic strategies. J. Mol. Cell. Cardiol. *52*, 1213–1225.

Oken, M.M., Creech, R.H., Tormey, D.C., Horton, J., Davis, T.E., McFadden, E.T., and Carbone, P. (1982). Toxicity and response criteria of the Eastern Cooperative Oncology Group. Am. J. Clin. Oncol. *5*, 649–656.

Ola, M.S., Nawaz, M., and Ahsan, H. (2011). Role of Bcl-2 family proteins and caspases in the regulation of apoptosis. Mol. Cell. Biochem. *351*, 41–58.

Olmeda, D., Jordá, M., Peinado, H., Fabra, A., and Cano, A. (2007). Snail silencing effectively suppresses tumour growth and invasiveness. Oncogene *26*, 1862–1874.

Pajic, M., Iyer, J.K., Kersbergen, A., van der Burg, E., Nygren, A.O.H., Jonkers, J., Borst, P., and Rottenberg, S. (2009). Moderate increase in Mdr1a/1b expression causes in vivo resistance to doxorubicin in a mouse model for hereditary breast cancer. Cancer Res. *69*, 6396–6404.

Pal, M., Moffa, A., Sreekumar, A., Ethier, S.P., Barder, T.J., Chinnaiyan, A., and Lubman, D.M. (2006). Differential phosphoprotein mapping in cancer cells using protein microarrays produced from 2-D liquid fractionation. Anal. Chem. *78*, 702–710.

Palchaudhuri, R., and Hergenrother, P.J. (2007). DNA as a target for anticancer compounds: methods to determine the mode of binding and the mechanism of action. Curr. Opin. Biotechnol. *18*, 497–503.

Parisis, N., Metodieva, G., and Metodiev, M. V (2013). Pseudopodial and β-arrestin-interacting proteomes from migrating breast cancer cells upon PAR2 activation. J. Proteomics *80C*, 91–106.

Peinado, H., Olmeda, D., and Cano, A. (2007). Snail, Zeb and bHLH factors in tumour progression: an alliance against the epithelial phenotype? Nat. Rev. Cancer *7*, 415–428.

Pickup, M.W., Mouw, J.K., and Weaver, V.M. (2014). The extracellular matrix modulates the hallmarks of cancer. EMBO Rep. *15*, 1243–1253.

Piskareva, O., Harvey, H., Nolan, J., Conlon, R., Alcock, L., Buckley, P., Dowling, P., O'Sullivan, F., Bray, I., and Stallings, R.L. (2015). The development of cisplatin resistance in neuroblastoma is accompanied by epithelial to mesenchymal transition in vitro. Cancer Lett. *364*, 142–155.

Polyak, K., and Weinberg, R.A. (2009). Transitions between epithelial and mesenchymal states: acquisition of malignant and stem cell traits. Nat. Rev. Cancer *9*, 265–273.

Prada, I., Cocucci, E., Racchetti, G., and Meldolesi, J. (2007). The Ca2+-dependent exocytosis of enlargeosomes is greatly reinforced by genistein via a non-tyrosine kinase-dependent mechanism. FEBS Lett. *581*, 4932–4936.

Prevarskaya, N., Skryma, R., and Shuba, Y. (2011). Calcium in tumour metastasis: new roles for known actors. Nat. Rev. Cancer *11*, 609–618.

Racchetti, G., Lorusso, A., Schulte, C., Gavello, D., Carabelli, V., D'Alessandro, R., and Meldolesi, J. (2010). Rapid neurite outgrowth in neurosecretory cells and neurons is sustained by the exocytosis of a cytoplasmic organelle, the enlargeosome. J. Cell Sci. *123*, 165–170.

Racchetti, G., D'Alessandro, R., and Meldolesi, J. (2012). Astrocyte stellation, a process dependent on Rac1 is sustained by the regulated exocytosis of enlargeosomes. Glia *60*, 465–475.

Rantanen, V., Engblom, P., Raitanen, M., Hietanen, S., Haarala, M., Grénman, S., and Syrjänen, S. (2002). Mutations of TP53 do not correlate with the sensitivity to paclitaxel—a study using 27 gynaecological cancer cell lines. Eur. J. Cancer *38*, 1783–1791.

Rebbaa, A., Zheng, X., Chou, P.M., and Mirkin, B.L. (2003). Caspase inhibition switches doxorubicin-induced apoptosis to senescence. Oncogene *22*, 2805–2811.

Reinhardt, H.C., and Yaffe, M.B. (2009). Kinases that control the cell cycle in response to DNA damage: Chk1, Chk2, and MK2. Curr. Opin. Cell Biol. *21*, 245–255.

Reinhardt, H.C., Aslanian, A.S., Lees, J.A., and Yaffe, M.B. (2007). p53-Deficient Cells Rely on ATM- and ATR-Mediated Checkpoint Signaling through the p38MAPK/MK2 Pathway for Survival after DNA Damage. Cancer Cell *11*, 175–189.

Rescher, U., and Gerke, V. (2008). S100A10/p11: Family, friends and functions. Pflugers Arch. *455*, 575–582.

Rezvanpour, A., Santamaria-Kisiel, L., and Shaw, G.S. (2011). The S100A10-annexin A2 complex provides a novel asymmetric platform for membrane repair. J. Biol. Chem. *286*, 40174–40183.

Ritter, C.A., Perez-Torres, M., Rinehart, C., Guix, M., Dugger, T., Engelman, J.A., and Arteaga, C.L. (2007). Human Breast Cancer Cells Selected for Resistance to Trastuzumab In vivo Overexpress Epidermal Growth Factor Receptor and ErbB Ligands and Remain Dependent on the ErbB Receptor Network. Clin. Cancer Res. *13*, 4909–4919.

Rogalska, A., Gajek, A., Szwed, M., Jóźwiak, Z., and Marczak, A. (2011). The role of reactive oxygen species in WP 631-induced death of human ovarian cancer cells: a comparison with the effect of doxorubicin. Toxicol. In Vitro *25*, 1712–1720.

Ron, D., and Mochly-Rosen, D. (1995). An autoregulatory region in protein kinase C: the pseudoanchoring site. Proc. Natl. Acad. Sci. U. S. A. *92*, 492–496.

Roninson, I.B., Broude, E.V., and Chang, B.-D. (2001). If not apoptosis, then what? Treatment-induced senescence and mitotic catastrophe in tumor cells. Drug Resist. Updat. *4*, 303–313.

Rosenkranz, K.M., Bedrosian, I., Feng, L., Hunt, K.K., Hartman, K., Lucci, A., Meric-Bernstam, F., Kuerer, H.M., Singletary, E.S., Hwang, R., et al. (2006). Breast cancer in the very elderly: treatment patterns and complications in a tertiary cancer center. Am. J. Surg. *192*, 541–544.

Ruth, A.C., and Roninson, I.B. (2000). Effects of the Multidrug Transporter P-Glycoprotein on Cellular Responses to Ionizing Radiation. Cancer Res. *60*, 2576–2578.

Salim, C., Boxberg, Y. V, Alterio, J., Féréol, S., and Nothias, F. (2009). The giant protein AHNAK involved in morphogenesis and laminin substrate adhesion of myelinating Schwann cells. Glia *57*, 535–549.

Sánchez, C., Mendoza, P., Contreras, H.R., Vergara, J., McCubrey, J.A., Huidobro, C., and Castellón, E.A. (2009). Expression of multidrug resistance proteins in prostate cancer is related with cell sensitivity to chemotherapeutic drugs. The Prostate *69*, 1448–1459.

Sánchez-Tilló, E., Liu, Y., de Barrios, O., Siles, L., Fanlo, L., Cuatrecasas, M., Darling, D.S., Dean, D.C., Castells, A., and Postigo, A. (2012). EMT-activating transcription factors in cancer: beyond EMT and tumor invasiveness. Cell. Mol. Life Sci. *69*, 3429–3456.

Savagner, P. (2001). Leaving the neighborhood: Molecular mechanisms involved during epithelial-mesenchymal transition. BioEssays *23*, 912–923.

Sayeed, S., Asano, E., Ito, S., Ohno, K., Hamaguchi, M., and Senga, T. (2013). S100A10 is required for the organization of actin stress fibers and promotion of cell spreading. MolCell Biochem *374*, 105–111.

Schwarz, J.K., Lovly, C.M., and Piwnica-Worms, H. (2003). Regulation of the Chk2 Protein Kinase by Oligomerization-Mediated cis- and trans-Phosphorylation1. Am. Assoc. Cancer Res. *1*, 598–609.

Seidman, C., Struhl, K., Sheen, J., and Jessen, Y. (1997). Escherichia coli, Plasmids, and Bacteriophages. In Current Protocols in Molecular Biology, F. Ausubel, R. Brent, R. Kingston, D. Moore, J. Siedman, J. Smith, and K. Struhl, eds. (John Wiley & Sons, Inc.), p. 1.8.0-1.8.10.

Sekiya, F., Bae, Y.S., Jhon, D.Y., Hwang, S.C., and Rhee, S.G. (1999). AHNAK, a protein that binds and activates phospholipase C-gamma1 in the presence of arachidonic acid. J. Biol. Chem. *274*, 13900–13907.

Senkus, E., Kyriakides, S., Penault-Llorca, F., Poortmans, P., Thompson, A., Zackrisson, S., and Cardoso, F. (2013). Primary breast cancer: ESMO Clinical Practice Guidelines for diagnosis, treatment and follow-up. Ann. Oncol.

Seol, D.-W. (2008). Up-regulation of IAPs by PI-3K: A cell survival signal-mediated anti-apoptotic mechanism. Biochem. Biophys. Res. Commun. *377*, 508–511.

Shankar, J., Messenberg, A., Chan, J., Underhill, T.M., Foster, L.J., and Nabi, I.R. (2010). Pseudopodial Actin Dynamics Control Epithelial-Mesenchymal Transition in Metastatic Cancer Cells. Cancer Res. *70*, 3780–3790.

Shao, Y., Czymmek, K.J., Jones, P. a, Fomin, V.P., Akanbi, K., Duncan, R.L., and Farach-Carson, M.C. (2009). Dynamic interactions between L-type voltage-sensitive calcium channel Cav1.2 subunits and ahnak in osteoblastic cells. Am. J. Physiol. Cell Physiol. *296*, C1067–C1078.

Shapiro, G.I., and Harper, J.W. (1999). Anticancer drug targets: cell cycle and checkpoint control. J. Clin. Invest. *104*, 1645–1653.

Sheppard, H.M., Feisst, V., Chen, J., Print, C., and Dunbar, P.R. (2015). AHNAK is downregulated in melanoma, predicts poor outcome, and may be required for the expression of functional cadherin-1. Melanoma Res. *0*, 1.

Shin, J.H., Kim, I.Y., Kim, Y.N., Shin, S.M., Roh, K.J., Lee, S.H., Sohn, M., Cho, S.Y., Lee, S.H., Ko, C.-Y., et al. (2015a). Obesity Resistance and Enhanced Insulin Sensitivity in Ahnak-/- Mice Fed a High Fat Diet Are Related to Impaired Adipogenesis and Increased Energy Expenditure. Plos One *10*, e0139720.

Shin, J.H., Kim, Y.N., Kim, I.Y., Choi, D.-H., Yi, S.S., and Seong, J.K. (2015b). Increased Cell Proliferations and Neurogenesis in the Hippocampal Dentate Gyrus of Ahnak Deficient Mice. Neurochem. Res. *40*, 1457–1462.

Shin, S., Seong, J.K., and Bae, Y.S. (2016). Ahnak stimulates BMP2-mediated adipocyte differentiation through Smad1 activation. Obesity *0*, n/a-n/a.

Shtivelman, E., Cohen, F.E., and Bishop, J.M. (1992). A human gene (AHNAK) encoding an unusually large protein with a 1.2-microns polyionic rod structure. Proc. Natl. Acad. Sci. U. S. A. *89*, 5472–5476.

Shukla, A., Hillegass, J.M., MacPherson, M.B., Beuschel, S.L., Vacek, P.M., Pass, H.I., Carbone, M., Testa, J.R., and Mossman, B.T. (2010). Blocking of ERK1 and ERK2 sensitizes human mesothelioma cells to doxorubicin. Mol. Cancer *9*, 314.

Silva, T.A., Smuczek, B., Valadão, I.C., Dzik, L.M., Iglesia, R.P., Cruz, M.C., Zelanis, A., de Siqueira, A.S., Serrano, S.M.T., Goldberg, G.S., et al. (2016). AHNAK enables mammary carcinoma cells to produce extracellular vesicles that increase neighboring fibroblast cell motility. Oncotarget.

Sinha, B.K., Mimnaugh, E.G., Rajagopalan, S., and Myers, C.E. (1989). Adriamycin activation and oxygen free radical formation in human breast tumor cells: Protective role of glutathione peroxidase in adriamycin resistance. Cancer Res. *49*, 3844–3848.

Sishi, B.J.N., Loos, B., van Rooyen, J., and Engelbrecht, A.-M. (2013). Autophagy upregulation promotes survival and attenuates doxorubicin-induced cardiotoxicity. Biochem. Pharmacol. *85*, 124–134.

Sköldberg, F., Rönnblom, L., Thornemo, M., Lindahl, A., Bird, P.I., Rorsman, F., Kämpe, O., and Landgren, E. (2002). Identification of AHNAK as a novel autoantigen in systemic lupus erythematosus. Biochem. Biophys. Res. Commun. *291*, 951–958.

Sleeman, J., and Steeg, P.S. (2010). Cancer metastasis as a therapeutic target. Eur. J. Cancer *46*, 1177–1180.

Sos, M.L., Koker, M., Weir, B.A., Heynck, S., Rabinovsky, R., Zander, T., Seeger, J.M., Weiss, J., Fischer, F., Frommolt, P., et al. (2009). PTEN Loss Contributes to Erlotinib Resistance in EGFR-Mutant Lung Cancer by Activation of Akt and EGFR. Cancer Res. *69*, 3256–3261.

Spano, D., Heck, C., De Antonellis, P., Christofori, G., and Zollo, M. (2012). Molecular networks that regulate cancer metastasis. Semin. Cancer Biol. *22*, 234–249.

Steeg, P.S. (2006). Tumor metastasis: mechanistic insights and clinical challenges. Nat Med *12*, 895–904.

Steelman, L.S., Navolanic, P.M., Sokolosky, M.L., Taylor, J.R., Lehmann, B.D., Chappell, W.H., Abrams, S.L., Wong, E.W.T., Stadelman, K.M., Terrian, D.M., et al. (2008). Suppression of PTEN function increases breast cancer chemotherapeutic drug resistance while conferring sensitivity to mTOR inhibitors. Oncogene *27*, 4086–4095.

Stiff, T., Shtivelman, E., Jeggo, P., and Kysela, B. (2004). AHNAK interacts with the DNA ligase IV-XRCC4 complex and stimulates DNA ligase IV-mediated double-stranded ligation. DNA Repair *3*, 245–256.

Stronach, E.A., Chen, M., Maginn, E.N., Agarwal, R., Mills, G.B., Wasan, H., and Gabra, H. (2011). DNA-PK Mediates AKT Activation and Apoptosis Inhibition in Clinically Acquired Platinum Resistance. Neoplasia *13*, 1069–IN35.

Sudo, H., Tsuji, A.B., Sugyo, A., Abe, M., Hino, O., and Saga, T. (2014). AHNAK is highly expressed and plays a key role in cell migration and invasion in mesothelioma. Int. J. Oncol. *44*, 530–538.

Sussman, J., Stokoe, D., Ossina, N., and Shtivelman, E. (2001). Protein kinase B phosphorylates AHNAK and regulates its subcellular localization. J. Cell Biol. *154*, 1019–1030.

Svensson, S., Nilsson, K., Ringberg, A., and Landberg, G. (2003). Invade or Proliferate? Two Contrasting Events in Malignant Behavior Governed by p16INK4a and an Intact Rb Pathway Illustrated by a Model System of Basal Cell Carcinoma. Cancer Res. *63*, 1737–1742.

Swift, L.P., Rephaeli, A., Nudelman, A., Phillips, D.R., and Cutts, S.M. (2006). Doxorubicin-DNA Adducts Induce a Non-Topoisomerase II − Mediated Form of Cell Death Doxorubicin-DNA Adducts Induce a Non-Topoisomerase II – Mediated. *9*, 4863–4871.

Syljuasen, R.G., Jensen, S., Bartek, J., and Lukas, J. (2006). Adaptation to the Ionizing Radiation-Induced G2 Checkpoint Occurs in Human Cells and Depends on Checkpoint Kinase 1 and Polo-like Kinase 1 Kinases. Cancer Res. *66*, 10253–10257.

Szakács, G., Paterson, J.K., Ludwig, J. a, Booth-Genthe, C., and Gottesman, M.M. (2006). Targeting multidrug resistance in cancer. Nat. Rev. *5*, 219–234.

Tacar, O., Sriamornsak, P., and Dass, C.R. (2013). Doxorubicin: an update on anticancer molecular action, toxicity and novel drug delivery systems: Doxorubicin cell and molecular biological activity. J. Pharm. Pharmacol. *65*, 157–170.

Takemura, H., Rao, V.A., Sordet, O., Furuta, T., Miao, Z.-H., Meng, L., Zhang, H., and Pommier, Y. (2006). Defective Mre11-dependent Activation of Chk2 by Ataxia Telangiectasia Mutated in Colorectal Carcinoma Cells in Response to Replication-dependent DNA Double Strand Breaks. J. Biol. Chem. *281*, 30814–30823.

Tamura, S., Shiozaki, H., Miyata, M., Kadowaki, T., Inoue, M., Matsui, S., Iwazawa, T., Takayama, T., Takeichi, M., and Monden, M. (1996). Decreased E-cadherin expression is associated with haematogenous recurrence and poor prognosis in patients with squamous cell carcinoma of the oesophagus. Br J Surg *83*, 1608–1614.

Tanaka, M., and Grossman, H.B. (2003). In vivo gene therapy of human bladder cancer with PTEN suppresses tumor growth, downregulates phosphorylated Akt, and increases sensitivity to doxorubicin. Gene Ther. *10*, 1636–1642.

Tanida, S., Mizoshita, T., Ozeki, K., Tsukamoto, H., Kamiya, T., Kataoka, H., Sakamuro, D., and Joh, T. (2012). Mechanisms of Cisplatin-Induced Apoptosis and of Cisplatin Sensitivity: Potential of BIN1 to Act as a Potent Predictor of Cisplatin Sensitivity in Gastric Cancer Treatment. Int. J. Surg. Oncol. *2012*, 1–8.

Thiery, J.P., and Sleeman, J.P. (2006). Complex networks orchestrate epithelial–mesenchymal transitions. Nat. Rev. Mol. Cell Biol. *7*, 131–142.

Thomson, S., Petti, F., Sujka-Kwok, I., Mercado, P., Bean, J., Monaghan, M., Seymour, S.L., Argast, G.M., Epstein, D.M., and Haley, J.D. (2011). A systems view of epithelial–mesenchymal transition signaling states. Clin. Exp. Metastasis *28*, 137–155.

Thorn, C.F., Oshiro, C., Marsh, S., Hernandez-Boussard, T., McLeod, H., Klein, T.E., and Altman, R.B. (2011). Doxorubicin pathways. Pharmacogenet. Genomics *21*, 440–446.

Tsang, W.P., Chau, S.P.Y., Kong, S.K., Fung, K.P., and Kwok, T.T. (2003). Reactive oxygen species mediate doxorubicin induced p53-independent apoptosis. Life Sci. *73*, 2047–2058.

Ubezio, P., and Civoli, F. (1994). Flow cytometric detection of hydrogen peroxide production induced by doxorubicin in cancer cells. Free Radic. Biol. Med. *16*, 509–516.

Valastyan, S., and Weinberg, R. a. (2011). Tumor metastasis: Molecular insights and evolving paradigms. Cell *147*, 275–292.

Van der Veldt, A.A.M., Lubberink, M., Bahce, I., Walraven, M., de Boer, M.P., Greuter, H.N.J.M., Hendrikse, N.H., Eriksson, J., Windhorst, A.D., Postmus, P.E., et al. (2012). Rapid Decrease in Delivery of Chemotherapy to Tumors after Anti-VEGF Therapy: Implications for Scheduling of Anti-Angiogenic Drugs. Cancer Cell *21*, 82–91.

Vandewalle, C., Comijn, J., De Craene, B., Vermassen, P., Bruyneel, E., Andersen, H., Tulchinsky, E., Van Roy, F., and Berx, G. (2005). SIP1/ZEB2 induces EMT by repressing genes of different epithelial cell-cell junctions. Nucleic Acids Res. *33*, 6566–6578.

Vega, S., Morales, A.V., Ocaña, O.H., Valdés, F., Fabregat, I., and Nieto, M.A. (2004). Snail blocks the cell cycle and confers resistance to cell death. Genes Dev. *18*, 1131–1143.

Wallace, G.Q., and McNally, E.M. (2009). Mechanisms of muscle degeneration, regeneration, and repair in the muscular dystrophies. Annu. Rev. Physiol. *71*, 37–57.

Wang, F., Hansen, R.K., Radisky, D., Yoneda, T., Barcellos-Hoff, M.H., Petersen, O.W., Turley, E.A., and Bissell, M.J. (2002). Phenotypic Reversion or Death of Cancer Cells by Altering Signaling Pathways in Three-Dimensional Contexts. J. Natl. Cancer Inst. *94*, 1494–1503.

Wang, S., Konorev, E.A., Kotamraju, S., Joseph, J., Kalivendi, S., and Kalyanaraman, B. (2004). Doxorubicin Induces Apoptosis in Normal and Tumor Cells via. Biochemistry (Mosc.) *279*, 25535–25543.

Weaver, V.M., Lelièvre, S., Lakins, J.N., Chrenek, M.A., Jones, J.C.R., Giancotti, F., Werb, Z., and Bissell, M.J. (2002). β4 integrin-dependent formation of polarized three-dimensional architecture confers resistance to apoptosis in normal and malignant mammary epithelium. Cancer Cell *2*, 205–216.

Weller, P., Bankfalvi, A., Gu, X., Dominas, N., Lehnerdt, G.F., Zeidler, R., Lang, S., Brandau, S., and Dumitru, C. a (2014). The role of tumour FoxP3 as prognostic marker in different subtypes of head and neck cancer. Eur. J. Cancer Oxf. Engl. 1990 *50*, 1291–1300.

White, N.M. a, Masui, O., Desouza, L. V, Krakovska, O., Metias, S., Romaschin, A.D., Honey, R.J., Stewart, R., Pace, K., Lee, J., et al. (2014). Quantitative proteomic analysis reveals potential diagnostic markers and pathways involved in pathogenesis of renal cell carcinoma. Oncotarget *5*, 506–518.

Willipinski-Stapelfeldt, B., Riethdorf, S., Assmann, V., Woelfle, U., Rau, T., Sauter, G., Heukeshoven, J., and Pantel, K. (2005). Changes in Cytoskeletal Protein Composition Indicative of an Epithelial-Mesenchymal Transition in Human Micrometastatic and Primary Breast Carcinoma Cells. Clin. Cancer Res. *11*, 8006–8014.

Winck, F. V., Belloni, M., Pauletti, B. a., Zanella, J.D.L., Domingues, R.R., Sherman, N.E., and Paes Leme, A.F. (2014). Phosphoproteome analysis reveals differences in phosphosite profiles between tumorigenic and non-tumorigenic epithelial cells. J. Proteomics *96*, 67–81.

World Health Organization (2014). WHO | The top 10 causes of death. http://www.who.int/mediacentre/factsheets/fs310/en/. Acessed: 06/09/2016.

Xiao, Z., Chen, Z., Gunasekera, A.H., Sowin, T.J., Rosenberg, S.H., Fesik, S., and Zhang, H. (2003). Chk1 Mediates S and G2 Arrests through Cdc25A Degradation in Response to DNA-damaging Agents. J. Biol. Chem. *278*, 21767–21773.

Xu, X., Hou, Y., Yin, X., Bao, L., Tang, A., Song, L., Li, F., Tsang, S., Wu, K., Wu, H., et al. (2012). Single-Cell Exome Sequencing Reveals Single-Nucleotide Mutation Characteristics of a Kidney Tumor. Cell *148*, 886–895.

Yamada, A., Irie, K., Hirota, T., Ooshio, T., Fukuhara, A., and Takai, Y. (2005). Involvement of the annexin II-S100A10 complex in the formation of E-cadherin-based adherens junctions in madin-darby canine kidney cells. J. Biol. Chem. *280*, 6016–6027.

Yamazaki, D., Kurisu, S., and Takenawa, T. (2005). Regulation of cancer cell motility through actin reorganization. Cancer Sci. *96*, 379–386.

Yang, Z., and Klionsky, D.J. (2010). Mammalian autophagy: core molecular machinery and signaling regulation. Curr. Opin. Cell Biol. *22*, 124–131.

Yang, J., Mani, S. a, Donaher, J.L., Ramaswamy, S., Itzykson, R. a, Come, C., Savagner, P., Gitelman, I., Richardson, A., and Weinberg, R.A. (2004). Twist, a Master Regulator of Morphogenesis, Plays an Essential Role in Tumor Metastasis. Cell *117*, 927–939.

Yang, S., Zhou, Q., and Yang, X. (2007). Caspase-3 status is a determinant of the differential responses to genistein between MDA-MB-231 and MCF-7 breast cancer cells. Biochim. Biophys. Acta BBA - Mol. Cell Res. *1773*, 903–911.

Yao, J., Ong, S.-E., and Bajjalieh, S. (2014). Huntingtin is associated with cytomatrix proteins at the presynaptic terminal. Mol. Cell. Neurosci. *63*, 96–100.

Yeh, P.Y., Chuang, S.-E., Yeh, K.-H., Song, Y.C., and Cheng, A.-L. (2003). Involvement of nuclear transcription factor-κB in low-dose doxorubicin-induced drug resistance of cervical carcinoma cells. Biochem. Pharmacol. *66*, 25–33.

Yilmaz, M., and Christofori, G. (2009). EMT, the cytoskeleton, and cancer cell invasion. Cancer Metastasis Rev. *28*, 15–33.

Yoo, H.Y., Kumagai, A., Shevchenko, A., Shevchenko, A., and Dunphy, W.G. (2009). The Mre11-Rad50-Nbs1 Complex Mediates Activation of TopBP1 by ATM. Mol. Biol. Cell *20*, 2351–2360.

Yook, J.I., Li, X.-Y., Ota, I., Hu, C., Kim, H.S., Kim, N.H., Cha, S.Y., Ryu, J.K., Choi, Y.J., Kim, J., et al. (2006). A Wnt-Axin2-GSK3beta cascade regulates Snail1 activity in breast cancer cells. Nat. Cell Biol. *8*, 1398–1406.

Zaccaria, M.L., Di Tommaso, F., Brancaccio, A., Paggi, P., and Petrucci, T.C. (2001). Dystroglycan distribution in adult mouse brain: a light and electron microscopy study. Neuroscience *104*, 311–324.

Zacharias, U., Purfürst, B., Schöwel, V., Morano, I., Spuler, S., and Haase, H. (2011). Ahnak1 abnormally localizes in muscular dystrophies and contributes to muscle vesicle release. J. Muscle Res. Cell Motil. *32*, 271–280.

Zeisberg, M., and Neilson, E.G. (2009). Biomarkers for epithelial-mesenchymal transitions. J. Clin. Invest. *119*, 1429–1437.

Zhang, Y.W., Shi, J., Li, Y.J., and Wei, L. (2009). Cardiomyocyte death in doxorubicin-induced cardiotoxicity. Arch. Immunol. Ther. Exp. (Warsz.) *57*, 435–445.

Zhao, S., Venkatasubbarao, K., Lazor, J.W., Sperry, J., Jin, C., Cao, L., and Freeman, J.W. (2008). Inhibition of STAT3 Tyr705 phosphorylation by Smad4 suppresses transforming growth factor beta-mediated invasion and metastasis in pancreatic cancer cells. Cancer Res. *68*, 4221–4228.

del Zoppo, G.J., Milner, R., Mabuchi, T., Hung, S., Wang, X., and Koziol, A. (2006). Vascular matrix adhesion and the blood-brain barrier. Biochem. Soc. Trans. *34*, 1261–1266.

Zuber, J., Tchernitsa, O.I., Hinzmann, B., Schmitz, A.C., Grips, M., Hellriegel, M., Sers, C., Rosenthal, a, and Schäfer, R. (2000). A genome-wide survey of RAS transformation targets. Nat. Genet. *24*, 144–152.

Chapter 7 : Addendum

7.1 Additional cell cycle results

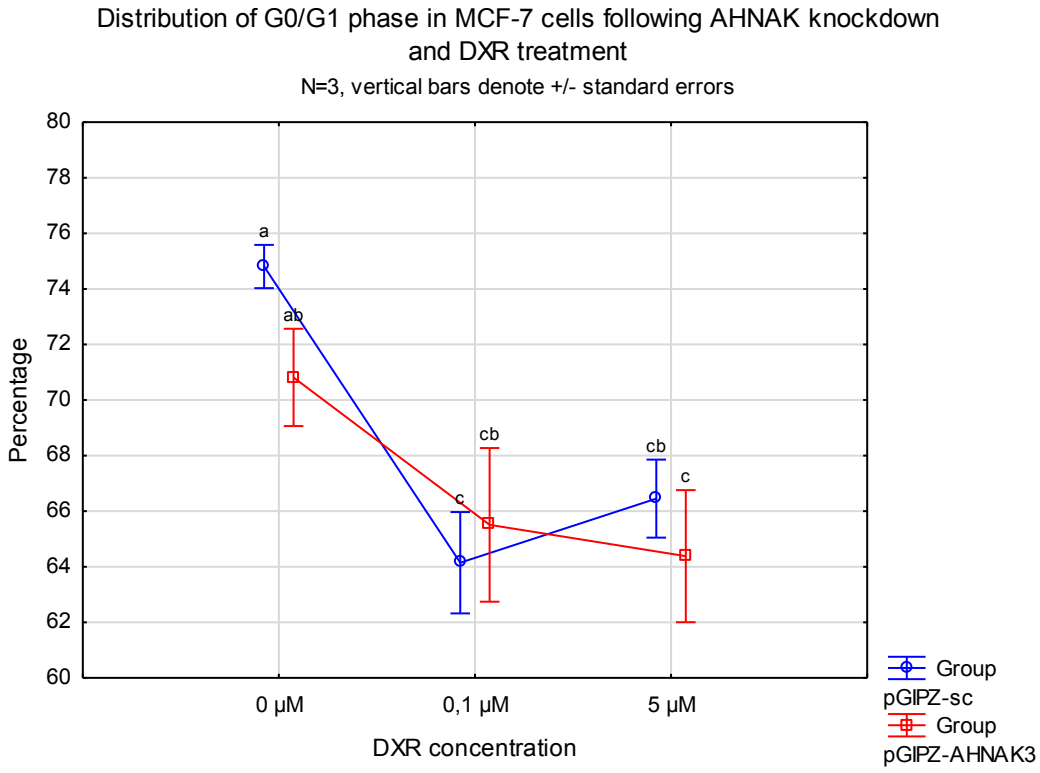

Figure 7.1: Distribution of MCF-7 cells in G_0/G_1 phase following AHNAK knockdown with pGIPZ-AHNAK3 and DXR treatment for 24 hrs.

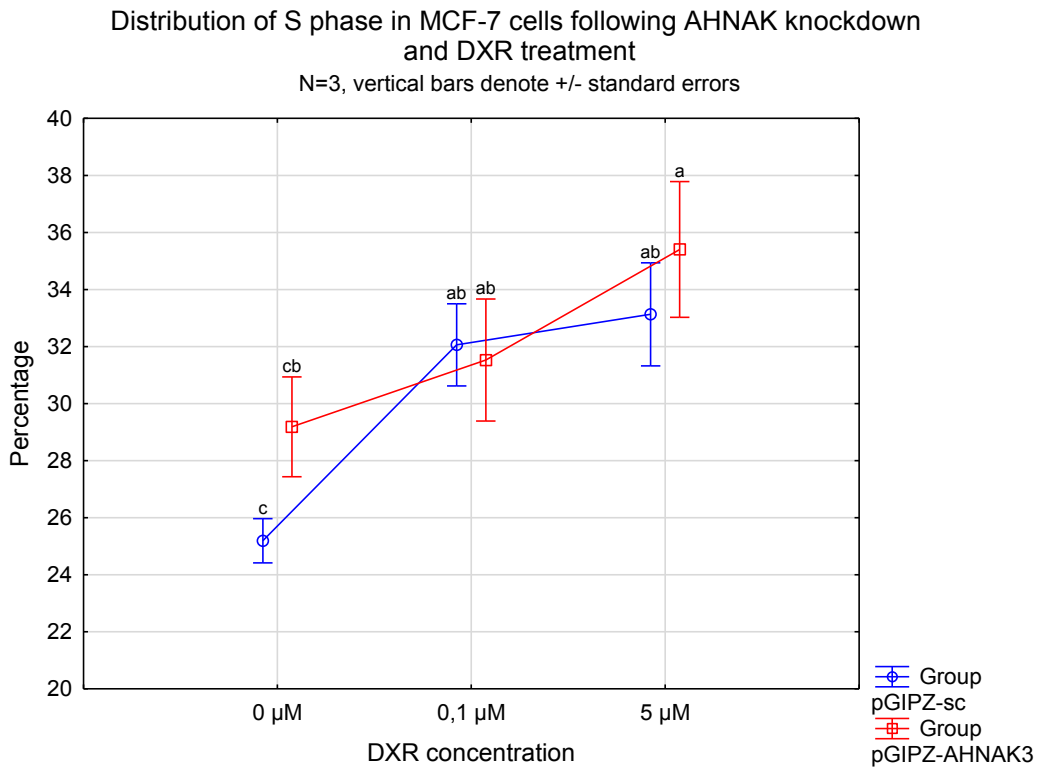

Figure 7.2: Distribution of MCF-7 cells in S phase following AHNAK knockdown with pGIPZ-AHNAK3 and DXR treatment for 24 hrs.

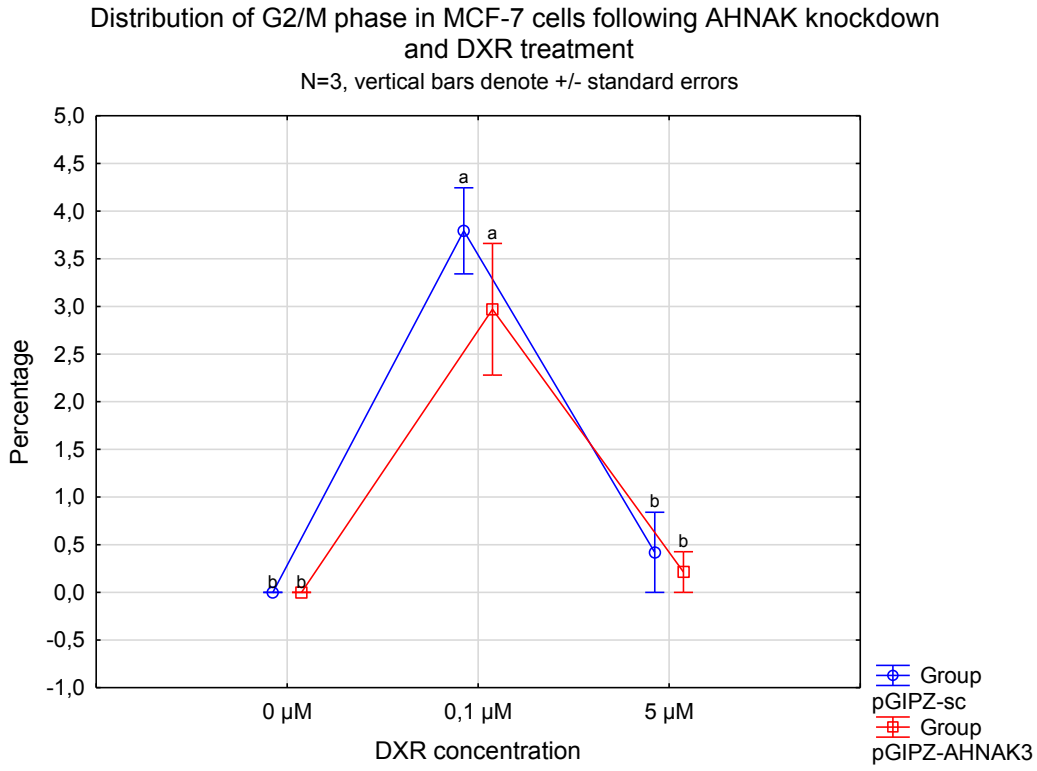

Figure 7.3: Distribution of MCF-7 cells in G_2/M phase following AHNAK knockdown with pGIPZ-AHNAK3 and DXR treatment for 24 hrs.

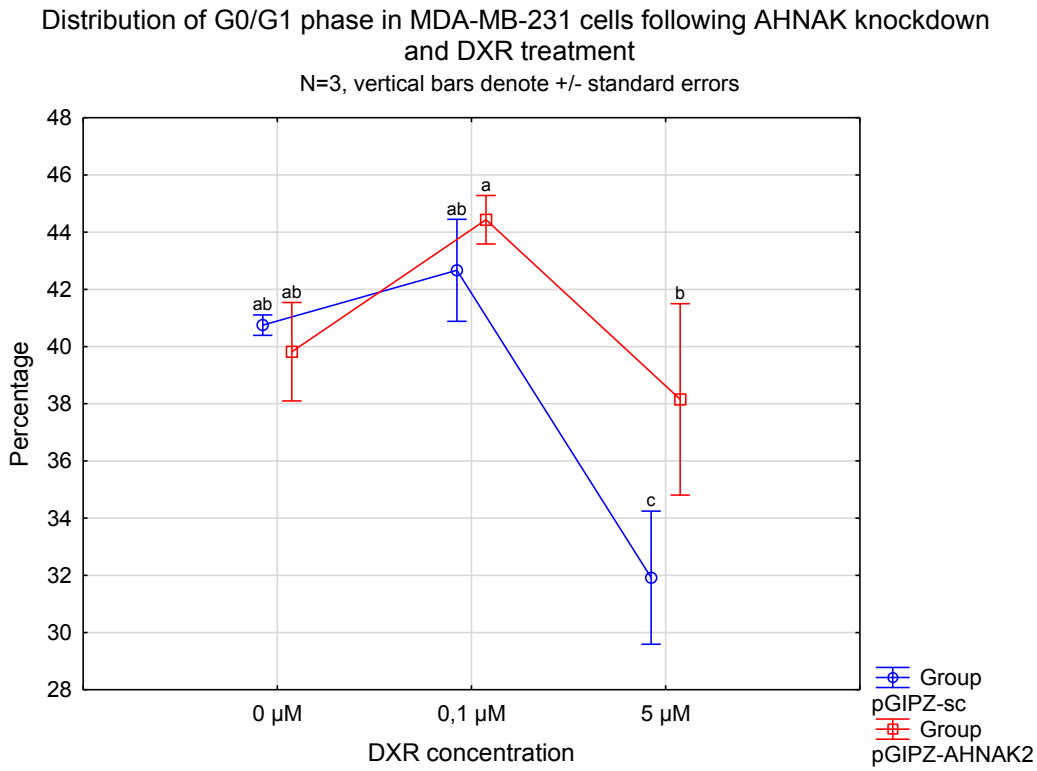

Figure 7.4: Distribution of MDA-MB-231 cells in G_0/G_1 phase following AHNAK knockdown with pGIPZ-AHNAK2 and DXR treatment for 24 hrs.

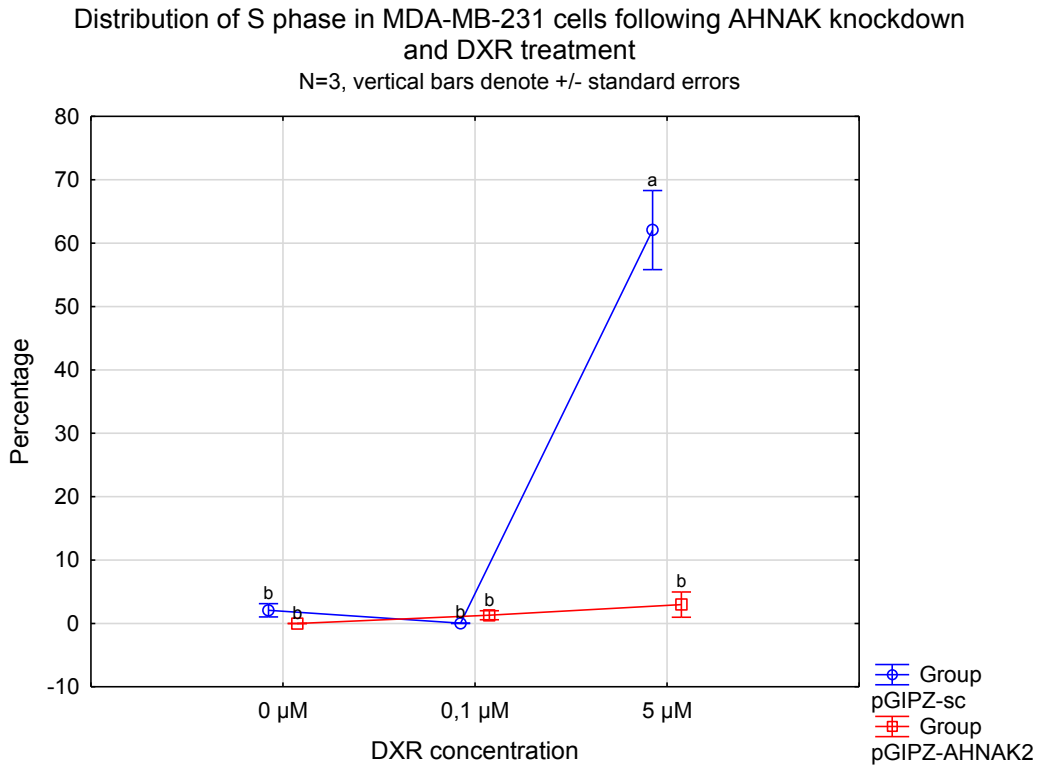

Figure 7.5: Distribution of MDA-MB-231 cells in S phase following AHNAK knockdown with pGIPZ-AHNAK2 and DXR treatment for 24 hrs.

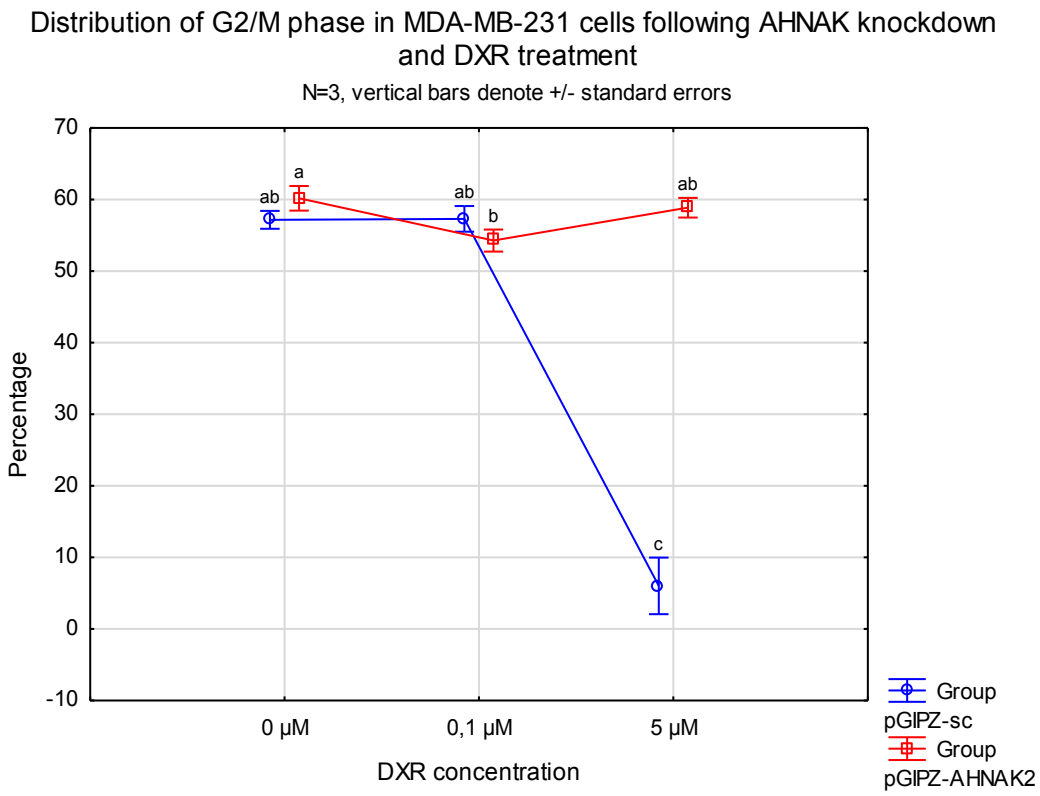

Figure 7.6: Distribution of MDA-MB-231 cells in G_2/M phase following AHNAK knockdown with pGIPZ-AHNAK2 and DXR treatment for 24 hrs.

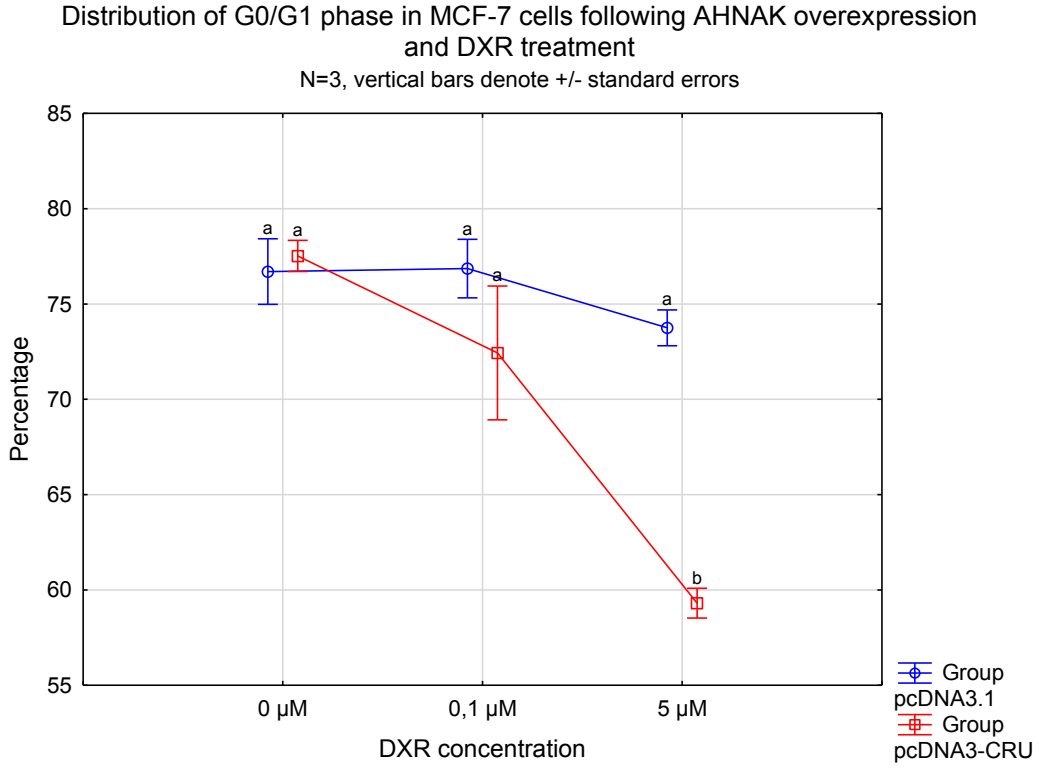

Figure 7.7: Distribution of MCF-7 cells in G_0/G_1 phase following AHNAK overexpression with pcDNA3-CRU and DXR treatment for 24 hrs.

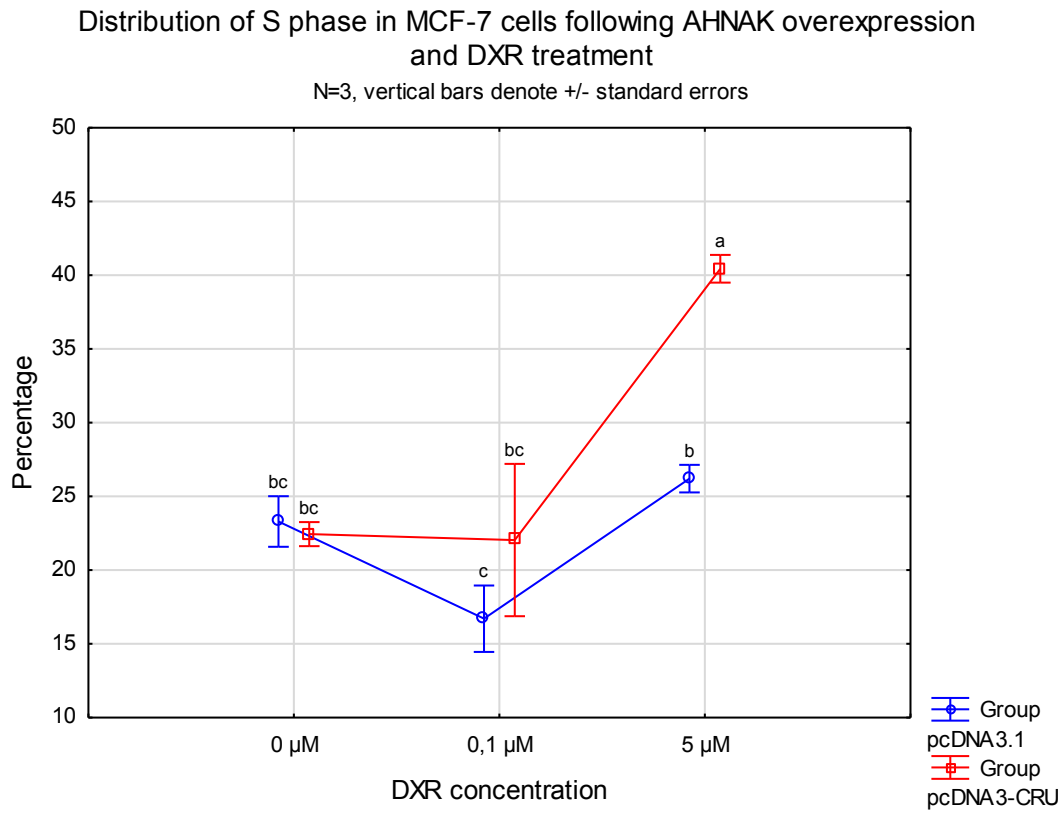

Figure 7.8: Distribution of MCF-7 cells in S phase following AHNAK overexpression with pcDNA3-CRU and DXR treatment for 24 hrs.

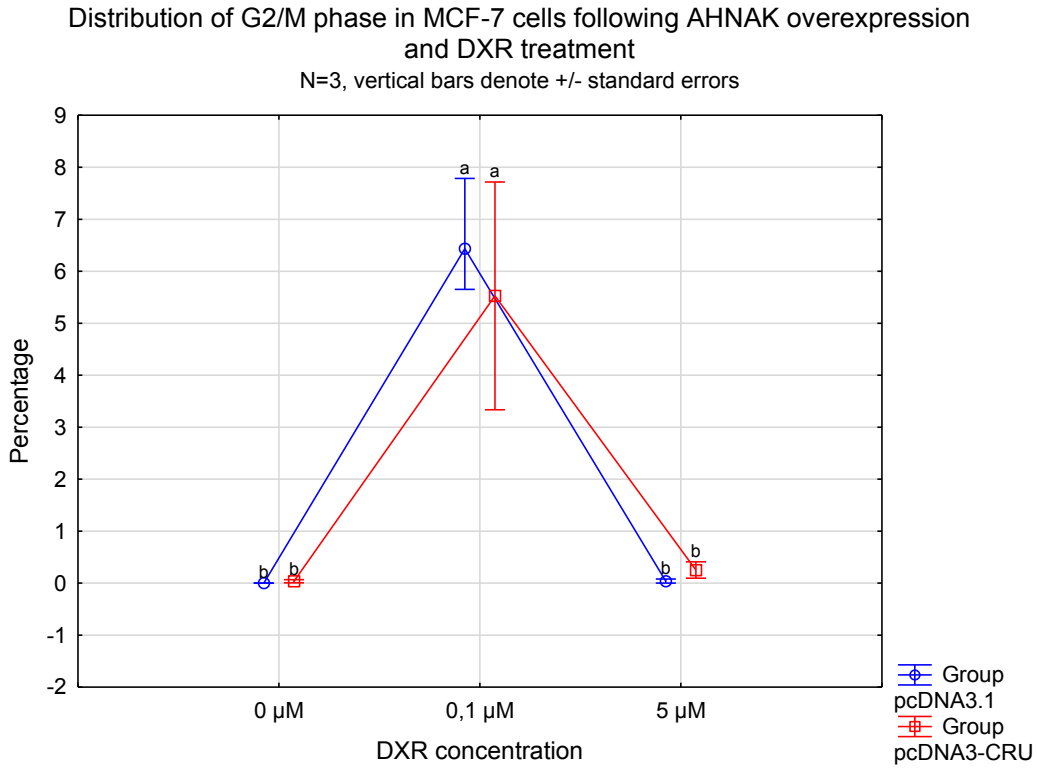

Figure 7.9: Distribution of MCF-7 cells in G_2/M phase following AHNAK overexpression with pcDNA3-CRU and DXR treatment for 24 hrs.

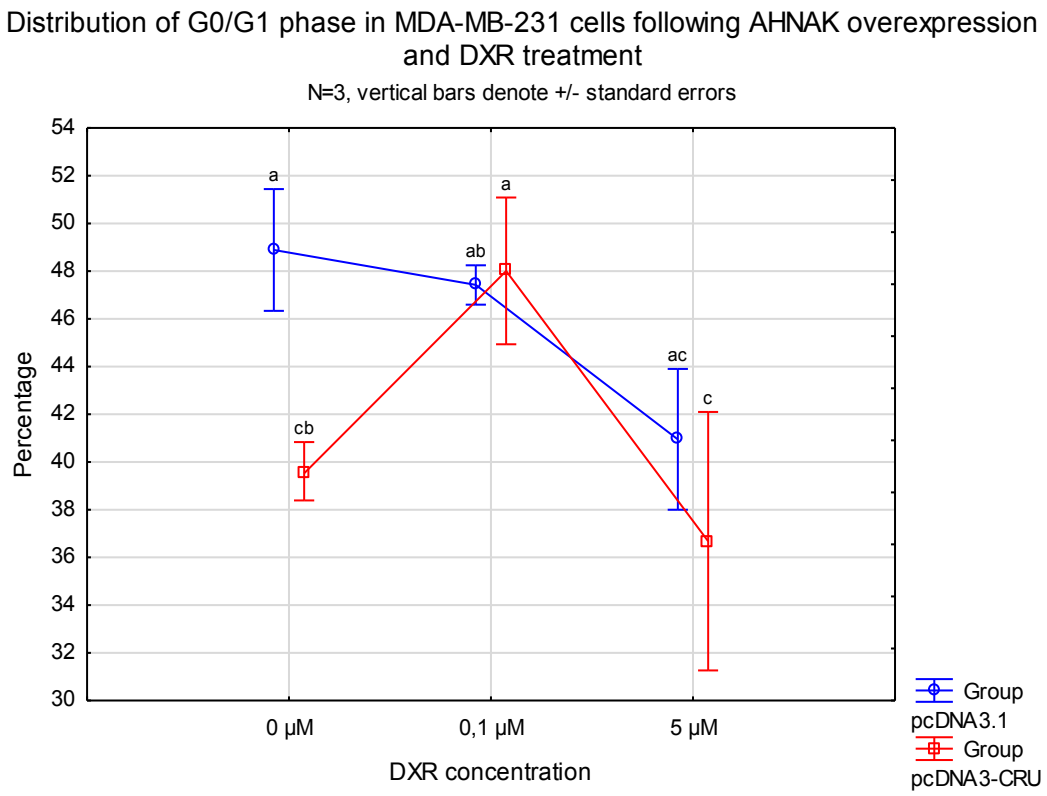

Figure 7.10: Distribution of MDA-MB-231 cells in G_0/G_1 phase following AHNAK overexpression with pcDNA3-CRU and DXR treatment for 24 hrs.

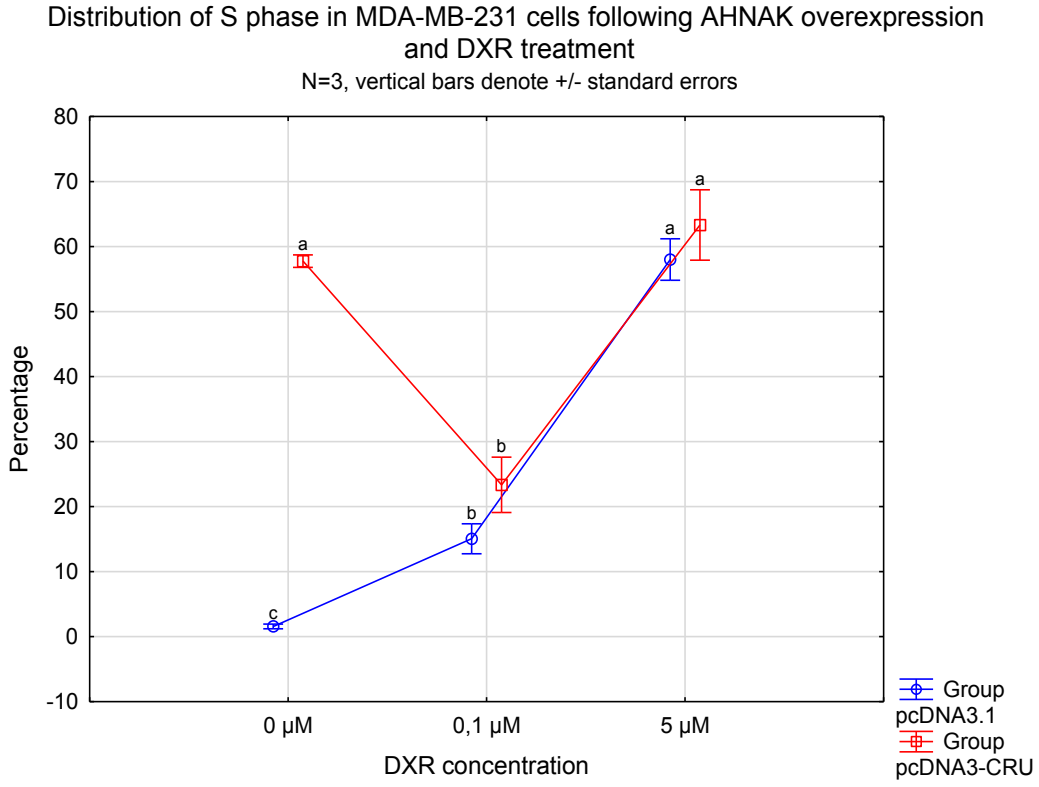

Figure 7.11: Distribution of MDA-MB-231 cells in S phase following AHNAK overexpression with pcDNA3-CRU and DXR treatment for 24 hrs.

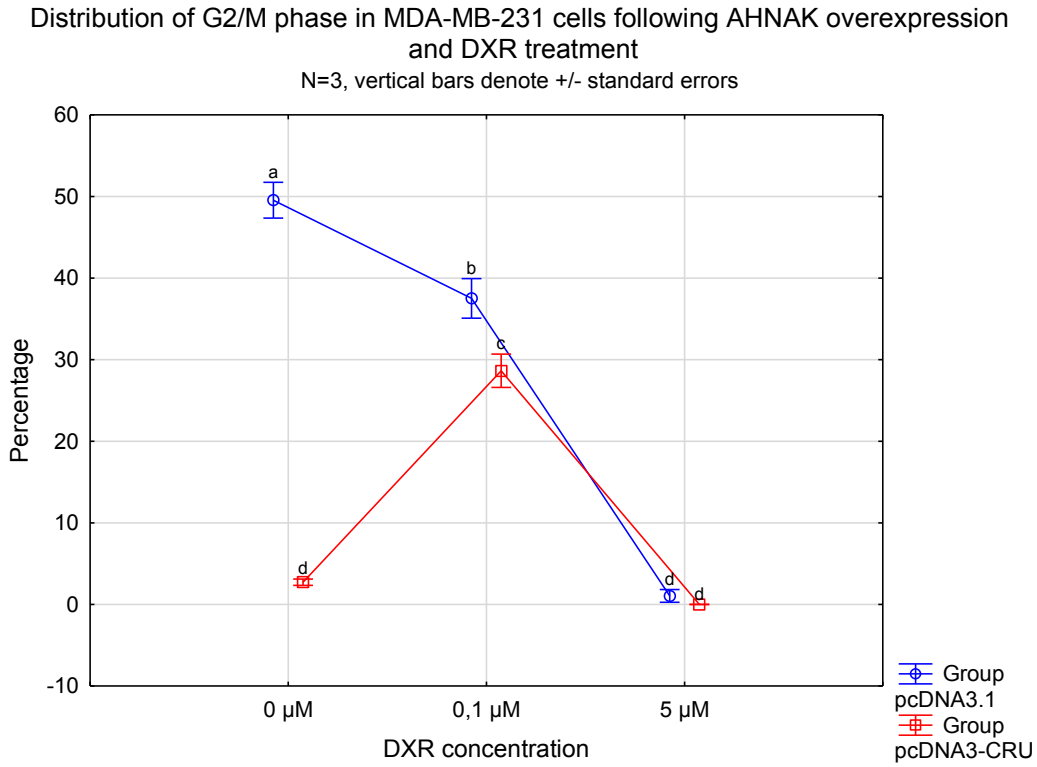

Figure 7.12: Distribution of MDA-MB-231 cells in G_2/M phase following AHNAK overexpression with pcDNA3-CRU and DXR treatment for 24 hrs.

7.2 Additional scratch assay results

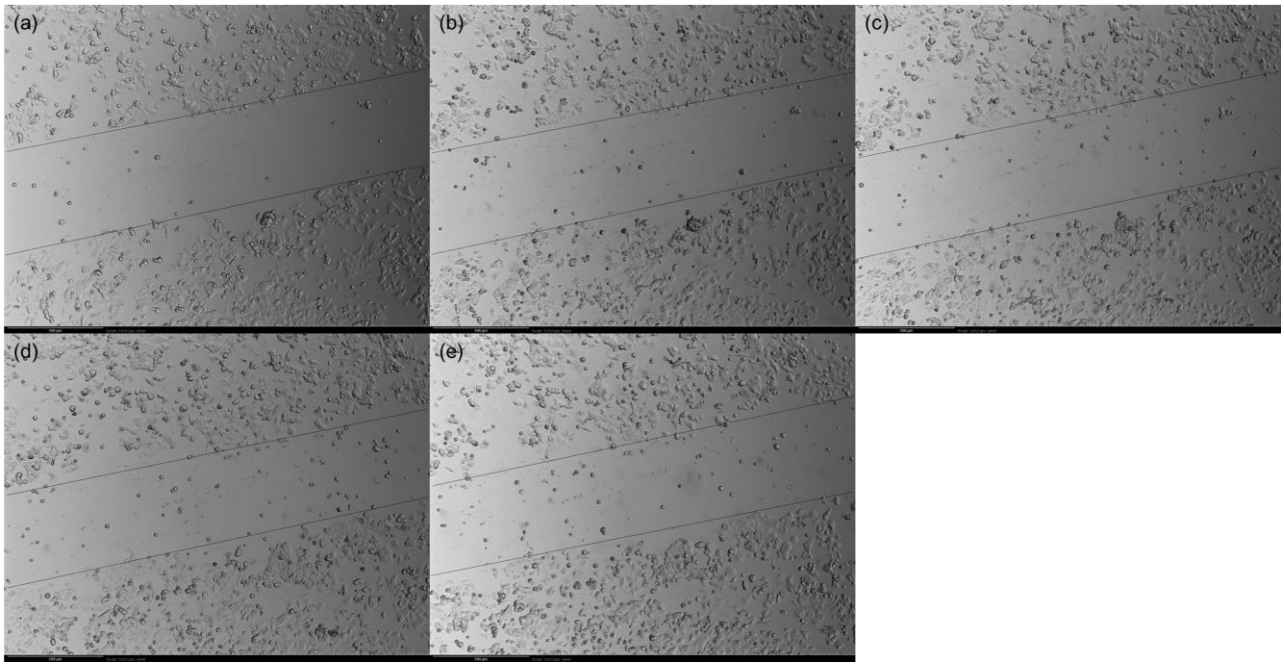

Figure 7.13: Representative brightfield microscopy images of wound closure over 24 hrs in pGIPZ-sc transfected MCF-7 cells without DXR treatment. Lines serve as an indication of wound area and where drawn to fit the general migration front across the imaged area. (a) 0 hrs; (b) 6 hrs: (c) 12 hrs; (d) 18 hrs; (e) 24 hrs. Scale = 500 µm, 4x objective.

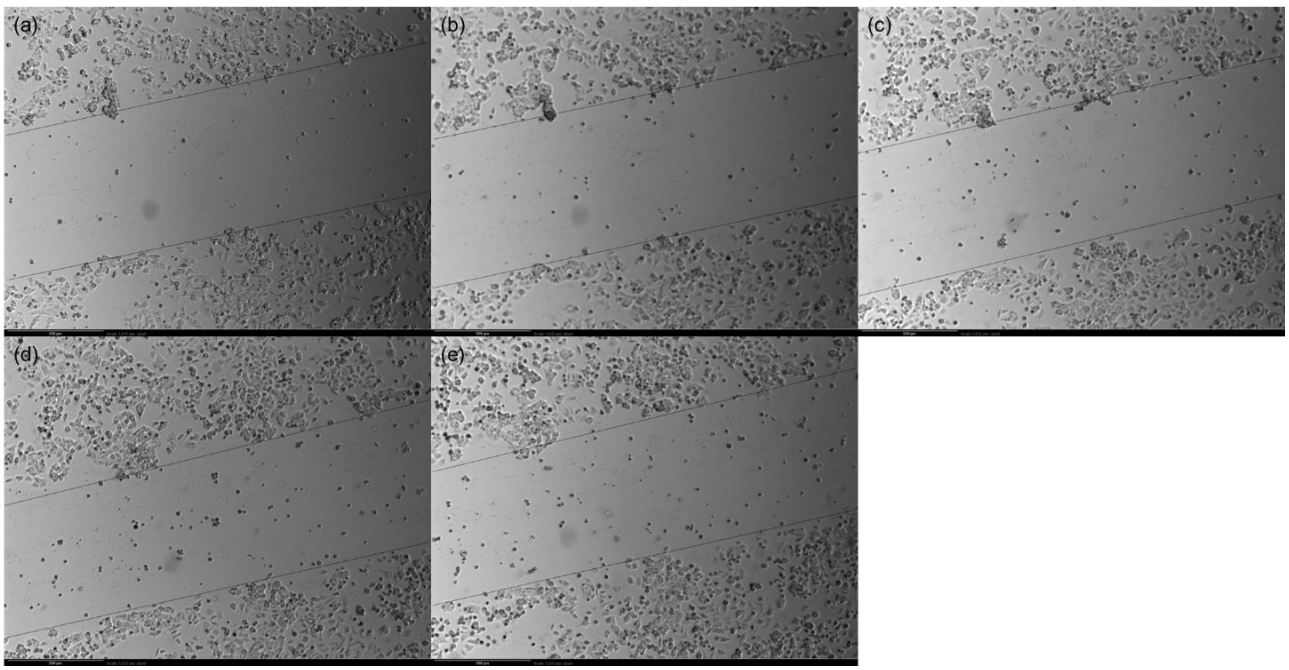

Figure 7.14: Representative brightfield microscopy images of wound closure over 24 hrs in pGIPZ-sc transfected MCF-7 cells treated with 0.1 µM DXR. Lines serve as an indication of wound area and where drawn to fit the general migration front across the imaged area. (a) 0 hrs; (b) 6 hrs: (c) 12 hrs; (d) 18 hrs; (e) 24 hrs. Scale = 500 µm, 4x objective.

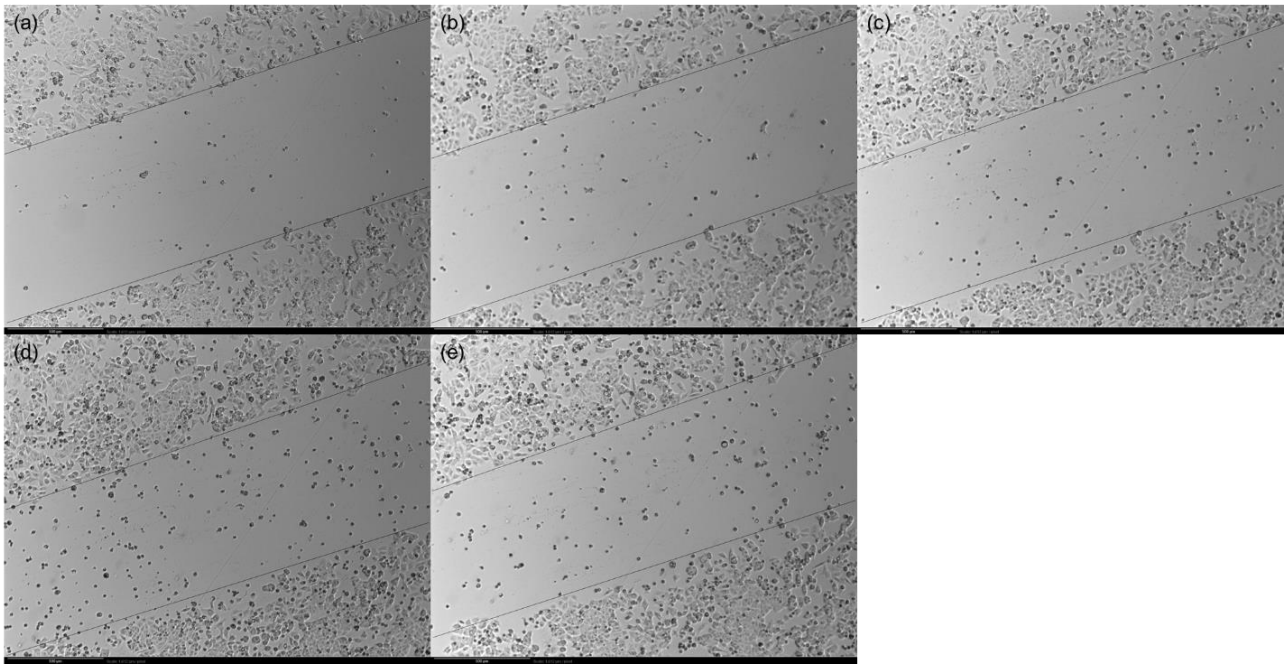

Figure 7.15: Representative brightfield microscopy images of wound closure over 24 hrs in pGIPZ-AHNAK3 transfected MCF-7 cells without DXR treatment. Lines serve as an indication of wound area and where drawn to fit the general migration front across the imaged area. (a) 0 hrs; (b) 6 hrs: (c) 12 hrs; (d) 18 hrs; (e) 24 hrs. Scale = 500 µm, 4x objective.

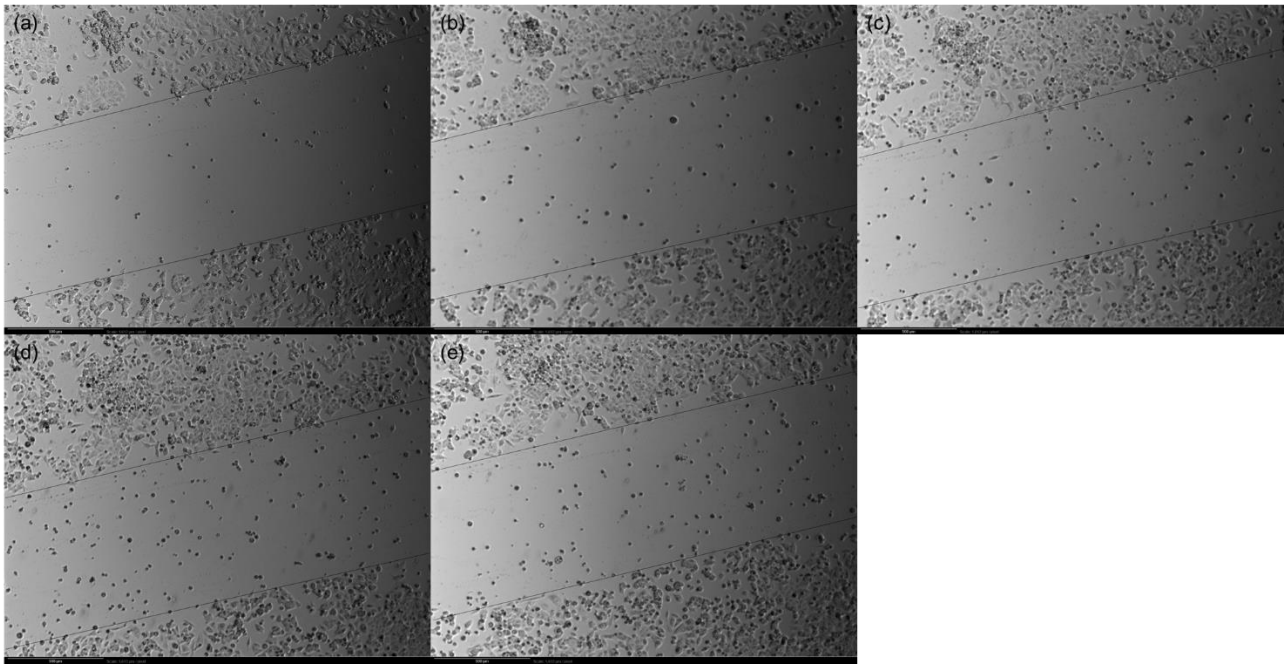

Figure 7.16: Representative brightfield microscopy images of wound closure over 24 hrs in pGIPZ-AHNAK3 transfected MCF-7 cells treated with 0.1 µM DXR. Lines serve as an indication of wound area and where drawn to fit the general migration front across the imaged area. (a) 0 hrs; (b) 6 hrs: (c) 12 hrs; (d) 18 hrs; (e) 24 hrs. Scale = 500 µm, 4x objective.

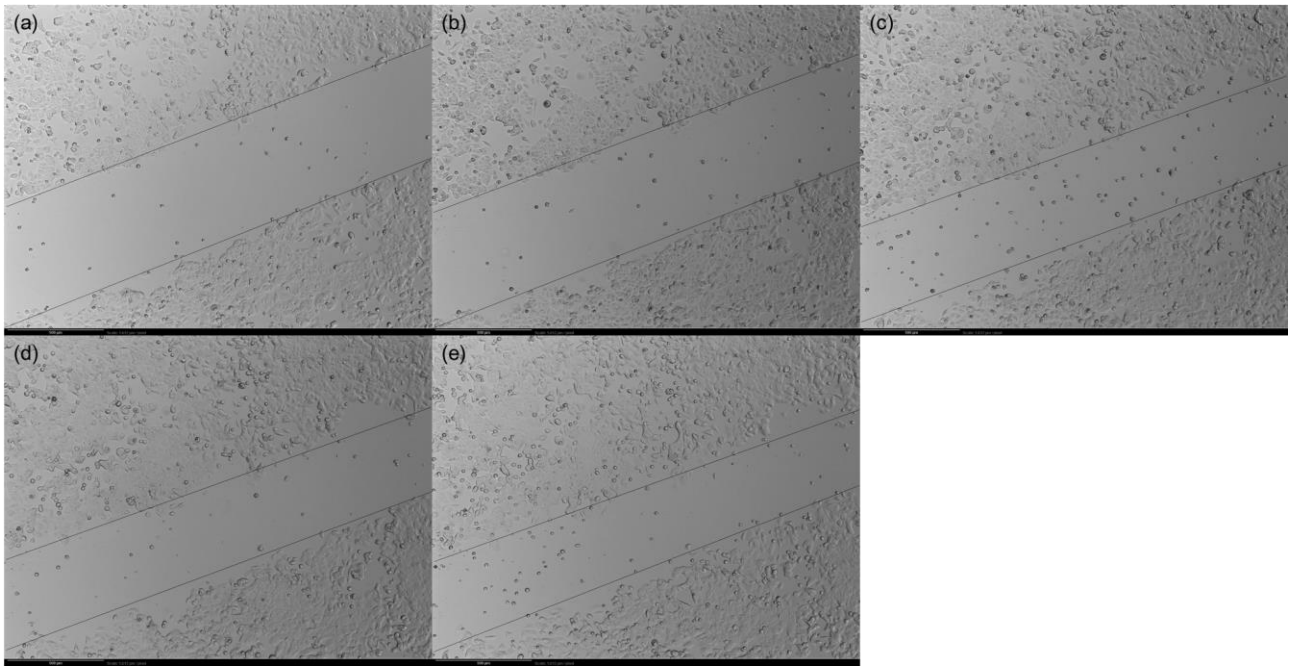

Figure 7.17: Representative brightfield microscopy images of wound closure over 24 hrs in MMC control MCF-7 cells. Lines serve as an indication of wound area and where drawn to fit the general migration front across the imaged area. (a) 0 hrs; (b) 6 hrs: (c) 12 hrs; (d) 18 hrs; (e) 24 hrs. Scale = 500 µm, 4x objective.

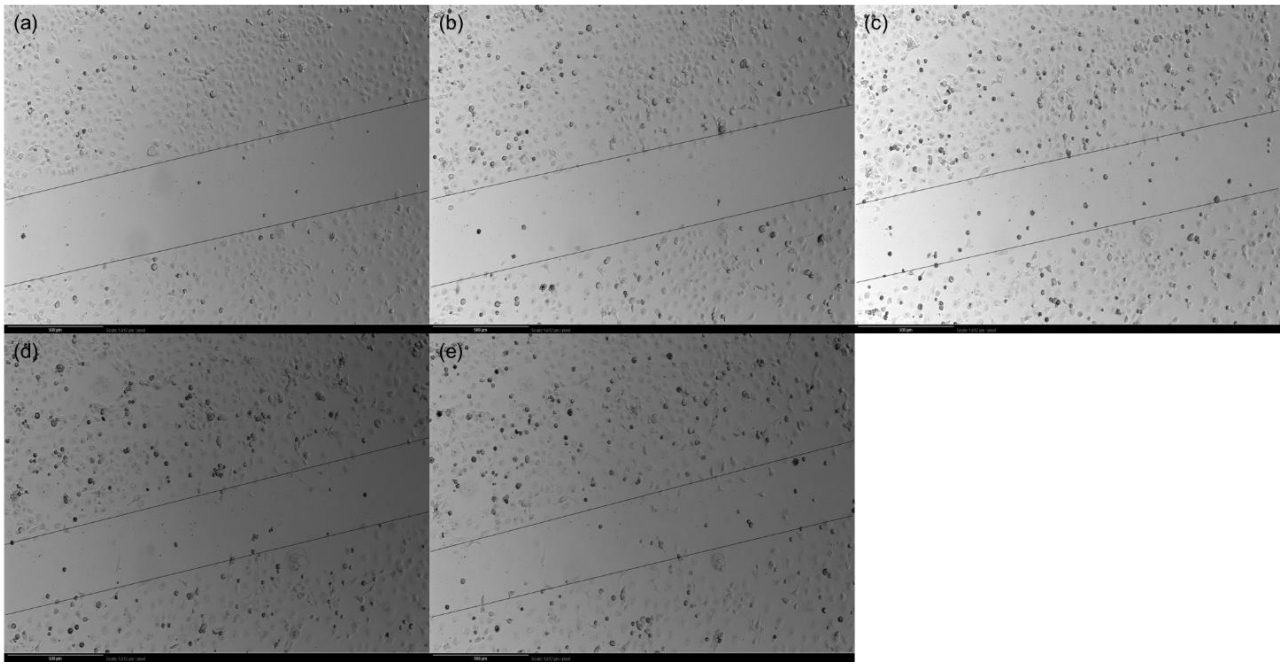

Figure 7.18: Representative brightfield microscopy images of wound closure over 24 hrs in pGIPZ-sc transfected MDA-MB-231 cells without DXR treatment. Lines serve as an indication of wound area and where drawn to fit the general migration front across the imaged area. (a) 0 hrs; (b) 6 hrs: (c) 12 hrs; (d) 18 hrs; (e) 24 hrs. Scale = 500 µm, 4x objective.

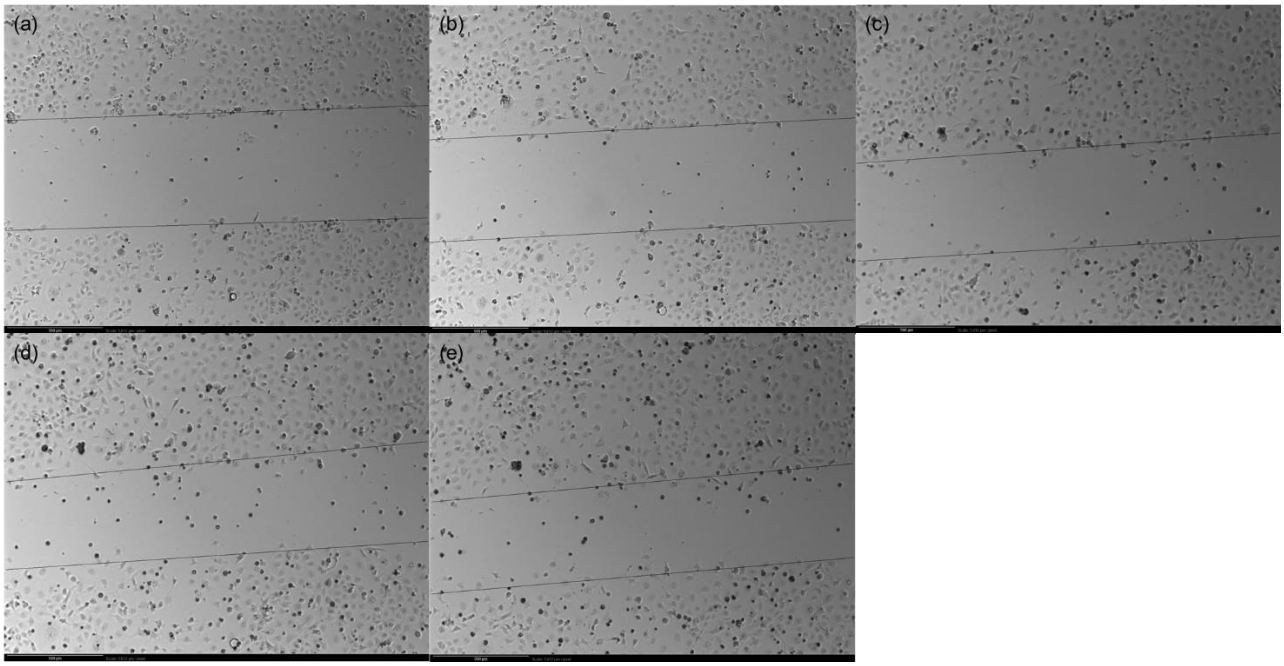

Figure 7.19: Representative brightfield microscopy images of wound closure over 24 hrs in pGIPZ-sc transfected MDA-MB-231 cells treated with 0.1 µM DXR. Lines serve as an indication of wound area and where drawn to fit the general migration front across the imaged area. (a) 0 hrs; (b) 6 hrs: (c) 12 hrs; (d) 18 hrs; (e) 24 hrs. Scale = 500 µm, 4x objective.

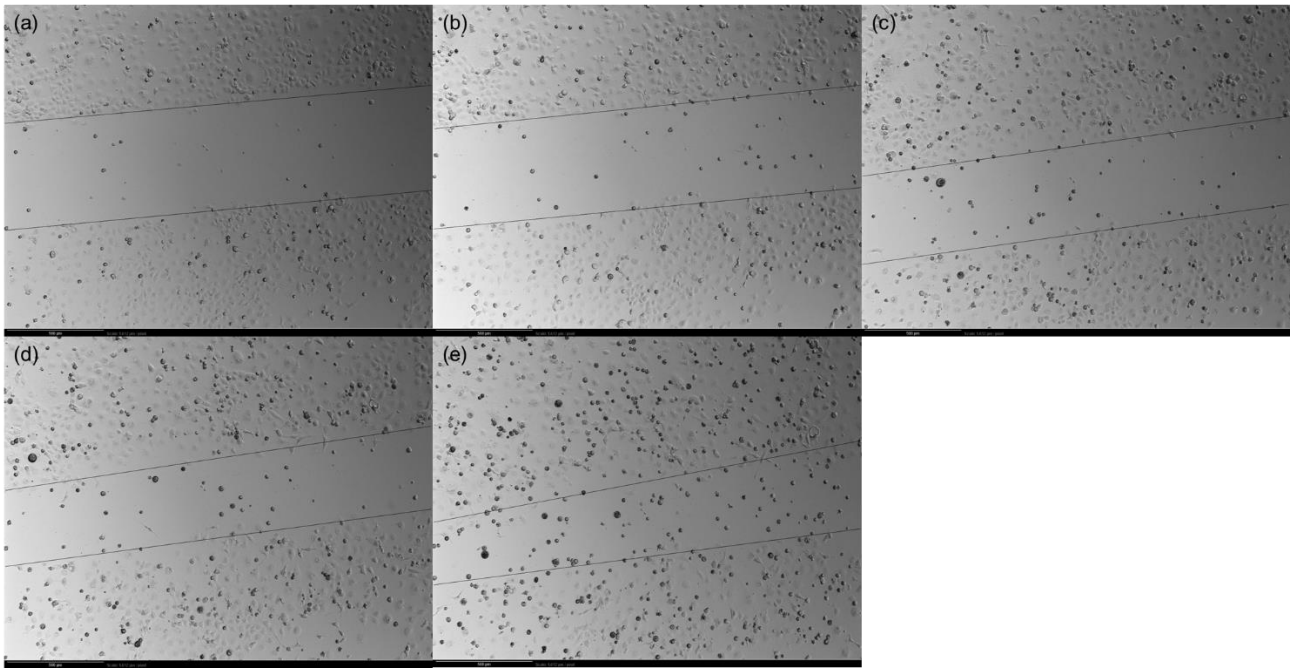

Figure 7.20: Representative brightfield microscopy images of wound closure over 24 hrs in pGIPZ-sc transfected MDA-MB-231 cells treated with 5 µM DXR. Lines serve as an indication of wound area and where drawn to fit the general migration front across the imaged area. (a) 0 hrs; (b) 6 hrs: (c) 12 hrs; (d) 18 hrs; (e) 24 hrs. Scale = 500 µm, 4x objective.

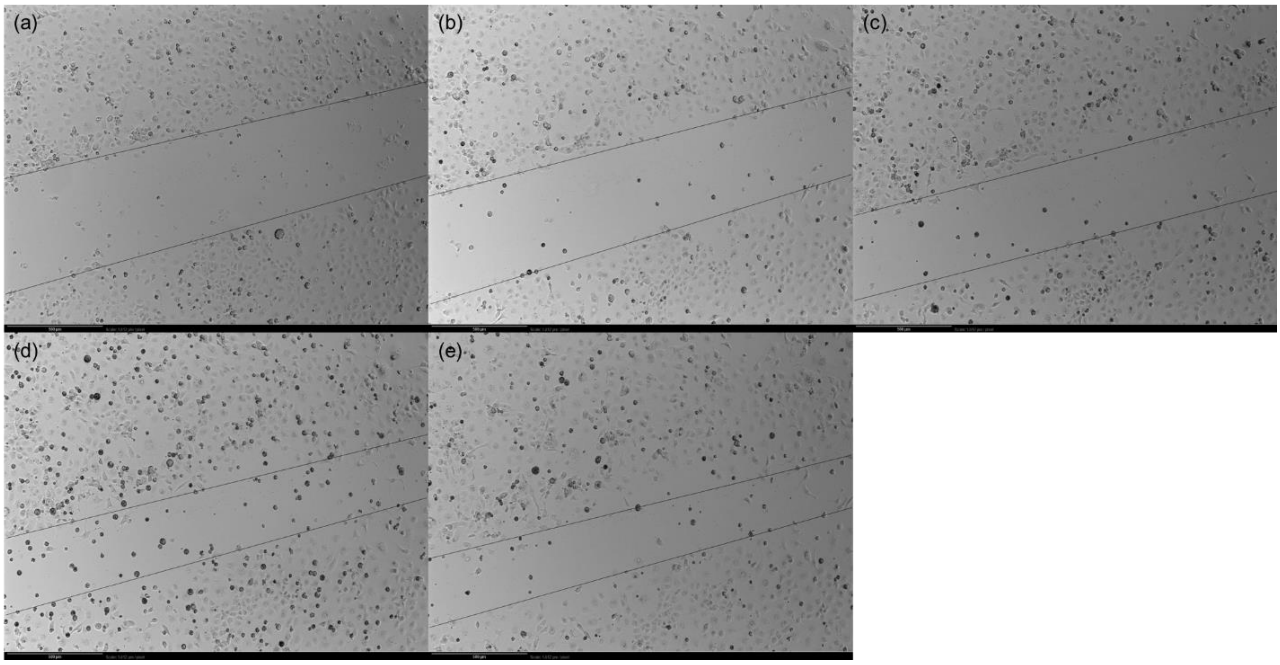

Figure 7.21: Representative brightfield microscopy images of wound closure over 24 hrs in pGIPZ-AHNAK2 transfected MDA-MB-231 cells without DXR treatment. Lines serve as an indication of wound area and where drawn to fit the general migration front across the imaged area. (a) 0 hrs; (b) 6 hrs: (c) 12 hrs; (d) 18 hrs; (e) 24 hrs. Scale = 500 µm, 4x objective.

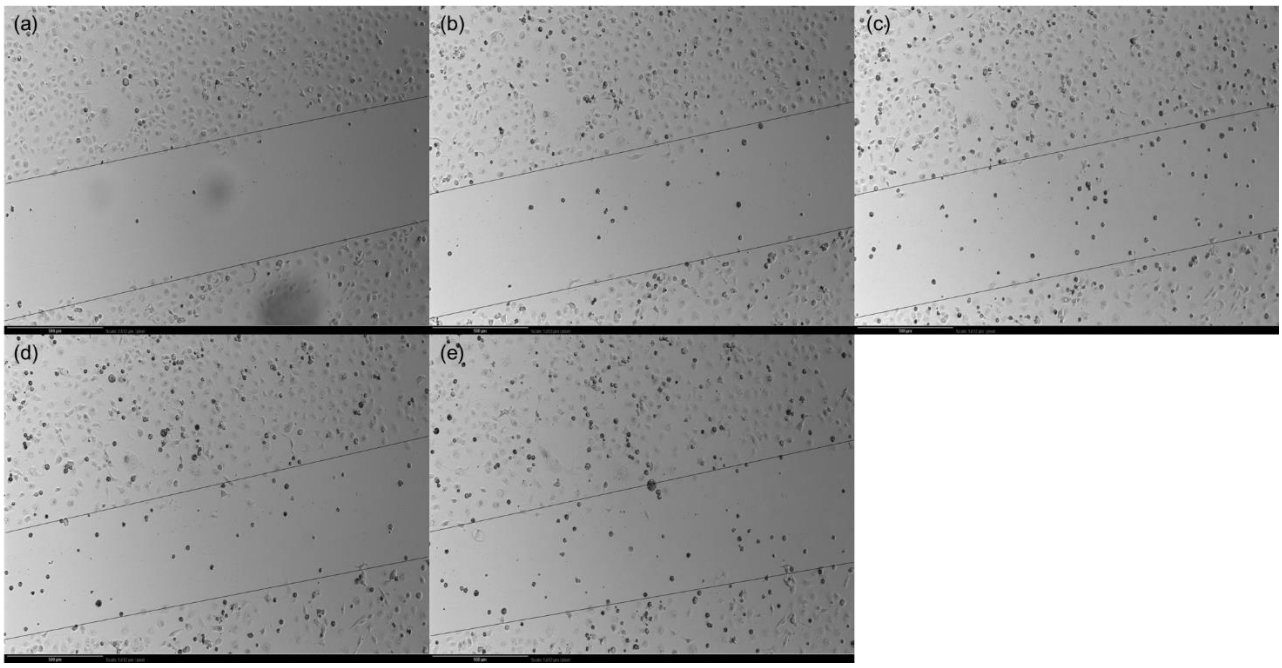

Figure 7.22: Representative brightfield microscopy images of wound closure over 24 hrs in pGIPZ-AHNAK2 transfected MDA-MB-231 cells treated with 0.1 µM DXR. Lines serve as an indication of wound area and where drawn to fit the general migration front across the imaged area. (a) 0 hrs; (b) 6 hrs: (c) 12 hrs; (d) 18 hrs; (e) 24 hrs. Scale = 500 µm, 4x objective.

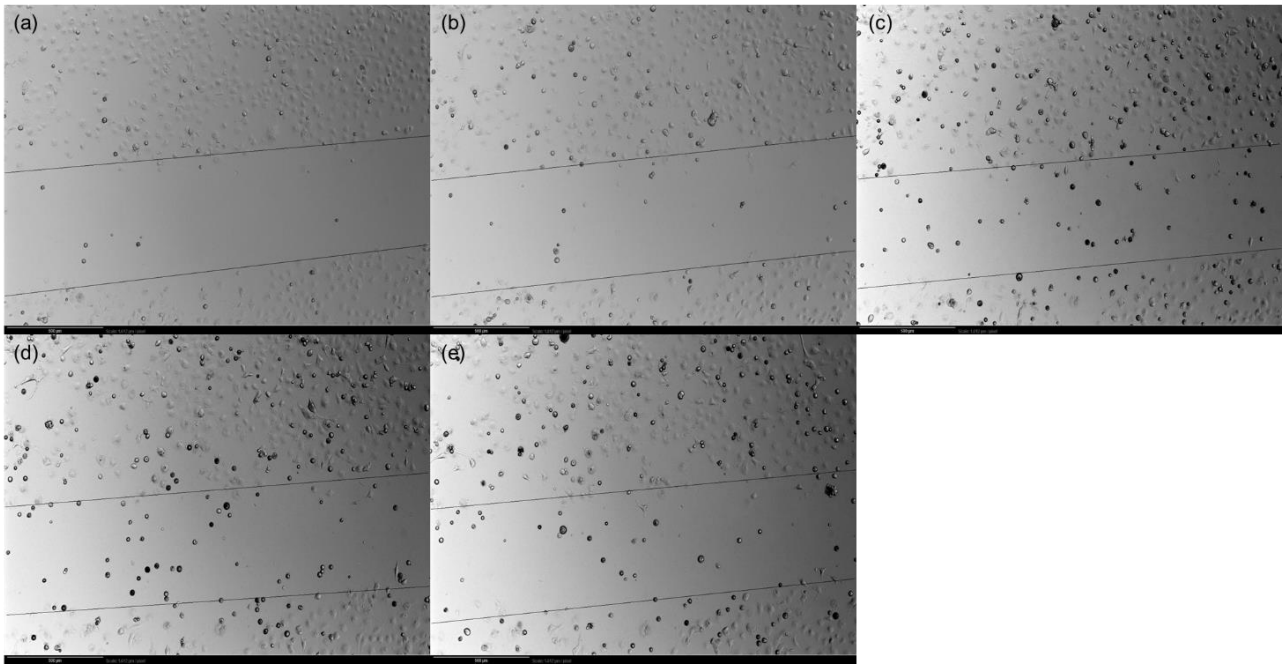

Figure 7.23: Representative brightfield microscopy images of wound closure over 24 hrs in pGIPZ-AHNAK2 transfected MDA-MB-231 cells treated with 5 µM DXR. Lines serve as an indication of wound area and where drawn to fit the general migration front across the imaged area. (a) 0 hrs; (b) 6 hrs: (c) 12 hrs; (d) 18 hrs; (e) 24 hrs. Scale = 500 µm, 4x objective.

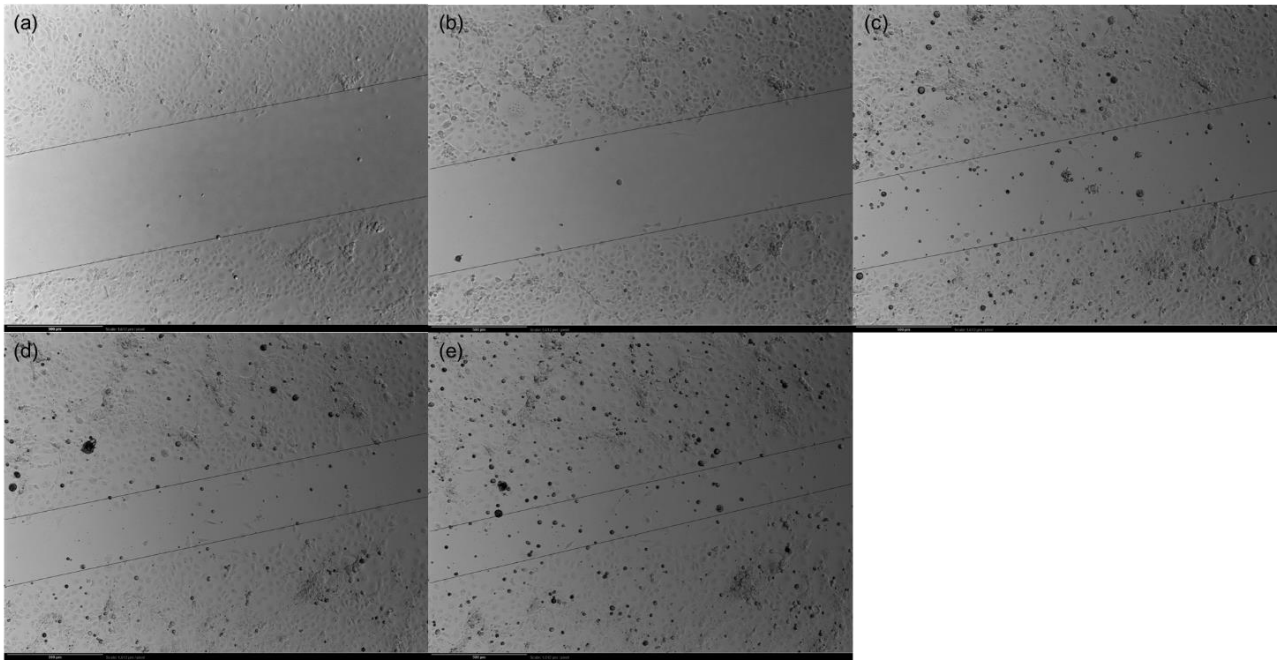

Figure 7.24: Representative brightfield microscopy images of wound closure over 24 hrs in MMC control MDA-MB-231 cells. Lines serve as an indication of wound area and where drawn to fit the general migration front across the imaged area. (a) 0 hrs; (b) 6 hrs: (c) 12 hrs; (d) 18 hrs; (e) 24 hrs. Scale = 500 µm, 4x objective.

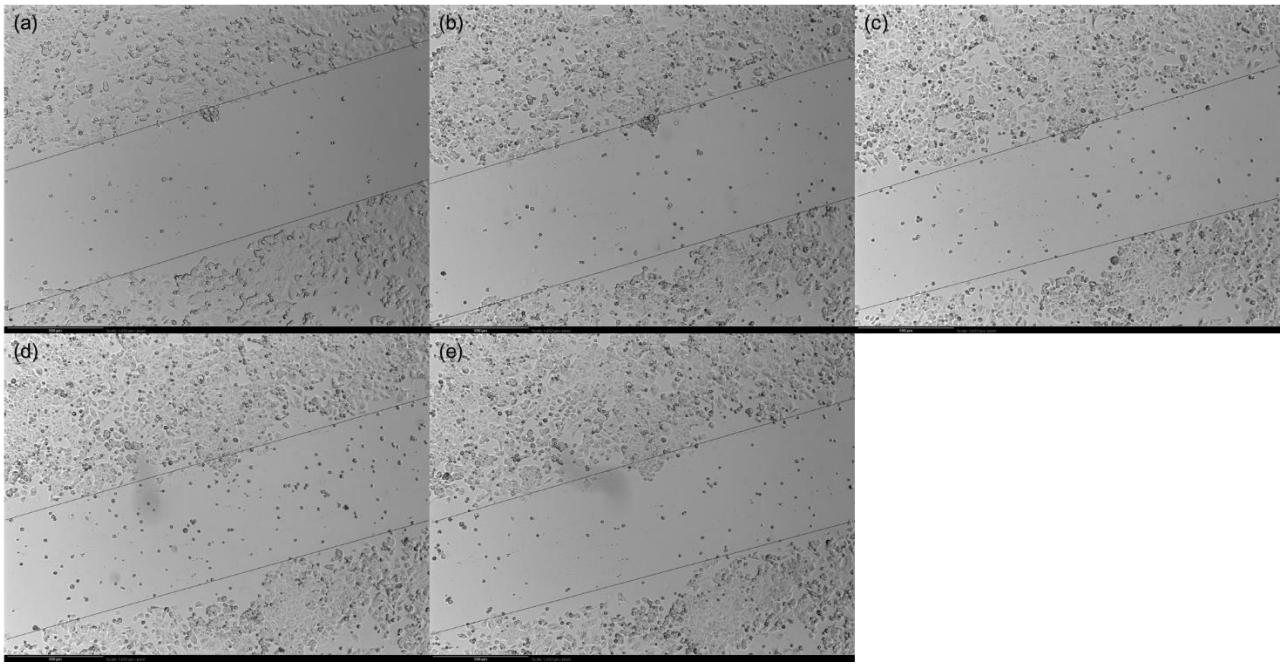

Figure 7.25: Representative brightfield microscopy images of wound closure over 24 hrs in pcDNA3.1 transfected MCF-7 cells without DXR treatment. Lines serve as an indication of wound area and where drawn to fit the general migration front across the imaged area. (a) 0 hrs; (b) 6 hrs: (c) 12 hrs; (d) 18 hrs; (e) 24 hrs. Scale = 500 µm, 4x objective.

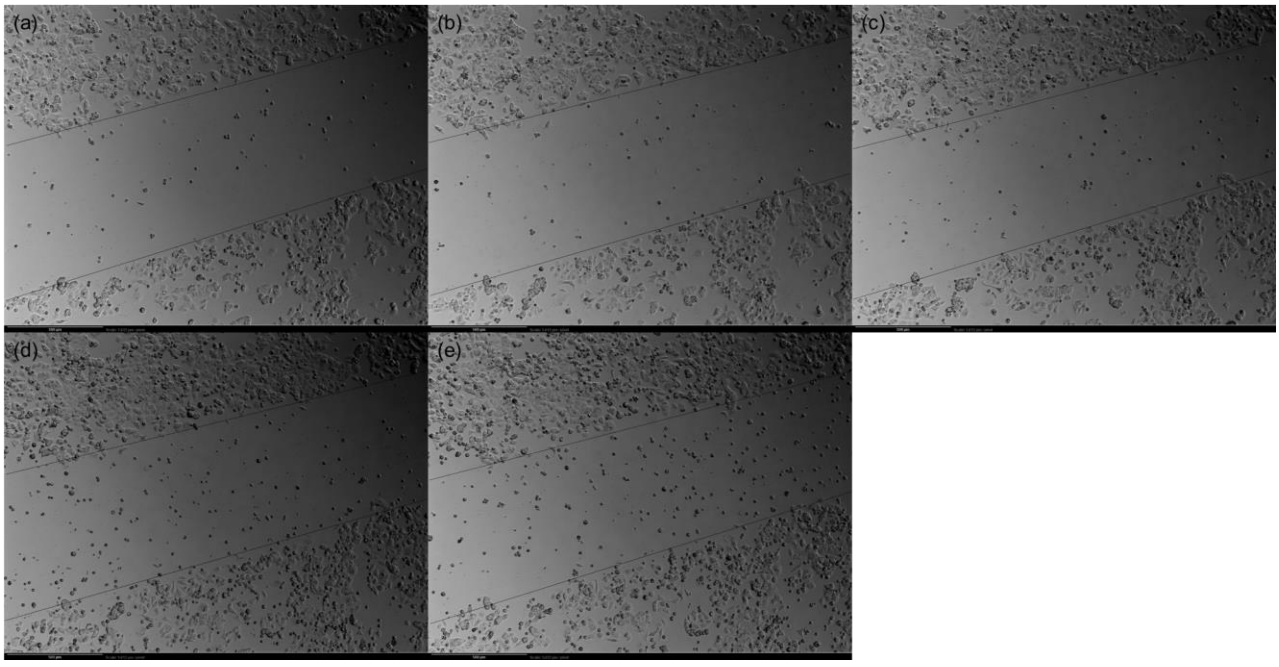

Figure 7.26: Representative brightfield microscopy images of wound closure over 24 hrs in pcDNA3.1 transfected MCF-7 cells treated with 0.1 µM DXR. Lines serve as an indication of wound area and where drawn to fit the general migration front across the imaged area. (a) 0 hrs; (b) 6 hrs: (c) 12 hrs; (d) 18 hrs; (e) 24 hrs. Scale = 500 µm, 4x objective.

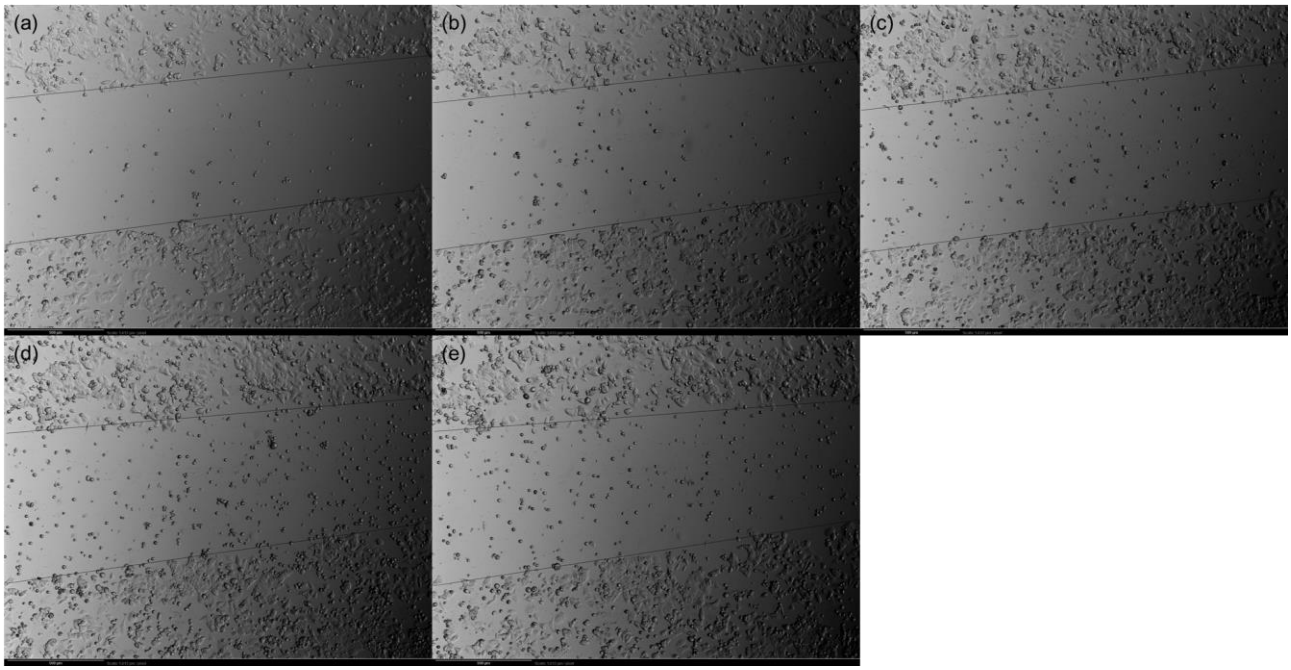

Figure 7.27: Representative brightfield microscopy images of wound closure over 24 hrs in pcDNA3-CRU transfected MCF-7 cells without DXR treatment. Lines serve as an indication of wound area and where drawn to fit the general migration front across the imaged area. (a) 0 hrs; (b) 6 hrs: (c) 12 hrs; (d) 18 hrs; (e) 24 hrs. Scale = 500 µm, 4x objective.

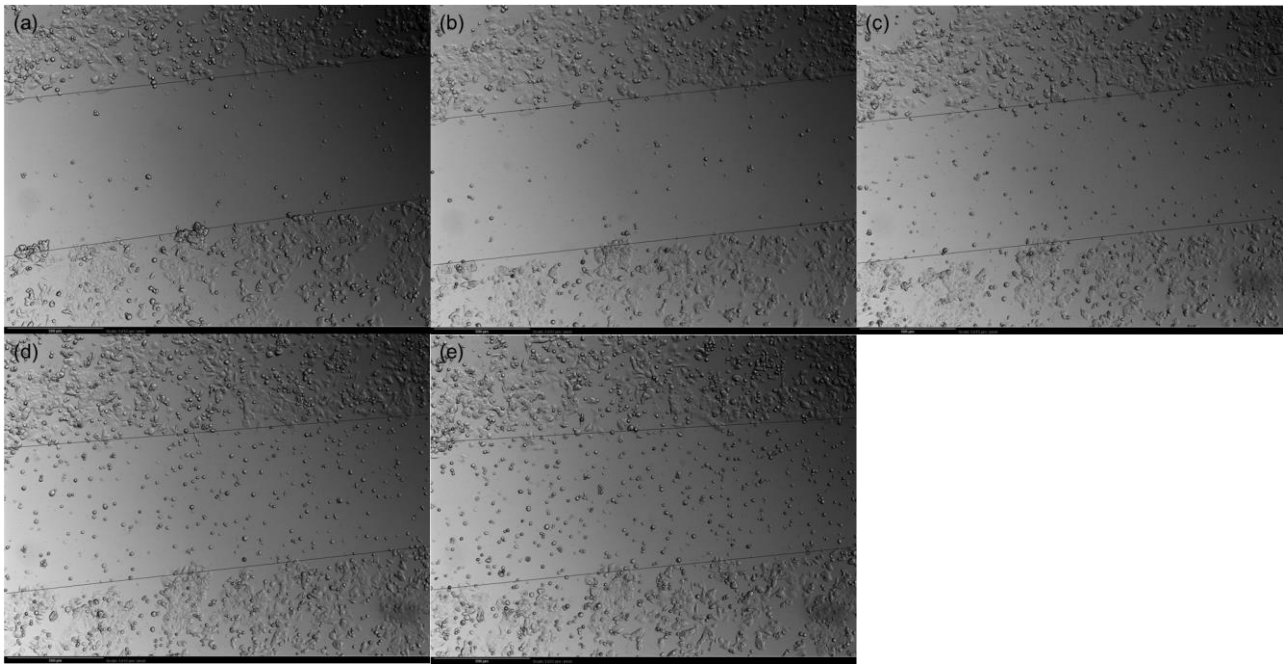

Figure 7.28: Representative brightfield microscopy images of wound closure over 24 hrs in pcDNA3-CRU transfected MCF-7 cells treated with 0.1 µM DXR. Lines serve as an indication of wound area and where drawn to fit the general migration front across the imaged area. (a) 0 hrs; (b) 6 hrs: (c) 12 hrs; (d) 18 hrs; (e) 24 hrs. Scale = 500 µm, 4x objective.

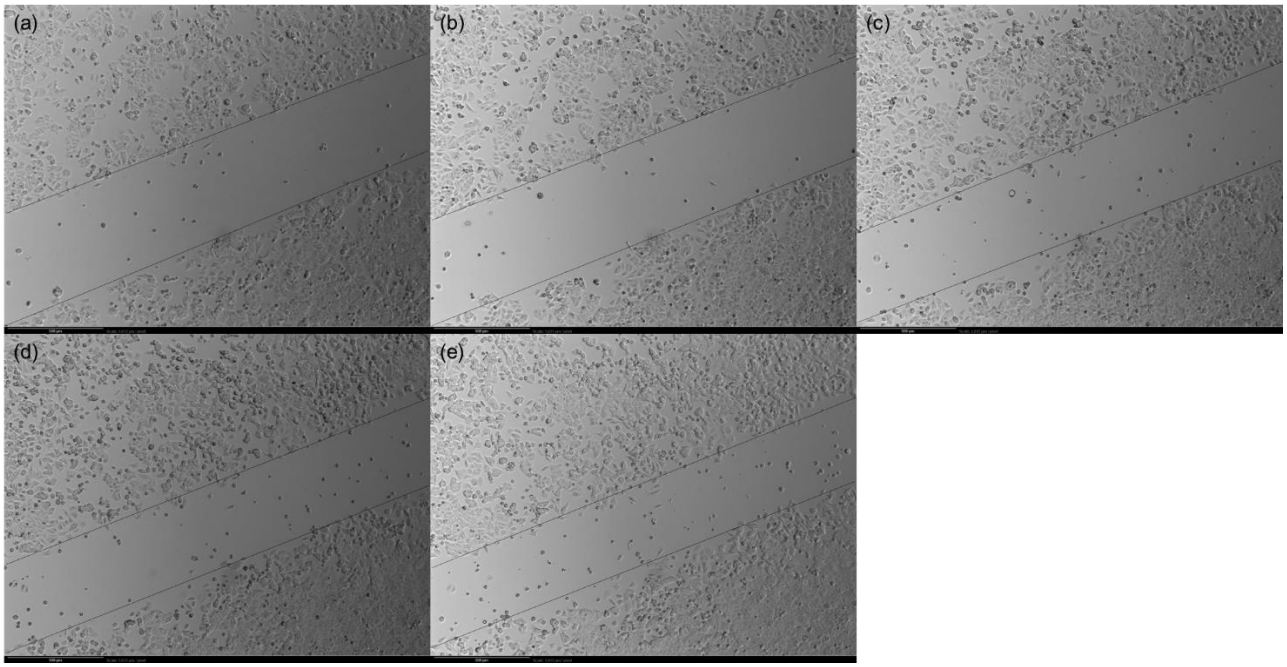

Figure 7.29: Representative brightfield microscopy images of wound closure over 24 hrs in MMC control MCF-7 cells. Lines serve as an indication of wound area and where drawn to fit the general migration front across the imaged area. (a) 0 hrs; (b) 6 hrs: (c) 12 hrs; (d) 18 hrs; (e) 24 hrs. Scale = 500 µm, 4x objective.

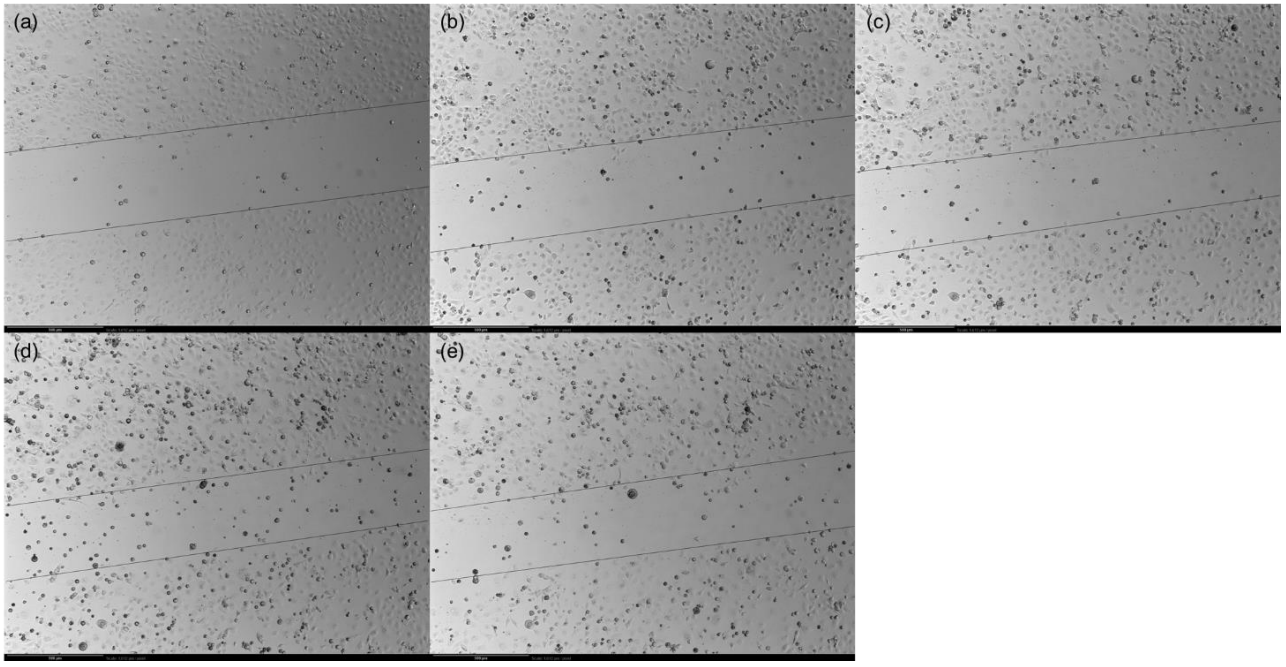

Figure 7.30: Representative brightfield microscopy images of wound closure over 24 hrs in pcDNA3.1 transfected MDA-MB-231 cells without DXR treatment. Lines serve as an indication of wound area and where drawn to fit the general migration front across the imaged area. (a) 0 hrs; (b) 6 hrs: (c) 12 hrs; (d) 18 hrs; (e) 24 hrs. Scale = 500 µm, 4x objective.

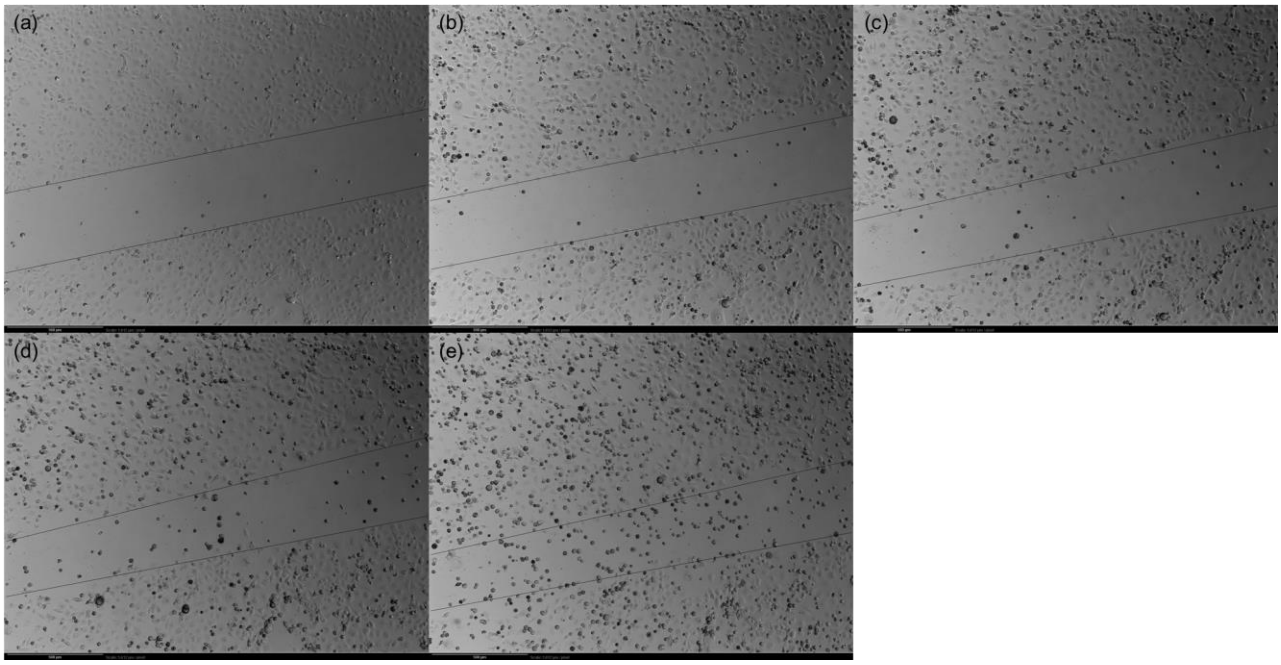

Figure 7.31: Representative brightfield microscopy images of wound closure over 24 hrs in pcDNA3.1 transfected MDA-MB-231 cells treated with 0.1 µM DXR. Lines serve as an indication of wound area and where drawn to fit the general migration front across the imaged area. (a) 0 hrs; (b) 6 hrs: (c) 12 hrs; (d) 18 hrs; (e) 24 hrs. Scale = 500 µm, 4x objective.

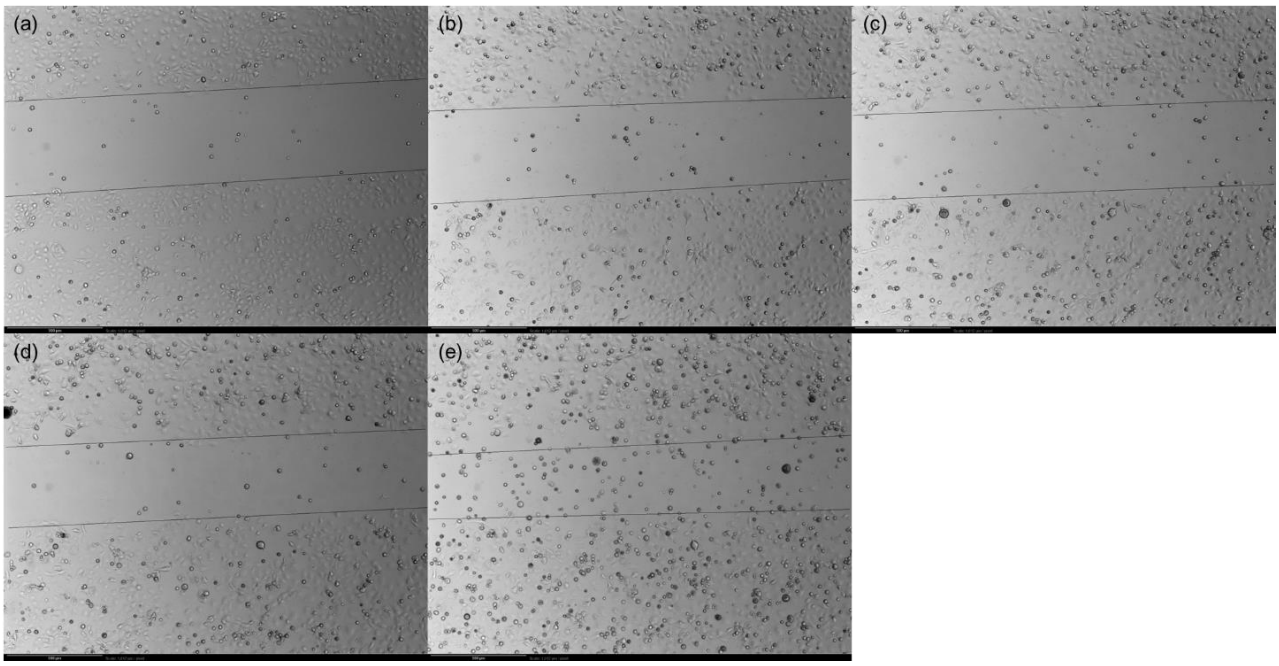

Figure 7.32: Representative brightfield microscopy images of wound closure over 24 hrs in pcDNA3.1 transfected MDA-MB-231 cells treated with 5 µM DXR. Lines serve as an indication of wound area and where drawn to fit the general migration front across the imaged area. (a) 0 hrs; (b) 6 hrs: (c) 12 hrs; (d) 18 hrs; (e) 24 hrs. Scale = 500 µm, 4x objective.

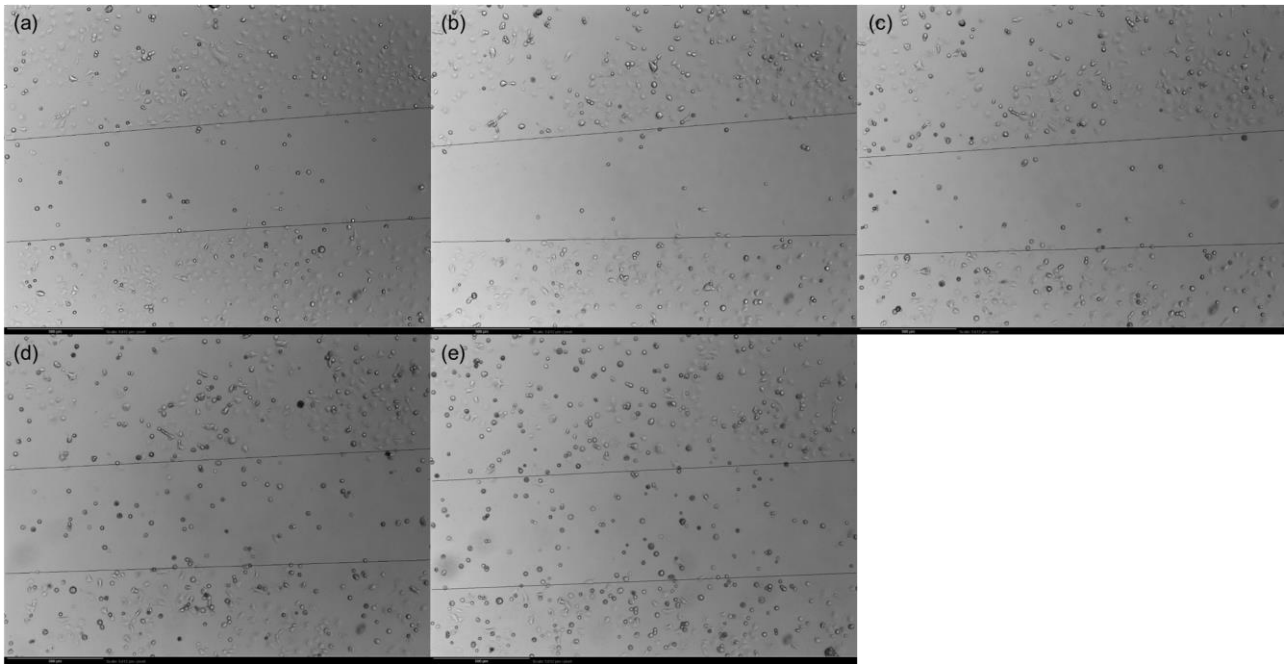

Figure 7.33: Representative brightfield microscopy images of wound closure over 24 hrs in pcDNA3-CRU transfected MDA-MB-231 cells without DXR treatment. Lines serve as an indication of wound area and where drawn to fit the general migration front across the imaged area. (a) 0 hrs; (b) 6 hrs: (c) 12 hrs; (d) 18 hrs; (e) 24 hrs. Scale = 500 µm, 4x objective.

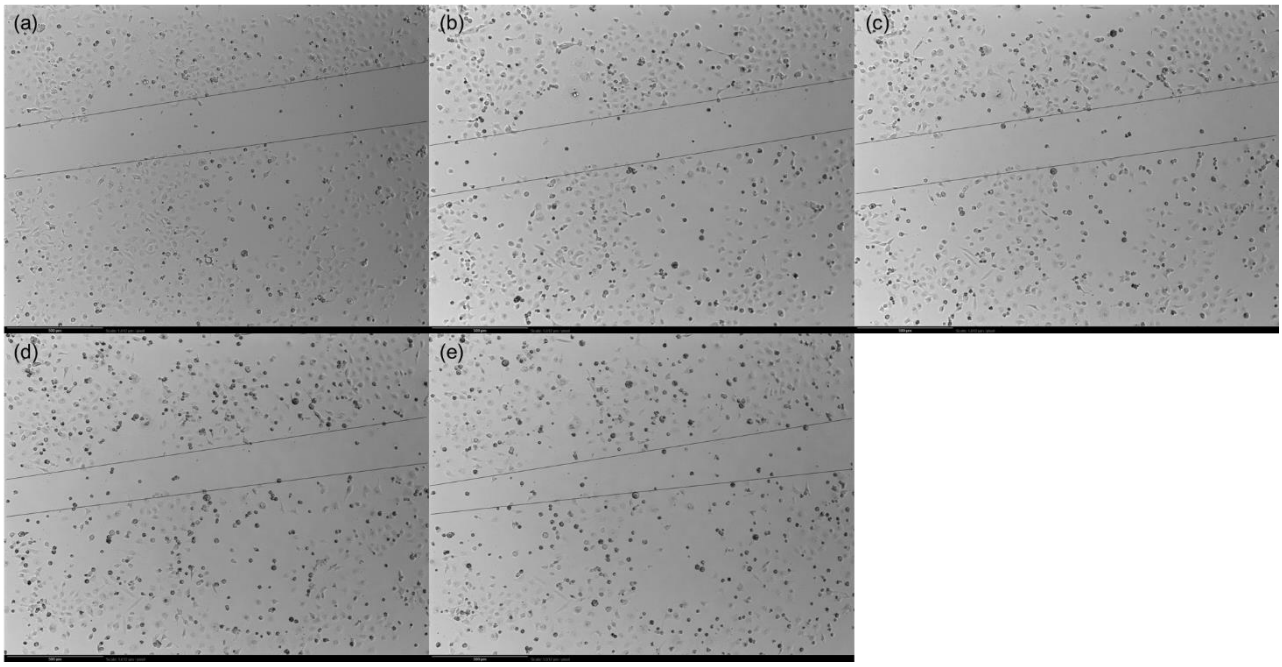

Figure 7.34: Representative brightfield microscopy images of wound closure over 24 hrs in pcDNA3-CRU transfected MDA-MB-231 cells treated with 0.1 µM DXR. Lines serve as an indication of wound area and where drawn to fit the general migration front across the imaged area. (a) 0 hrs; (b) 6 hrs: (c) 12 hrs; (d) 18 hrs; (e) 24 hrs. Scale = 500 µm, 4x objective.

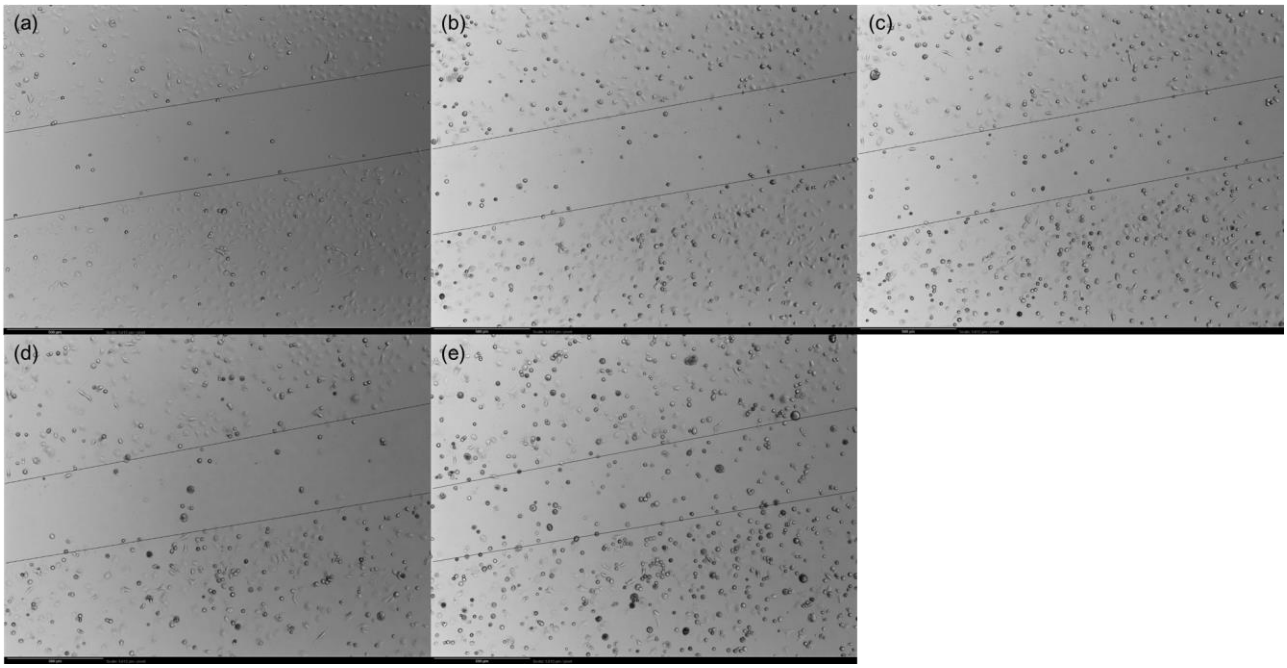

Figure 7.35: Representative brightfield microscopy images of wound closure over 24 hrs in pcDNA3-CRU transfected MDA-MB-231 cells treated with 5 µM DXR. Lines serve as an indication of wound area and where drawn to fit the general migration front across the imaged area. (a) 0 hrs; (b) 6 hrs: (c) 12 hrs; (d) 18 hrs; (e) 24 hrs. Scale = 500 µm, 4x objective.

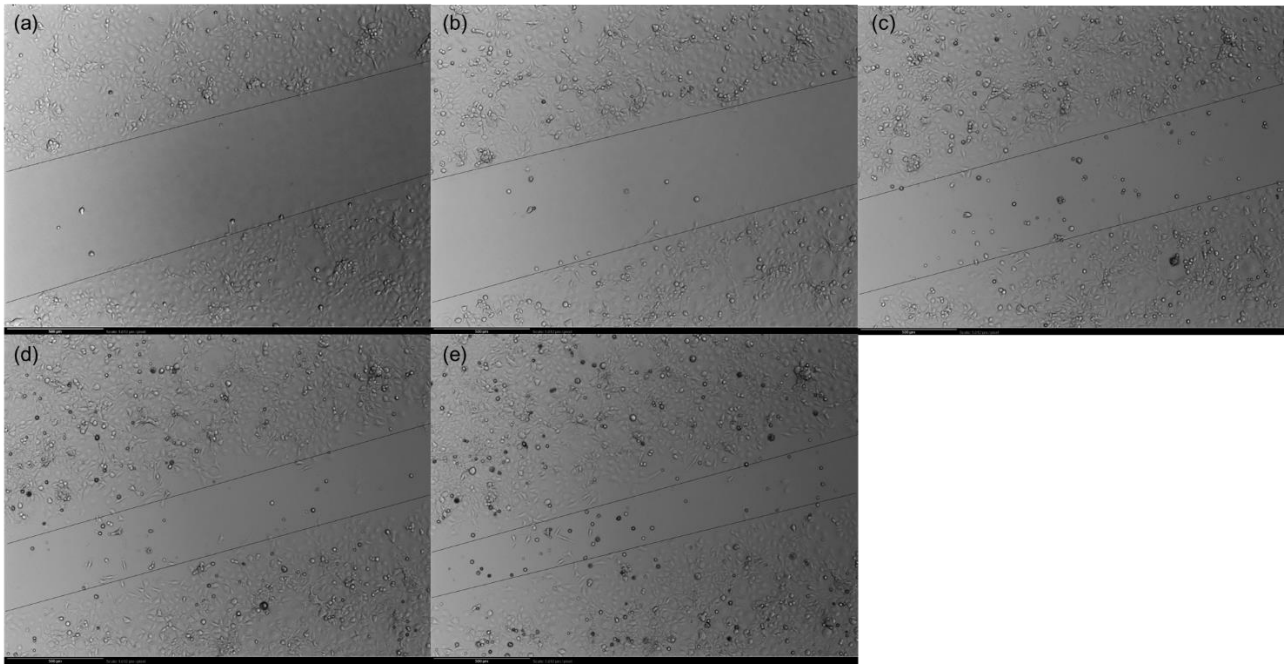

Figure 7.36: Representative brightfield microscopy images of wound closure over 24 hrs in MMC control MDA-MB-231 cells. Lines serve as an indication of wound area and where drawn to fit the general migration front across the imaged area. (a) 0 hrs; (b) 6 hrs: (c) 12 hrs; (d) 18 hrs; (e) 24 hrs. Scale = 500 µm, 4x objective.

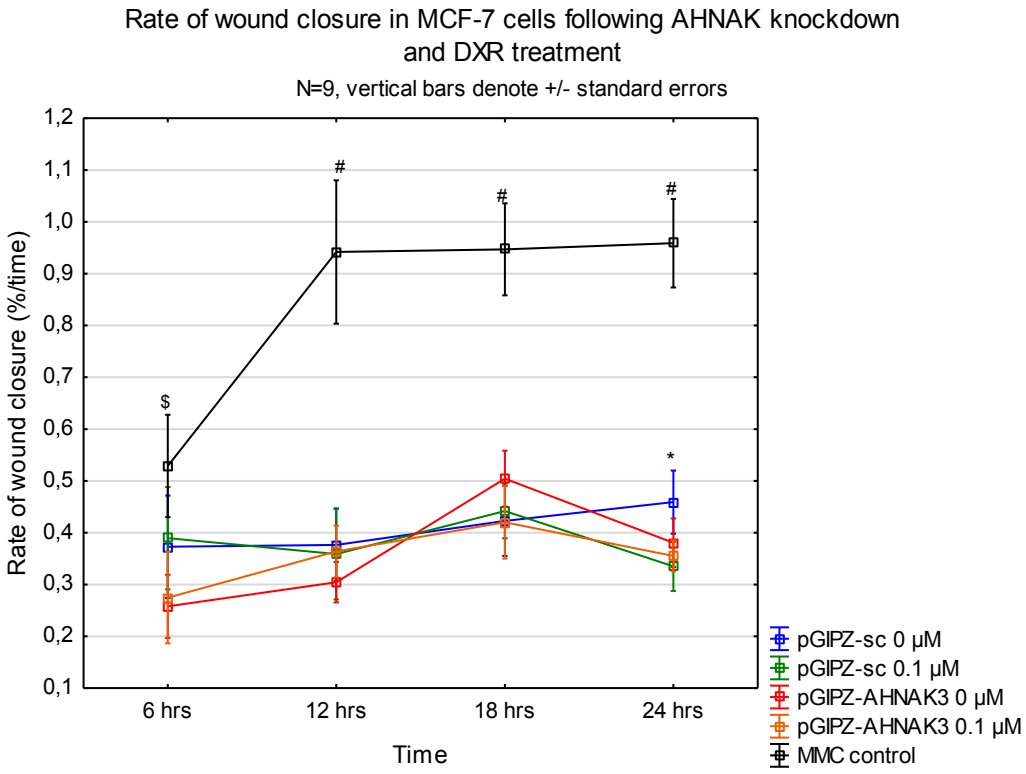

Figure 7.37: Rate of wound closure in MCF-7 cells following AHNAK knockdown and DXR treatment. Statistical significance between groups per time point is indicated by symbols. $ - MMC control vs. pGIPZ-AHNAK3 0 µM, $p < 0.05$; # - MMC control group vs. all other groups, $p < 0.0001$; * - pGIPZ-sc 0 µM vs. pGIPZ-sc 0.1 µM, $p < 0.05$.

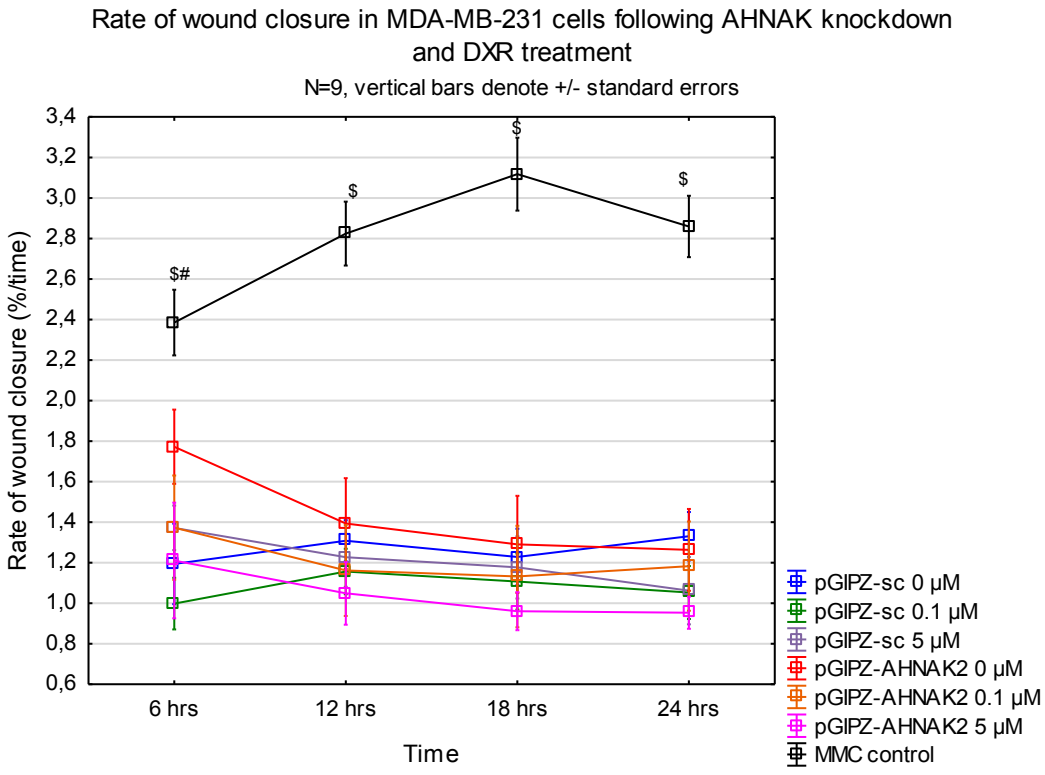

Figure 7.38: Rate of wound closure in MDA-MB-231 cells following AHNAK knockdown and DXR treatment. Statistical significance between groups per time point is indicated by symbols. $ - MMC

control vs. all other groups, $p < 0.05$ at 6hrs, $p < 0.0001$ at 12-24 hrs; # - pGIPZ-sc 0 µM vs. pGIPZ-AHNAK2 0 µM, $p < 0.05$.

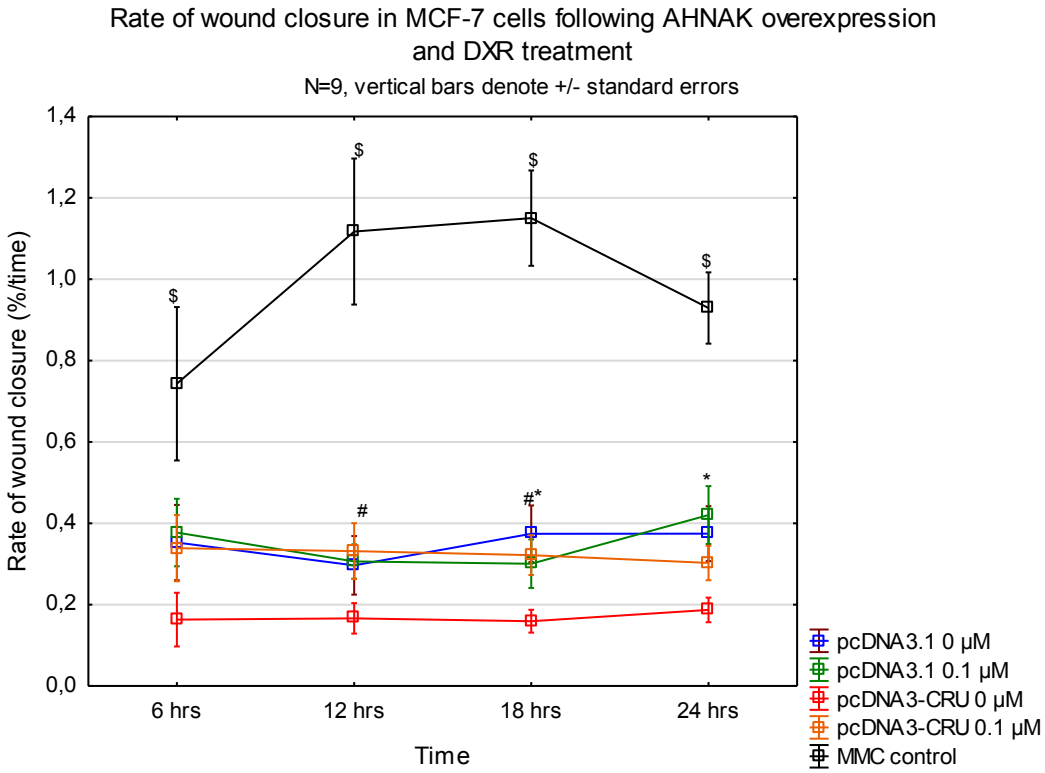

Figure 7.39: Rate of wound closure in MCF-7 cells following AHNAK overexpression and DXR treatment. Statistical significance between groups per time point is indicated by symbols. $ - MMC control vs. all other groups, $p < 0.05$ at 6 hrs, $p < 0.0001$ at 12-24 hrs; # - pcDNA3-CRU 0 µM vs. pcDNA3-CRU 0.1 µM, $p < 0.05$; * - pcDNA3.1 0 µM vs. pcDNA3-CRU 0 µM, $p < 0.05$.

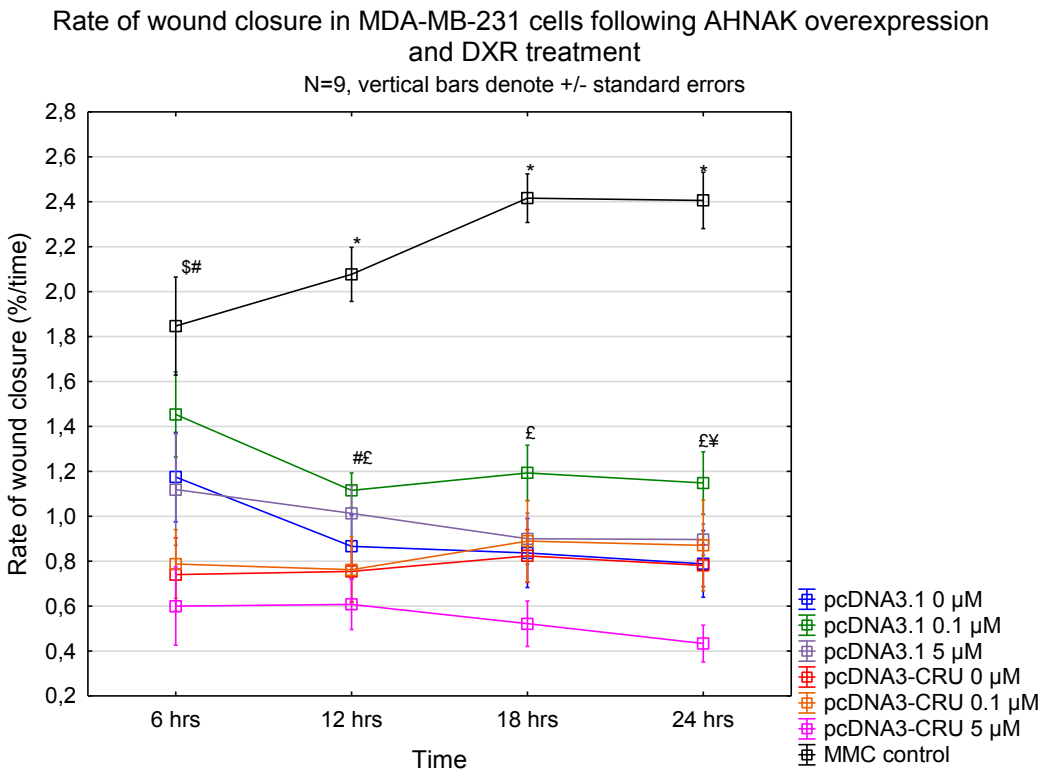

Figure 7.40: Rate of wound closure in MDA-MB-231 cells following AHNAK overexpression and DXR treatment. Statistical significance between groups per time point is indicated by symbols. $ - MMC control vs. all other groups except pcDNA3.1 0.1 µM, $p < 0.05$; # - pcDNA3.1 0.1 µM vs. pcDNA3-CRU 0.1 µM, $p < 0.05$; * - MMC control vs. all other groups, $p < 0.0001$; £ - pcDNA3.1 5 µM vs. pcDNA3-CRU 5 µM, $p < 0.05$; ¥ - pcDNA3-CRU 0 µM vs. pcDNA3-CRU 5 µM, $p < 0.05$.